NASA CONTRACTOR REPORT

NASA CR-336

SCOUT MOTOR PERFORMANCE ANALYSIS AND PREDICTION STUDY (PAPS)

by C. K. Whitney, T. F. Owens, J. Paskind, and M. B. Rubin

Prepared under Contract Nos. NAS 1-3683,
NAS 1-3684, NAS 1-3685, and NAS 1-3686
for Langley Research Center

NATIONAL AERONAUTICS AND SPACE ADMINISTRATION - WASHINGTON, D. C. - DECEMBER 1965

NASA CR-336

SCOUT MOTOR PERFORMANCE ANALYSIS AND PREDICTION STUDY (PAPS)

By

C. K. Whitney, LTV Astronautics Division

T. F. Owens, Thiokol Chemical Corp.

J. Paskind, Aerojet-General Corp.

M. B. Rubin, Hercules Powder Co.

Prepared under Contract Nos. NAS 1-3683, NAS 1-3684, NAS 1-3685, and NAS 1-3686

for Langley Research Center

NATIONAL AERONAUTICS AND SPACE ADMINISTRATION

For sale by the Clearinghouse for Federal Scientific and Technical Information
Springfield, Virginia 22151 – Price $5.00

TABLE OF CONTENTS

LIST OF ILLUSTRATIONS

LIST OF TABLES

NOMENCLATURE

a_L	-	Longitudinal acceleration, ft./sec./sec.
A_e	-	Area, nozzle exit, sq. in.
A_s	-	Propellant burning surface area, sq. in.
A_t	-	Area, throat, sq. in.
C	-	Constant
C*	-	Characteristic velocity (propellant weight), ft./sec.
$\overline{C_c^*}$	-	Characteristic velocity (consumed weight), ft./sec.
C_D	-	Coefficient, discharge
C_F	-	Coefficient, thrust, for motor exit half angle
C_F^o	-	Coefficient, thrust, zero degree exit half angle
C_N	-	Coefficient
D	-	Drag, lb.
e	-	Base of natural logarithms
f	-	Mass fraction
F	-	Thrust, lb.
$\overline{F_b}$	-	Thrust, web average, lb.
F_{SL}	-	Thrust, sea level, lb.
F_V	-	Thrust, vacuum, lb.
g	-	Acceleration of gravity, ft./sec./sec.
I_{SP}	-	Propellant specific impulse, lb. - sec./lb.
I_T	-	Total impulse, lb. - sec.
K_n	-	Propellant surface to throat area ratio
l_b	-	Propellant thickness burned, in.
l_w	-	Geometric propellant web length, in.
$l_{w_{eff}}$	-	Propellant thickness burned during web time, in.

n - Burning rate exponent

P - Head-cap pressure, psi

P_a - Pressure, ambient, psia

$\overline{P_b}$ - Pressure, web average, psia

P_c - Pressure, stagnation, psia

P_e - Pressure, exit, psia

Q - Ratio of inerts C* to propellant C*

r - Burning rate, in./sec.

T - Temperature, ^{o}F

t - time, sec.

t_b - Time, "effective" burning, sec. (Refer to following special definitions)

t_T - Time, total burning, sec.

t_w - Time, web burn, sec.

W - Weight, lb.

$\dot{w}$ - Weight rate, lb./sec.

W_C - Weight, Consumed, lb.

W_I - Weight, inert, lb.

W_{IC} - Weight, inert consumed, lb.

W_P - Weight, propellant, lb.

W_R - Weight, remaining, lb.

ϵ - Expansion area ratio

γ - Specific heat ratio

λ - Nozzle divergence loss factor

π_k - Propellant temperature sensitivity coefficient (Algol II)

ρ - Density, lb./cu. in.

σ - Standard deviation

σ_k - Temperature coefficient of burning rate (Castor I)

SPECIAL DEFINITIONS

"EFFECTIVE" BURNING TIME, t_b:

The "effective" burning time has but one significance. It is precisely representative of the time required (from the first disturbance in performance measurements) to burn a given percentage of the propellant in a given motor type. As such it correlates precisely with the average burning rate during burning through the web thickness. It is defined as:

$$t_b = f_{PI} \times \frac{\int_o^{t_T} P\,dt}{\bar{P}_b} = f_{FI} \frac{\int_o^{t_T} F_v dt}{\bar{F}_{bV}}$$

where

Motor Type	f_{PI}
Algol II	0.8502
Castor I	0.8719
X259	0.9275
X258	0.8980
10 KS 2500 (round bore)	0.9550
10 KS 2500 (keyhole bore)	0.9680

WEB BURNING TIME, t_w:

Each of the motor manufacturers has one or more definitions of "web burning time" for each of the motor types. The differences in definitions reflect differences in motor performance characteristics, differences in customer requirements, differences in manufacturers practices, etc.

The different definitions that were encountered in the PAPS program were:

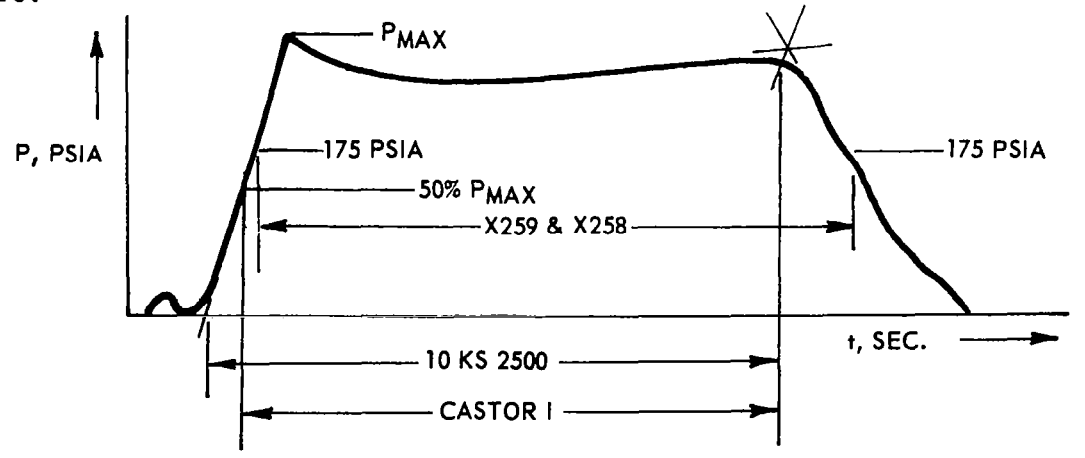

The "web burn time" values from static test data are correlated with the "effective" burning time, t_b, from flight data by the following equations:

Algol II

$t_w = t_b$

Castor I

$t_w = t_b - 0.060$

X259

$t_w = t_b/0.930$

X258

$t_w = t_b/0.910$

SUMMARY

The Scout Motor Performance Analysis and Prediction Study was initiated by identifying and acquiring the available data that would be needed to establish Scout motor performance prediction and evaluation procedures. A basic improvement in predicting/evaluating motor burn times and thrust levels was provided by changing the concept of "web burn time." The appropriate changes in the procedure for reducing this value eliminate error that results from subjective interpretation of an analog trace. More accurate correlations of Scout motor burn rate with propellant test burn rate were developed. Nominal curves of Scout motor thrust, and chamber pressure, versus burning time, were derived from sea level ambient test data and AEDC vacuum tunnel test data. Nominal propellant specific impulse values were based upon available AEDC test data, with confirmation by data from ground tests with ambient pressure conditions. Curves of motor inerts consumption versus time were developed. A rational equation was derived for calculating the propellant flow rate according to the inerts flow rate and other motor operating conditions that change during burning time. Flight motor performance was compared with ground test performance, considering burn rate, shape of thrust and pressure time histories, and the total integrals of pressure and thrust.

The objectives of the study did not include advances in the state of the science/art. The effected improvements in prediction practices do not represent advanced technology. Rather, the practices are based upon concepts and techniques which had been demonstrated previously. In some instances available techniques could not be applied in the prediction procedures of all three motor manufacturers, for lack of prerequisite test data.

Procedures for reducing flight telemeter (T/M) data were modified to obtain more accurate values for motor head-cap pressure. Step-by-step procedures for evaluating flight motor performance and stage acceleration were prepared, including formats for LTV post-flight reports of motor performance data. Special studies performed included: (1) X259 specific impulse change, (2) X258 impulse deficiency, (3) variation in motor tail-off characteristics, (4) rational estimates of true variability of Scout motor specific impulse, (5) prediction error allowances for use in orbital error analyses, (6) instrumentation and weighing accuracies, (7) Q. C. checkpoints affecting motor prediction accuracy, (8) comparisons of radar indicated trajectories with computed trajectories based upon original predictions and PAPS repredictions. Pre-flight, motor performance predictions by the PAPS engineers for the motors in the first three stages were used by LTV in preparing the pitch programs for Scout vehicles beginning with S-133.

A problem encountered was the lack of accurate measures of motor impulse in flight. Neither telemetry data (motor head-cap pressure or longitudinal acceleration) or radar data is an adequate basis for estimating a normal impulse deviation. Head-cap pressure telemetered data does permit an accurate evaluation of the burning rate (web-average) and instantaneous weight flow rate of a motor, when the true impulse of the motor is normal. An abnormally large deviation or a prevailing shift in motor impulse is detected and evaluated best only when all the available flight data are considered.

Further improvements in motor prediction accuracy can be effected by acquisition of experimental data that are lacking. Additional significant improvements will require advances in the state of the science/art. Particularly, the fourth stage impulse variation anomaly may justify intensive, fundamental research into the mechanism of solid propellant pyrolysis and combustion under various environments. Such study could contribute also to a more complete and rational explanation of the different behavior of a propellant test motor from its related Scout motor.

Over-all, the repredicted motor data analyzed show an improvement over the originally predicted motor data. The significance of the improvement is somewhat obscured by the relatively large error sources elsewhere than in motor predictions, evidenced by the large reduction in error by using post-flight data.

1.0 INTRODUCTION

The Scout was developed as an inexpensive launch vehicle for space experiments which would not require a very precise trajectory. Solid propellant motors were selected for the propulsion of all four stages because of the lower cost of solid motors and their simpler operation and launch facilities and the resulting higher reliability. The "guidance" system is a preplanned pitch program with attitude control during burning of the first three stages.

The precision of the Scout trajectory was limited partly by the variability in performance of the motors. Vehicle error analyses were performed by the NASA and LTV (References 1 and 2). Among the motor variables, the trajectory was particularly senstive to deviations of the first stage motor burning rate, affecting the thrust level and burning time, as shown in Table 1. This sensitivity to burning rate variation reduces as successive stages burn. Conversely, the trajectory was most sensitive to fourth stage deviations in propellant consumption, in weight of motor inerts, and to any error in establishing the specific impulse of the propellant.

The error analyses considered the basic error sources in all the motor performance predictions to be (1) specific impulse, (2) propellant weight, and (3) burn rate. Respective motor error values of 1.0%, 0.67%, and 3.3% (considered, then, to be two sigma values) and the other vehicle errors produced an 85 n. mi. altitude error in a circular orbit. Correspondingly, motor error values of 0.20%, 0.20%, and 1.5% with the same vehicle errors reduced the altitude error to 55 n. mi. The lower values, as two sigma allowances for prediction error, seemed to be within the state of the art.

Each of the Scout motor manufacturers (Aerojet, Thiokol and Hercules) had acquired significant amounts of motor measurements and test data from normal quality control practice. Available data could be used in correlations with Scout motor performance as a basis for performance prediction procedures. The manufacturers' practices could be reviewed to determine any critical need for additional data and improvements in data accuracy.

Accordingly, the Scout Motor Performance Analysis and Prediction Study (PAPS) was initiated. An engineer, experienced in solid rocket motors, was assigned to the study by each of the motor manufacturers. Four engineers were assigned by LTV, one for vehicle and flight data coordination and three for PAPS assistance and for monitoring the motor manufacturers' quality control in Scout motor manufacturing and inspection practices. The seven engineers assembled in an office near the NASA Scout Project Office, which provided the direction of the study. Each of the four companies represented provided "home plant" manning and computer time.

The basic approach of the PAPS group was to prepare more accurate nominal motor data (vacuum specific impulse, weights, and instantaneous values of vacuum thrust and weight-remaining) and burn rate prediction procedures. The vacuum specific impulse ratings of the motors would be based as much on

TABLE I

APPROXIMATE ORBITAL ACCURACY EFFECT
OF INDIVIDUAL MOTOR DEVIATIONS (ARBITRARY)
(Nominal Orbit: 540 n. mi. circular, Wallops Launch, 52° Inclination)

STAGE	MOTOR VARIABLE (See Note 1)	INJECTION CONDITION DEVIATIONS			ORBIT CONDITION DEVIATIONS	
		Δh, ft.	ΔV, fps	Δγ deg.	ΔApogee, n. mi.	ΔPerigee, n. mi.
I	I_{sp} + 0.1%	5500	-0.05	0.03	3.7	-0.2
(Algol IIA)	W_p + 0.1%	6000	-0.08	0.03	3.9	-0.5
	$\dot{w}$ + 1.0%	5500	-9.4	0.01	1.2	-2.8
2	I_{sp} + 0.1%	4400	1.9	0.02	4.2	-0.1
(Castor I)	W_p + 0.1%	4400	1.8	0.03	4.4	-0.3
	$\dot{w}$ + 1.0%	4000	-1.9	0.01	1.0	-0.9
3	I_{sp} + 0.1%	4700	3.5	0.03	5.7	-0.1
(X259A3)	W_p + 0.1%	5000	3.5	0.03	5.8	-0.2
	$\dot{w}$ + 1.0%	3000	-3.2	0.01	0.7	-0.8
4	I_{sp} + 0.1%	4	10.3	Nil	6.9	Nil
(X258B1)	W_p + 0.1%	28	15.8	Nil	9.2	0.3
	$\dot{w}$ + 1.0%	36	0.4	Nil	0.4	-0.2

Notes:

1. Motor deviations are arbitary, one sigma approximations of prediction error. Effects of negative deviations are essentially **symmetrical.**

2. Deviations of injection conditions and orbit parameters are interpolated from values computed for the same launch conditions but for the following motor deviations:

Motor Variable	DEVIATIONS, %, BY STAGE			
	1	2	3	4
I_{sp}	0.672	1.5	1.38	1.38
W_p	1.0	1.0	1.0	1.0
$\dot{w}_p$	6.48	4.95	9.96	9.03

Arnold Engineering and Development Center (AEDC) test data as possible. The nominal weights of the motors would be based upon a review of manufacturers' weight data and the weighing procedures and equipment used in acquiring the weight data. The basic approach to burn rate prediction was to construct preliminary correlations of ground-tested Scout motor and (related) propellant test motor burn rates. Improvements in burn rate correlation techniques, testing practices and data reduction procedures could be verified by any significant reduction in the scatter of data about the burn rate correlation. The improved method could then be applied in correlating flight motor burn rate data, giving the best opportunity to detect any effect of flight conditions on motor burn rate.

This study used only the state of the science/art that was available at the outset of the study. The procedures and practices investigated were based upon concepts that had been demonstrated previously to yield improved results in motor performance prediction/evaluation.

Further improvement in prediction accuracy can be achieved within the state of the science/art by acquiring the data which are prerequisite to the application of available concepts. Also, additional accuracy in predictions can be expected with application of advances in the state of the science/art. Avoidable limitations on prediction accuracy were investigated and recommendations were provided accordingly.

2.0 THE SCOUT VEHICLE

The Scout is a solid propellant, four-stage rocket propelled vehicle equipped with a preprogrammed guidance system. The basic vehicle, shown in Figure 1, is made up of the rocket motors, structural transition sections and a payload section. Dualized ignition circuits have been employed to enhance ignition reliability. Dual squibs are used in all motor igniters. Each one of the squibs is in a separate circuit and is connected to a separate battery. Ignition of the first stage is accomplished by a direct electrical signal provided by launch blockhouse command. Second, third and fourth stage ignitions are controlled by the guidance program timer.

The guidance and control system provides the attitude reference, control signals, and forces necessary for stabilization of the vehicle in its three orthogonal axes (pitch, yaw and roll) during boost of the first three stages. Normally, the yaw and roll axes are maintained at the launch reference while the pitch attitude is programmed through a pre-set angle corresponding to the desired trajectory. However, a yaw torquing capability is incorporated to provide programming of the yaw axis if desired. Miniature integrating rate gyros, contained within the inertial reference package, detect any angular deviation from the programmed vehicle attitude and generate proportional error signals. These error signals are then summed with corresponding rate signals and are transmitted to the appropriate control subsystem. In addition to the "strapped down" gyro sensors, the system contains a relay unit for power and ignition switching, an intervalometer to provide precise scheduling of events during flight, a programmer to provide torquing voltages to the pitch or yaw gyro and the associated power supplies.

In the lift-off configuration, the vehicle is aerodynamically stable. Control of the first stage is effected by a proportional system using a combination of jet vanes and aerodynamic surfaces, operated by hydraulic servo actuators. The second and third stage control forces are provided by hydrogen peroxide fueled, reaction motors operated as an "on-off" system. The attitude of the fourth stage is maintained by spinning just prior to third stage separation. Four solid propellant motors provide spin-up forces prior to fourth stage ignition.

A pitch program is designed to fly a gravity turn zero-lift trajectory to meet the specific requirements of the mission. The gravity turn trajectory is achieved by proper selection of the effective launch angle, launch azimuth and stage coast times. Following the design of the pitch program, a sequence of events is established for the boost trajectory, and the timer functions thus established, together with the pitch program, are incorporated into the vehicle before it leaves the LTV plant in Dallas. Neither the timed events nor the commanded pitch rates can be changed during flight. There is no ground control of the vehicle after command ignition of the first stage motor. The only deviations from the predicted trajectory which are corrected in flight are errors in vehicle attitude. There is no provision for correcting deviations in velocity, altitude or flight path angle.

The four propulsion motors of the Scout are joined by interstage structures referred to as "transition sections." Each transition section is

THE SCOUT

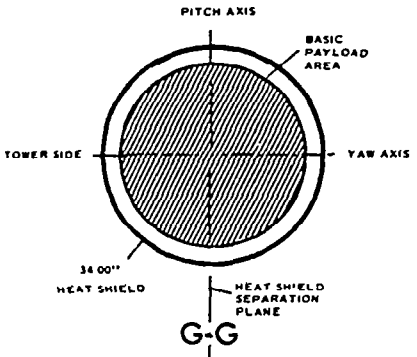
PITCH AXIS
BASIC PAYLOAD AREA
TOWER SIDE
YAW AXIS
34.00"
HEAT SHIELD
HEAT SHIELD SEPARATION PLANE
G-G

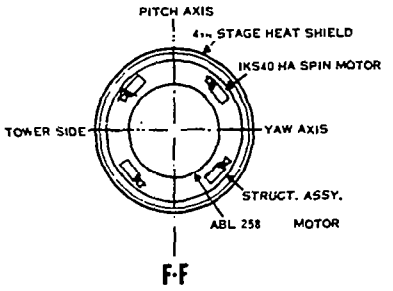
PITCH AXIS
4TH STAGE HEAT SHIELD
IKS40 HA SPIN MOTOR
TOWER SIDE
YAW AXIS
STRUCT. ASSY.
ABL 258 MOTOR
F-F

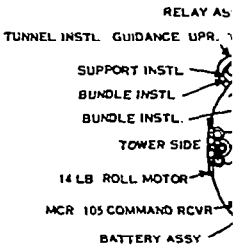
RELAY AS
TUNNEL INSTL GUIDANCE UPR.
SUPPORT INSTL
BUNDLE INSTL
BUNDLE INSTL.
TOWER SIDE
14 LB ROLL MOTOR
MCR 105 COMMAND RCVR
BATTERY ASSY

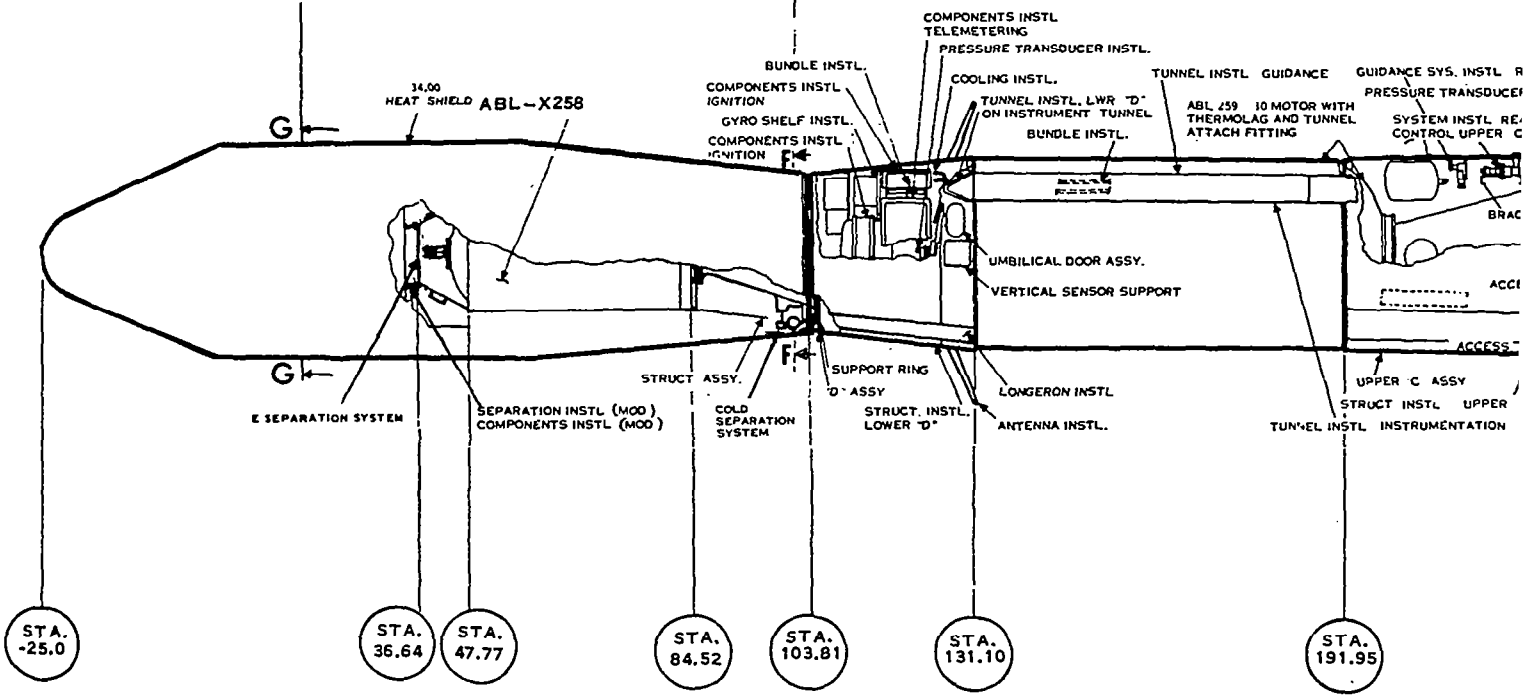
34.00
HEAT SHIELD
ABL-X258
G
F
COMPONENTS INSTL TELEMETERING
PRESSURE TRANSDUCER INSTL.
BUNDLE INSTL.
COMPONENTS INSTL IGNITION
COOLING INSTL.
GYRO SHELF INSTL.
TUNNEL INSTL. LWR "D" ON INSTRUMENT TUNNEL
BUNDLE INSTL.
TUNNEL INSTL GUIDANCE
ABL 259 10 MOTOR WITH THERMOLAG AND TUNNEL ATTACH FITTING
GUIDANCE SYS. INSTL
PRESSURE TRANSDUCER
SYSTEM INSTL
CONTROL UPPER
UMBILICAL DOOR ASSY.
VERTICAL SENSOR SUPPORT
ACCESS
STRUCT ASSY.
SUPPORT RING
"D" ASSY
STRUCT. INSTL. LOWER "D"
LONGERON INSTL
ANTENNA INSTL.
UPPER C ASSY
STRUCT INSTL UPPER
TUNNEL INSTL INSTRUMENTATION
E SEPARATION SYSTEM
SEPARATION INSTL (MOD)
COMPONENTS INSTL (MOD)
COLD SEPARATION SYSTEM
STA. -25.0
STA. 36.64
STA. 47.77
STA. 84.52
STA. 103.81
STA. 131.10
STA. 191.95

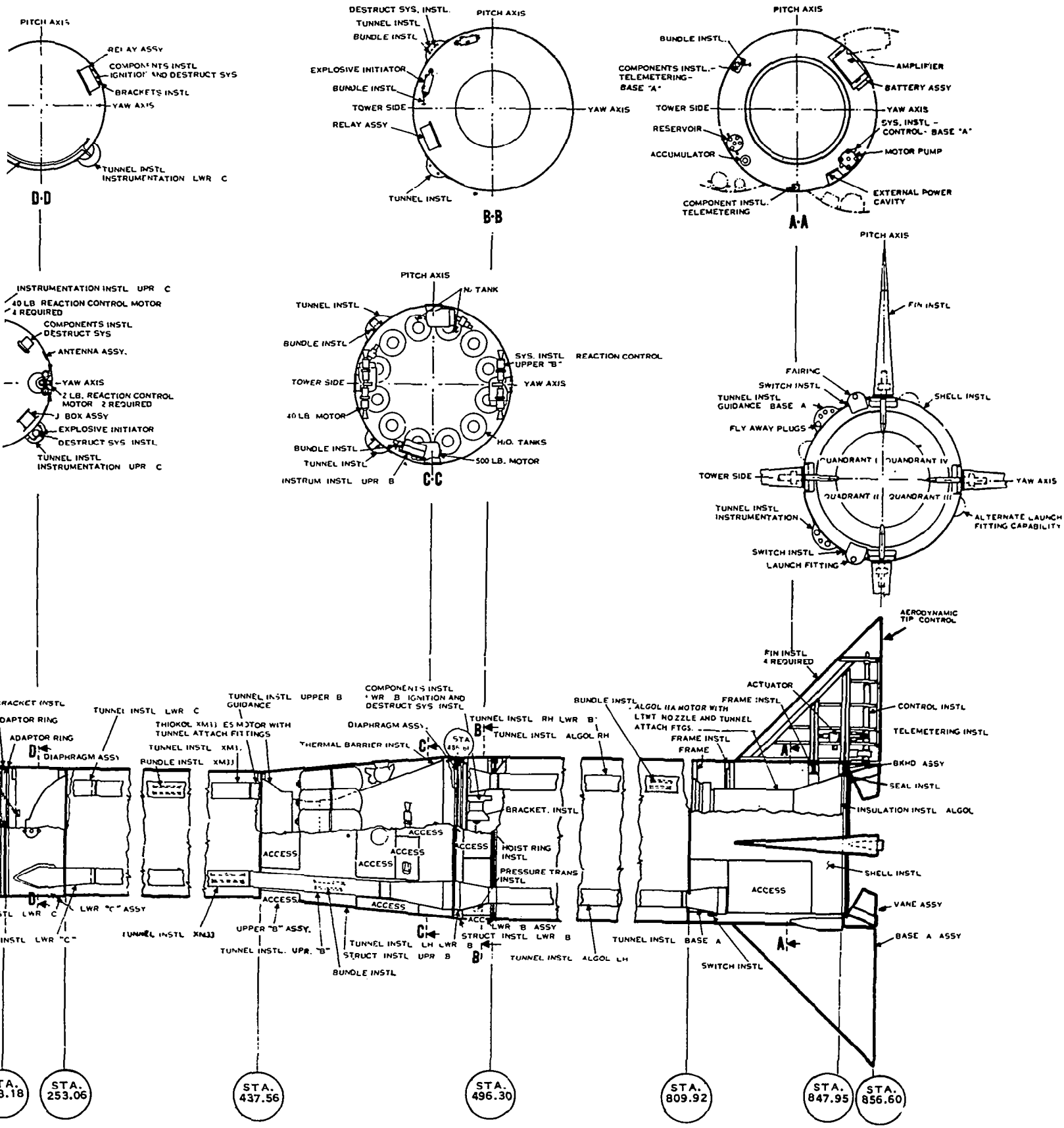

FIGURE 1 SCOUT INBOARD PROFILE

divided into lower and upper portions at the stage separation plane. A diaphragm separation system is used in the transition sections B and C. The diaphragm performs as an internal clamp with a threaded periphery that engages the two portions of a transition section. Exhaust pressure from the ignited upstage motor deforms the diaphragm periphery and separates the upper stage. A spring ejection system is used in transition section D. Explosive bolt clamps are actuated to disengage the two portions of the transition section D and separation is effected by the loaded spring.

The telemetry system of the Scout vehicle is a standard IRIG PAM/FM/FM system capable of handling 18 standard IRIG sub-carrier channels.

Separation of the third stage, and the lower D section, discontinues the telemetry and radar tracking beacon systems from the powered fourth stage.

2.1 PROPULSION MOTORS

2.1.1 FIRST STAGE

The Algol IIB motor, shown in Figure 2. is a composite propellant solid rocket motor which produces a web-average thrust of approximately 102,000 pounds force for about 46 seconds at 77°F and vacuum conditions. The overall motor length is 358 inches, the diameter is 40 inches and the total weight is 23,750 pounds, of which 21,139 pounds is propellant. The total vacuum impulse of the motor is 5,472,350 pound-seconds, the propellant vacuum specific impulse is 258.875 pound-seconds/pound, and the mass fraction of the motor is 0.891.

The Algol IIB motor case is fabricated from rolled and welded AISI 4130 heat treated steel. The case is 318.4 inches long with an outside diameter of 40 inches and a nominal wall thickness of 0.112 inch.

The nozzle assembly consists of an AISI 4130 steel closure which forms the motor aft closure and main structural member, a plastic exit cone and entrance section and a National Carbon grade RVA graphite throat insert. The ablative inner layer of the exit cone is a high-silica laminate, impregnated with phenolic resin, wound on a conical mandrel parallel to the axis of the nozzle. The entrance section is fabricated of the same material, with the fiber orientation perpendicular to the exposed flow surface.

The ignition system for the Algol IIB motor utilizes an "Alclojet" igniter containing a 2030 gram pyrotechnic charge and two Holex type 3184A initiator squibs. Each of the initiators has dual bridgewires. Ignition of any one of the four independently circuited bridgewires is sufficient to ignite the rocket motor. The pressure integral produced by the igniter is approximately 200 psia-seconds and the duration is about 50 milliseconds.

ANP-2872 JM Mod I/31 propellant is used in the Algol motor. The composition of the propellant is 61 percent oxidizer, 19 percent aluminum, and 20 percent fuel/binder. The propellant is cast with a cross shaped port as shown in Figure 2.

The chamber is lined with asbestos-filled rubber insulation. The aft chamber section has an insulation buildup to improve flow conditions and to

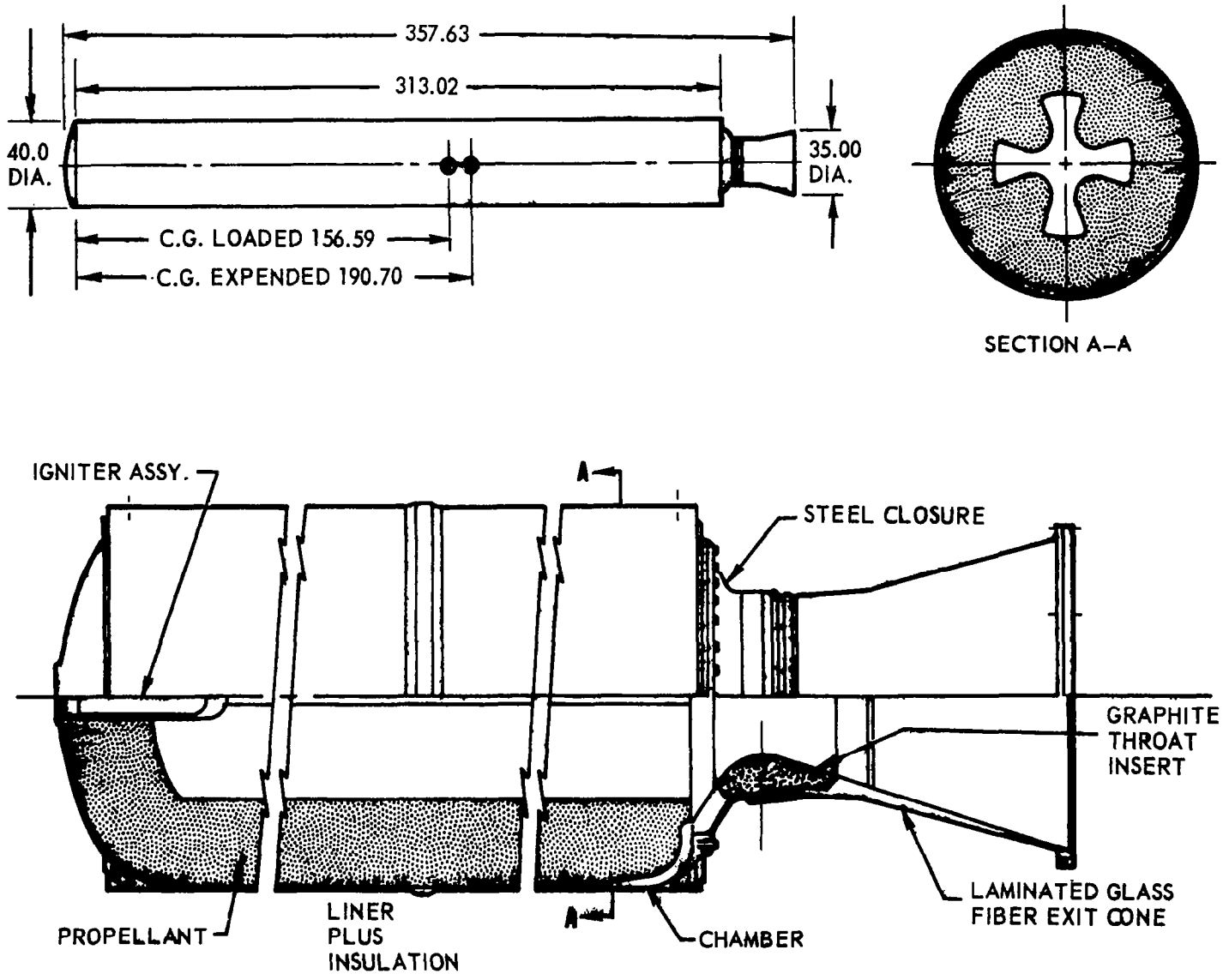

FIGURE 2 ALGOL IIB MOTOR

protect the aft chamber flange. To provide a bond of the propellant to the insulation, a brush coat of liner material is applied to the inner surface of the insulation prior to casting the propellant. When the propellant has cured, the core is removed and the propellant at the aft end of the motor is trimmed to a specified distance from the aft end of the case. Installation of the nozzle and igniter completes the motor assembly.

In addition to the 21,139 pounds of propellant burned during motor operation, 216 pounds of inert material are also consumed. The bulk of this inert material is insulation and liner which is lost after web burn time when the inside surface of the chamber wall is exposed. During the web burning period, the sources of inert material are the exit cone and entrance section of the nozzle, the graphite throat, and the insulation at the aft end of the motor. The igniter charge is also considered a part of the inert weight.

2.1.2 SECOND STAGE

The XM33E5 Castor motor, shown in Figure 3, is 246 inches long, has a case diameter of 31 inches and a nozzle exit plane diameter of 40 inches. This motor, at 77°F and vacuum conditions, produces an average thrust of 63,100 pounds during a 27.5 second web burning time and a total impulse of 2,000,000 pound-seconds. The gross weight of the XM33E5 rocket motor is 8861 pounds which includes 7321 pounds of TP-H8038 propellant with a vacuum specific impulse of 273.2 pound-seconds/pound and has a mass fraction of 0.827.

The XM33E5 motor case is cylindrical with hemispherical head and aft end closures. The case is constructed from rolled and welded AISI 4130 heat treated steel. The motor case is 202 inches long with an outside diameter of 31 inches and a nominal wall thickness of 0.110 inch.

The XM33E5 motor uses a one piece conical nozzle machined from normalized AISI 4130 steel. The throat section is formed by a machined insert of National Carbon CS-312 graphite. A ceramic coating of Rockide "A," with a flame-sprayed nickle-chromium alloy under-coating as an aid to bonding, is used to coat the expansion cone. The nozzle expansion cone has a 21° 40' divergent half-angle and internal threads at the exit plane for engagement with the "B" section separation diaphragm.

The motor case is insulated in the forward and aft domes with a polysulfide/epoxy filled with ground asbestos. The insulation, being trowelable, is applied to the case with a sweep mold having the desired insulation geometry. After application and cure of the insulation, the case is lined with a dual liner system. The first coat, a polysulfide liner, is bond-compatible with the insulation. The second coat, a PBAA liner, is bond-compatible with the polysulfide liner and the PBAA propellant. An epoxy wash is applied between the two liner coats to facilitate a bond between the two liner systems. The nominal liner thickness is 0.120 inch over the forward section of the motor case and 0.180 inch over the aft 90 inches.

The XM33E5 motor, after application and partial cure of the last coat of liner, is cast with TP-H8038 propellant. The propellant configuration, shown in Figure 3, is a standard five point star with a head end web producing a loading density of 86 percent at a 45 percent web fraction. The propellant

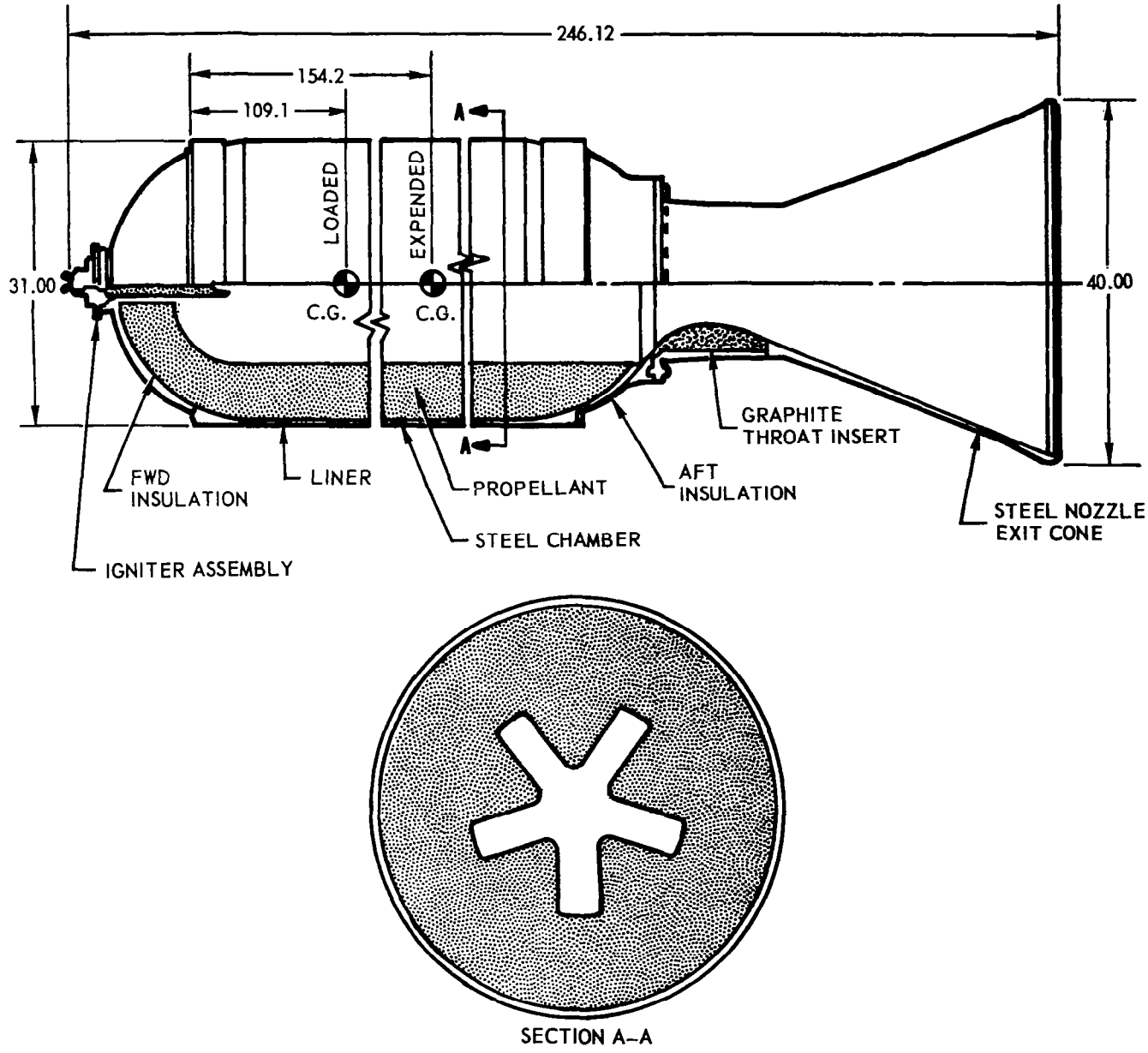

FIGURE 3 XM33E5 CASTOR MOTOR

is a composite of 70% oxidizer, 16% fuel and binder, and 14% aluminum. The propellant produces a vacuum specific impulse of 273.2 pound-seconds/pound in the Castor motor.

The pyrogen ignition system used in the XM33E5 motor has a fiberglass case loaded with TP-E8035 propellant in a 12 point star configuration. The pyrogen case is fitted with a steel adapter to house the pyrotechnic booster charge and the two McCormick-Selph M-125 Mod 1 initiators. Each initiator has dual bridgewires. Ignition of any one of the four bridgewires is sufficient to ignite the Castor motor. The pyrogen unit loads approximately three pounds of propellant and nominally produces an average propellant flow rate of 11 pounds per second during a 0.25 second web burning time.

2.1.3 THIRD STAGE

The X259 Antares II rocket motor, shown in Figure 4, is 113.8 inches long, has a case diameter of 30.05 inches, and has a nozzle exit cone diameter of 29.32 inches. This motor, at 77°F and vacuum conditions, produces an average thrust of 21,700 pounds force, during an average web burn time of 31.5 seconds, and a total impulse of 719,500 pound-seconds. The gross weight of the X259 is 2778 pounds which includes 2557 pounds of propellant. The X259 has a propellant vacuum specific impulse of 281.4 pound-seconds/pound weight and a mass fraction of 0.92.

The X259 case is made of Hercules Spiralloy, which is oriented, continuously wound fiberglass strands bonded together with an epoxy resin. This structure incorporates aluminum forward and aft adapters and attach rings as integral parts of the case. The motor case is 76.11 inches long with an outside diameter of 30.05 inches and a nominal wall thickness of 0.140 inch.

The X259 nozzle consists of a graphite throat insert, a retaining ring, and a 15° half-angle expansion cone. The retaining ring assembly is manufactured by compression molding an asbestos phenolic material to a forged aluminum ring. The inner surface of the phenolic portion of this assembly is subsequently machined to receive an ATJ graphite throat which is bonded into place with an epoxy resin. The expansion cone is a composite molding of graphite tape and silica phenolic tape. The cone exterior is reinforced with a fiberglass structure, and the interior contains, for venting purposes, 0.060 inch diameter holes drilled on 0.50 inch centers through the graphite tape and forty-eight longitudinal slots through the phenolic and fiberglass interface. The phenolic-fiberglass expansion cone is bonded to the retainer ring-graphite throat assembly with an epoxy resin and the whole assembly is machined.

The X259 insulation consists of a two piece contoured, asbestos filled Buna-S rubber material which is molded on a removable plaster mandrel prior to the manufacture of the case. The insulator is then made an integral part of the case during the winding operation which is done prior to removing the plaster mandrel.

The X259 propellant is a high energy, composite, double-based propellant and is bonded directly to the insulator and case in a slotted configuration with four radial slots spaced 60° and 120° apart. This propellant

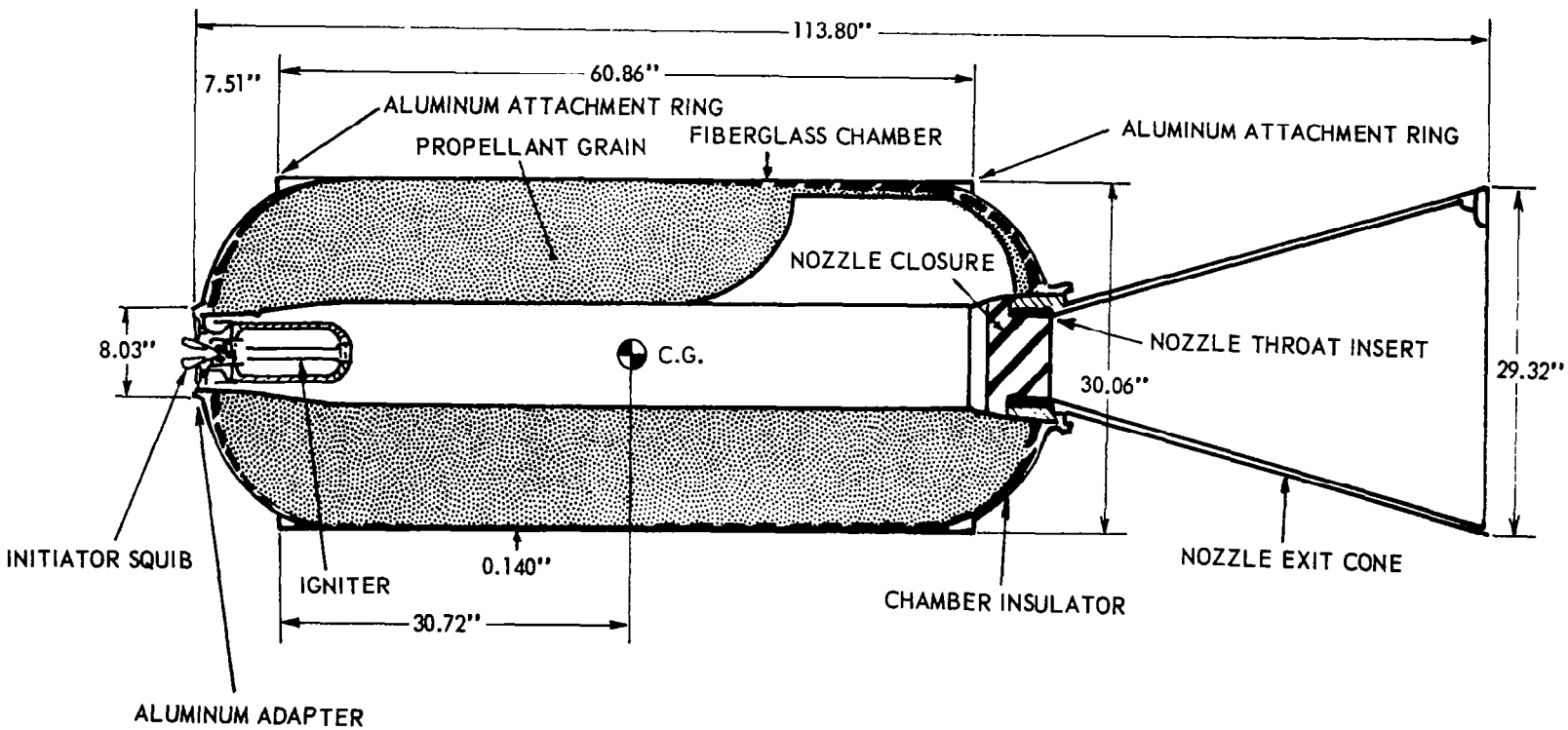

FIGURE 4 X259-A2 MOTOR

gives a vacuum specific impulse of 281.4 pound-seconds/pound weight with a nozzle expansion ratio of 16.2.

The X259 utilizes a pyrogen (rocket-type) igniter with a propellant mass flow rate of 6.67 pounds/second. The propellant charge, which weighs 8 pounds, is cast in an eight pointed star configuration. It is overwound with fiberglass after being assembled with an aluminum headcap and asbestos phenolic forward and aft domes. Ignition of the propellant is accomplished by 25 grams of boron-potassium-nitrate (BKNO3) pellets. The pellets are ignited by two SD55A3 squibs, each containing dual bridgewires. These squibs are inserted into the aluminum headcap at the forward end of the igniter.

2.1.4 FOURTH STAGE

The X258 Altair II rocket motor (C model), shown in Figure 5, is 59.25 inches long, has a case diameter of 18.04 inches, and has nozzle exit cone diameter of 16.28 inches. This motor, at 77°F and vacuum conditions, produces an average thrust of 5800 pounds-force, during an average web burn time of 22 seconds, and a total impulse of 140,000 pounds-seconds. The gross weight of the X258 is 576 pounds, which includes 502 pounds of propellant. The X258 has a propellant vacuum specific impulse of 281.2 pound-seconds/pound weight and a mass fraction of 0.87.

The X258 case is made of Hercules Spiralloy similar to the way the X259, third stage, case is made. The motor case is 42.82 inches long with an outside diameter of 18.04 inches and a minimum wall thickness of 0.80 inch.

The X258 nozzle consists of a graphite throat insert, a retaining ring, and a 18° half-angle expansion cone. The retaining ring assembly is manufactured by compression molding an asbestos phenolic material to a forged aluminum ring. The inner surfaces of the phenolic portion of this assembly are subsequently machined to receive an ATJ graphite throat which is bonded into place with an epoxy resin. The expansion cone is a composite molding of graphite tape reinforced with asbestos phenolic and overwound with fiberglass. The interior of the cone contains, for venting purposes, 0.62 inch holes drilled on 0.5 inch centers through the graphite tape and 24 longitudinal slots through the phenolic-fiberglass interface. The phenolic-fiberglass expansion cone is bonded to the retainer ring-graphite throat assembly with an epoxy resin and the whole assembly is machined.

The X258 "C" model insulation consists of forward and aft dome insulators, made of asbestos filled Buna-S rubber, molded on a removable plaster mandrel prior to winding the chamber. These insulators are made an integral part of the case during the winding operation. After removal of the plaster mandrel, additional boric acid filled rubber is applied to the cylindrical portion of the chamber where no previous insulation exists. At the present time a new model of the X258 ("E" model) is being developed. This model will contain a one-piece boric acid, ablative insulator for the complete inside case wall.

The X258 propellant is a high energy, composite, double-based propellant and is bonded directly to the insulator in a slotted, test tube configuration with twelve radial slots, four major slots and eight minor slots.

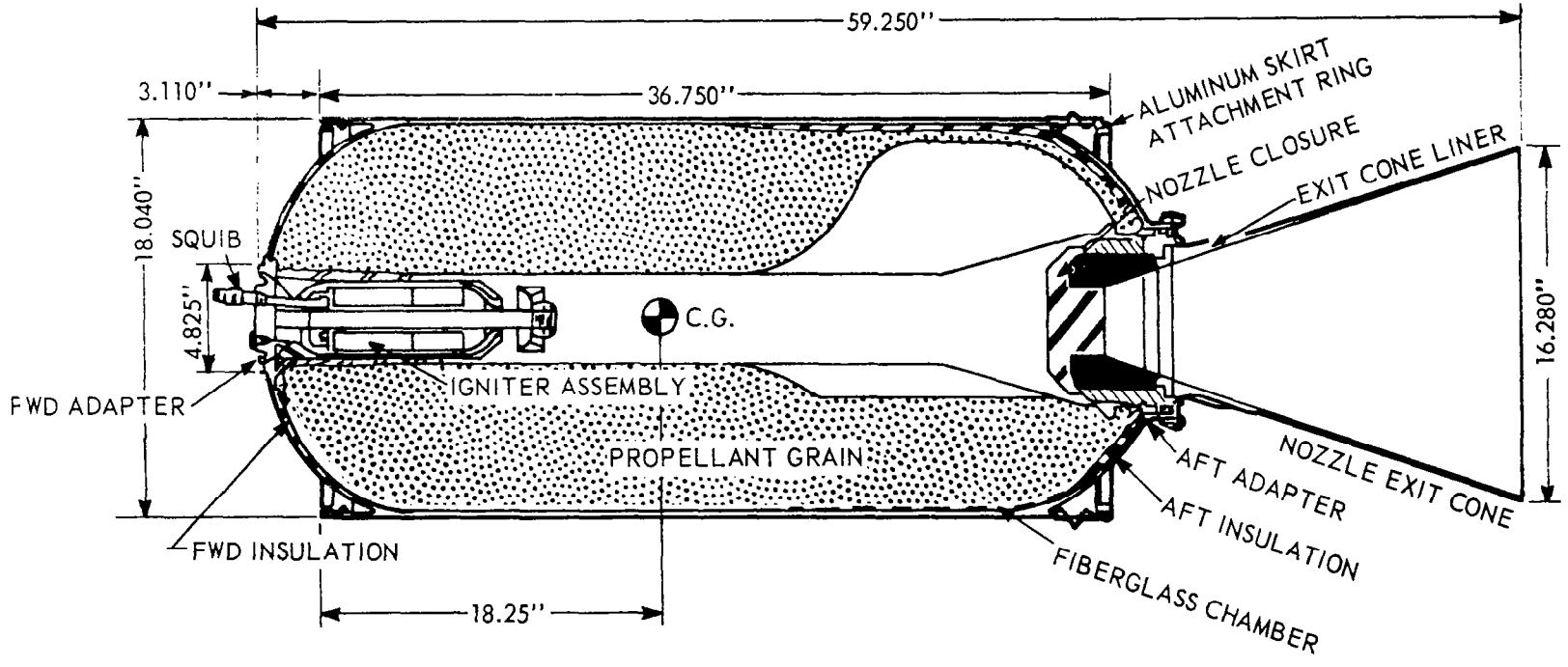

FIGURE 5 X258-C ALTAIR II MOTOR

The propellant, designated CYI-75, is similar to the X259 propellant except for a lower burning rate.

The X258 utilizes a pyrogen (rocket-type) igniter with a propellant mass flow rate of 1.67 pounds/seconds. The propellant charge, which weighs 2 pounds, is overwound with fiberglass after being assembled with an aluminum headcap and asbestos phenolic forward and aft domes. Ignition of the propellant is accomplished by 10 grams of boron-potassium-nitrate ($BKNO_3$) pellets. The pellets are ignited by two SD6A0 squibs, each containing dual bridgewires. These squibs are inserted into the aluminum headcap at the forward end of the igniter. A tantalum core, phenolic rod running through the center port of the propellant charge connects the forward headcap with a phenolic cusp which is used to deflect the igniter gases for better ignition of the motor propellant.

3.0 MOTOR PERFORMANCE CONCEPTS

3.1 WEB BURN TIME

The primary objective of this study was to develop a system which could be used to accurately predict the thrust level, burn time, and weight remaining of the Scout motors. The prediction of thrust level and burn time could conceivably be based on a correlation of pressure, thrust, time, or burning rate of the full scale motor with either pressure, time, or burning rate of a test motor. Time measurements were selected since they are the most precise measurements obtained. The choice of prediction techniques is then resolved to a correlation between the full scale motor and test motor based on either time or burning rate. Since a correlation based on burning rate allows adjustments, if needed, for known differences in the propellant web thickness, this approach was used. In developing the burn rate correlation it was essential to develop precise techniques for determining the propellant burning rate in both the full scale motors and the test motors.

A major difficulty in determining a precise estimate of burning rate in the past has been associated with the tangent method of obtaining web burn time. The propellant burning rate was calculated as the ratio of the propellant web thickness, l_w, and a web burn time, t_w. The web thickness value was obtained from the geometry of the motor, either as designed or as measured. The web burn time was obtained by the "tangent" method using an analog trace of pressure versus time. The interval of web burn time ends at the intercept of the trace with the bisector of the area, or angle, formed by two tangents to the trace at the decay transient as shown in Figure 6 .

The tangent method of determining web burn time is particularly susceptible to two types of errors:

1. Slight deviations in the trace shape at the decay transient can significantly affect the time determination independently of the average burning rate and thrust level. Deviations in the trace characteristics can result from a number of factors such as differences in burning rate between the propellant mixes loaded into the motor and differences in web thickness within the motor.

2. The interpretation of the data necessary in constructing tangents to the curve results in different times being obtained for the same data by different individuals. Also, different proportioning of the pressure and time scales on analog records leads to different times being derived for the same motor.

An example of the first type of error is shown in Figure 6 . If the performance of two motors differed only as indicated by the dashed line, a significant difference in web burn time would be obtained. However, this difference in time would not be indicative of a real difference in the average burning rate, pressure level, or thrust level of the motors.

The second type of error, that of the individual interpretation of the data, is probably the most significant error associated with the tangent method. To demonstrate the error introduced from this source, NASA personnel

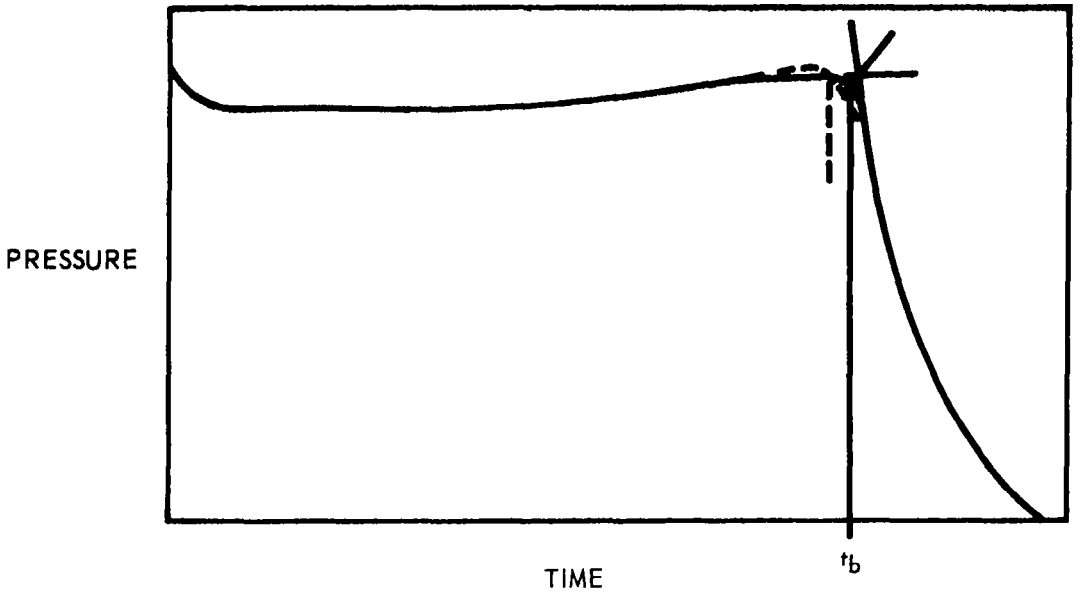

FIGURE 6 TANGENT METHOD OF DETERMINING WEB BURNING TIME

and PAPS personnel together reviewed the flight records for a series of Algol IIA motors and determined web burn times by the tangent method. In addition, the Aerojet representative determined web burn times for the same series of motors from the reduced data plots provided by LTV. A comparison of the times determined from these two sets of data with the web burn times determined independently by LTV from different analog records is shown in Table 2 .

TABLE 2

ALGOL IIA

FLIGHT WEB BURN TIME COMPARISON

DATA SOURCES:

Source I - LTV Flight Reports
Source II - Read from Oscillograph Records at LRC
Source III - Read from LTV Data Plot

VEHICLE	ALGOL IIA	SOURCE I Sec	SOURCE II Sec	SOURCE III Sec
S-113	13	46.5	46.8	47.4
S-114	5	44.5	43.0	44.0
S-115	6	46.0	46.5	47.4
S-116	8	47.0	47.4	48.3
S-118	4	--	--	45.3
S-119	7	46.0	--	47.5
S-120	12	47.0	--	48.1
S-122	21	43.0	--	44.6
S-127	10	--	47.9	48.0

Note: dashes indicate data not available.

A comparison of the tabulated times shows that in some cases a difference in excess of three percent existed. As a consequence, when the burning rate is then determined by ratioing the design or measured web thickness to these different time values, the result is an apparent difference in burning rate for the same motor. Therefore, other techniques were investigated as a means of obtaining more consistent burning rate and time data. The basis of the other techniques was a recognition of the relationship between the accumulated pressure integral and the propellant weight discharged which can be expressed as follows:

$$\int_{t_o}^{t} P\,dt = \int_{t_o}^{t} \dot{w}\,dt \;\frac{C^*}{gA_t} \qquad (1)$$

$$= A_s l_b \;\frac{\rho C^*}{gA_t}$$

Further, the average propellant burning rate during any interval of motor operation can be expressed mathematically as follows:

$$r = l_b/t_b \qquad (2)$$

Figure 7 (a) illustrates two times, t_1, and t_2, which would be required to burn through the respective distances, l_1, and l_2, in Figure 7 (b). Figure 7 (c) illustrates that the average burning surface area is very nearly the same through both of the burning times although the thicknesses burned are quite different. However, the thickness burned at each of these time points can be calculated from Equation (1) since all factors other than the distance burned are well defined in the two cases. The time and thickness burned in each case can then be entered in Equation (2) to obtain consistent burning rate data.

Thiokol experience had shown that consistent burning rate data could be obtained using the tangent time value if the average distance burned were allowed to be a variable. This approach recognizes the dependence of the pressure integral on the propellant weight burned; hence on the average burning surface and the propellant thickness burned. Burning rate calculated in this manner is relatively insensitive to the normal errors in determining web burn time. Arbitrarily selecting time values from 25.9 sec to 28.7 sec (about 10% range) from the nominal Castor I pressure-time curve results in only a 0.3% range of burn rate values when the propellant thickness burned is adjusted based on the pressure integral ratio. This pressure integral ratio-burn rate relationship is shown in Figure 8 .

Although the above approach provides an adequate representation of the propellant burning rate, it was deemed advisable to redefine web burn time such that it too would be more indicative of motor performance. If the end of the web burn time is defined as occurring when a given percentage of the total pressure integral has been accumulated, the burn times would be as consistent as the burning rate data. Hence, this definition of web burn time was used in developing the burning rate correlations.

Two criteria were established to evaluate any improvement in performance predictions resulting from the change in burn time definition and its effect on the burning rate calculation:

1. Better correlation of the burning rate and thrust levels for individual motors.

2. An improvement in the burning rate correlation between the batch test and full scale motors.

The improvement in each of the above areas is exemplified by test data available for the Algol IIA motor. Two burning rate correlations between batch and full scale motors, shown in Figures 9 and 10, were constructed for the Algol II motor. The first correlation, Figure 9 , was constructed using burning rates for both the test motor and the Algol motor obtained by dividing the design or measured web thicknesses by the time determined by the tangent method. This approach resulted in a correlation having a standard deviation

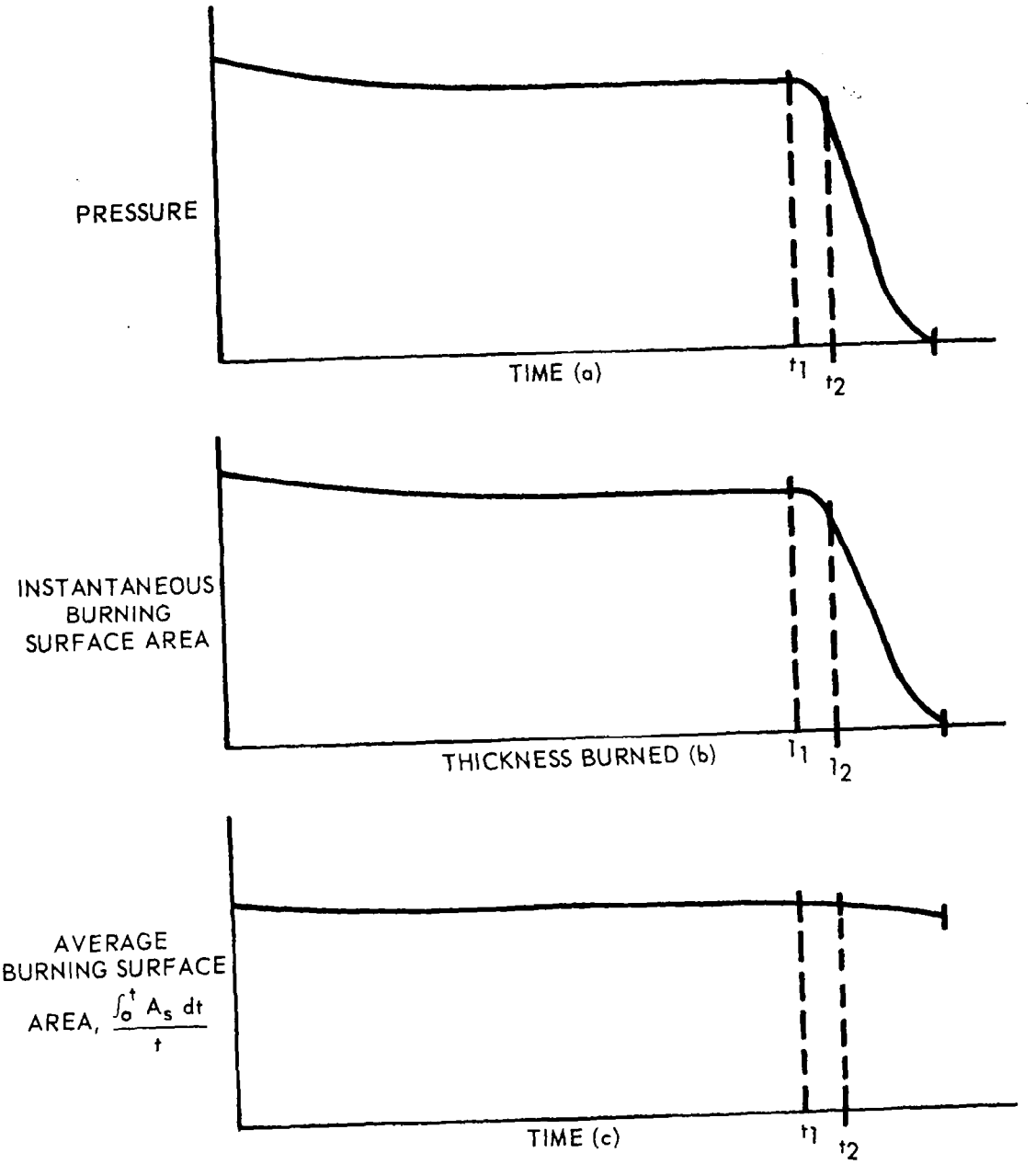

FIGURE 7 PRESSURE VERSUS TIME AND BURNING SURFACE AREA VERSUS WEB THICKNESS

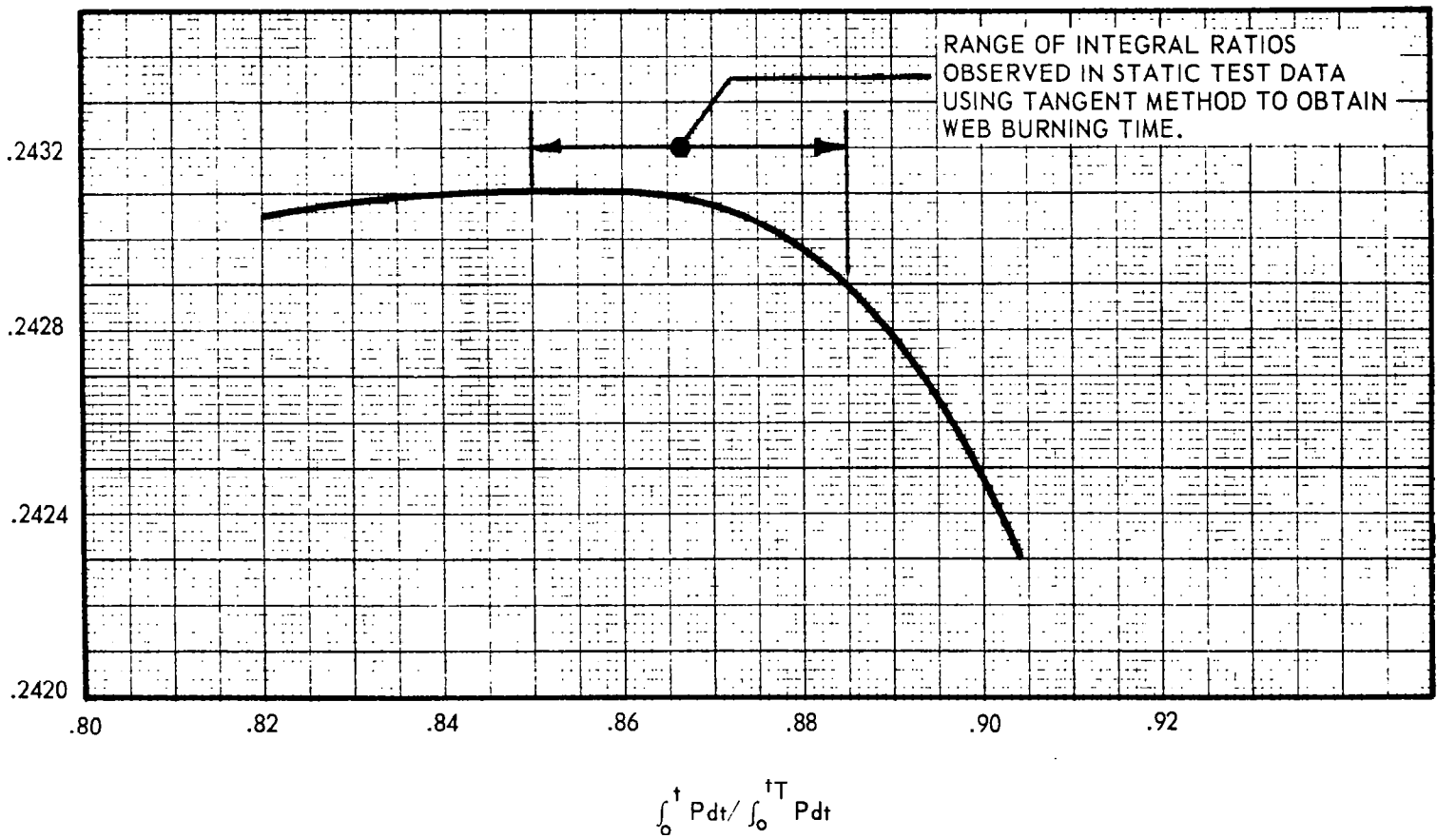

FIGURE 8 CASTOR I BURN RATE VERSUS PRESSURE INTEGRAL RATIO

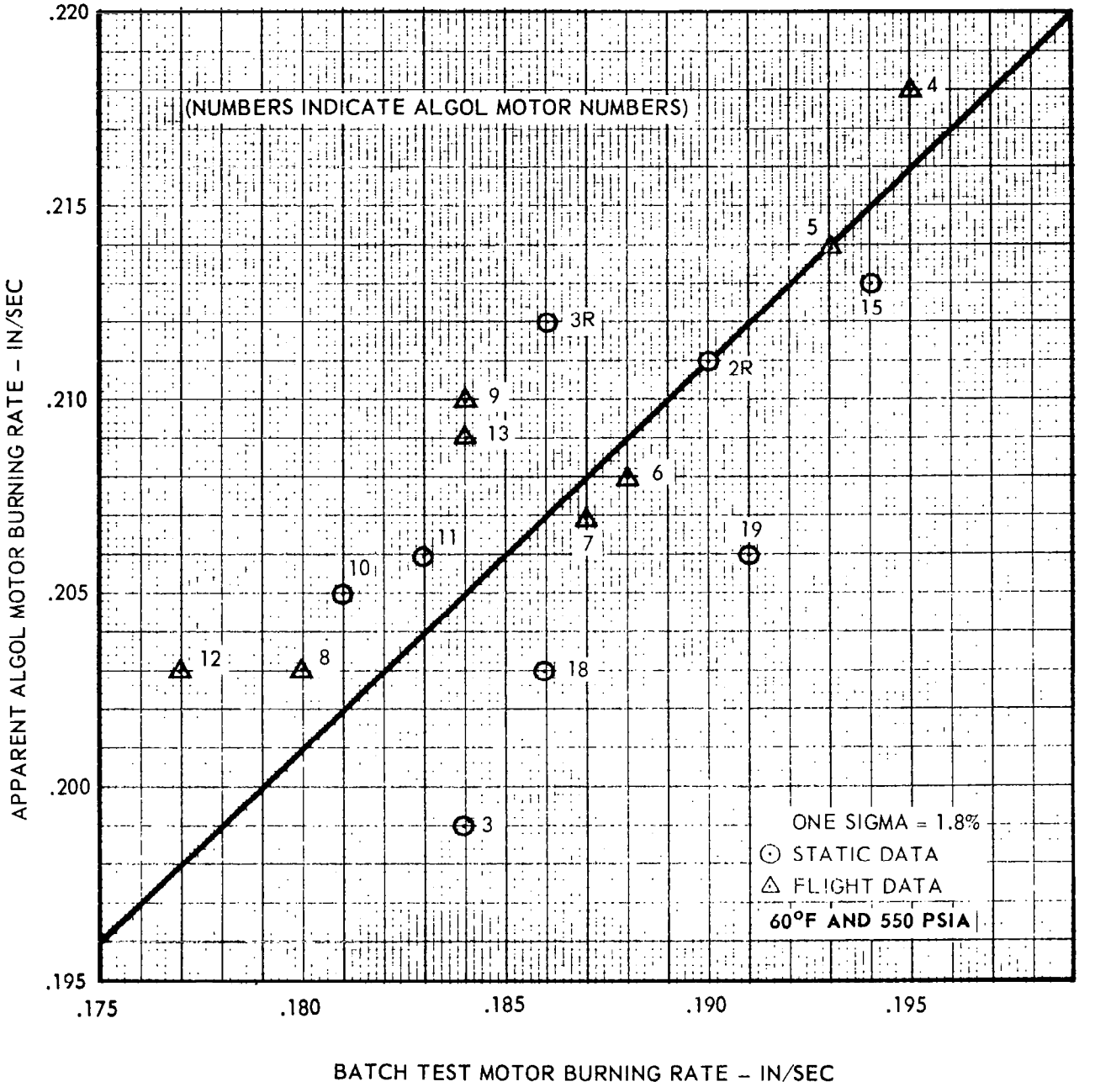

FIGURE 9 ALGOL IIA BURNING RATE CORRELATION – TANGENT METHOD

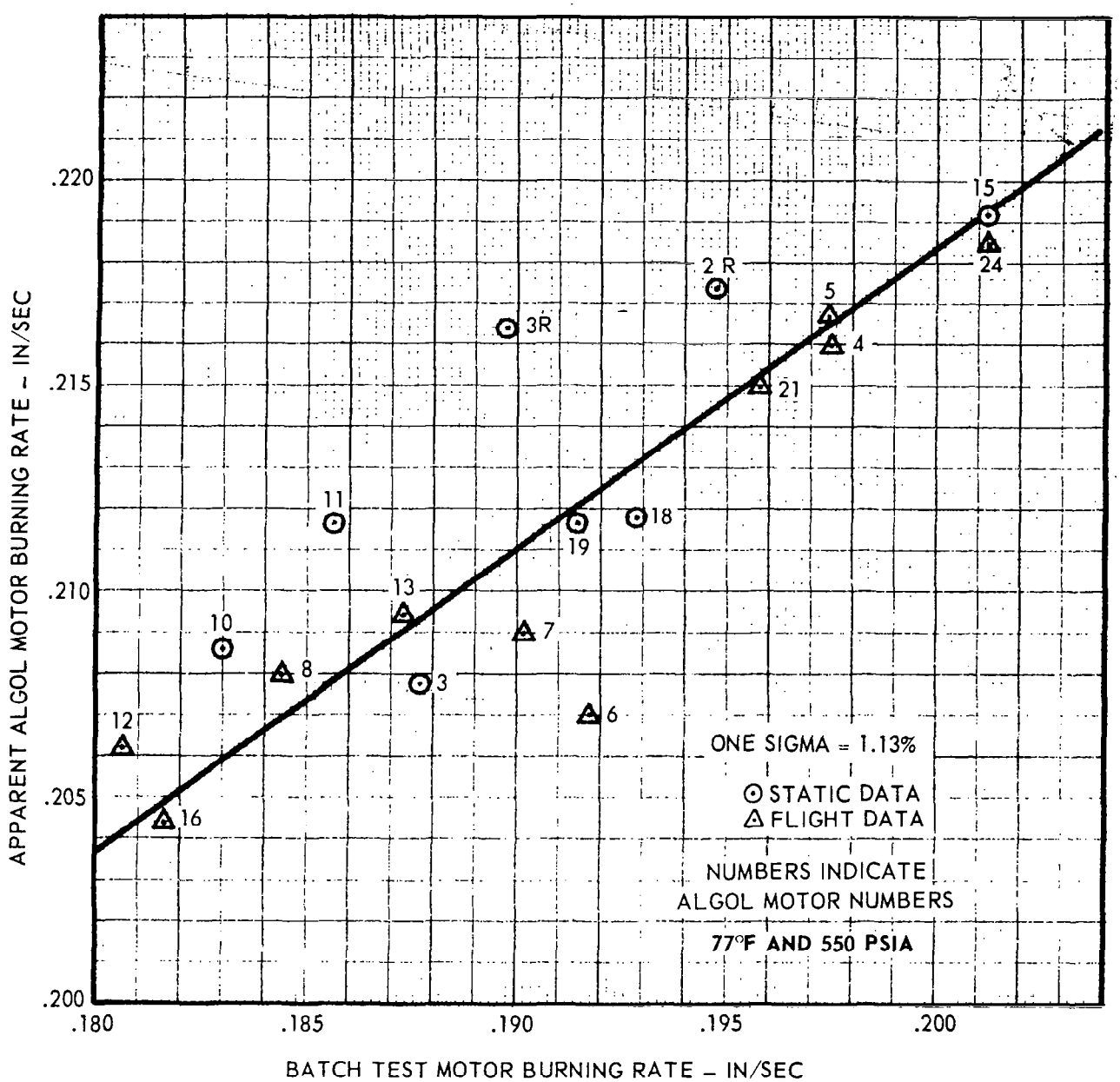

FIGURE 10 ALGOL IIA AND B BURNING RATE CORRELATION — INTEGRAL RATIO METHOD

of 1.87 percent. The next correlation, Figure 10 , was constructed in the same manner, except using the revised definition of web burn time. In this correlation 1.49 percent standard deviation of the rate errors was eliminated, leaving a net burn rate prediction error having a standard deviation of 1.13 percent.

A comparison of the agreement between the burning rate and sea level thrust of the Algol motor is shown in Figures 11 and 12 . In Figure 11 the tangent method was used to determine web burn time while in Figure 12 the integral ratio method was used. The thrust data shown on each plot represent data obtained from the same static test Algol motors. The scatter about the line of correlation results not only from the inconsistency in the burning rate or time data but also from other sources such as instrumentation error and slight differences in propellant weight and nozzle expansion area ratio. When the tangent method was used, Figure 11, the scatter about the line had a standard deviation of 1.04 percent. By merely using the integral ratio method of determining web burn time, Figure 12, the standard deviation of the scatter was reduced to 0.60 percent. Thus, the latter method of determining web burn time results in a significant improvement in the agreement between the thrust level and burning rate (and burn time) for this series of motors.

3.2 CONSUMABLE WEIGHT REMAINING

The flight of the vehicle is dependent only upon its accelerations which are most strongly a function of vehicle weight remaining, versus time. Most of the vehicle weight change is in motor consumables: 1) propellant and 2) a relatively small amount of "inert" materials such as internal case insulation and inside surfaces of the nozzle. There appears to be no way feasible for acquiring instantaneous measurements, in flight, of motor consumable weight remaining. Such measurements, by any technique, have not been acquired during static tests of Scout motors either. The problem of not having instantaneous measurements of consumable weight is further complicated by the independent rates of consumption of the propellant and the inerts.

Based on a simplified theory, the instantaneous rate of propellant consumption would vary during burning in direct proportion to chamber pressure or to vacuum thrust. However, the presence of pyrolyzed inert materials in the discharge stream affects chamber pressure and thrust, versus time. Any change, during burning, of the proportion of inerts in the total discharge causes a related, changing effect on pressure and thrust, versus time. In addition, any change in the nozzle throat size during burning affects the pressure-weight rate relationship, and any change in the nozzle exit/throat ratio or exit cone "half-angle" affects the vacuum thrust-weight rate relationship. Also, the generation and flow of gas through the port of a motor causes an increase in pressure toward the head end of the motor. This effect diminishes with burning time (with increasing port size) and affects the pressure-weight rate relationship.

In the history of the Scout program, the weight consumption rate was considered to vary in proportion to head-cap pressure, initially. Later the weight consumption rate was assumed to vary in direct proportion to the

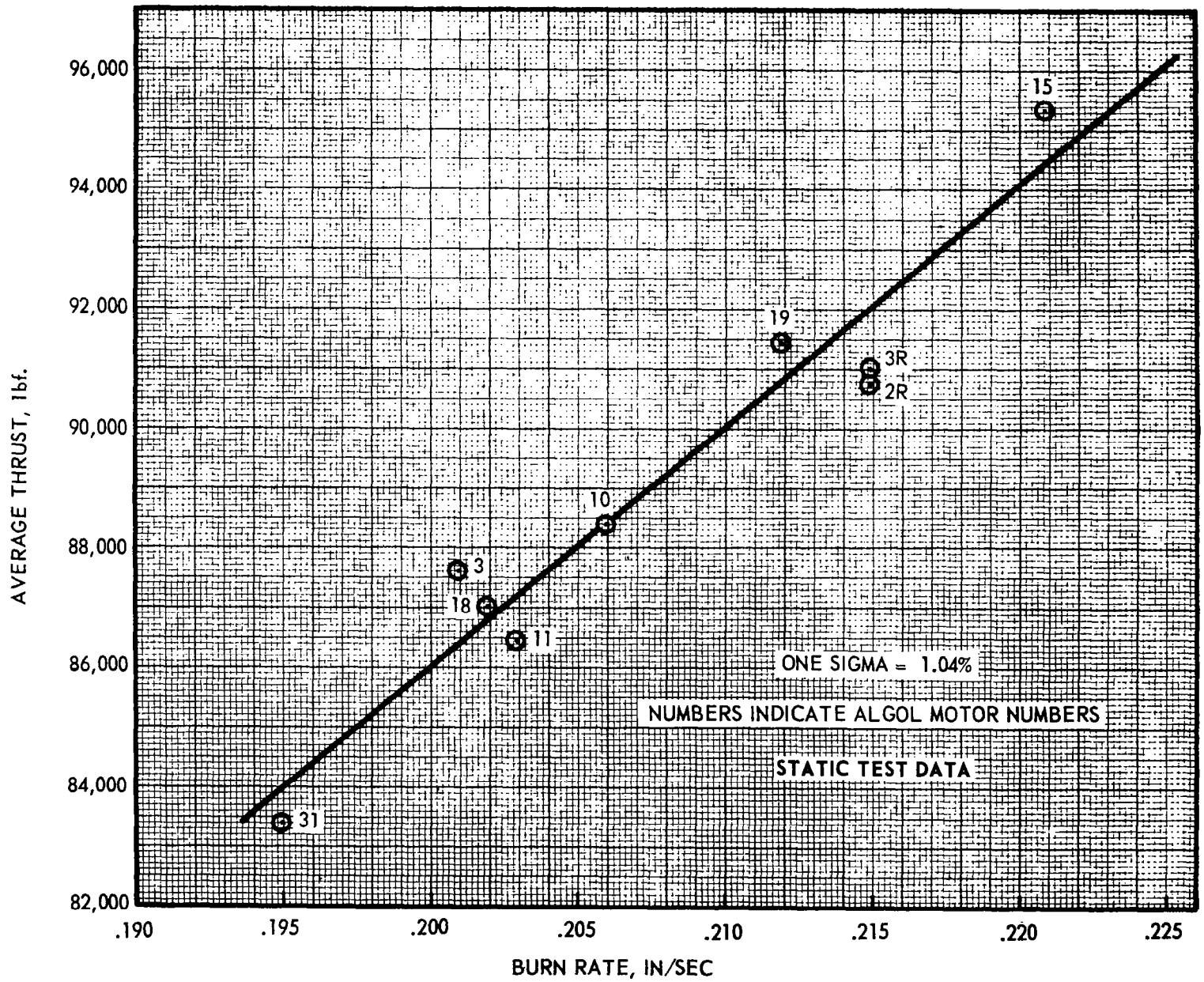

FIGURE 11 ALGOL IIA AVERAGE THRUST VERSUS BURNING RATE – TANGENT METHOD

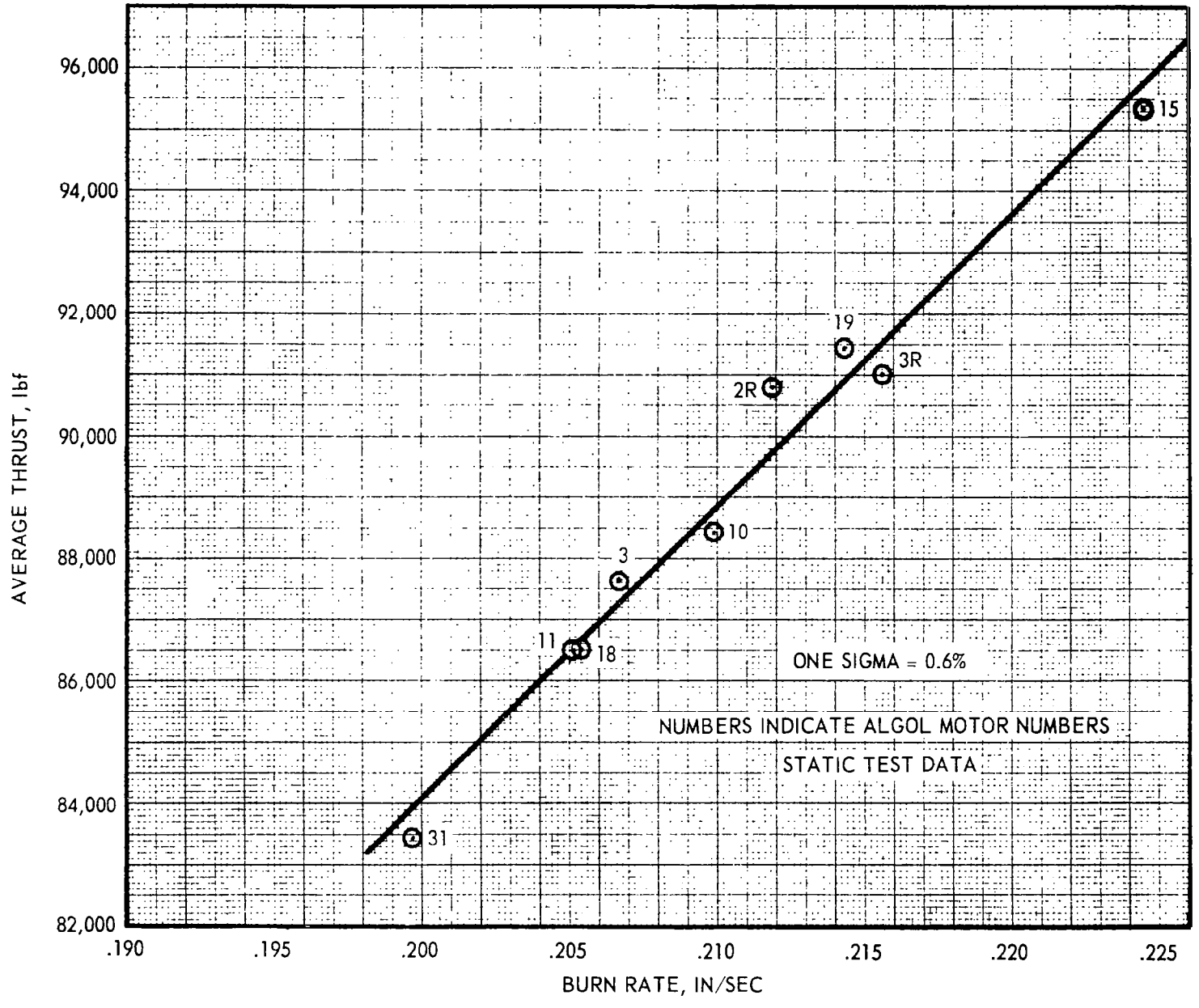

FIGURE 12 ALGOL IIA AVERAGE THRUST VERSUS BURNING RATE – INTEGRAL RATIO METHOD

vacuum thrust. Being based upon thrust, not pressure, the method avoids the port flow effects, and the neglected effect of change in the nozzle area ratio was small; but the assumption that the inerts weight flow rate varies with thrust might result in a significant error that could be avoided.

An equation was derived (Appendix B, Eq. 9) to permit calculation of the propellant flow rate according to chamber pressure, throat area, characteristic velocities of the propellant and inerts gases, and an independently estimated inerts flow rate.

The development of nominal data for more accurate predictions of consumable weight remaining provided a basis for development of an equivalent method for evaluating the consumable weight remaining in Scout flight motors. A corollary to the equation for propellant flow rate was derived for calculating the consumable weight remaining according to flight telemetry data on motor head-cap pressure versus time (Appendix C). This equation for flight data evaluation by LTV was designed to permit inputs of the basic nominal motor data as they were developed by the motor engineers for predicting motor weight remaining.

The effect of the change in method for calculating the consumable weight remaining was examined. Weight remaining versus time was calculated three ways: 1) by the new equation, 2) based upon head-cap pressure, and 3) based upon vacuum thrust. New nominals for pressure and thrust were used in each of the three calculations, so the difference in results would be due to the differences in equations only. The increased amount of weight remaining, calculated by the new equation over the amounts calculated by the pressure and thrust equations, is shown in the upper set of curves in Figures 13 and 14 . The dashed line shows the increase in weight remaining by the new equation over the weight remaining by the pressure equation. The solid line shows the increase in weight remaining by the new equation over the weight remaining by the thrust equation.

Similarly, the differences in velocity increments (ideal) that result from the new weight remaining equation were investigated. The greater weight remaining during burning calculated by the new equation resulted in a lower velocity increment than calculated by either the pressure or thrust equation. The resulting curves are at the bottom of Figures 13 and 14 .

Another effect of the new weight remaining equation is a slightly greater value of "apparent" impulse for flight motors when calculated on the basis of longitudinal acceleration.

3.3 THRUST

The new nominal thrust versus time data for the Scout motors are based upon static test data, with the exception of the X-258 fourth stage. The data from this motor reflect a difference between flight behavior and AEDC test vehavior. The static and flight pressure versus time trace shapes and pressure integrals for the first three stages are not significantly different. Chamber pressure of the fourth stage is not usually measured in flight. Nominal vacuum thrust for the first stage was computed from the sea level

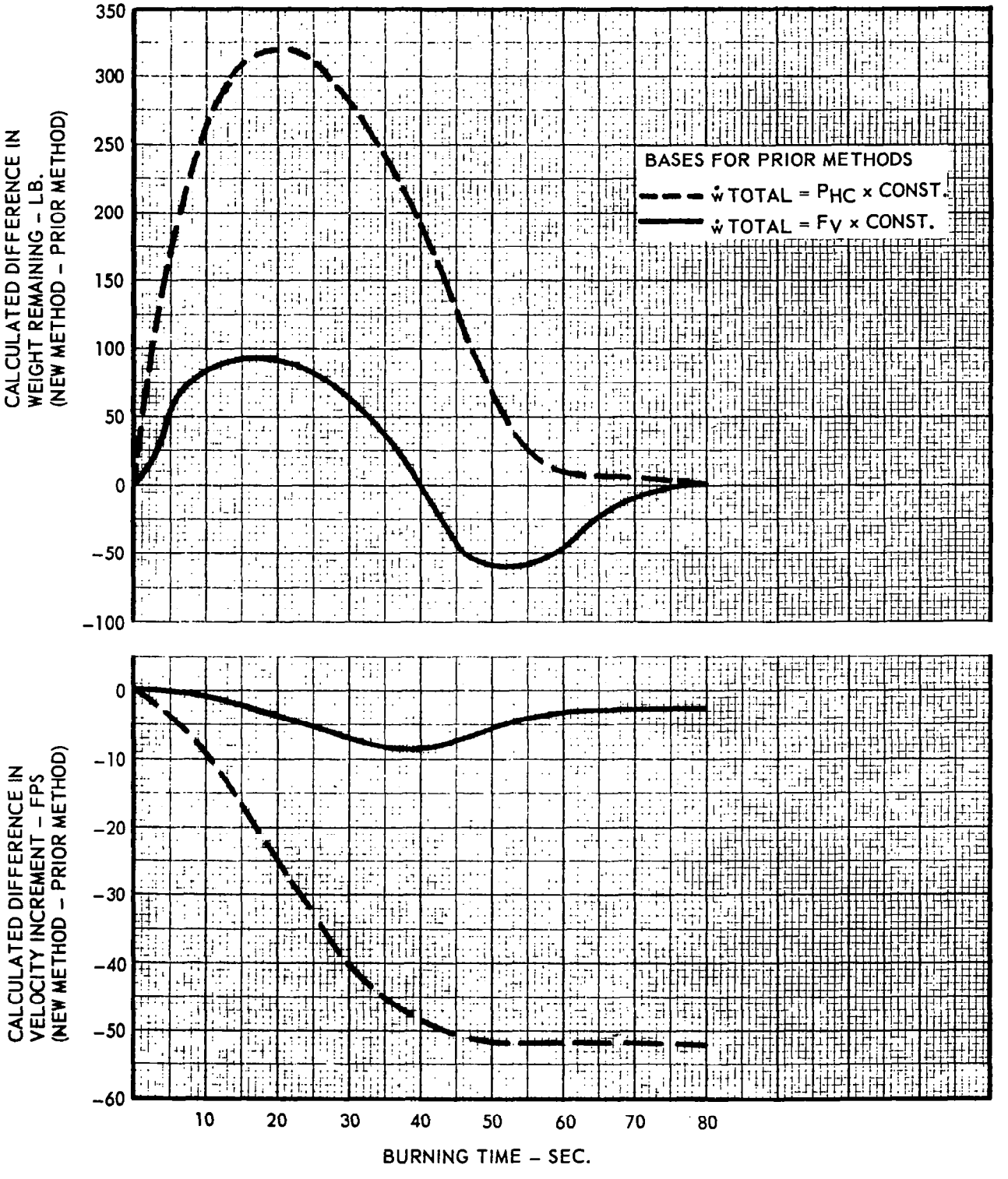

FIGURE 13 ALGOL II B EFFECT OF METHOD FOR CALCULATING WEIGHT REMAINING ON THE VELOCITY INCREMENT

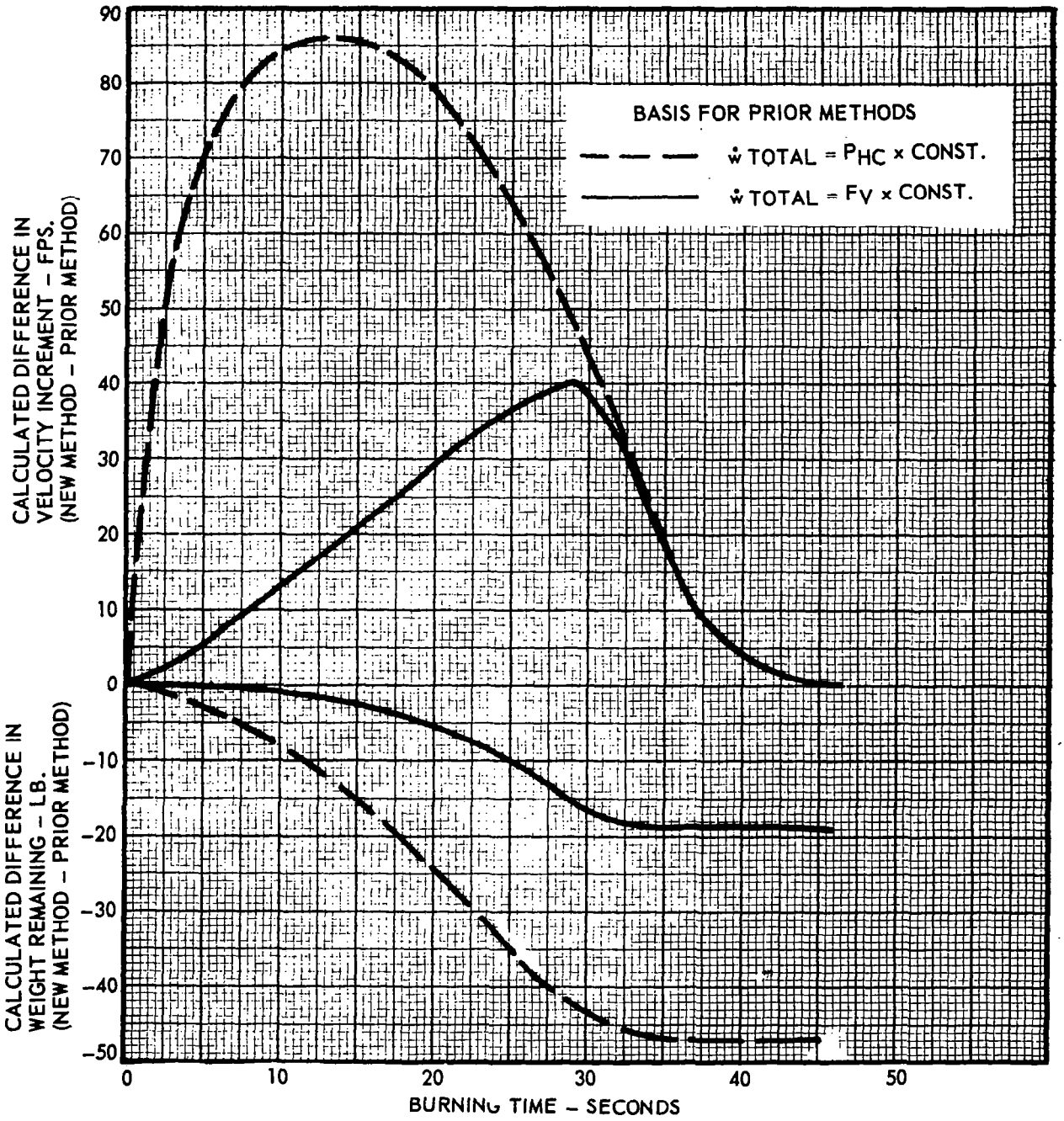

FIGURE 14 CASTOR I EFFECT OF METHOD FOR CALCULATING WEIGHT REMAINING ON THE VELOCITY INCREMENT

thrust, employing the theoretical effects of ambient pressure. The nominal vacuum thrusts for the second and third stages are based upon altitude test chamber data at AEDC because this static test thrust data is the most accurate data available. For the same reason, the X258 propellant specific impulse rating is based upon AEDC tests. However, during flight, a performance degradation of the X258 occurs. Accepting the AEDC tests of propellant specific impulse, this degradation is possibly caused by a propellant sliver remaining at motor burnout or incomplete combustion and discharge of aluminum particles.

The vacuum thrust versus time of a Scout propulsion motor may be inferred from the telemetry data on instantaneous acceleration, drag and vehicle weight remaining, or from the instantaneous head-cap pressure. The first method has been standard practice and is based upon the relationship:

$$F = \Sigma D + \left[\alpha_L \cdot W_R\right] + P_a A_e \qquad (1)$$

The second method is based upon the following relationships:

$$F_V = P \quad (F_V/P)_{NOM} \left[\int_o^{t_T} Pdt \;_{PRED} \Big/ \int_o^{t_T} Pdt \;_{MEAS} \right] \qquad (2)$$

Where:

NOM = Nominal

PRED = Predicted

MEAS = Measured.

This latter method is preferred as the more accurate method of representing flight thrust. The reasons for this preference are:

1. The curve shape of the telemetry pressure trace has been found to be more realistic than the calculated thrust trace shape prepared from accelerometer data. The accelerometer traces and calculated thrust traces exhibit unexplained wiggles. See Figure 15 .

2. Flight total pressure integral values have generally been found to be as accurate as flight total impulse values derived from accelerometer data.

However, neither type of telemetry data is a sufficiently accurate source of data for the calculation of the impulse of a given motor. The accuracy and utility of telemetry data are further discussed in Section 7.0.

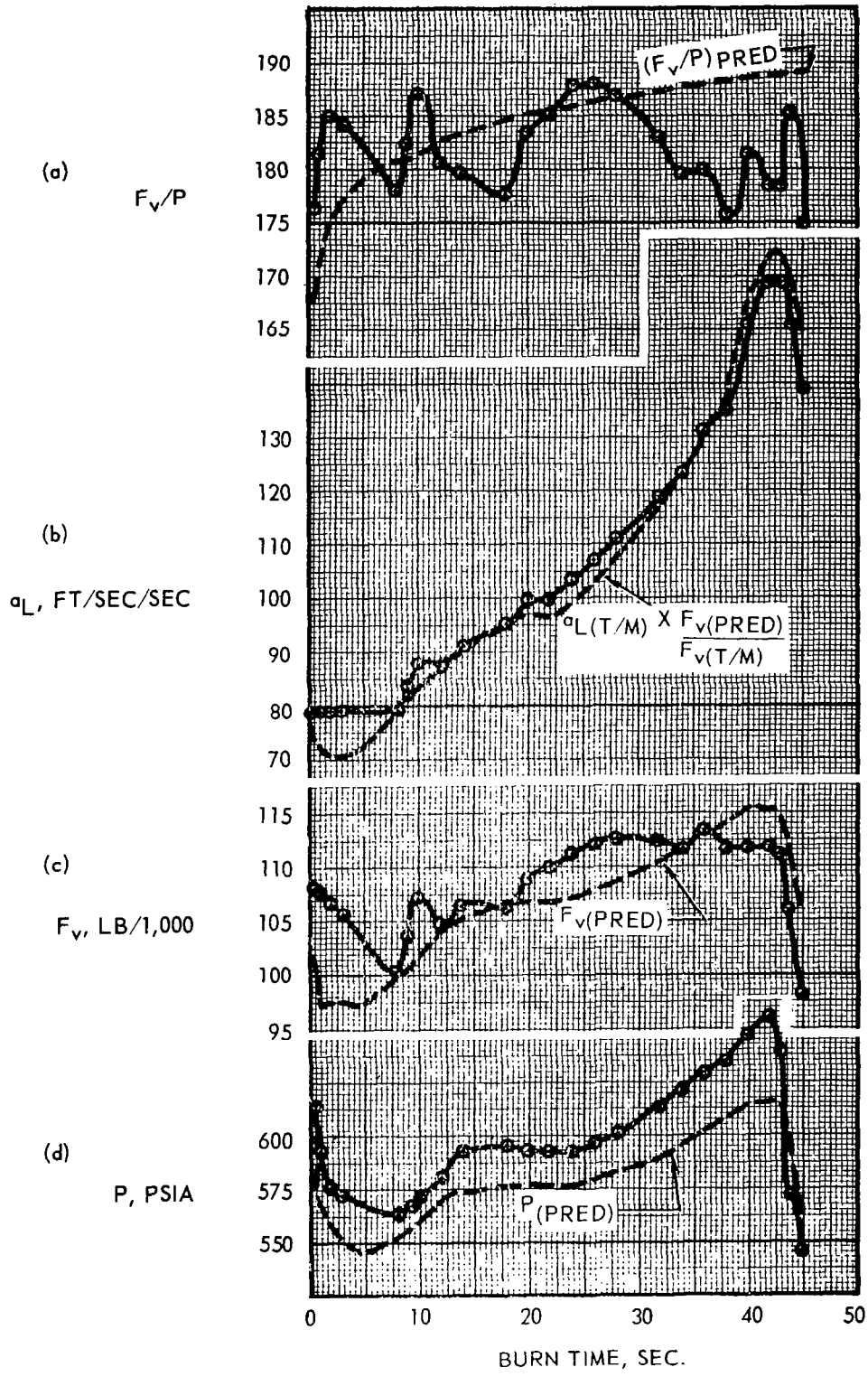

FIGURE 15 COMPARISON OF PRESSURE AND ACCELERATION TELEMETRY DATA WITH PREDICTED PERFORMANCE

4.0 MOTOR BURN RATE CORRELATIONS

4.1 FIRST STAGE

4.1.1 INTRODUCTION

The performance of an Algol IIB motor is predicted by firing a series of twelve 10KS-2500 test motors, one motor representing each of the twelve batches of propellant in the Algol motor, to determine the propellant batch burn rates. These motors are fired at 77°F with a standard throat size to produce approximately 550 psia chamber pressure. These batch rates are adjusted to the standard condition of 550 psia and 77°F and are then averaged. This average batch rate is translated to an "apparent" full scale burning rate at 550 psia and 77°F by the use of a correlation. The "apparent" full scale burning rate is then translated to a "true" full scale rate, at actual operating pressure, by the use of a second correlation. The "true" full scale rate is converted to a predicted web time for the new motor.

4.1.2 DATA PREPARATION

4.1.2.1 Calculation of the 10KS-2500 Batch Test Burning Rate

The batch test burn rate is calculated from the following equations:

$$r = l_w/t_b \qquad (1)$$

$$t_b = fPI \int_o^{tT} Pdt/\bar{P}b \qquad (2)$$

$$\bar{P}_b = \int_o^{t_b} Pdt/t_w \qquad (3)$$

The time interval for the web pressure integral and web time is defined in the Nomenclature. Any small variation in the selection of the web time, t_w, for the determination of the web average pressure, $\bar{P}_b$, has a negligible effect on the calculated value of the average pressure because the web pressure integral is determined to the same time point.

4.1.2.2 Calculation of the Algol Motor Burning Rate

The "effective" burning time, t_b, for the Algol motor is defined as that time at which 85 percent of the total pressure integral has been accumulated. The 85 percentage level of the total pressure integral was selected as the effective web time for the Algol II motor because the average ratio of the web pressure integral determined by the tangent method to the total pressure integral is approximately 85 percent. The effective burning time includes a nominal ignition interval of 150 milliseconds. If the ignition interval exceeds 150 milliseconds, as a result of a delayed ignition, a correction should be applied. The interval is defined as the time interval from fire switch to 565 psia chamber pressure.

It is not possible to define the start of web burn time for flight motors with any greater precision because the flight telemetry system provides an Algol pressure value only every 200 milliseconds. Furthermore, longitudinal acceleration data are not lucid in showing ignition and liftoff for a majority of the flights during this period.

The burning rate of an Algol motor is calculated from:

$$r = l_w/t_b \qquad (4)$$

4.1.2.3 Conversion of Burning Rate Data to Standard Conditions

To convert the batch test or Algol motor burning rates to the standard condition of 550 psia and 77°F, the temperature sensitivity coefficient, π_k, and the pressure exponent, n, are used.

$$\pi_k = \left|(\ln r_1 - \ln r_2)/(T-77)\right| \qquad (5)$$

where r_1 and r_2 are the burning rates of a motor at temperatures T and 77. The data are for a constant K_n condition.

π_k = .0011 per degree F for Algol IIB propellant

and,

$$n = \left|(\ln r_2 - \ln r_3)/(\ln P_2 - \ln 550)\right| \qquad (6)$$

where r_2 and r_3 are the calculated burning rates of a propellant under pressure conditions P_2 and 550 for a constant propellant temperature.

n = 0.22 for Algol IIB propellant

In use,

$$r_2 = r_1 (e)^{\pi_k (77 - T)} \qquad (7)$$

$$P_2 = P_1 (e)^{\pi_k (77 - T)} \qquad (8)$$

and

$$r_3 = r_2 (550/P_2)^n \qquad (9)$$

where

r_1 = the measured burning rate at T and P_1, in/sec

r_2 = the burning rate at 77° and P_2, in/sec

r_3 = the burning rate at 77° and 550 psia, in/sec

P_1 = the measured pressure at T, psia

P_2 = the pressure at 77°F and r2, psia

T = the measured temperature of the propellant, °F

4.1.3 CORRELATION METHOD

4.1.3.1 Integral Ratio Method

The burning rate data for statically tested and flight Algol II motors are correlated with batch test burning rate data at the standard condition of 550 psia and 77°F in Figure 16 . Two correlation lines are shown for the two oxidizer blend ratio systems used in the motors. The flight and static motors are both distributed over the range of the data and both types of motors are scattered approximately equally on both sides of the respective lines. The nominal burning rate of Algol II propellant in full scale motors is 0.211 in/sec at 550 psia and 77°F.

These Algol motor burning rates are "apparent" burning rates and not actual motor burning rates because the full scale motors do not all operate at 550 psia. The full scale Algol motors, in accord with theory, exhibit a constant P/r ratio, hence the line of data with a slope of 1.0 on a log-log plot of burning rate versus operating pressure (Figure 17). This line intersects 550 psia at 0.211 in/sec burning rate. The propellant burning rate versus pressure relationship follows a constant temperature line with a slope of 0.22 (the pressure exponent for the propellant), also intersecting the 550 spia line at 0.211 in/sec. This relationship is used for Algol motor prediction.

The standard deviation for apparent motor burning rates predicted from the correlation (Figure 16) is 0.0024 in/sec which is 1.13 percent of the average. The standard deviation for actual motor burn rate prediction error is 1.4%.

4.1.3.2 Alternate Effective Burning Time Methods

Two alternate effective burning time methods involving the same concept were investigated for the Algol motor, and they produced correlation results almost identical to the method described in Paragraph 4.1.3.1 above. They are:

1. t_{b1} is the time obtained by dividing 85% of the total integral by the web average pressure,

2. and t_{b2} is the time interval between the points of accumulation of 10 percent and 80 percent of the total pressure integral.

4.1.3.3 Liquid Strand Burning Rate versus Algol Motor Burning Rates

The liquid strand burning rate is obtained by burning a strand of uncured propellant at constant temperature and pressure. The average liquid strand burning rates for Algol motors were "effective" time correlated with the full scale burning rates determined by the method described in Paragraph 4.1.3.1. This correlation is shown in Figure 18 . The standard deviation for Algol motor burning rates predicted from this correlation is 0.0031 in/sec which is 1.47 percent of the average. The slope of this correlation line is 1.681 as compared with a slope of 0.733 for the batch test versus the same

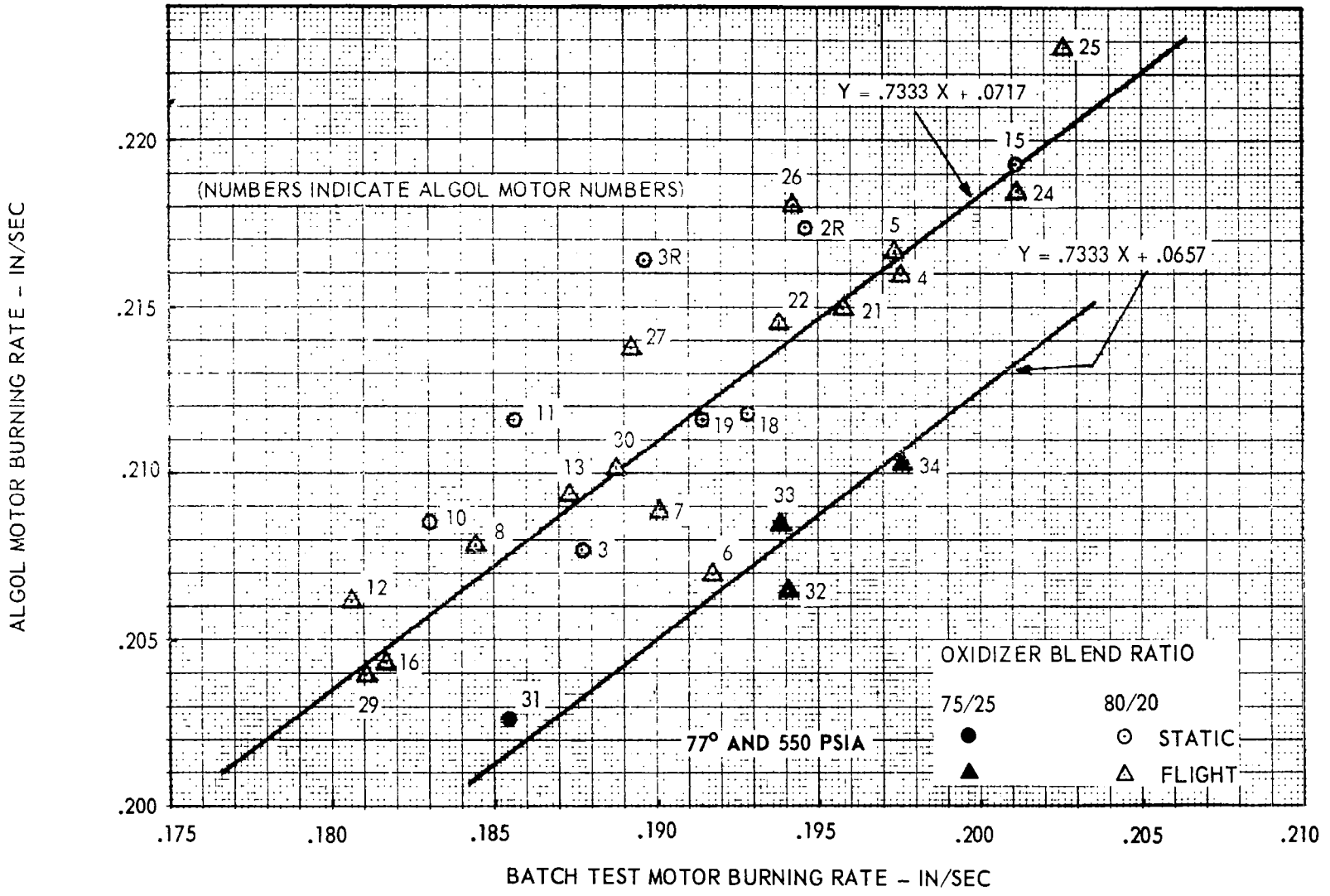

FIGURE 16 ALGOL II BURNING RATE CORRELATION EFFECTIVE TIME METHOD

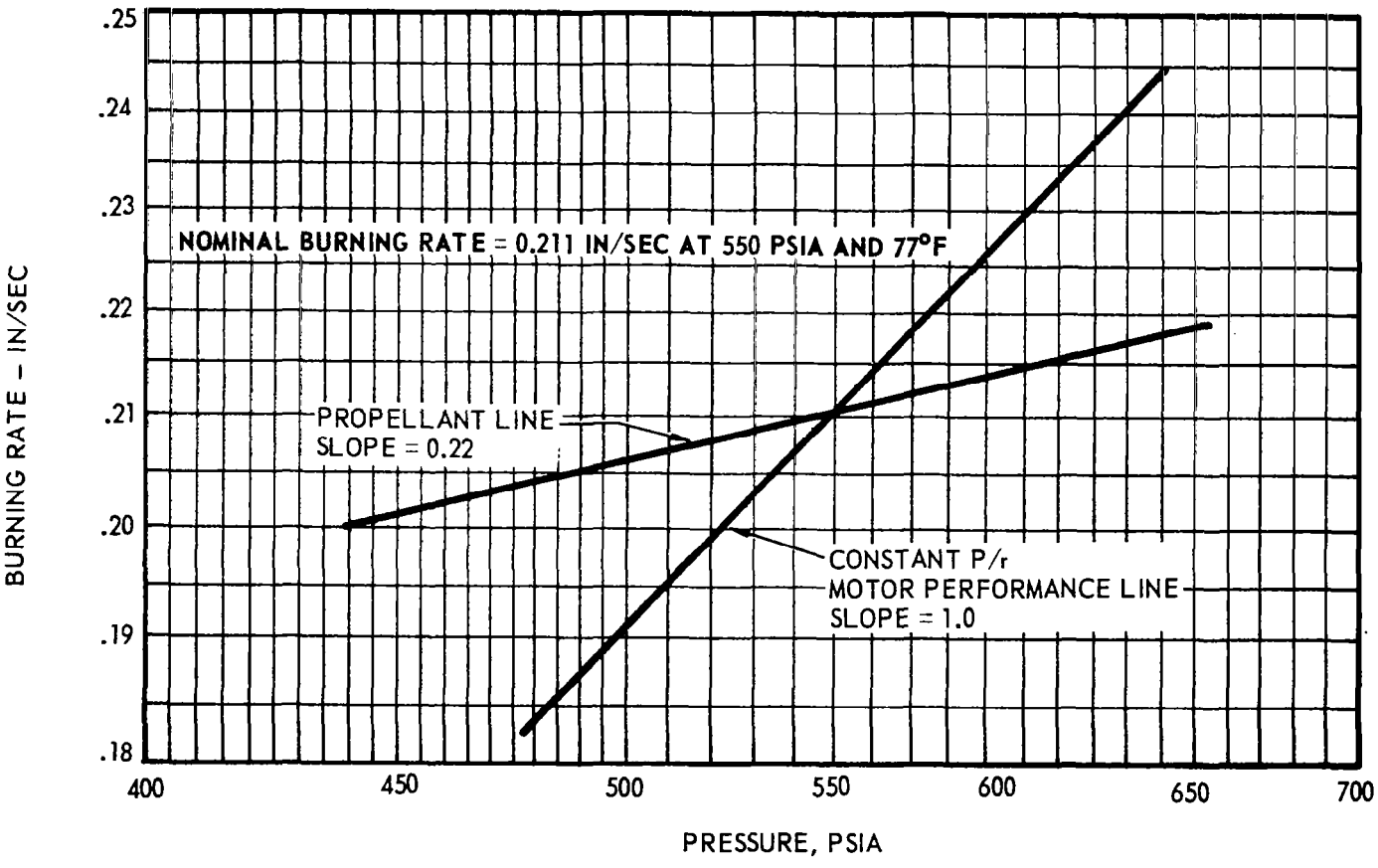

FIGURE 17 ALGOL IIB BURN RATE VS PRESSURE CORRELATIONS

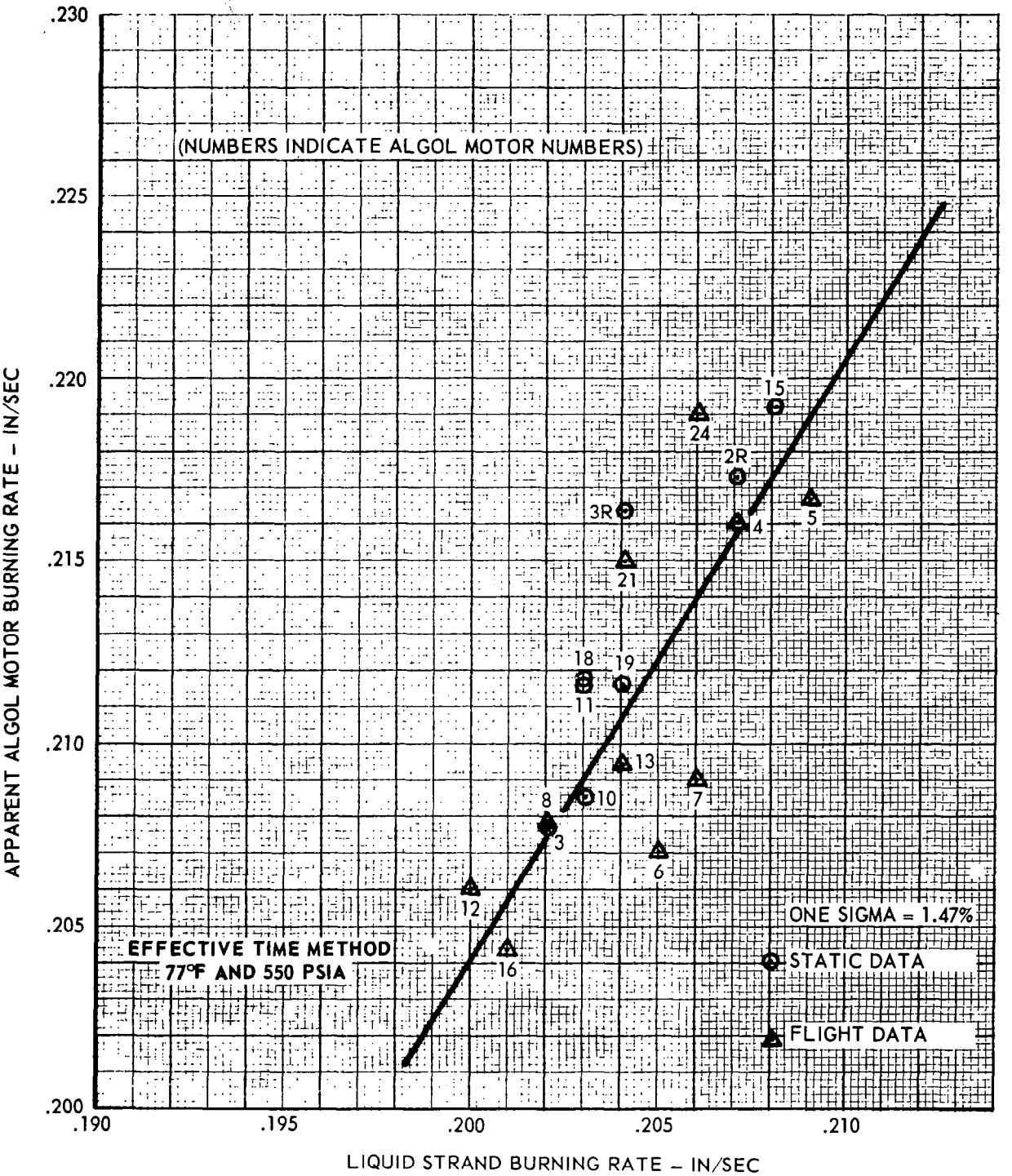

FIGURE 18 ALGOL IIA AND B BURNING RATE VS LIQUID STRAND BURN RATE

full scale data correlation. Thus, the liquid strand burning rate data cover a range approximately one-half that of either the batch test or full scale burning rate data and is a less satisfactory parameter for motor prediction.

4.2 SECOND STAGE

The correlation of Castor I burning rates between the batch check (TX-3) motors and the Castor motor provides the basis for predicting burn time and thrust. Several correlation techniques were tested, and the best of these techniques was selected for use in predicting the performance of the Castor motor.

The data available for constructing the burn rate correlation consisted of eighteen static test and eleven flight motors. In constructing the correlation it was necessary to develop a precise technique for estimating the propellant burning rate of both the test motor and the Castor motor.

The methods discussed in Paragraph 3.1 have been applied to the Castor by determining the web burn time by the tangent method, and adjusting the thickness burned based on the geometric design of the motor and the percentage of the total pressure integral accumulated to web time. Thus, the propellant thickness burned during the web burn time of a Castor motor was calculated as follows:

$$l_{w_{eff}} = K_3 \frac{\int_o^{t_w} P\,dt}{\int_o^{t_T} P\,dt} \qquad (1)$$

where: K_3 = a characteristic thickness based on the motor geometry

(K_3 = design web thickness x $\frac{\text{total fuel volume}}{\text{web fuel volume}}$

= 7.685)

The average burning rate of the Castor motor was determined by dividing the propellant thickness burned by the web burn time determined for the motor as follows:

$$r = \frac{l_{w_{eff}}}{t_w} \qquad (2)$$

The above procedure is used to derive burning rates for the static test Castor motors. The equivalent procedure of defining web burn time, as occurring when a given percentage of the total pressure integral is accumulated, produces consistent time values. The burning rate is determined by dividing this time into a constant thickness burned. The web burn time of the flight motors was defined as beginning 0.060 second after the first indication of acceleration on the flight records and ending when 87.19 percent of the total pressure integral had been accumulated. The 0.060 second delay is an estimate of the time required to attain 50% of the maximum chamber pressure on ignition, and was necessitated because of the poor definition of the transient conditions available from flight records. The accumulation of 87.19 percent of the total

pressure integral was selected to define the end of web burn time since this represents the nominal pressure integral ratio observed in the static test motors and therefore results in no time bias between the two time measurement systems. The average burning rate of the flight motors was then determined by dividing the thickness burned, a constant of 6.701 inches, by the web burn time determined for the motor. The same basic procedure, described in Section 6.0 of this report, was used to determine the burning rate of the burn rate test motors.

Since the Castor static test data were expected to be superior to the flight data, the initial correlation was constructed for only the static test Castor motors. The technique used in the initial correlation was to determine the ratio of the Castor burn rate to the batch test motor burn rate (scale factor) when the batch test burn rate was evaluated at the temperature and K_n of the Castor motor. This technique produced a correlation (Figure 19) having a standard deviation of two percent. On examination, there appears to be a shift in the burn rate correlation between the first series of static test motors (denoted by circles in Figure 19) and the later motors (denoted by squares in Figure 19).

Review of the ballistic and physical property control charts for TPH8038 propellant used in the Castor motor revealed that the oxidizer grind ratio (the percent of the total oxidizer that was ground) had been varied from 20% to 45% in order to maintain the desired propellant burning rate. There was an apparent shift in the burn rate correlation coinciding with changes in the oxidizer grind ratio.

The batch test motors were tested in two basic firing patterns. The first series of Castor motors (20% grind ratio) had eight batch test motors cast from each propellant mix and tested in a pattern of temperature and K_n conditions to obtain measures of the propellant burning rate, burning rate exponent, and temperature sensitivity. The remaining Castor motors (30 to 40% grind ratio) normally had two batch test motors tested from each propellant mix at a single point (K_n = 200, T_f = 70°F). In these later motors special propellant mixes were made and tested to standardize new lots of raw materials. Batch test motors from these mixes were fired in the pattern of multiple test conditions to obtain a measure of the propellant ballistic properties. From the batch test motors associated with propellant standardization mixes, a history of the effect of changes in the oxidizer grind ratio on the ballistic properties of the propellant was available. From the standardization mix data it was apparent that the burning rate exponent was significantly lower for high oxidizer grind ratios, as shown in Figure 20. Using the curve of Figure 20 except where measures were obtained on an individual mix basis, a correlation was constructed (Figure 21) showing the dependence of the scale factor on the burning rate exponent when the batch test motor burn rate was evaluated at the K_n (207) of the Castor motor.

As a result, a technique of correlating the full scale and batch check burning rates at the chamber pressure level of the related full scale motor was investigated. This technique required the use of a burning rate exponent to calculate batch test data for the pressure level of the Castor motor. For mixes involving only one test condition, the burning rate

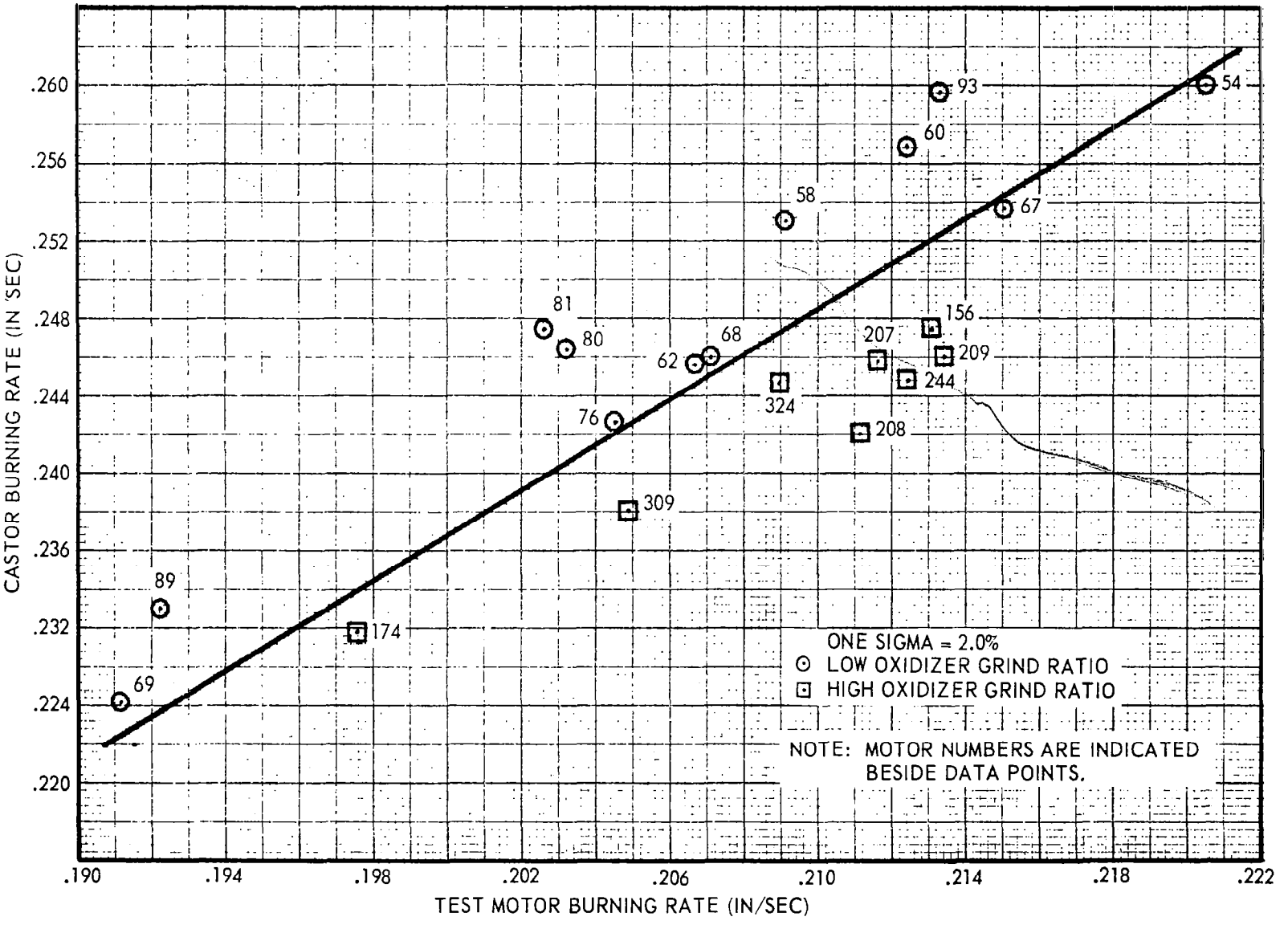

FIGURE 19 CASTOR I BURNING RATE CORRELATION – TEST MOTOR K_n = CASTOR K_n

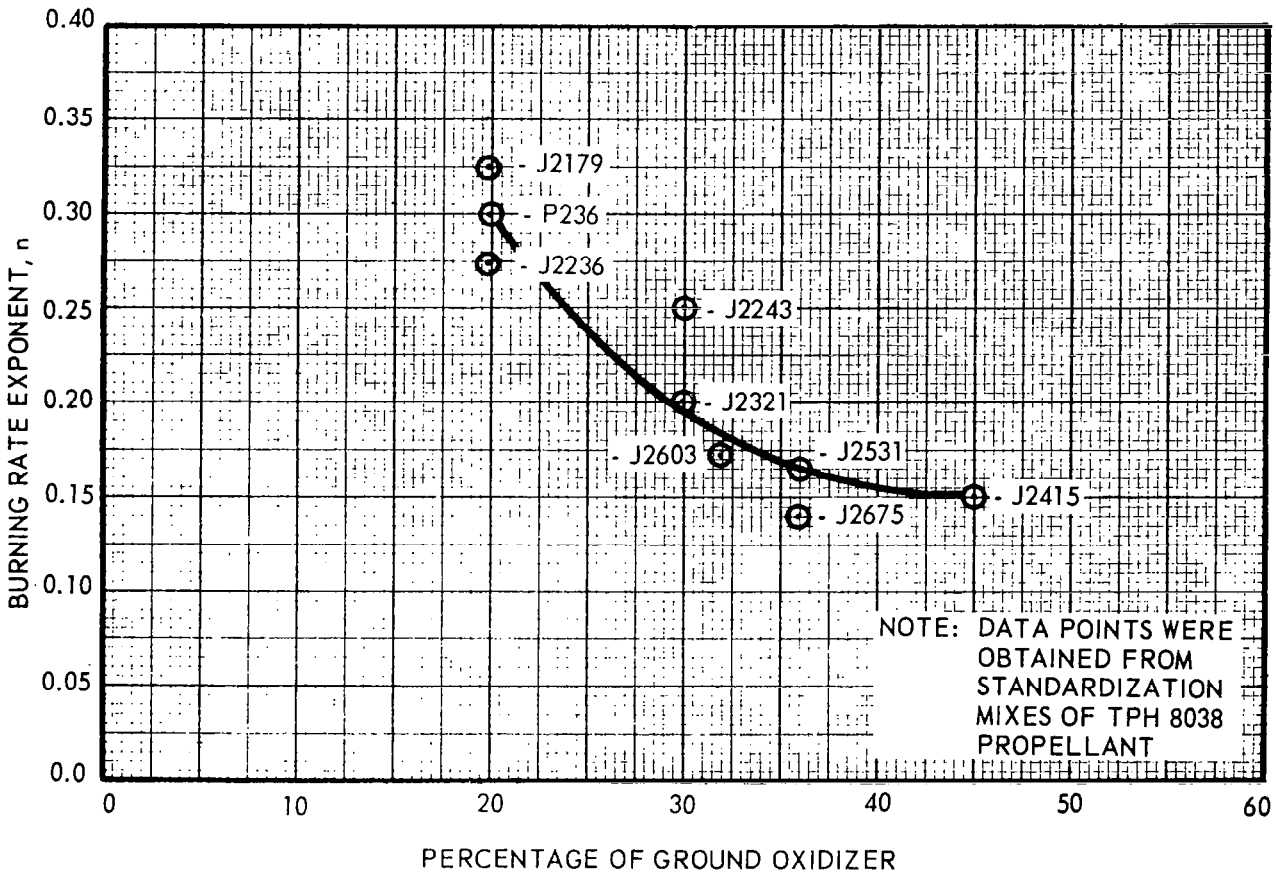

FIGURE 20 CASTOR I BURNING RATE EXPONENT VERSUS OXIDIZER GRIND RATIO

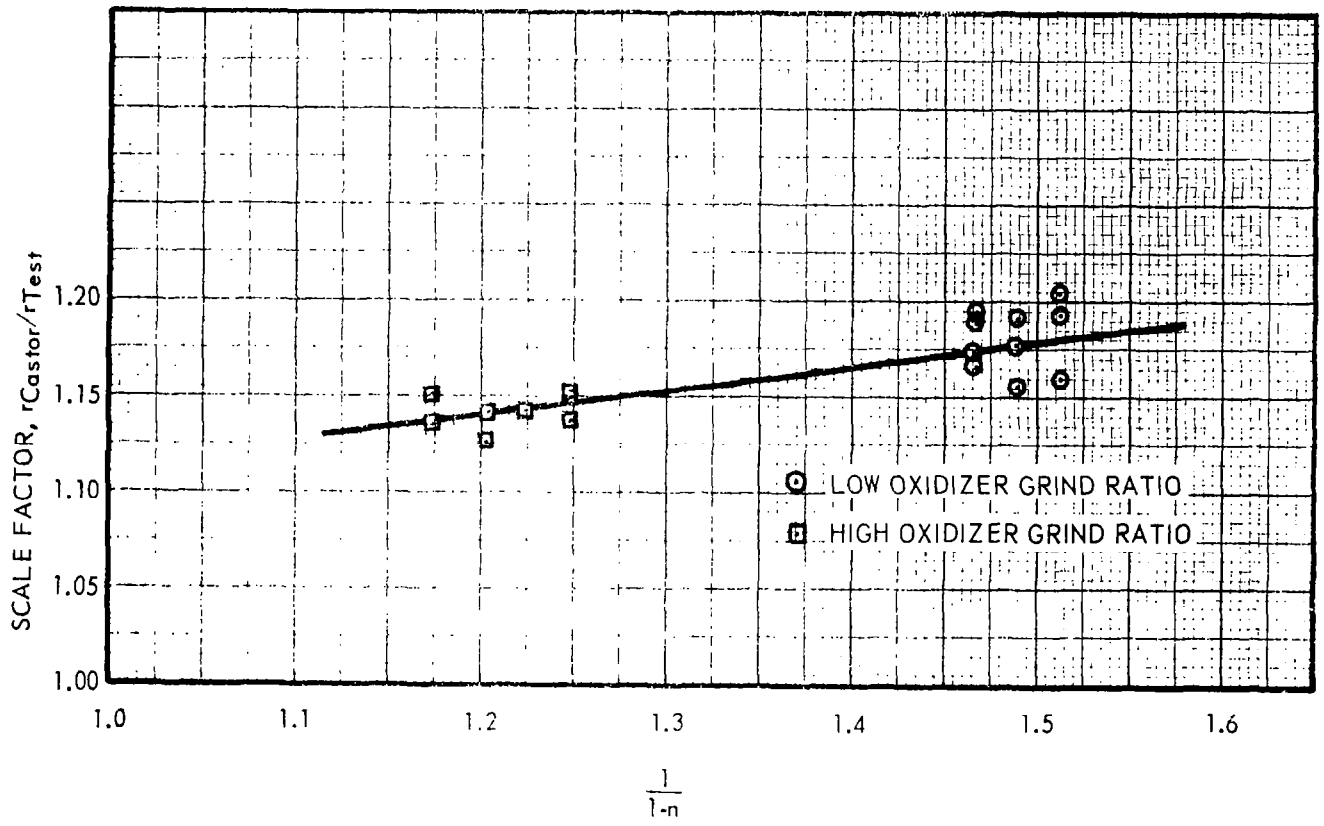

FIGURE 21 EFFECT OF BURNING RATE EXPONENT ON SCALE FACTOR – TEST MOTOR K_n = 207

exponent was estimated from related standardization mix data (Figure 20). The correlation obtained by this technique (Figure 22) was much improved, having a standard deviation of 0.9% with no apparent stratification of the data. Although the correlation obtained by the equal pressure approach was more precise then by the equal K_n approach, predictions of motor performance could not be obtained directly from this correlation, nor could prediction accuracy be inferred since the chamber pressure of the Castor motor is not known prior to the test.

The last burning rate correlation constructed is a practical version of the equal pressure approach and can readily be used to predict the performance of the Castor motor. This correlation, shown in Figure 23 , was constructed by evaluating the test motor burn rate at a K_n condition (K_n = 231) where normally the pressure level of the test motor is equal to the pressure level of the Castor motor. When the test motors are evaluated at the higher K_n condition, the scale factor need no longer be corrected according to the burning rate exponent, as shown in Figure 24. At this K_n condition any percent change in burn rate is the same in both the Castor motor and the test motor, resulting in a constant scale factor. Using this correlation technique all required test motor data is available prior to the Castor test. Also, a conservative estimate of the prediction error can be determined directly from the scatter about the correlation line (the scatter includes Castor test measurement error which is not encountered in predictions). The correlation shown in Figure 23 includes eleven flight and eighteen static test motors, and has a standard deviation of 0.98%. The same correlation fits both flight and static test Castor data as shown in Figure 23, hence there is no effect on the burning rate of the Castor motor due to the flight environment.

4.3 THIRD AND FOURTH STAGES

A burning rate correlation is not directly used in predicting the X259 and X258 flight performance. There is, however, a correlation between small scale acceptance tests used in evaluating a new casting powder lot and the large scale motor acceptance of the powder lot. This correlation is made for the X259 to determine the nozzle throat size to be used in the large scale test so that the chamber maximum pressure can be kept within the specified limits. The correlation is based on previous powder lot burn rates in small tests and burn rates in full scale tests. A graph of this correlation for the X259 is shown as Figure 25. The high burning rate type casting powder lots, ZI-193 and ZI-207, are shown on Figure 25 separated from the other lots. The motor burn rates for these lots reflect the use of the larger nozzle throat. Current motors will utilize either of two lots, ZI-207 (high rate powder) and ZI-246 (low rate powder). The full scale evaluation is used as the basis for predicting flight performance.

The X258 motor has used only one powder lot since its development, therefore, no burn rate correlation has been conducted.

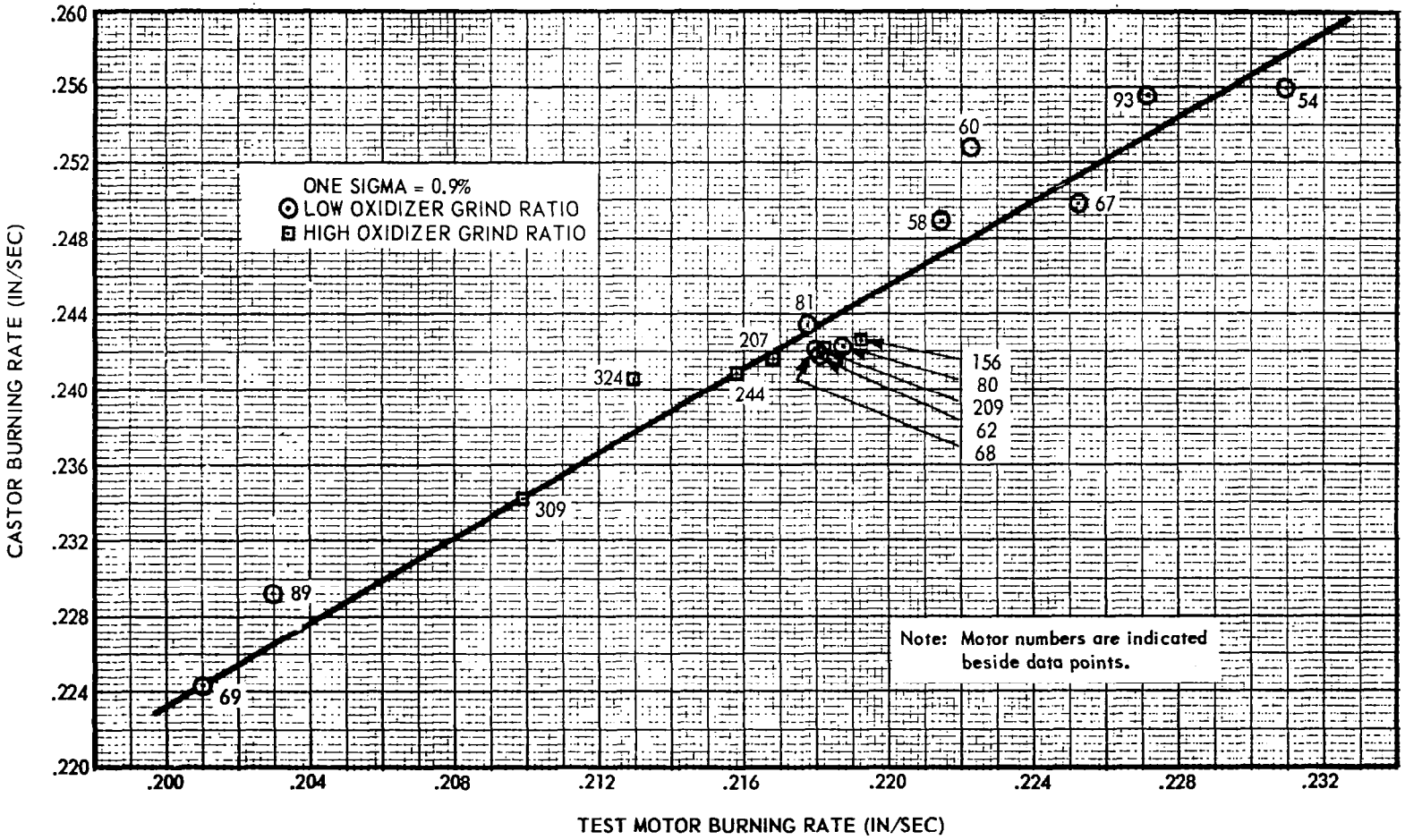

FIGURE 22 CASTOR I BURNING RATE CORRELATION – TEST MOTOR PRESSURE = CASTOR PRESSURE

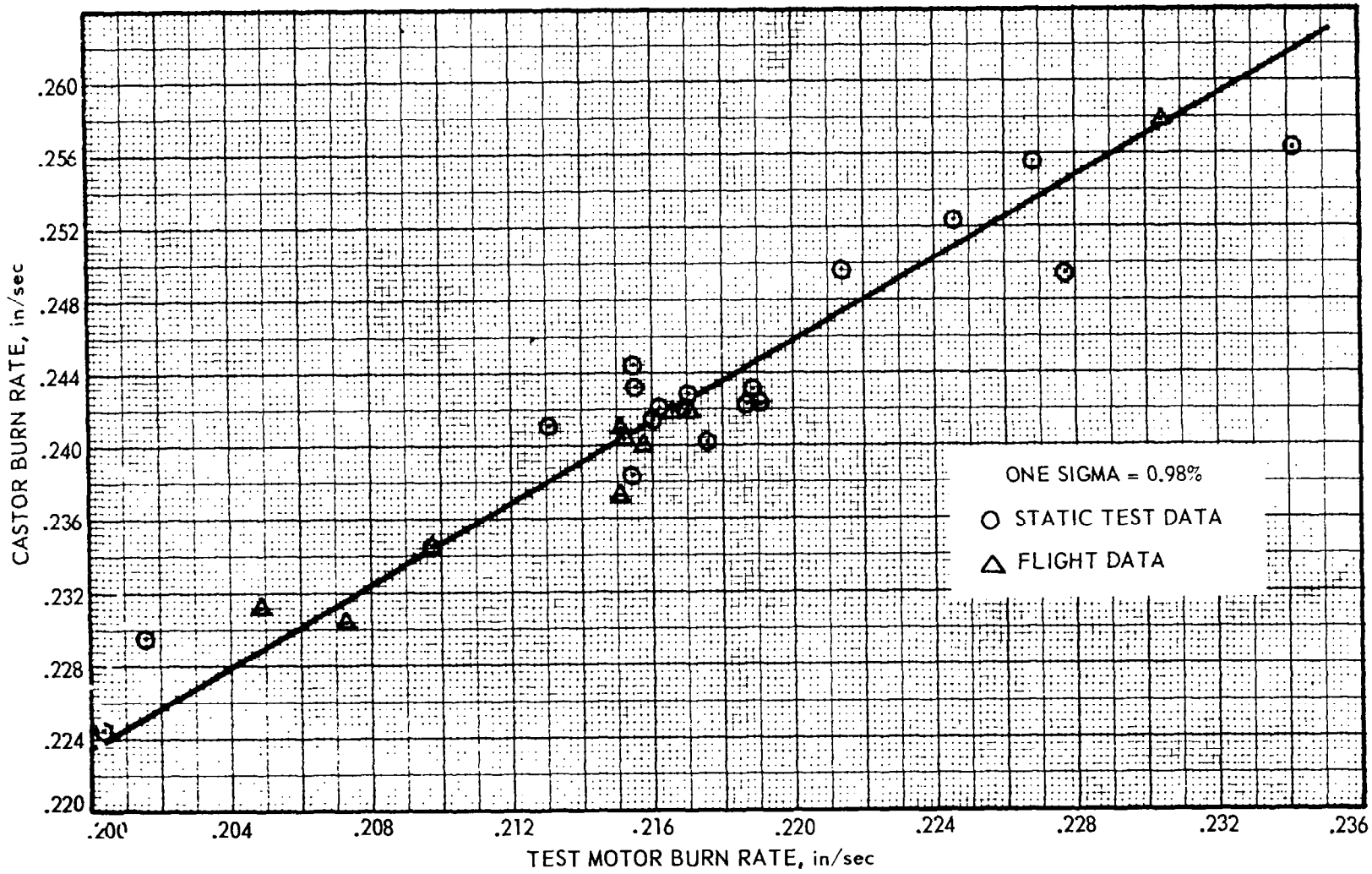

FIGURE 23 CASTOR I BURNING RATE CORRELATION – TEST MOTOR K_n = 231

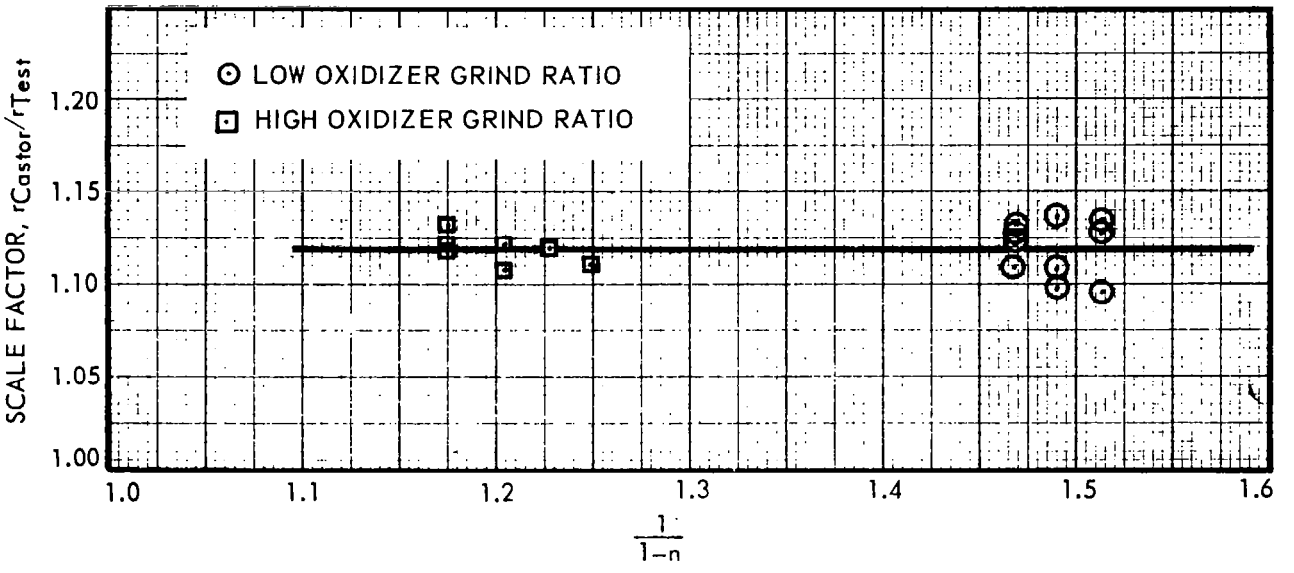

FIGURE 24 EFFECT OF BURNING RATE EXPONENT ON SCALE FACTOR – TEST MOTOR K_n = 231

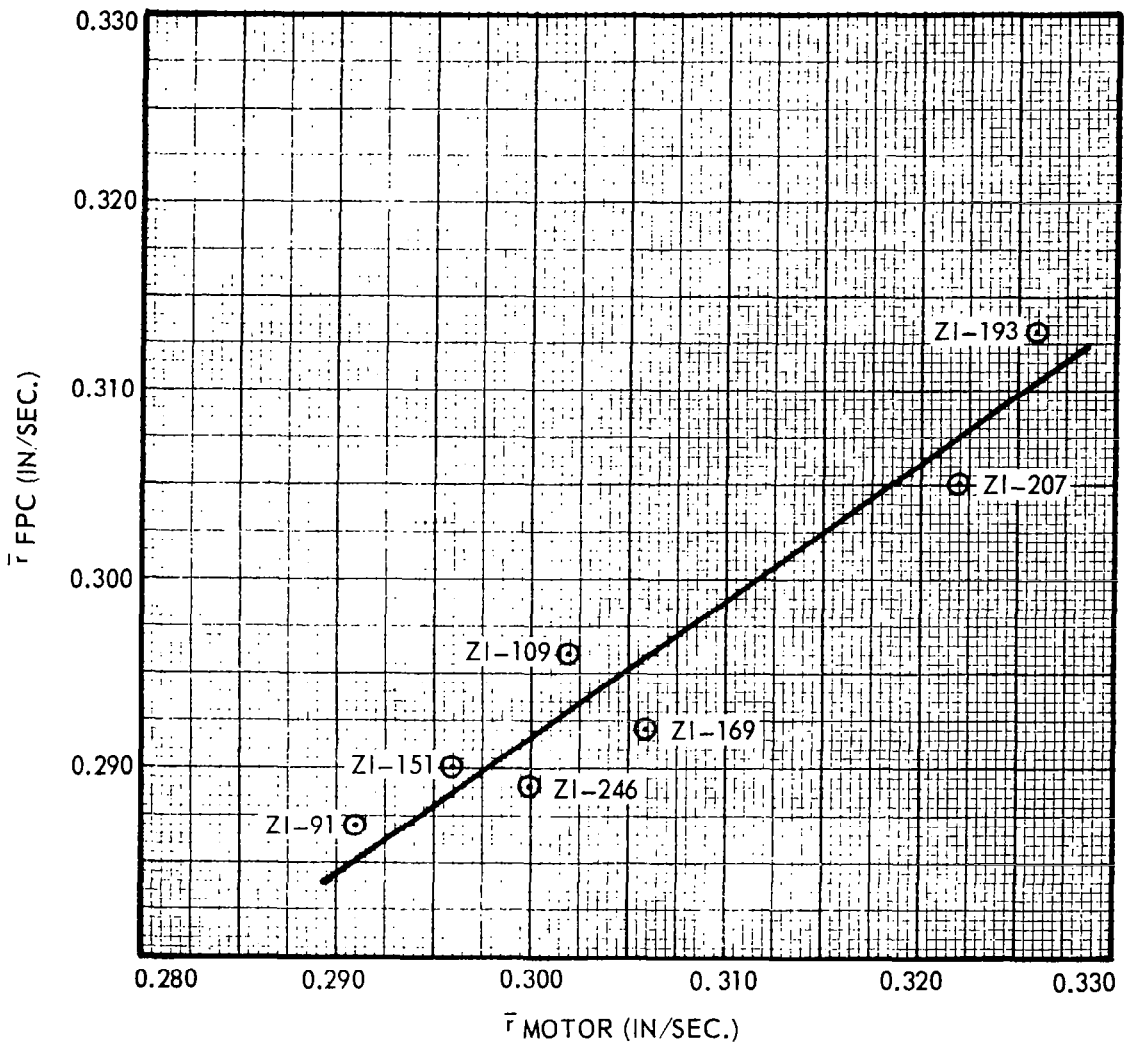

FIGURE 25 SMALL SCALE BURNING RATE VERSUS X259 MOTOR BURNING RATE

5.0 NOMINAL MOTOR CHARACTERISTICS

5.1 FIRST STAGE

A tabulation of nominal Algol IIB characteristics is provided in Table 3.

5.1.1 HEAD-CAP PRESSURE

The Algol IIA static test pressure data were reduced to a common temperature condition (77°F) and the pressure traces were averaged. Arithmetical averaging of pressure was used at intervals during the web burning period, and graphical techniques were employed during the tail-off portion of the pressure traces. The flight pressure data were averaged in the same manner, and the resulting curve shape was almost identical to the average static pressure trace. The nominal pressure data presented in Table 4 and Figures 26 and 27 represents both static and flight motors. The nominal pressure integral, 29,450 psia-sec, is the average integral of the static test firings.

5.1.2 SEA LEVEL THRUST

Sea level thrust-to-pressure ratios (Table 5) were computed for each static test firing at frequent time intervals. These ratios, taken at the same times for each firing, were averaged to produce a nominal thrust to pressure ratio versus time. These values were then multiplied by the corresponding pressure values to obtain the nominal sea level thrust. The nominal total impulse at sea level, 4,731,650 psia-sec, is the average impulse of the static test firings.

5.1.3 VACUUM THRUST

The nominal vacuum thrust was computed from the sea level thrust using the following equations:

$$C_F vac = [C^\circ_F vac - \epsilon(P_e/P_c)]\,\lambda + \epsilon(P_e/P_c) \qquad (1)$$

$$C_{Fact} = C_{F_{vac}} - \epsilon(P_a/P_c) \qquad (2)$$

$$F_{vac} = F_{act}\,(C_{F_{vac}}/C_{Fact}) \qquad (3)$$

The values obtained are presented in Table 4 and Figure 27. The nominal vacuum thrust integral, 5,472,350 lbf-sec, approximates the average of the integrals acquired from flight data.

Nominal thrust to pressure ratios for both vacuum and sea level are tabulated in Table 5 .

TABLE 3
ALGOL IIB
NOMINAL DATA
(PERFORMANCE AT 77°F AND VACUUM)

Propellant Weight	21,139	lb.
Inert Weight Loss	216	lb.
Consumable Weight	21,355	lb.
Total Motor Weight (less nozzle closure)	23,750	lb.
Burnout Weight	2,392	lb.
Nozzle Closure Weight	3	lb.
Head Cap Pressure Integral	29,450	psia-sec
Sea Level Impulse	4,731,650	lbf-sec
Sea Level Specific Impulse (Propellant)	223,835	lbf-sec/lbm
Vacuum Impulse	5,472,350	lbf-sec/lbm
Vacuum Specific Impulse (Propellant)	258,875	lbf-sec/lbm
Propellant Burn Rate	0.211	in/sec.
Web Burn Time	45.70	sec.
Total Burn Time	80.00	sec.
Average Vacuum Thrust (web)	101,783	lbf
Average Sea Level Thrust (web)	88,007	lbf
Maximum Vacuum Thrust	109,610	lbf
Maximum Sea Level Thrust	97,390	lbf
Average Pressure (web)	548	psia
Maximum Pressure	584	psia
Average Throat Area	113.76	in^2
Exit Area	5.666	in^2
Initial Expansion Ratio	7.36	
Propellant Density	0.0627	lb/in^3
Specific Heat Ratio	1.18	
Characteristic Velocity	5,082	ft/sec.
Temperature Sensitivity of Burn Rate	0.11	%/°F
Motor K_n	224.0	
Propellant Web Length	9.64	in.

TABLE 4

ALGOL II B

NOMINAL PERFORMANCE DATA AT 77°F

PRESSURE, THRUST, AND WEIGHT REMAINING

Point	Time (SEC)	Chamber Pressure (PSIA)	Sea Level Thrust (LBF)	Vacuum Thrust (LBF)	Consumable Weight (LB)	Jet Vane Drag (LBF)
1	0	0	0	0	21,355	0
2	0.2	610	89,670	101,695	21,317	1407
3	0.5	578	84,619	96,559	21,204	1278
4	0.7	560	82,040	94,010	21,131	1298
5	1.3	539	80,172	92,182	20,919	1220
6	2.7	524	80,130	92,270	20,436	1241
7	5.0	515	79,901	91,926	19,637	1244
8	9.0	523	82,748	94,721	18,201	1282
9	13.4	542	87,232	99,244	16,544	1343
10	19.0	546	89,033	101,115	14,358	1368
11	25.5	546	89,429	101,529	11,776	1374
12	34.0	559	92,588	104,745	8,319	1417
13	42.6	582	97,389	109,611	4,659	1483
14	45.7	584	97,228	109,343	3,310	1479
15	46.4	563	94,458	106,746	3,010	1444
16	47.5	532	88,505	100,780	2,556	1364
17	48.4	487	81,278	93,762	2,210	1269
18	51.4	321	49,859	62,493	1,296	846
19	54.8	177	24,663	33,024	663	447
20	56.8	123	16,237	23,702	441	321
21	59.2	78	8,912	17,298	263	234
22	66.0	17	290	3,360	24	45
23	67.1	14.7	0	1,100	10	15
24	67.2	14.7	0	1,000	9	14
25	80.0	0	0	0	0	0

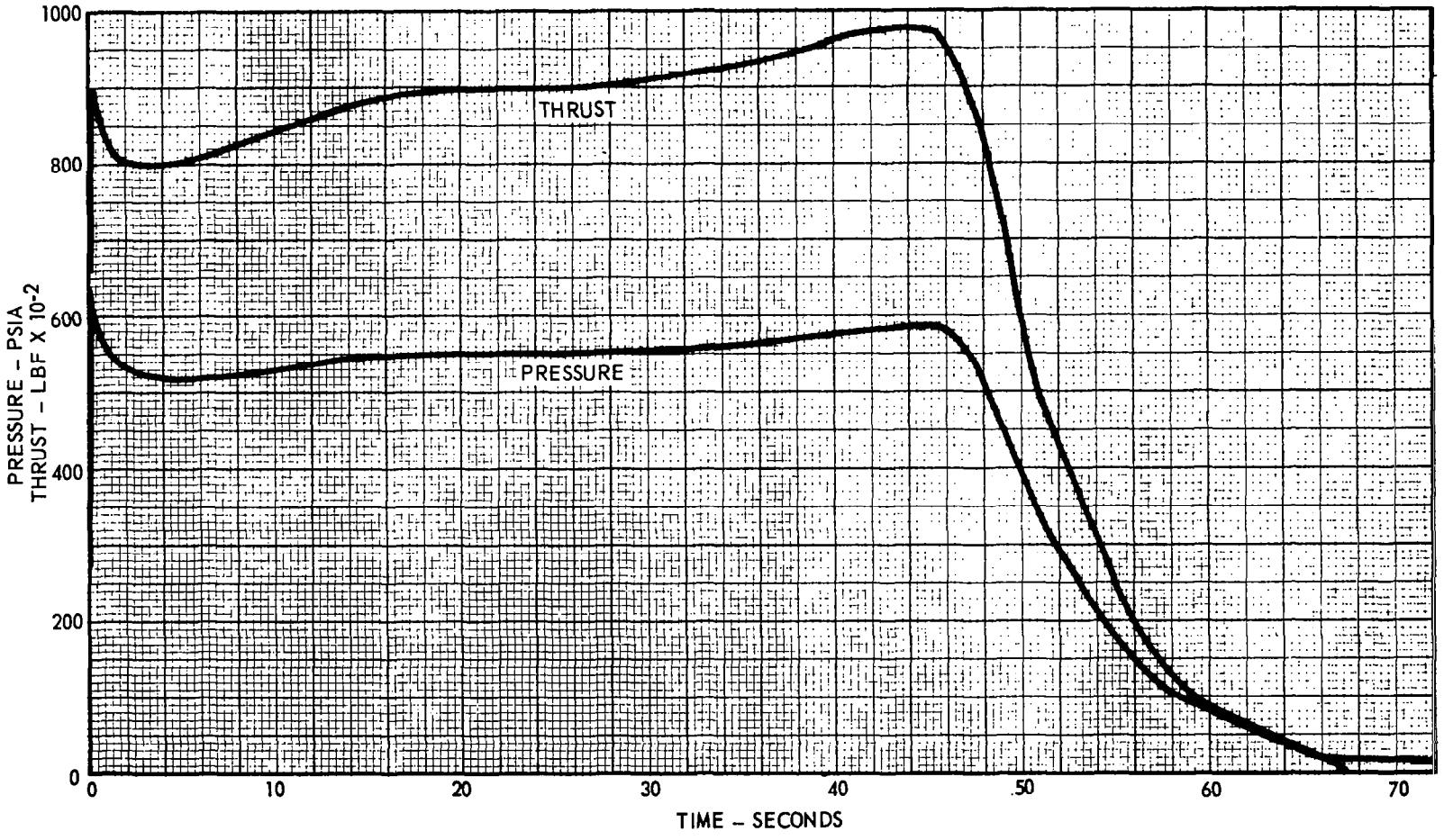

FIGURE 26 ALGOL IIB NOMINAL PERFORMANCE – SEA LEVEL

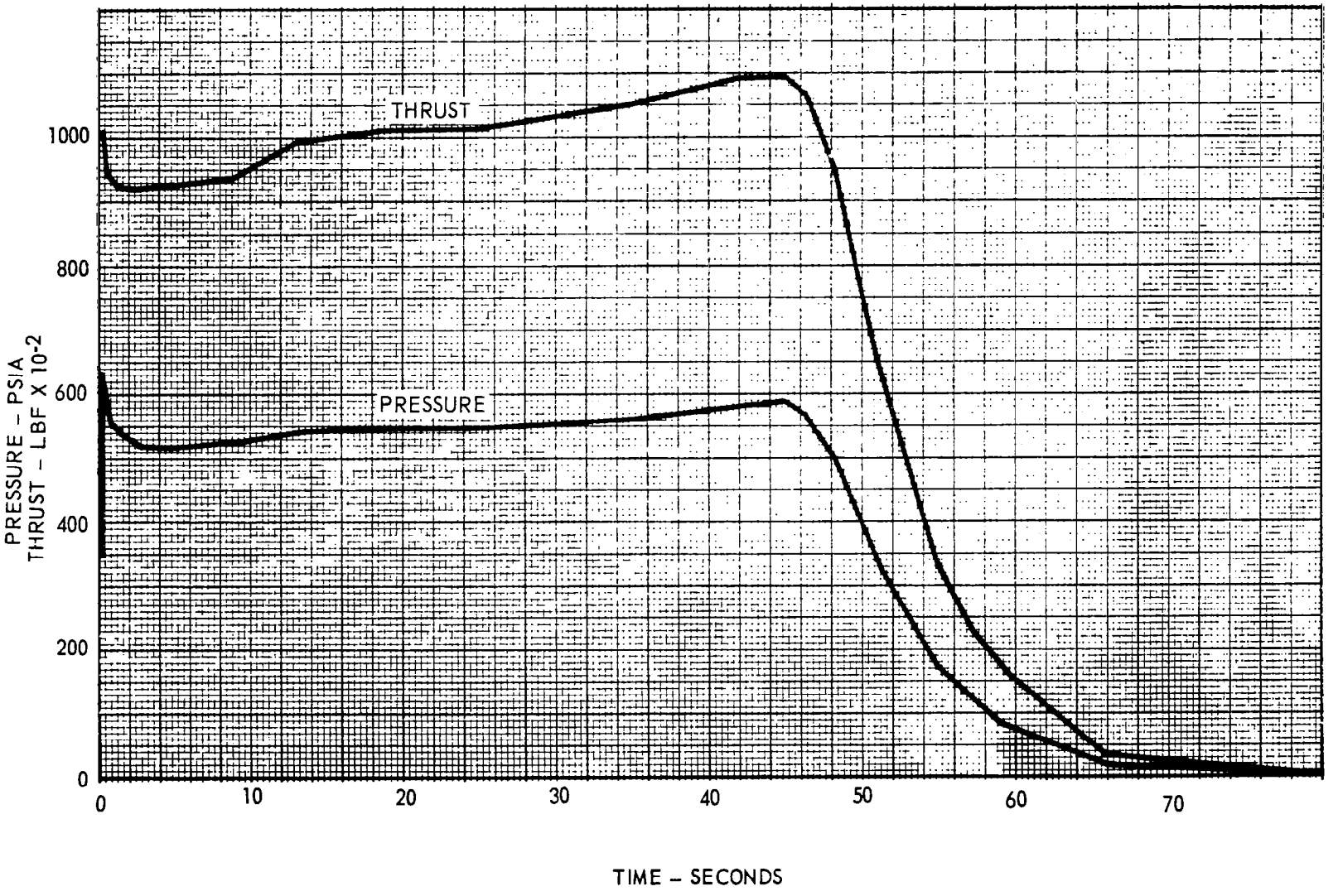

FIGURE 27 ALGOL IIB NOMINAL PRESSURE AND THRUST VS TIME – VACUUM

TABLE 5
ALGOL II B
NOMINAL PERFORMANCE DATA AT 77°F
THRUST/PRESSURE RATIOS

Point	Time (SEC)	Thrust/Pressure Ratio, Sea Level (LBF/PSIA)	Thrust/Pressure Ratio, Vacuum (LBF/PSIA)
1	0	0	0
2	0.2	147.00	166.71
3	0.5	146.40	167.06
4	0.7	146.50	167.88
5	1.3	148.74	171.02
6	2.7	132.92	176.09
7	5.0	155.15	178.50
8	9.0	158.22	181.11
9	13.4	160.95	183.11
10	19.0	163.06	185.19
11	25.5	163.79	185.95
12	34.0	165.63	187.38
13	42.6	167.34	188.34
14	45.7	167.49	189.00
15	46.4	167.78	189.00
16	47.5	166.36	189.00
17	48.4	165.90	189.00
18	51.4	155.32	189.00
19	54.8	139.34	189.00
20	56.8	132.01	189.00
21	59.2	114.26	189.00
22	66.0	17.06	189.00
23	67.1	-	-
24	67.2	-	-
25	80.0	-	-

5.1.4 INERT WEIGHT FLOW

A new nominal inert weight loss, 216 pounds, was established, replacing the old nominal value of 283 pounds. The old value was based upon the first four static firings. The motor design was finalized after the fourth static test firing, and these early inert weight loss values were not valid. The average inert weight loss for Algol motors IIA-3R, IIA-10, IIA-11, IIA-18, IIA-19, and IIB-15 was 216 pounds. This weight includes the igniter charge. Although the value reflects an average of both Algol IIA and IIB data, it is appropriate for Algol IIB predictions because the interior nozzle materials subject to erosion are unchanged. The Algol IIB design features a reinforced nozzle shell and new nozzle fabrication procedure. A detailed analysis of the sources of the inert material consumed (Figure 28) led to the new inert loss distribution. The inert weight loss rate is presented in Figure 29.

5.1.5 PROPELLANT WEIGHT FLOW

The nominal propellant weight of 21,139 pounds is the average of recent production motors. Instantaneous values for propellant weight flow were calculated using Equation 9 in Appendix B. This concept associates propellant weight flow with the stagnation pressure and a varying throat area. Nominal throat area, versus time, was established by averaging before-firing and after-firing throat sizes of statically tested Algol motors and estimating the intermediate sizes during burning time. The characteristic velocity, C*, of the inert gases was approximated as one-half that of the propellant (Ref. 3). Both of these C* values were deduced according to a nominal characteristic velocity of the propellant and inerts gas mixture, based upon test data. The nominal flow rate of inerts was based upon measures of total inerts consumption in static tests and upon a dependence of the linear pyrolysis rate upon the chamber pressure and the local gas flow velocity (Figure 29). The local linear pyrolysis rates were applied to the exposed area of the inerts to estimate the total flow rate of inerts, versus time.

5.1.6 CONSUMABLE WEIGHT REMAINING

The total weight flow is the sum of the inert weight flow and the propellant weight flow. The nominal consumable weight remaining derived from these flow values is tabulated in Table 4 and plotted in Figure 30.

5.2 SECOND STAGE

The establishment of nominal motor performance characteristics in conjunction with the burn rate correlation provides the basis for predicting instantaneous values of thrust and weight remaining during motor operation. An analysis of all previous motor data was conducted to establish the performance characteristics of the Castor I motor.

Static test data were available from six models of the Castor I motor. Since only three XM-33E5 motors had been static tested, it was necessary to use the data available from tests of other models of the TX-33 motor (-36, -37, -39, -41, and -52) to supplement the XM-33E5 data. This is possible because these models are the same except for various external modifications.

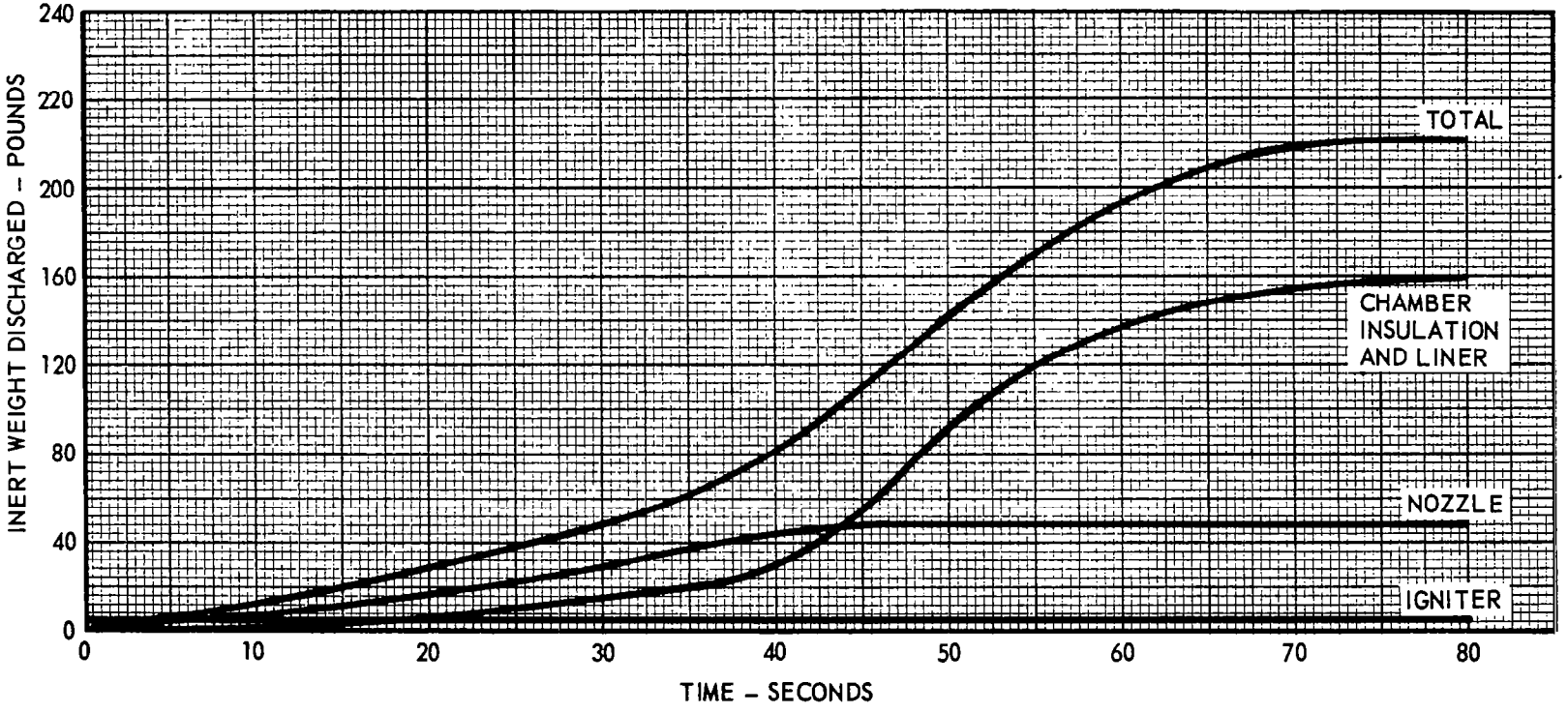

FIGURE 28 ALGOL IIB INERT WEIGHT DISCHARGED VS TIME

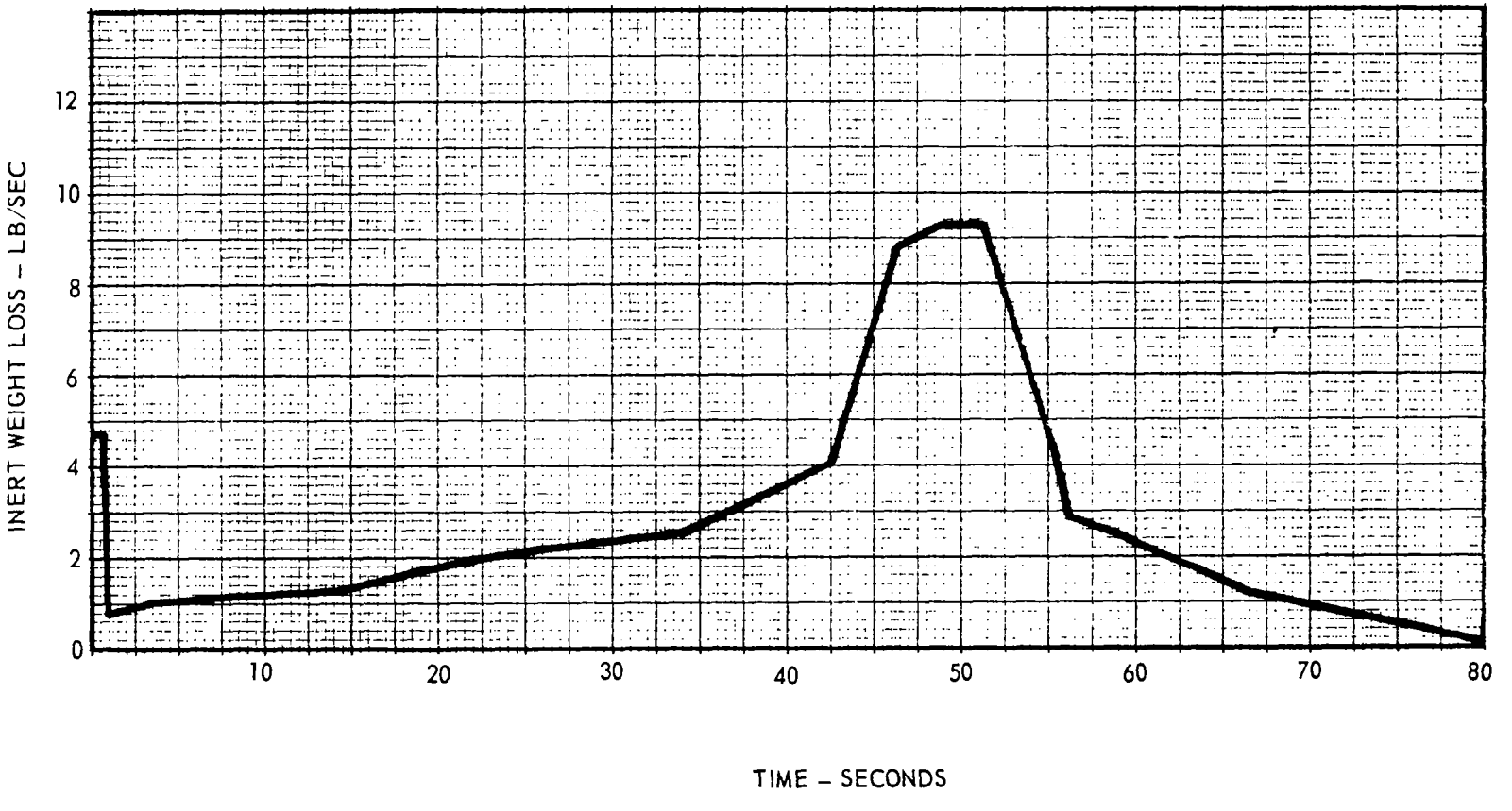

FIGURE 29 ALGOL II B INERT WEIGHT LOSS VS TIME

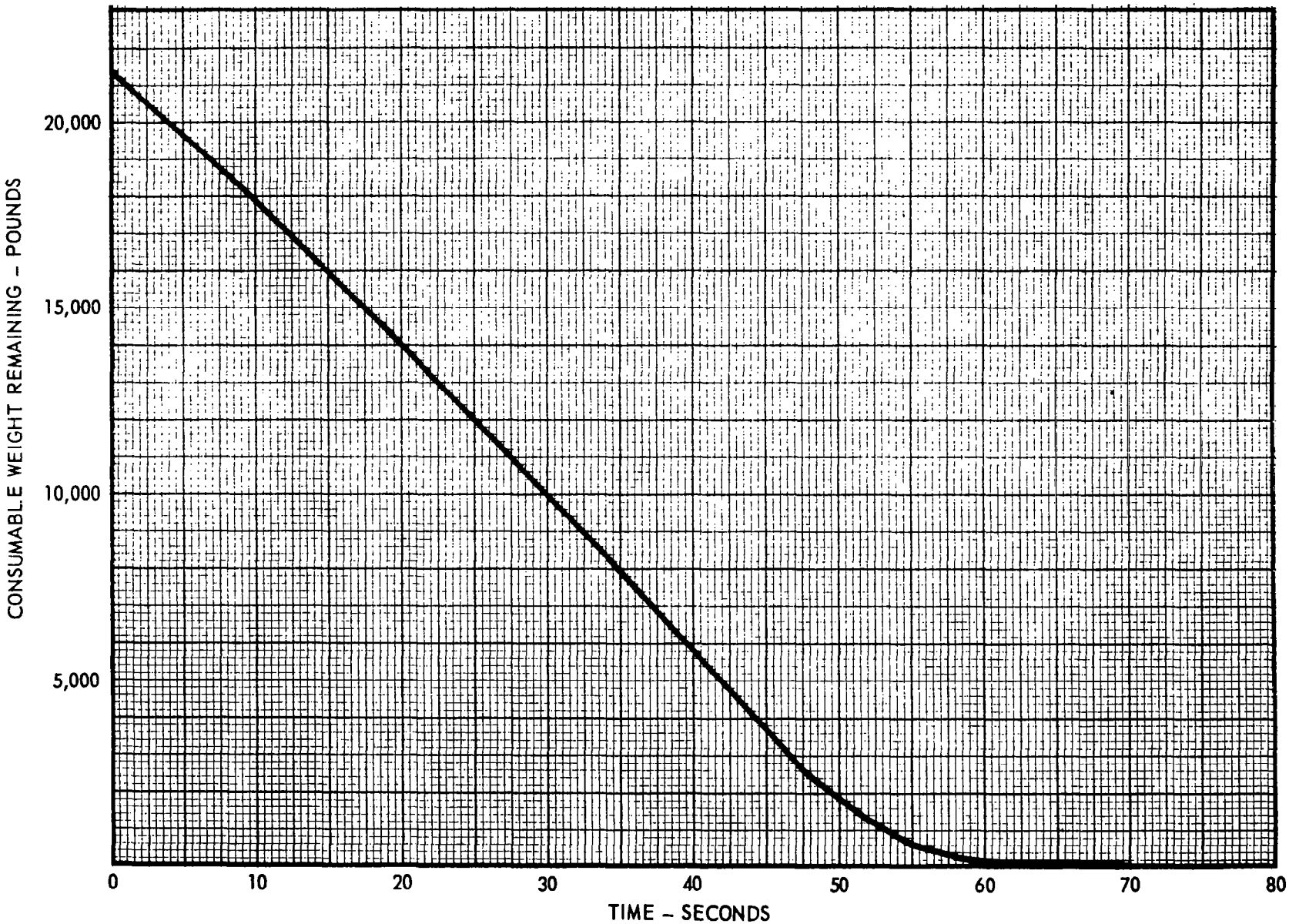

FIGURE 30 ALGOL IIB NOMINAL CONSUMABLE WEIGHT REMAINING VS TIME

The data available for analysis to define the nominal performance characteristics of the Castor motor consisted of 11 flight and 23 static test motors. Of the 23 static test motors, 22 motors were tested at Redstone Arsenal and one motor was tested at AEDC under simulated altitude conditions. No significant difference in performance due to the flight environment was detected by a comparison of the burning rate correlations, energy levels, and trace characteristics of the two groups of motors. The nominal performance of the Castor I (XM-33E5) motor is shown in Table 6 .

5.2.1 NOMINAL THRUST AND PRESSURE VERSUS TIME

The static test Castor motor data provide the basis of constructing the nominal thrust-time configuration of the Castor motor. The pressure-time and thrust-time characteristics for each Castor motor were tabulated and processed through a Thiokol computer program. This program generates a series of dimensionless ratios for each motor representing each instantaneous value of pressure, thrust, and time as a percentage of the average pressure, average thrust, and web burning time, respectively. The program then averages these ratios to establish the nominal performance characteristics. This approach eliminates the time difference factor between motors and minimizes the effect of an instrumentation bias between motors, resulting in a common basis for deriving the trace characteristics most descriptive of nominal motor operation. The pressure-time curve established by this approach was considered to be representative of static test motor performance. The data available from sea level static tests and from the test of the Castor I (XM-33E5) motor under simulated altitude conditions at AEDC were used in constructing the nominal thrust trace for vacuum operation. The vacuum thrust-time curve was based on the nominal pressure-time curve derived from all static test motors, and the vacuum thrust to chamber pressure ratios observed in the AEDC test. The performance of the Castor motor tested at AEDC was in excellent agreement with the vacuum performance projected from sea level static tests. Instantaneous thrust points were established by calculating the F_v/P ratios, shown in Table 7 , from the AEDC test and multiplying this ratio by the instantaneous pressure value from the nominal pressure-time curve.

The nominal performance was represented by values at the twenty-eight time points available in the vehicle trajectory computer program. The resulting curves of chamber pressure and thrust time are shown in Figure 31.

5.2.2 INERT WEIGHT LOSS

A review of the before firing and after firing weight measurements of the Castor motor indicated a total weight loss of inert materials of 131 pounds distributed as follows:

1. Liner and insulation - 108 pounds
2. Nozzle - 15 pounds
3. Igniter - 8 pounds

The inert weight loss of the nozzle, igniter, and case insulation was assumed to occur linearly over the burning time of the motor, except for the charge weight of the igniter (included in this analysis as an inert

TABLE 6
CASTOR I
NOMINAL DATA
(PERFORMANCE AT 77°F AND VACUUM)

Propellant Weight	7321	lb.
Inert Weight Loss	131	lb.
Consumable Weight	7452	lb.
Total Motor Weight (less nozzle closure)	8861	lb.
Burnout Weight	1409	lb.
Nozzle Closure Weight	7	lb.
Heat Cap Pressure Integral	16,000	psia-sec
Total Impulse	2,000,000	lb-sec
Propellant Specific Impulse	273.2	lb-sec/lb
Propellant Burn Rate	0.244	in/sec
Effective Burn Time	27.57	sec.
Total Burn Time	46.00	sec.
Average Thrust (web)	63,100	lb.
Maximum Thrust	75,000	lb.
Average Pressure (web)	507	psia
Maximum Pressure	680	psia
Average Throat Area	74.658	$in.^2$
Exit Area	1167.8	$in.^2$
Average Expansion Area Ratio	15.642	
Propellant Density	0.0616	lb/in^3
Specific Heat Ratio	1.15	
Characteristic Velocity	5250	ft/sec
Temperature Sensitivity of Burn Rate	0.089	%/°F
Motor K_n	207.0	
Propellant Web Length	6.701	in.

TABLE 7
CASTOR I
NOMINAL PERFORMANCE DATA
(VACUUM AND 77°F)

Point	Time (SEC)	Vacuum Thrust (LBF)	Consumable Weight Remaining (LB)	Chamber Pressure (PSIA)	F_v/P
1	0.000	0	7452	0	-
2	0.120	74,798	7434	679	110.0
3	0.326	68,567	7379	613	111.7
4	0.601	66,396	7310	583	113.8
5	2.803	62,022	6787	515	120.3
6	4.179	61,215	6473	499	122.6
7	5.555	61,256	6161	494	123.8
8	11.059	62,845	4897	502	125.2
9	15.186	63,140	3935	501	126.0
10	19.314	63,126	2970	498	126.7
11	22.617	63,811	2194	501	127.3
12	24.268	64,402	1802	504	127.6
13	25.919	65,196	1406	509	127.9
14	26.469	65,386	1273	510	128.0
15	27.020	65,016	1140	507	128.1
16	27.570	63,284	1009	493	128.2
17	28.120	59,679	883	470	127.0
18	28.671	54,479	766	429	127.0
19	29.221	48,238	661	380	127.0
20	29.772	39,168	571	309	127.0
21	30.322	32,194	497	254	127.0
22	31.698	23,098	351	182	127.0
23	33.074	16,922	242	133	127.0
24	34.450	12,413	159	98	127.0
25	37.202	5,960	54	47	127.0
26	39.953	1,225	11	10	127.0
27	42.000	258	3	2	127.0
28	46.000	0	0	0	127.0

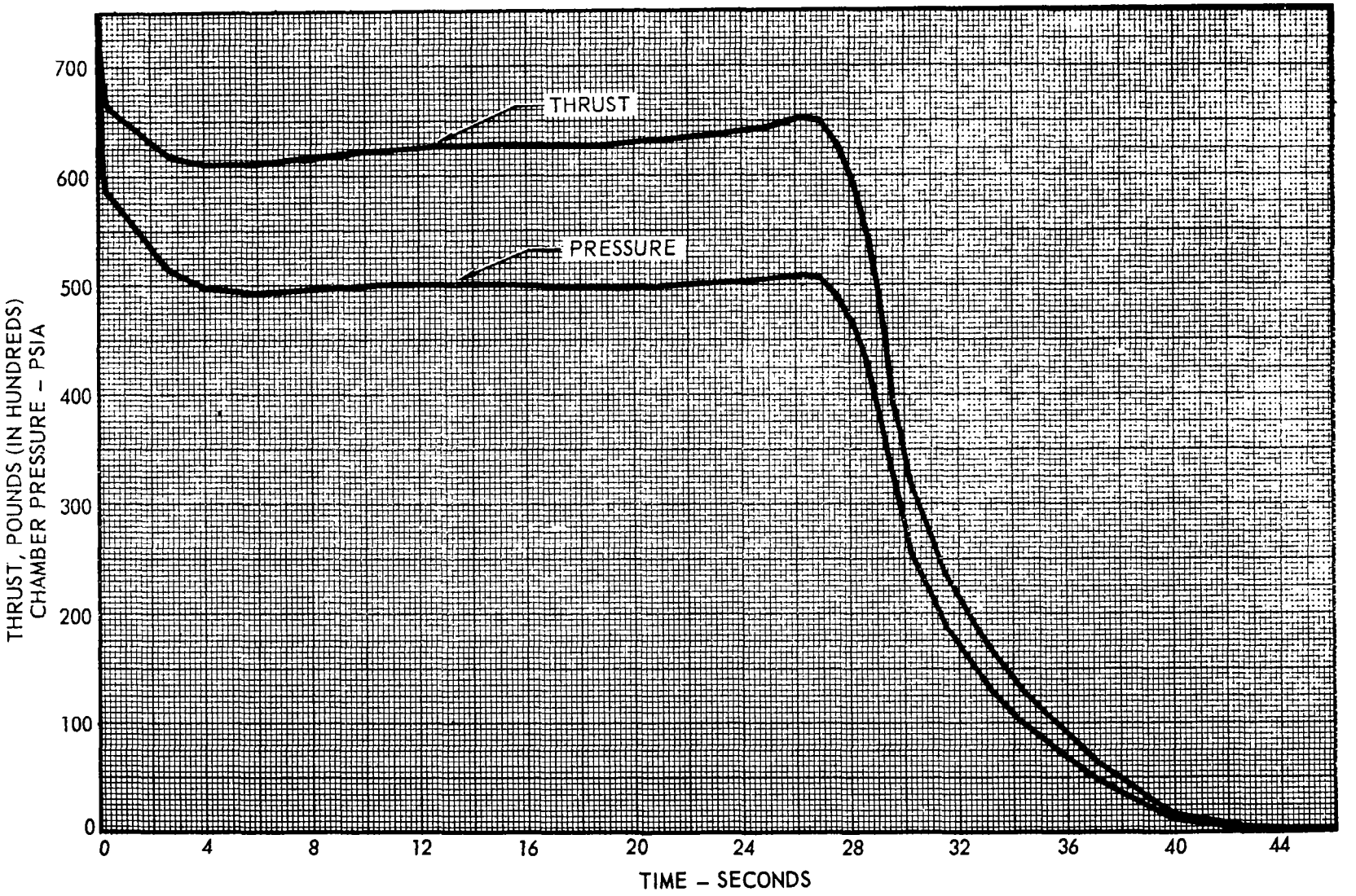

FIGURE 31 CASTOR I NOMINAL PRESSURE AND THRUST VERSUS TIME — VACUUM OPERATION

material) which was considered to be expended on ignition. The total weight loss of case insulation was estimated from char and erosion profiles constructed from previous Castor tests.

Since the consumption of liner material constitutes approximately 75% of the total inert weight loss, emphasis was placed on accurately establishing the discharge rate of this material. A heat transfer analysis computer program was used to determine the "melt" rate of the liner as a function of the time of exposure. The discharge rate of the liner was then estimated by applying the liner melt rate to the exposed liner surface, which was determined based on the geometric progression of the propellant burning surface, at increments of time. The resulting discharge rate was then adjusted to agree with the average, total liner weight consumed as determined from test data, while maintaining the characteristic shape of the curve. Figure 32 shows the nominal accumulated weight loss of the individual items and the nominal total inert weight loss as a function of time. Figure 33 shows the total discharge rate of inert materials from the Castor motor as a function of time. The sharp rise in the discharge rate shown in Figure 33 results from the rapid exposure of liner surface to the propellant gasses at burnout of the propellant web.

5.2.3 PROPELLANT DISCHARGE RATE

The propellant mass flow rate was derived from the nominal thrust line curve assuming the propellant specific impulse to be a constant throughout motor operations. The error introduced by this assumption is considered to be negligible since prior analyses had shown that the change in nozzle expansion area ratio during motor operation results in a range of variation of specific impulse of only 0.1%. Further, the inert material consumed was assumed to have a specific impulse equal to one-half the specific impulse of the propellant. The propellant weight discharged between two successive time points was then determined from the following relationship:

$$\int_{t_1}^{t_2} \dot{w}_p dt = \frac{\int_{t_1}^{t_2} F dt}{I_{SP}} - \frac{\int_{t_1}^{t_2} \dot{w}_I dt}{2} \qquad (1)$$

5.2.4 CONSUMABLE WEIGHT REMAINING VERSUS TIME

The motor weight remaining at any instant is a direct function of two factors: 1) the discharge rate of the inert materials, 2) the discharge rate of the propellant.

Weight discharge was calculated by summing the individual contributors to the mass flow rate. The nominal curve of consumable weight remaining versus time shown in Figure 34 was constructed by subtracting from the total consumable weight (7452 pounds) the weight of propellant plus inert material consumed during progressive time intervals. A tabulation of the consumable weight and vacuum thrust remaining at 28 time points during motor operation is shown in Table 7 .

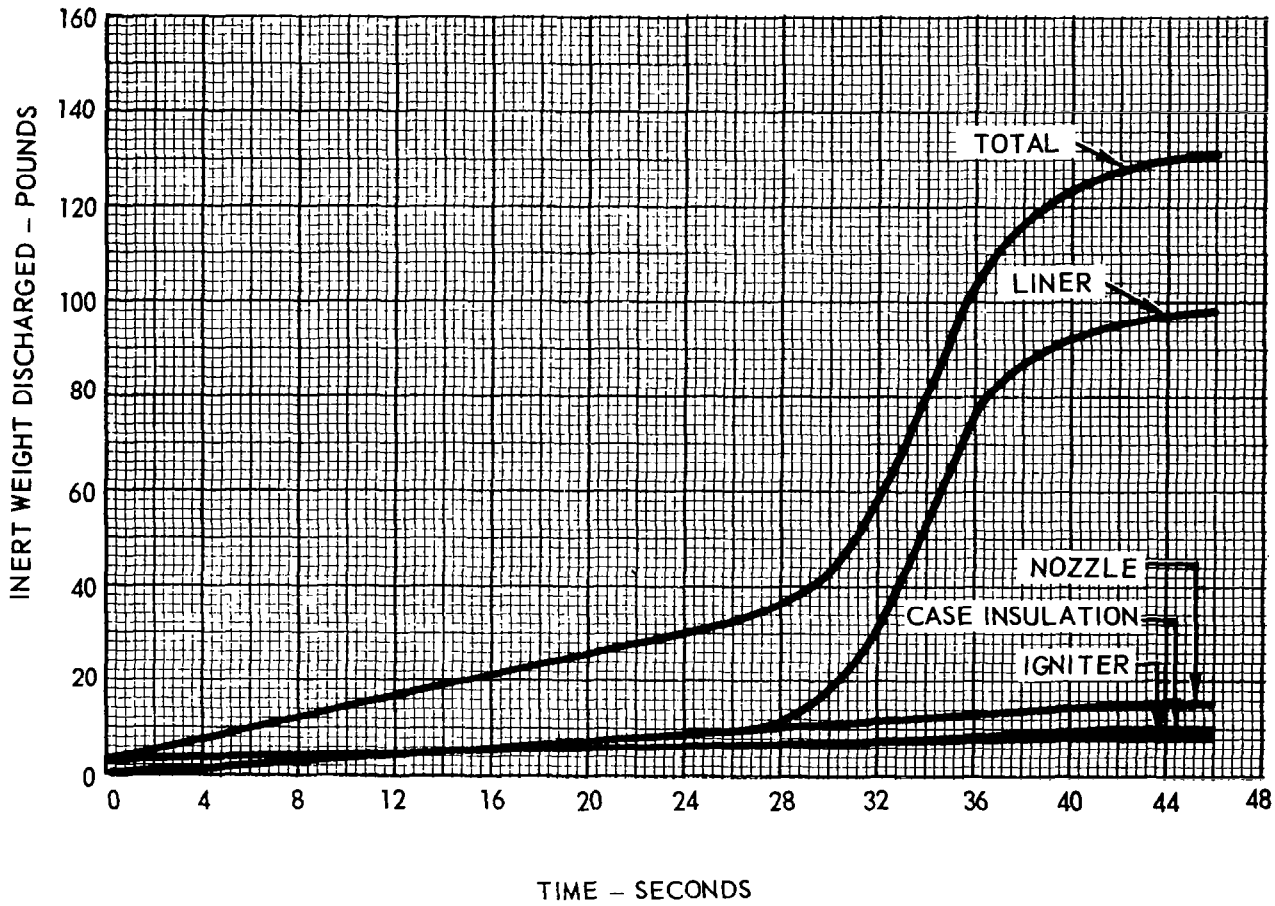

FIGURE 32 CASTOR I INERT WEIGHT DISCHARGED VERSUS TIME

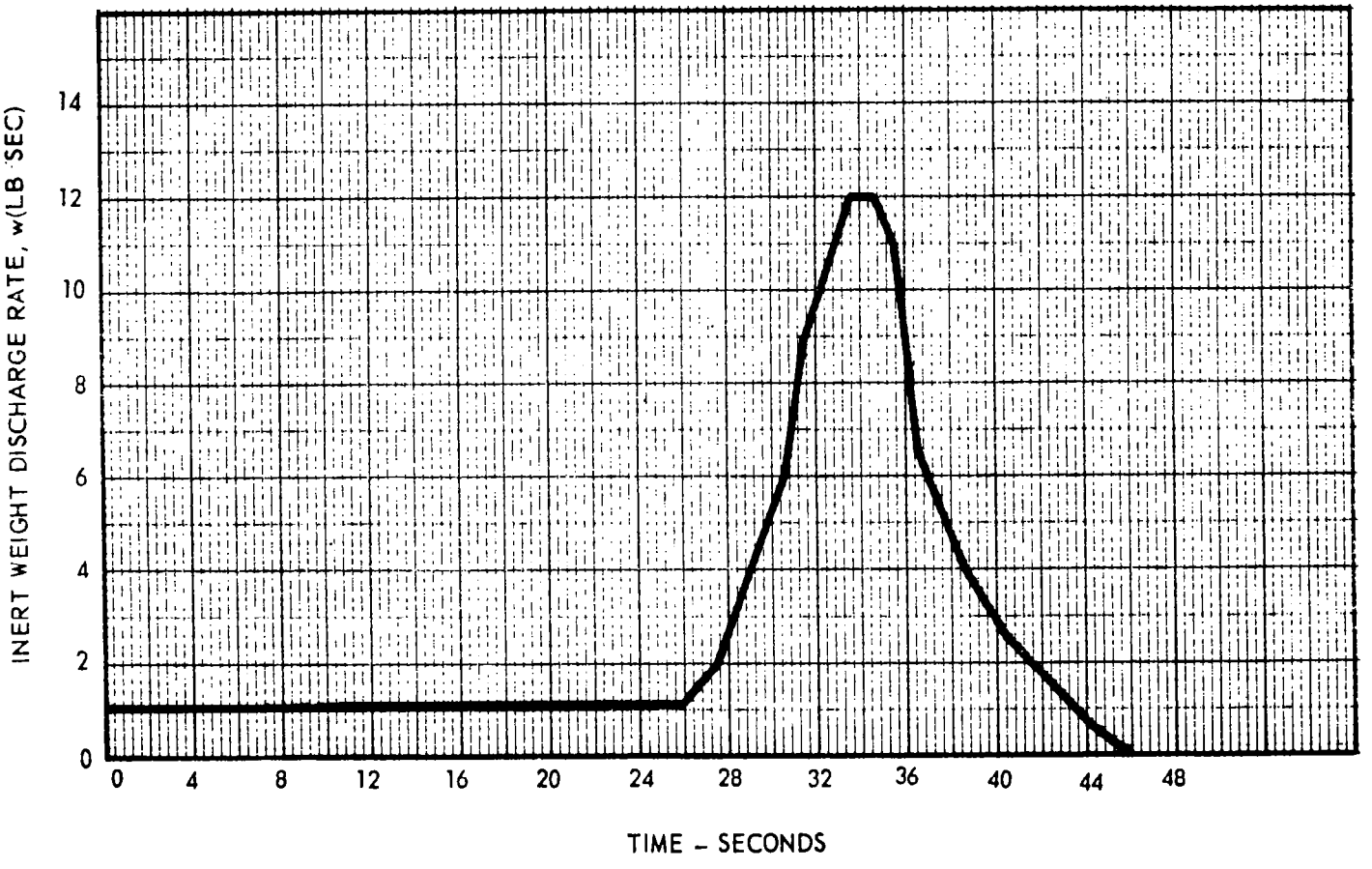

FIGURE 33 CASTOR I RATE OF INERT WEIGHT LOSS VERSUS TIME

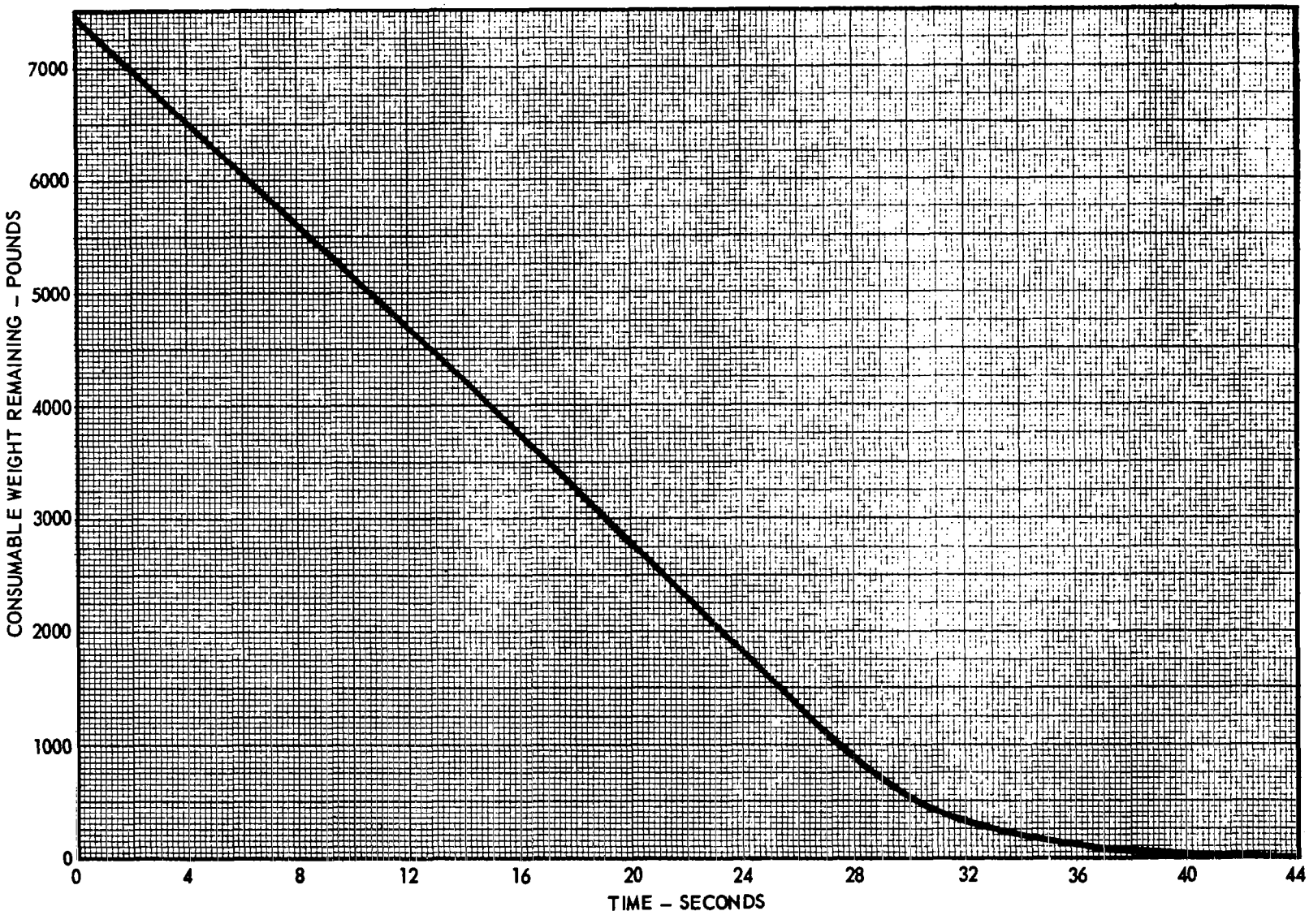

FIGURE 34 CASTOR I NOMINAL CONSUMABLE WEIGHT REMAINING VERSUS TIME

5.3 THIRD STAGE

5.3.1 INTRODUCTION

The establishment of nominal X259 motor performance characteristics for each of the two different burning rate casting powders provides the basis for predicting flight performance. These data were analyzed from the performance of five X259 motors static tested at AEDC and three motors static tested at Alleghany Ballistics Laboratory(ABL). The nominal motor characteristics are shown in Table 8.

5.3.2 NOMINAL THRUST AND PRESSURE TRACE CONFIGURATION

The static firing tests of the five X259 motors at AEDC provide data for the basis of the nominal pressure-time and vacuum thrust-time configuration for both burn rate types of casting powder. The normal (or low) rate powder was used in all five of the motors tested at AEDC. The nominal trace configuration was derived from these tests and the static firing at ABL of three X259 motors containing high burning rate powder. The traces for the normal burning rate and high burning rate powder lots are shown in Figures 35 and 36. The data from these tests were also used to derive the vacuum thrust/pressure (F/P) relationship for X259 motors using low rate powder. The high burning rate powder vacuum thrust values were obtained by using pressure data from the powder lot evaluation firing at ABL and adjusting the F/P relationship to take into account the increase in nozzle throat area from 35.78 in^2 to 38.63 in^2, i.e., expansion ratio change from 17.5 to 16.2. The F/P curves for both burning rate powders are shown in Figure 37.

A tabulation of the instantaneous values used to derive the vacuum thrust time curves for both burning rate powders are shown in Tables 9 and 10.

5.3.3 INERT WEIGHT FLOW

The amount of inert weight lost during X259 burning was measured in the AEDC tests. Measurements of the "before firing" and "after firing" inert weights gave an average value of 25 lbs. of inert material being consumed. This inert weight flow is assumed to be proportional to the thrust-time curve.

5.3.4 PROPELLANT WEIGHT FLOW

The nominal propellant weights for each burning rate type of casting powder were established by averaging previous production motors. The propellant weight flow at any instant is calculated from the instantaneous impulse (integral of thrust) assuming the specific impulse of the propellant is constant during motor burning.

5.3.5 CONSUMABLE WEIGHT REMAINING

The amount of consumable weight remaining at an instant of time is a function of the propellant weight flow and inert weights flow. Knowing the

TABLE 8

X259

NOMINAL DATA

(PERFORMANCE 77°F AND VACUUM)

	Powder Lots	
	Z1-193, Z1-207	Z1-246
Propellant Weight	2566 lbs.	2557 lbs.
Inert Weight Loss	25 lbs.	25 lbs.
Consumable Weight	2591 lbs.	2582 lbs.
Total Motor Weight (less nozzle closure)	2787 lbs.	2778 lbs.
Burnout Weight	196 lbs.	196 lbs.
Nozzle Closure Weight	0.25 lb.	0.25 lb.
Head Cap Pressure Integral	10,493 psia-sec	11,335 psia-sec
Total Impulse	715,400 lbf-sec	719,500 lbf-sec
Propellant Specific Impulse	278.8 lb-sec/lb	281.4 lb-sec/lb
Propellant Burn Rate	0.327 in/sec	0.300 in/sec
Web Burn Time	31.2 sec.	34.0 sec.
Total Burn Time	32.8 sec.	34.9 sec.
Average Thrust (Web)	21,810 lbf	20,620 lbf
Maximum Thrust	23,800 lbf	22,182 lbf
Average Pressure (Web)	320 psia	325 psia
Maximum Pressure	350 psia	350 psia
Average Throat Area	38.63 in^2	35.78 in^2
Exit Area	626.2 in^2	626.2 in^2
Average Expansion Area Ratio	16.2	17.5
Propellant Density	0.0636 lb/in^3	0.0636 lb/in^3
Specific Heat Ratio	1.18	1.18
Characteristic Velocity	5300 ft/sec	5300 ft/sec
Temperature Sensitivity of Burn Rate	0.25 %/°F	0.25 %/°F
Motor K_n	100	100
Propellant Web Length	10.40 in.	10.40 in.

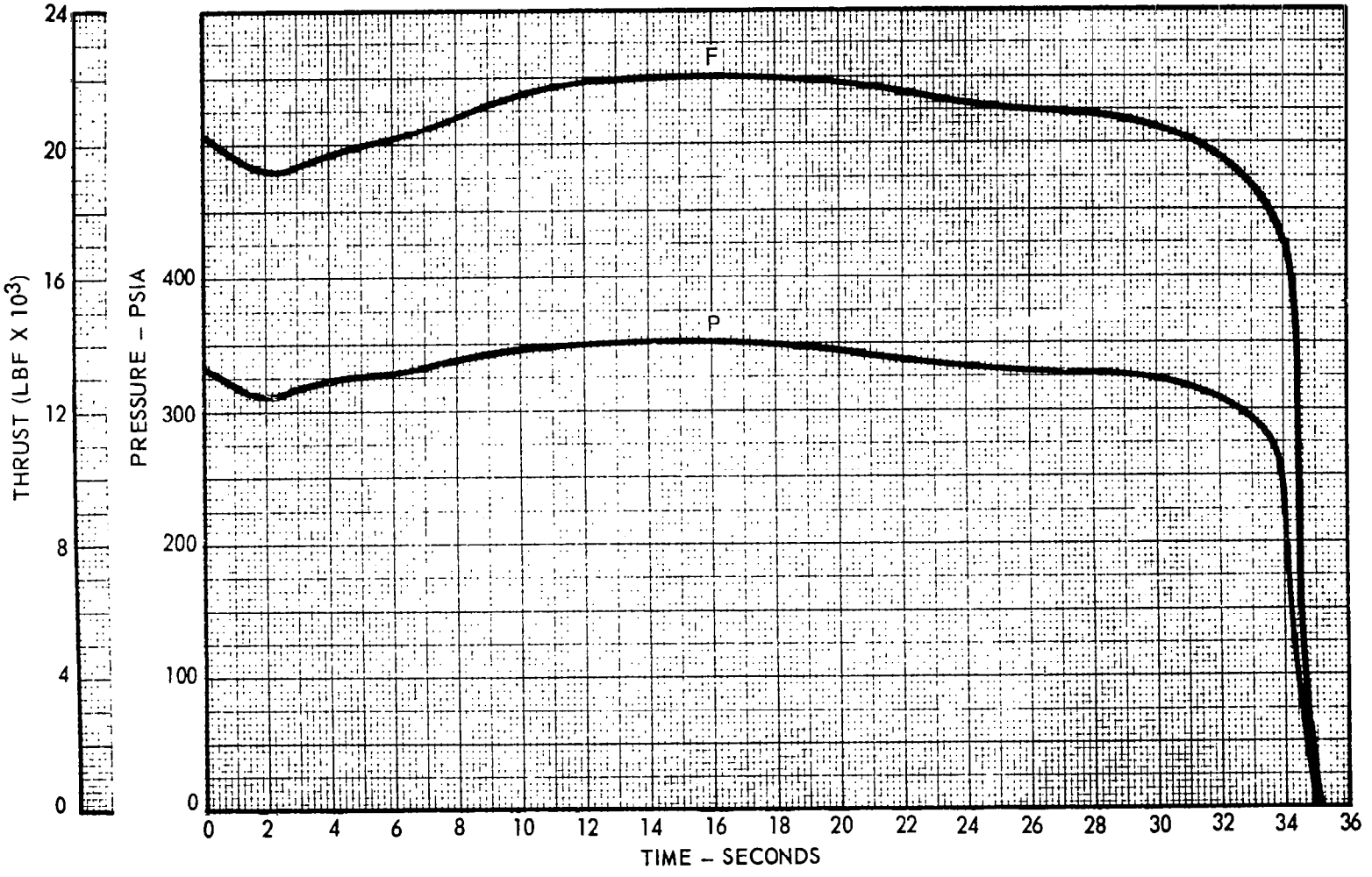

FIGURE 35 X259 NOMINAL PRESSURE AND VACUUM THRUST VERSUS TIME FOR LOW BURNING RATE POWDER LOT Z1–246

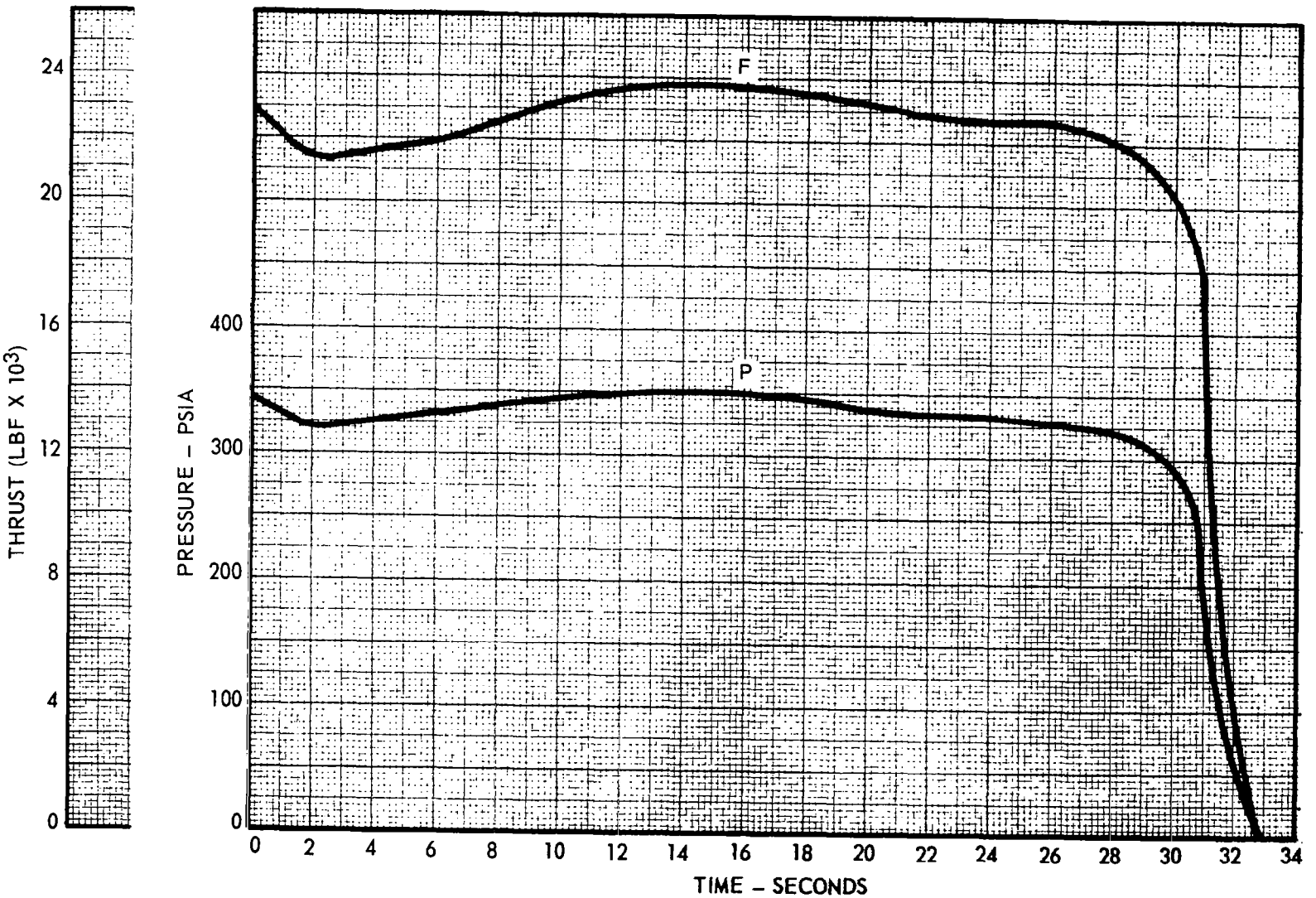

FIGURE 36 X259 NOMINAL PRESSURE AND VACUUM THRUST VERSUS TIME FOR HIGH BURNING RATE POWDER LOTS ZI–193 AND 207

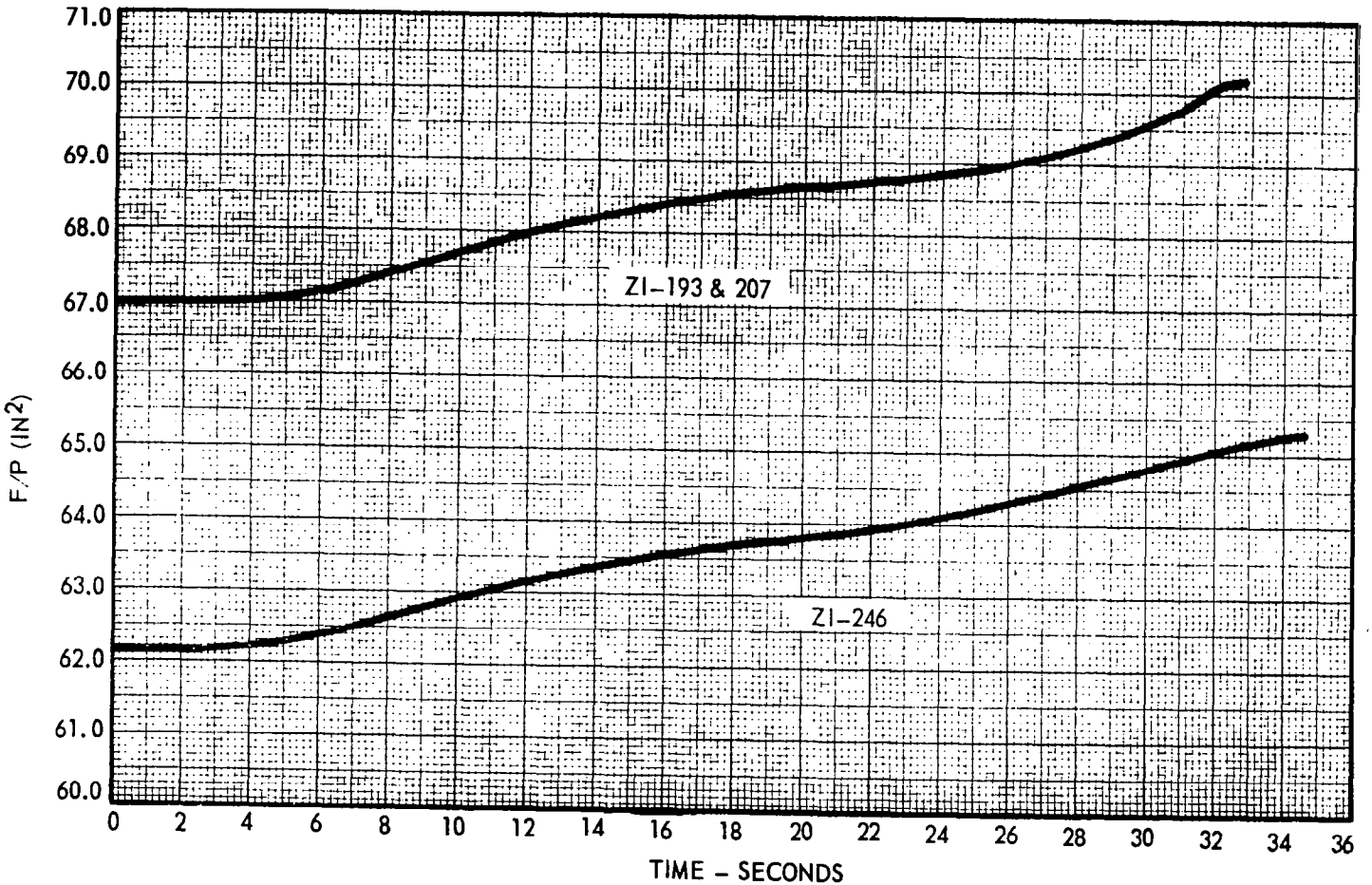

FIGURE 37 **X259 VACUUM THRUST/PRESSURE RELATIONSHIP VERSUS TIME FOR HIGH BURNING RATE POWDER LOTS ZI-193 AND 207 AND LOW BURNING RATE POWDER LOT ZI-246**

TABLE 9

X259 NOMINAL PERFORMANCE DATA

77°F AND VACUUM CONDITIONS

(Powder Lot ZI-246)

Point	Time (SEC)	Chamber Pressure (PSIA)	F/P (IN^2)	Vacuum Thrust (LBF)	Consumable Weight Remaining (LBS)
1	0	0	62.18	0	2582.0
2	0.1	325	62.18	20,210	2578.4
3	2.0	312	62.18	19,402	2443.3
4	5.0	323	62.29	20,122	2230.5
5	7.0	326	62.48	20,370	2085.2
6	10.0	343	62.93	21,587	1859.4
7	12.0	347	63.18	21,926	1703.1
8	14.0	350	63.37	22,182	1544.8
9	16.0	349	63.56	22,182	1386.7
10	19.0	345	63.73	21,990	1150.6
11	21.0	344	63.78	21,944	992.9
12	24.0	332	64.06	21,271	759.7
13	27.0	327	64.43	21,073	532.3
14	29.0	322	64.68	20,831	381.9
15	30.0	320	64.83	20,750	307.3
16	31.2	308	65.04	20,192	216.6
17	32.0	302	65.08	19,659	162.5
18	33.0	289	65.19	18,844	93.4
19	34.0	254	65.29	16,588	29.8
20	34.9	0	65.29	0	0

TABLE 10
X259 NOMINAL PERFORMANCE DATA
77°F AND VACUUM CONDITIONS
(Powder Lots ZI-193 and 207)

Point	Time (SEC)	Chamber Pressure (PSIA)	F/P (IN^2)	Vacuum Thrust (LBF)	Consumable Weight Remaining (LBS)
1	0	0	67.00	0	2591.0
2	0.1	343	67.00	22,981	2586.8
3	2.0	320	67.00	21,440	2434.0
4	3.0	322	67.00	21,574	2356.1
5	5.0	325	67.15	21,824	2199.0
6	7.0	333	67.30	22,413	2038.8
7	10.0	345	67.76	23,378	1790.1
8	12.0	348	67.98	23,658	1619.7
9	14.0	349	68.20	23,805	1447.9
10	16.0	347	68.40	23,734	1275.7
11	19.0	342	68.56	23,449	1015.8
12	21.0	336	68.61	23,054	847.4
13	24.0	333	68.89	22,941	597.5
14	27.0	325	69.26	22,509	350.6
15	28.0	319	69.38	22,132	269.8
16	29.0	311	69.50	21,615	190.6
17	30.0	296	69.64	20,614	114.1
18	31.0	261	69.74	18,201	43.9
19	32.0	50	70.16	3,507	6.4
20	32.8	0	70.16	0	0

relationship of the propellant weight flow and inert weights flow to time (proportional to thrust), the consumable weight remaining is derived by subtracting the instantaneous consumed weight from the total consumables which are propellant weight and 25 lbs. of inerts. The instantaneous consumed weight is calculated from the following equation:

$$W_c = \frac{(W_p + 25) \int_o^t F\,dt}{\int_o^{t_T} F\,dt} \qquad (1)$$

Curves representing the nominal consumed weight remaining during motor burning for both burning rate types of casting powder are shown in Figure 38.

5.4 FOURTH STAGE

5.4.1 INTRODUCTION

The establishment of nominal X258 "C" motor characteristics provides the basis for predicting flight performance. These data were prepared from the performance measurements of X258 motors at AEDC and during flight. The nominal motor characteristics are shown in Table 11.

5.4.2 NOMINAL THRUST AND PRESSURE TRACE CONFIGURATION

The static firing tests conducted at AEDC were the basis for the nominal pressure-time and vacuum thrust-time traces for the X258 motor. These tests consisted of both static and spin tests and a nominal trace configuration was determined. However, during flight, a consistent 1% to 2% degradation in performance was experienced. The trace configuration is shown in Figure 39. The F/P relationship shown in Figure 40 was also derived from the AEDC tests. A tabulation of the instantaneous values used to derive the nominal X258 "C" motor vacuum thrust-time curve is shown in Table 12 .

5.4.3 INERT WEIGHT FLOW

The amount of inert weight lost during X258 burning was measured in the AEDC spin tests. Measurements of the "before firing" and "after firing" inert weights gave an average value of 5.7 lbs. This inert weight flow is assumed to be proportional to the thrust time curve.

5.4.4 PROPELLANT WEIGHT FLOW

The nominal amount of propellant weight was established by averaging previous production motors. The propellant weight flow of the X258 "C" motor is calculated from the instantaneous thrust assuming the specific impulse of the propellant is constant during motor burning.

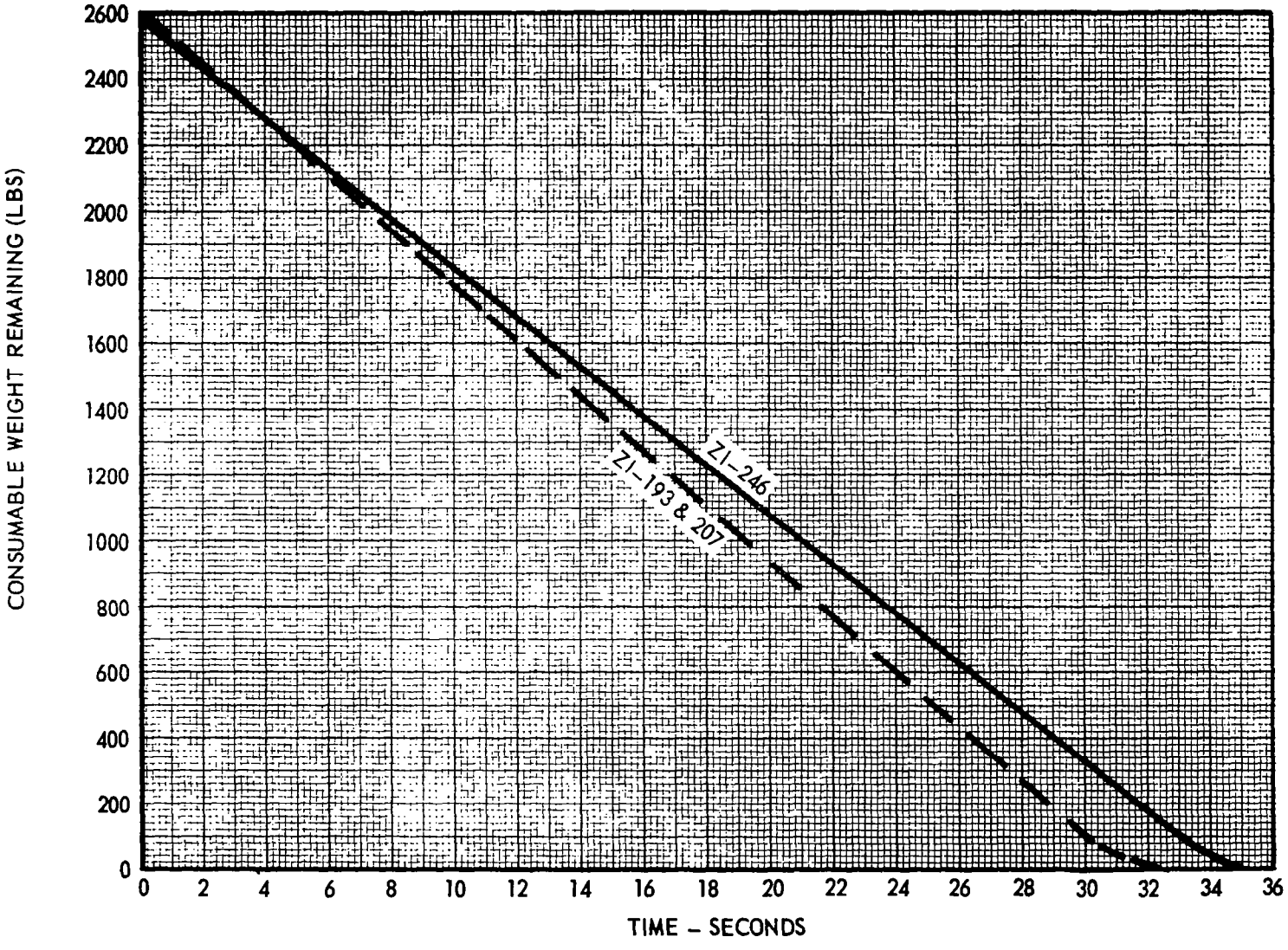

FIGURE 38 X259 NOMINAL CONSUMABLE WEIGHT REMAINING VS TIME

TABLE 11
X258 "C" MOTOR
NOMINAL DATA
(PERFORMANCE 77°F AND VACUUM)

Propellant Weight	502	lbs.
Inert Weight Loss	5.7	lbs.
Consumable Weight	503.6	lbs.
Total Motor Weight (less nozzle closure)	576.0	lbs.
Burnout Weight	76.5	lbs.
Nozzle Closure Weight	0.10	lb.
Head Cap Pressure Integral	9,582	psia-sec
Total Impulse	140,000	lb-sec
Propellant Specific Impulse	281.2	lb-sec/lb.
Propellant Burn Rate	0.286	in/sec
Web Burn Time	21.9	sec.
Total Burn Time	24.1	sec.
Average Thrust (web)	5,800	lbf
Maximum Thrust	6,700	lbf
Average Pressure (web)	428	psia
Maximum Pressure	453	psia
Average Throat Area	8.12	in^2
Exit Area	203.0	in^2
Average Expansion Area Ratio	25.0	
Propellant Density	0.06278	lb/in^3
Specific Heat Ratio	1.18	
Characteristic Velocity	5,300	ft/sec
Temperature Sensitivity of Burn Rate	0.25	%/°F
Motor K_n	145	
Propellant Web Length	6.82	in.

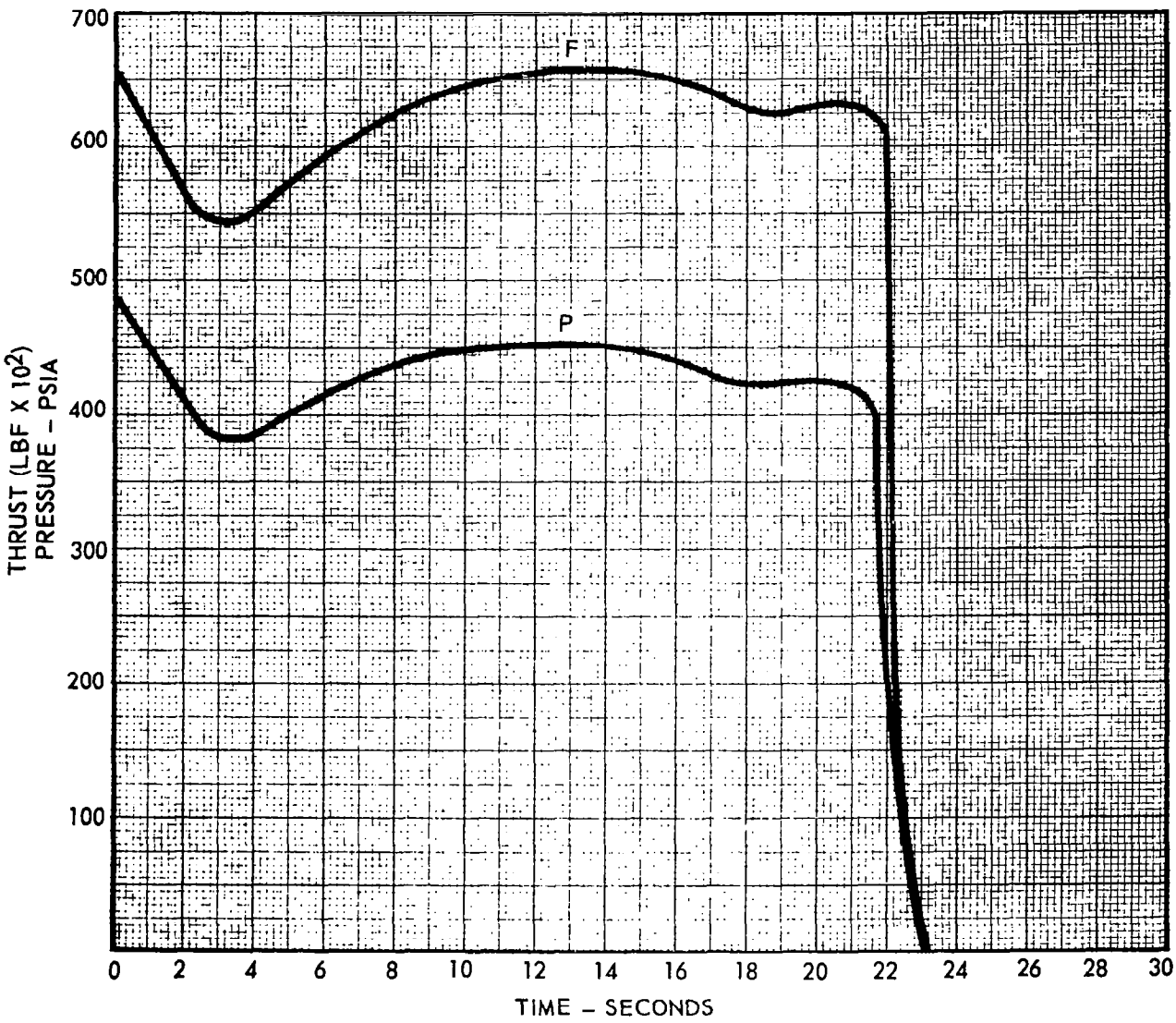

FIGURE 39 X258 "C" MOTOR NOMINAL PRESSURE AND VACUUM THRUST VERSUS TIME

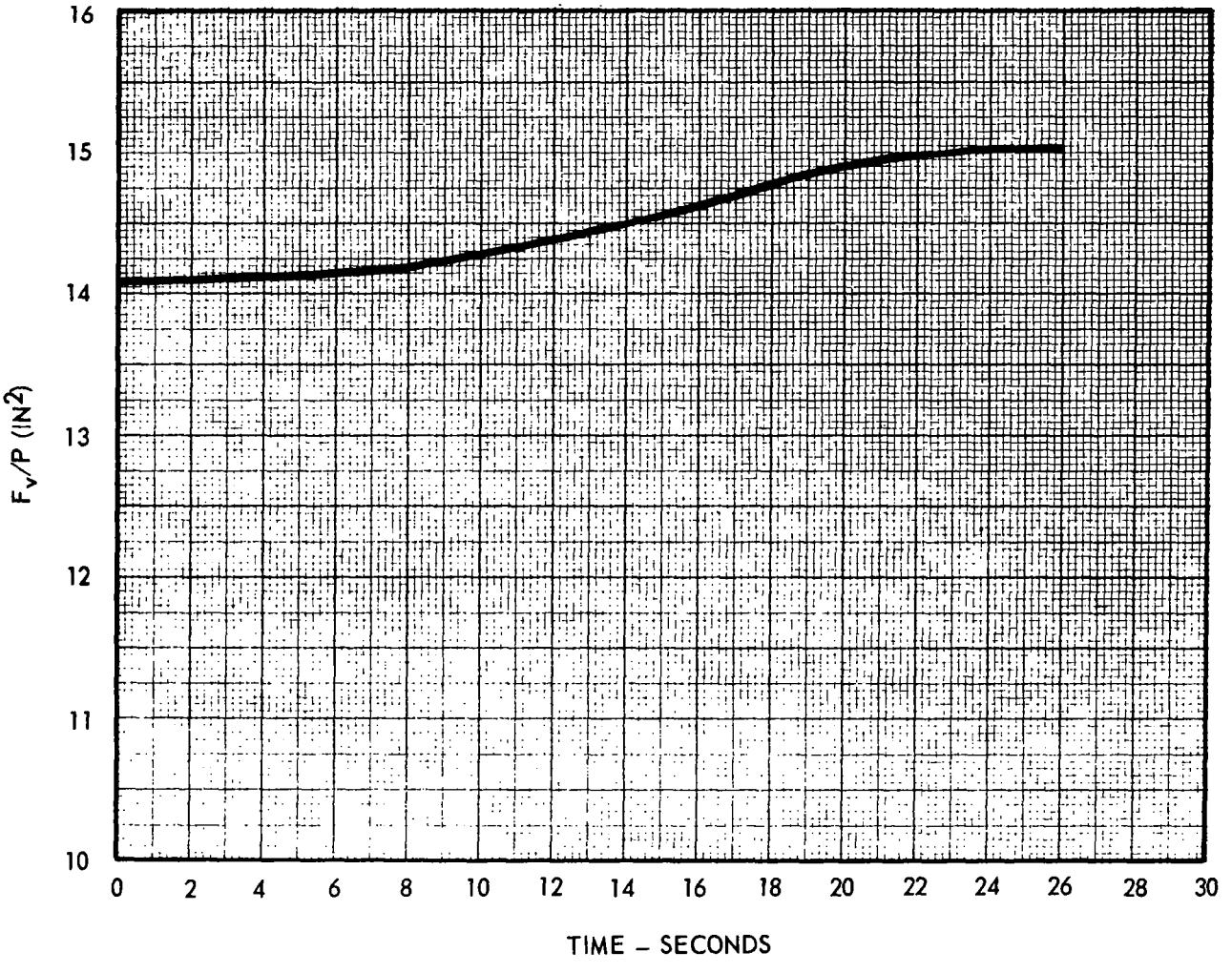

FIGURE 40 X258 "C" MOTOR VACUUM THRUST/PRESSURE RELATIONSHIP VERSUS TIME

TABLE 12
X258 "C" MOTOR NOMINAL PERFORMANCE DATA
77°F AND VACUUM CONDITIONS

Point	Time (SEC)	Chamber Pressure (PSIA)	F/P (IN^2)	Vacuum Thrust (LBF)	Consumable Weight Remaining (LBS)
1	0	0	14.10	0	503.6
2	0.1	482	14.10	6796	502.4
3	1.0	445	14.10	6275	475.3
4	2.0	385	14.10	5420	460.2
5	3.0	380	14.10	5413	440.7
6	4.0	391	14.10	5569	420.4
7	5.0	403	14.12	5690	400.2
8	6.0	418	14.15	5975	379.2
9	8.0	437	14.20	6268	334.8
10	10.0	450	14.30	6501	289.2
11	12.0	454	14.40	6605	242.0
12	14.0	453	14.50	6636	194.4
13	16.0	441	14.63	6452	147.3
14	18.0	425	14.76	6273	101.5
15	19.0	425	14.82	6298	78.9
16	20.0	425	14.90	6332	56.6
17	21.0	423	15.00	6345	33.8
18	22.0	405	15.04	6091	11.4
19	23.0	15	15.04	226	0.1
20	23.2	0	15.04	0	0

5.4.5 CONSUMABLE WEIGHT REMAINING

The amount of consumed weight remaining at an instant of time is a function of the propellant weight flow and inert weights flow. In the X258 "C" motor, the degradation of performance during flight environment (longitudinal acceleration) is accounted for by considering 4.1 lbs. of propellant as unburned. The consumable weight remaining for the X258 at an instant of time, as shown in Figure 41 , is calculated from the following equation:

$$W_c = \frac{(W_P - 4.1) + W_{Ic} \int_0^t F_{Vdt}}{\int_0^{t_T} F_{Vdt}} \qquad (1)$$

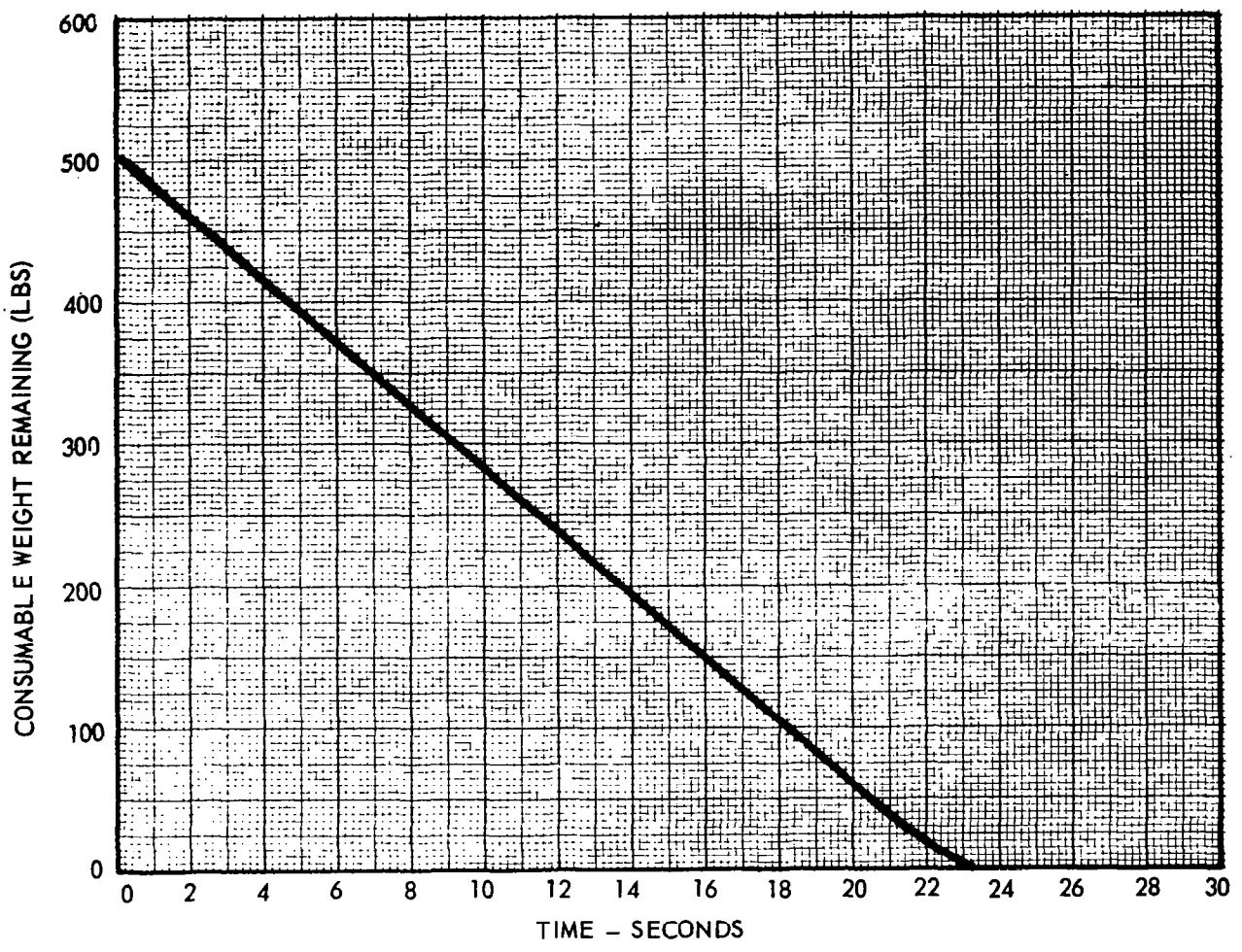

FIGURE 41 X258 NOMINAL CONSUMABLE WEIGHT REMAINING VS TIME

6.0 PERFORMANCE PREDICTION PROCEDURE

6.1 FIRST STAGE

The performance of an Algol IIB motor is predicted by firing a series of twelve 10KS-2500 test motors, one motor representing each of the twelve batches of propellant in the Algol motor, to determine the propellant batch burning rates. These motors are fired at 77°F with a standard throat size to produce approximately 550 psia chamber pressure. These batch rates are adjusted to the standard condition of 550 psia and 77°F and are then averaged. This average batch rate is translated to an "apparent" full scale burning rate at 550 psia and 77°F by the use of a correlation. The apparent full scale burning rate is then translated to a "true" full scale rate, at actual operating pressure, by the use of a second correlation. The true full scale rate is converted to a predicted web time for the new motor. Then the nominal time points, thrust, weight remaining, and jet vane drag, are multiplied by the appropriate time and propellant weight ratios to complete the performance prediction.

6.1.1 CORRELATION

The Algol motor burning rate at 77°F and 550 psia is calculated using the following equation for motors:

1. 80/20 oxidizer blend ratio
   Algol rate at 550 = 0.7333 (batch rate at 550) + 0.0717, in/sec.
2. 75/25 oxidizer blend ratio
   Algol rate at 550 = 0.7333 (batch rate at 550) + 0.657, in/sec.

Since the full scale motors do not all operate at 550 psia, a second correlation is required to convert the 550 psia burn rate to the true burning rate at operating pressure:

$$\text{Algol rate at operating pressure} = r_{(550)} \left[\frac{r(550)}{r_{(550\ \text{nominal})}} \right]^{\frac{n}{1-n}} \quad (2)$$

where $r_{(550\ \text{nominal})} = 0.211$ in/sec

Then, to calculate the new "effective" burn time, t_b,

$$t_b = 9.64/\text{Algol rate at operating pressure, sec.} \quad (3)$$

6.1.2 PREDICTION

The 25 nominal points for time, vacuum, thrust, jet vane drag, and consumable weight remaining are multiplied by the following ratios:

$$\text{New } t = \text{Nominal } t \times (\text{New } t_b/45.700) \text{ sec.} \quad (4)$$

$$\text{New } F = \text{Nominal } F \times (45.700/\text{New } t_b) \times (W_p/21{,}139) \text{ lbf} \quad (5)$$

$$\text{New JVD} = \text{Nominal JVD} \times (45.700/\text{New } t_b) \times (W_p/21{,}139) \text{ lbf.} \quad (6)$$

$$\text{New Cons. Wt. Rem.} = \text{Nominal C.W.R.} \times (W_p + 216)/(21{,}139 + 216) \text{ lb.} \quad (7)$$

$$\text{New Total Impulse} = W_p \times 258.875 \text{ lbf-sec} \quad (8)$$

6.1.3 COMPUTER PROGRAMS

Computer prediction programs are available at Sacramento for prediction of Algol II motor performance utilizing the average burning rate for the Algol motor and also by inputing the burning rates for each batch of propellant. The two methods are summarized below.

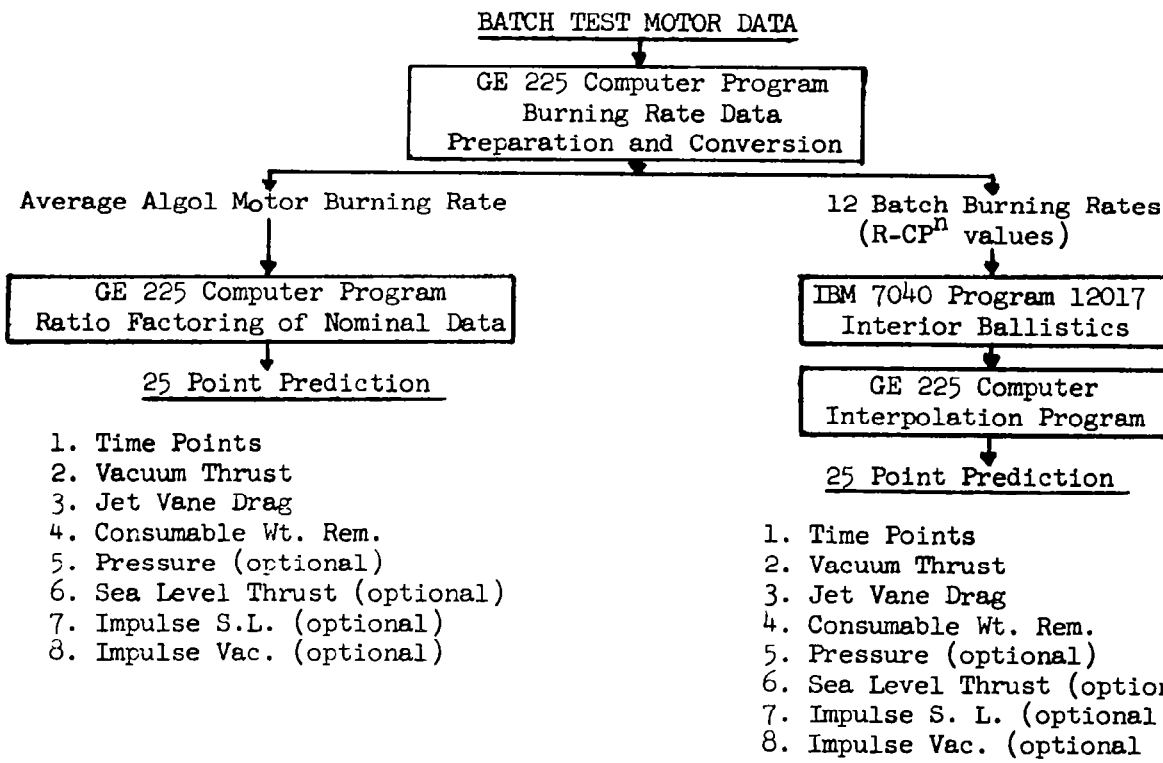

Algol II motors 2R, 3R, and 5 had a batch test motor fired for each batch of propellant. Performance predictions for each of these motors were prepared by both methods. The trace shapes produced by both methods were nearly identical and both prediction traces generally matched the actual motor pressure and thrust traces. The predictions showed a more rapid ignition than the actual motor data because the nominal motor trace is modeled after recent Algol II motors which utilize a larger ignition charg. than that employed in the early motors.

The short method for motor prediction, employing the average Algol motor burning rate, appears adequate for motor performance prediction.

6.2 SECOND STAGE

The prediction of Castor I motor performance is based on the ballistic properties of the propellant mixes loaded into the Castor motor. The burning rate of each propellant mix is currently determined by firing two or more batch test (TX-3) motors at a K_n of approximately 200 and a temperature of 70°F. The test motor burning rate (r_1) at the operating condition is determined for each motor using the following empirical equation:

$$r_1 = \frac{1}{t_w}\left[0.6415\ \frac{\int_o^{t_w} P\,dt}{\int_o^{t_T} P\,dt} - .00903\right] \tag{1}$$

$$K_{n_1} = \frac{76.5}{A_t} \tag{2}$$

where K_{n_1} = test motor K_n

The burning rate (r_2) determined from each test motor is then adjusted to the condition (K_n = 231) which serves as the basis for the correlation between the test motor and the Castor motor as follows:

$$r_2 = r_1\left(\frac{231}{K_{n_1}}\right)^{\frac{n}{1-n}} \tag{3}$$

where the burning rate exponent, "n," is measured for the lots of raw materials used in the manufacture of the propellant for the Castor motor, or in the absence of these data the burning rate exponent can be estimated from Figure 20.

The average burning rate of each propellant mix at a K_n of 231 is then determined as follows:

$$\bar{r}_2 = \frac{\Sigma r_2}{N} \tag{4}$$

where N = the number of rate values

The average burning rate of each propellant mix is then adjusted to the temperature at which the prediction of Castor performance is to be issued.

$$r_3 = \bar{r}_2\,(e)^{\sigma_K (T_f - T_1)} \tag{5}$$

where: $\sigma_K = \frac{d(\ln r)}{dT}$ temperature sensitivity of burning rate at a constant K_n, as measured for the propellant raw materials lots. (An average value of .00089 may be used in the absence of data for a particular propellant batch.)

T_f = temperature at which the Castor performance is to be predicted

T_1 = firing temperature of the test motors (normally 70°F)

After the above calculations have been made for each propellant batch loaded into the Castor motor, the overall average burning rate of the propellant batches loaded into the Castor motor is determined as follows:

$$r = \frac{\Sigma r_3}{N} \tag{6}$$

Equation 6 completes the adjustments to the batch test motor data. Knowing the burn rate of the propellant as measured by the batch test motors (Equation 6) and the characteristics of the Castor motor, the performance of the Castor motor can be predicted as follows:

$$\text{Burn rate} = r\ (1.11724) \tag{7}$$

$$\text{Web burning time, } t_w = 6.701/\text{burn rate} \tag{8}$$

$$\text{Effective burning time, } t_b = t_w + 0.060 \tag{9}$$

$$\text{Total impulse} = 273.2\ (\text{propellant weight}) \tag{10}$$

$$\text{Average thrust} = \frac{.86992\ (\text{total impulse})}{\text{burn time}} \tag{11}$$

$$\text{Consumable weight} = \text{propellant weight} + 131 \tag{12}$$

The above information can be used to modify the thrust-time and weight-time characteristics of the nominal Castor motor to predict a particular motor. This can be accomplished manually by multiplying each of the instantaneous performance values of the nominal tabulation by the following ratios to adjust for differences in web burn time and propellant weight.

$$\text{New t} = \text{Nominal t} \times \frac{t_b}{27.57} \tag{13}$$

$$\text{New F} = \text{Nominal F} \times \frac{27.57}{t_b} \times \frac{W_P}{7321} \tag{14}$$

$$\text{New Cons. Wt. Rem.} = \text{Nominal Cons. Wt. Rem.} \times \frac{W_P + 131}{7321 + 131} \tag{15}$$

A computer program is available at the Huntsville Plant for use in providing the tabulation of time, thrust, and weight remaining. The inputs required to operate the program are the predicted burn time, average thrust, and consumable weight obtained from Equations (9), (11), and (12), respectively.

6.3 THIRD STAGE

The predicted ballistic performance of any X259 flight motor is based on five static firings of the motor at AEDC in a simulated high-altitude environment and on static firings at ABL for casting powderacceptance. In the five AEDC firings the motor's ballistic performance characteristics--specific impulse, burn time, mass discharge coefficient, thrust and pressure-time trace configurations--were established. The flight prediction procedure was evolved from these vacuum test data.

The propellant burning rate of X259's cast from a given lot of casting powder is considered to be essentially constant from motor to motor. However, several lots of casting powder have been required through the years in the production of X259 motors. Due to lot-to-lot burning-rate variations, nozzle throat diameter changes have been necessary to maintain the motor operating pressure. Associated with all X259 motors cast from any one lot of casting powder is a particular nozzle throat size, and all motors within that lot are considered to be ballistically similar with respect to chamber pressure level, burn time, and specific impulse.

From the early AEDC tests of the X259, the specific impulse of the motor was established, together with the ratio of vacuum thrust to chamber pressure as a function of burn time. The F_V/P relationship determined at AEDC provides the means whereby vacuum thrust characteristics can be calculated for a different powder lot if chamber pressure data are available from an X259 test at sea level ambient pressure. This has been the case in the X259 development and production programs. Upon receipt of a new lot of casting powder, subscale motors are cast and fired at various K_n levels for preliminary acceptance of powder lot burning-rate characteristics.

One or more X259 quality assurance test firings are conducted to qualify the new powder lot and to obtain a burning rate prediction for flight motors. The vacuum-thrust curve is calculated by applying the AEDC F_V/P relationship and specific impulse to the static test pressure-time curve. Any changes in specific impulse resulting from a different nozzle throat size for the lot are properly accounted for in the vacuum thrust prediction procedure.

The prediction of X259 weight expended versus time is calculated as follows. The total propellant weight (main grain plus igniter charge) is added to the average inert weight consumed during burning time. The average inert weight consumed, as measured from the X259 AEDC tests, is 25 lbs. The instantaneous weight consumed is calculated from the equation:

$$W_c = \frac{\int_0^t F_V dt}{\int_0^{t_T} F_V dt} \qquad (1)$$

6.4 FOURTH STAGE

The X258C motor prediction procedure is similar to that of the X259, both in method and source of data; i.e., thrust and impulse predictions are based upon AEDC test results. All X258 motors cast to date and those remaining to be cast are from one lot of casting powder. Since the X258 motor is spin-stabilized in flight, the motor has also been spin fired in several ground tests. In the spin tests the propellant exhibits an approximate 15% increase in burning rate over the static test rate. Therefore, until recently, all predictions were based on the spin test results from AEDC. The prediction of vacuum thrust time curve for an X258 flight motor consisted of adjusting the nominal thrust level (determined from AEDC tests) such that the thrust-time integral equaled 281.2 times the unit's propellant weight. Weight expended was calculated by multiplying total expendable weight (propellant weight + 5.7 lbs. inert) by the ratio of impulse delivered to total impulse.

The X258 has been plagued by some phenomenon, encountered in the flight environment, which has caused the performance of the unit to be variable and generally lower in flights than sea level spinning/vacuum tests. Usually, the X258 motor flies without instrumentation, and it has not, therefore, been determined why motor performance is lower than expected. Some future Scout flights will include motor performance instrumentation--pressure transducers and accelerometers--and this will provide additional information. It is hoped this will help to define the problem. The deficiency has varied among flights with an approximately equivalent 1 to 2% degradation in specific impulse or approximately 4 pounds of unburned propellant. A reduction in either specific impulse or propellant weight burned results in similar flight trajectories. Therefore, the interim prediction procedure consists of using the specific impulse measured at AEDC, 281.2 seconds, but reducing the total propellant weight consumed by 4.1 pounds. The resultant thrust-time curve integral is lower than the AEDC measured value by an amount corresponding to 4.1 pounds of unburned propellant.

7.0 INSTRUMENTATION SYSTEMS

7.1 MOTOR MANUFACTURERS' FACILITIES

7.1.1 FIRST STAGE (Reference 4)

7.1.1.1 Chamber Pressure

Chamber pressure measurements are made with strain gage type pressure transducers manufactured by the Taber Instrument Corporation, specifically, a Model 206, with a range of 0 to 1000 psig (Specification AGC-32048/2). Each unit is compensated so the variation due to temperature is minimized in the range of 30 to 130°F.

The complete pressure measuring system consists of a Taber 206 pressure transducer, a dc power supply, an electrical shunt-calibration network, a dc amplifier, and a Beckman 210 analog-to-digital converter and recording system (ADC).

After completion of a static test firing, chamber pressure transducers are returned to the calibration laboratory for a cross check. If the temperature sensitivity, electrical shunt-to-pressure correlation, or zero offset exceeds the specification tolerance, the unit is adjusted and re-calibrated before it is reissued.

The maximum errors associated with low-level measurement of chamber pressure are shown in Table 13. The errors attributable to the transducer were determined by rigorous, repetitive laboratory calibrations, using a dead weight standard. Errors introducted by the strain gage channel and ADC were determined from repeated end-to-end calibrations of the data-transmission channels.

A root-square-summation of the individual errors yields a maximum inaccuracy of 0.19 $\pm$ 1.14% of-the-point, assuming the normal operating range (75% of full scale) for the transducer and the Beckman 210. The resulting standard deviation one sigma, repeatability for basic low-level chamber pressure measurements, is $\pm$ 0.38% of-the-point.

7.1.1.2 Axial Motor Force

Baldwin-Lima-Hamilton U3XXA force transducers (Specification AGC-32003/1) are used for force measurements. The thrust measurement system uses essentially the same components as the pressure measuring system.

In the range 10,000 to 50,000 lbf, maximum errors attributed to the load cells were determined from laboratory calibrations referenced directly to a dead weight standard. The force transducers are temperature compensated and trimmed to produce a standardized electrical output throughout the temperature range 30 to 130°F. Bending moments caused by alignment errors and dimensional variations in the thrust stand caused by deflection under load can

affect the measurement accuracy of the load cell. To minimize the structural effect, efficient and repeatable load-cell-isolation devices are used in all single and multiple degree-of-freedom thrust stands.

Since the thrust stand is considered an integral component of the force measurement system, an in-place calibration is essential for high-accuracy force measurements. A complete end-to-end force calibration of the measurement system is used to provide accuracy and repeatability and permit a complete analysis of all loads occurring during a test firing. Once the calibration factors have been established for a given stand, no further end-to-end calibration is required during the particular motor program.

The Aerojet calibration laboratories have a dead weight calibration capability from 0 to 60,000 lbf. Beyond 60,000 lbf., a secondary-standard calibration technique is used, with traceability to National Bureau of Standards (NBS) provided by proving rings. Furthermore, load cell hysteresis data are unobtainable because of facility limitations in the high-thrust range. Because of these variations in technique, the error analysis shown in Table 14 substitutes specification data for actual, observed variabilities.

Combining the individual errors by root-square-summation yields a maximum repeatability error of $\pm 0.43\%$ of-the-point at the normal operating range (75% full scale); the corresponding one-standard-deviation repeatability is $\pm$ 0.14% while the overall force measurement accuracy is -0.10% bias, $\pm 0.14\%$ repeatability, one sigma.

7.1.1.3 Propellant Weight

Propellant weight is determined by Cox and Stevens Weighing Kits comprised of three high-accuracy force transducers and a weight indicator. The accuracy of the weight kit is verified by a rigorous calibration procedure. Standard weights, certified Class C by NBS, are available for the motor-weight range, and weights kits are calibrated weekly against the appropriate standard weights.

Analysis of weight errors is separated into repeatability and accuracy. The repeatability parameters describe the variations in three redundant-calibration weighing procedures, accomplished during the weekly kit verification. In this context, repeatability includes random error in the weighing-kit load cells and indicator, together with human and systematic errors. The accuracy indicates the variation between the average of three redundant readings and the corresponding true calibration weight. Accuracy thus encompasses the repeatability parameters, along with random-bias variations of the equipment. The total weight-measurement error is therefore the root-square-summation (RSS) combination of the accuracy parameter and the Class C weight variability as indicated in Table 15 .

A RSS of the individual three sigma errors yields a maximum inaccuracy of -0.04 $\pm$ 0.19% of-the-point. The resulting one sigma repeatability for the basic weight measurement is 0.06%.

7.1.1.4 Definitions

The terms repeatability, bias, and accuracy, as used in this discussion, are defined as follows:

REPEATABILITY is the deviation from the average of data points obtained from repeated tests under identical, invariant conditions, i.e., the degree to which test results agree on a run-to-run basis with all test parameters held constant.

BIAS is the variation between the average value of a particular group of samples and the corresponding actual or reference value. As such, the term represents the average, inadvertent attenuation or amplification inherent in a measurement system.

ACCURACY is the overall ability of a measurement system to resolve a known physical quantity within a stated deviation. As such, the term accuracy encompasses both repeatability and bias.

For practical usage of weight measurement errors for the Algol motor, the accuracy and repeatability errors are the same since the bias error is removed by calibration of the weighing kit.

TABLE 13

ALGOL CHAMBER PRESSURE MEASUREMENT ERRORS

VARIABLES	PERCENT-OF-THE-POINT ERRORS	
	Bias	Repeatability (three sigma)
Transducer Variables		
(1) Linearity, hysteresis, and reproducibility	0.15	±0.47
(2) Electrical shunt to pressure correlation (30 to 130°F)	-0.01	±0.67
(3) Shift in calibration caused by use	0.08	±0.79
(4) Dead weight standard	--	±0.10
Channel Variables		
(1) Electrical calibration standard (2) ADC system (3) Amplifier	-0.03	±0.11
Root-square-summation (RSS)	--	±1.14
One-standard-deviation one sigma repeatability	--	±0.38
Accuracy one sigma	0.19	±0.38

TABLE 14

ALGOL AXIAL-FORCE MEASUREMENT ERRORS

VARIABLES	PERCENT-OF-THE-POINT ERRORS Bias	Repeatability (three sigma)
Measuring Load Cell Variables		
(1) Linearity, hysteresis, and reproducibility	--	±0.13
(2) Electrical shunt to force relationship (30 to 130°F)	--	±0.21
(3) Shift in calibration due to use	-0.00	±0.22
Thrust Stand Calibration Variables		
(1) NBS transfer standard	--	±0.10
(2) AGC working standard to NBS transfer standard	--	±0.15
(3) AGC working standard to measuring cell	--	±0.15
(4) Thrust stand and electrical system calibration	-0.07	±0.16
Channel Variables		
(1) Electrical calibration (2) ADC system (3) Amplifier	-0.03	±0.11
Root-square-summation (RSS)	--	±0.43
One-standard-deviation one sigma repeatability	--	±0.14
Accuracy one sigma	-0.10	±0.14

WEIGHING PROCEDURE FOR ALGOL IIB MOTOR

I. Empty Chamber Weight (approx. 1650 lbs.)
   A. Toledo Platform Scale-2000 lb. cap. in 1/4 lb. increments
   B. Scale accuracy 0.1% of indicated reading
   C. Scale is calibrated every 30 days
   D. Chamber weighed without tooling
   E. Zero set checked for each weighing

II. Insulated Chamber Weight (approx. 1960 lbs.)
   A. Toledo Platform Scale-2500 lb. cap. in 1/2 lb. increments
   B. Scale accuracy 0.1% of indicated reading
   C. Scale is calibrated every 30 days
   D. Chamber weighed without tooling
   E. Zero set checked for each weighing

III. Nozzle Weight, including bolts (approx. 550 lbs.)
- A. Toledo Platform Scale-1000 lb. cap. in 1/4 lb. increments
- B. Scale accuracy 0.1% of indicated reading
- C. Scale is calibrated every 15 days
- D. Nozzle weighed without tooling
- E. Zero set checked for each weighing

IV. Liner Weight (approx. 34 lbs.)
- A. Toledo Platform Scale-125 lb. cap. in 1/10 lb. increments
- B. Scale accuracy 0.1% of indicated reading
- C. Scale is calibrated every 15 days
- D. Zero set checked for each weighing
- E. Container is weighed before and after liner application

V. Igniter Weight (approx. 37 lbs.)
- A. Toledo Platform Scale-125 lb. cap. in 1/10 lb. increments
- B. Scale accuracy 0.1% of indicated reading
- C. Scale is calibrated every 15 days
- D. Zero set checked for each weighing
- E. Igniter weighed without tooling

VI. Final Assembly Weight (approx. 23,720 lbs.)
- A. Two Cox and Stevens 25,000 lb. load cells - 1 lb. reading increments
- B. Load cell accuracy 0.1% of indicated reading
- C. Load cells are calibrated every 60 days
- D. Zero set checked for each weighing
- E. Prior to lifting the motor, each load cell is checked against an NBS certified 12,000 lb. test weight.
- F. Motor is lifted with handling rings. Part No. and Serial No. of rings are recorded. (approx. wt. 1400 lb.)
- G. Motor is weighed three times, and the three readings are averaged.
- H. Front and rear load cell readings are added and the weight of the handling rings is subtracted.

VII. Propellant Weight
- A. The weights of the insulated chamber, liner, nozzle, hardware, and igniter are subtracted from the final assembly weight to establish the propellant weight.

TABLE 15

ALGOL PROPELLANT WEIGHT ERRORS

VARIABLES	PERCENT-OF-THE-POINT ERRORS Bias	Repeatability (three sigma)
(1) Weight measurement system reproducibility	--	±0.05
(2) Systematic errors	-0.04	±0.17
Accuracy	-0.04	±0.18
(3) NBS transfer standard	--	±0.05
Root-square-summation (RSS)	--	±0.19
One-standard-deviation one sigma repeatability	--	±0.06
Accuracy one sigma	-0.04	±0.06

7.1.2 SECOND STAGE

TX-33 motors are static tested at the Army Test and Evaluation Laboratory, Test Area 5, Redstone Arsenal. The TX-3 ballistic test motors are static tested at Thiokol, Test Facility B-7620. Digital data systems and oscillograph records are used by both agencies for data acquisition during static test of both the TX-33 and TX-3 motors. Both agencies use transducers providing state-of-the-art accuracies and recording equipment approaching state-of-the-art.

TX-33 Static Tests

TX-33 motors are fired in the horizontal position on a tracked dolly. One double bridge, main load transducer measures motor thrust during the static test. The test assembly (motor, tracked dolly, and mechanical adapters to the main load transducer) has a low natural frequency response to changes in motor thrust. The natural frequency of the system is increased by preloading the test assembly against the main load transducer. This preload is adjusted by two preload thrust transducers, and the outputs of these transducers are recorded during motor test so that any shift of preload during static test may be incorporated in the thrust determination.

TX-33 motor chamber pressure ports and pyrogen chamber pressure ports are located at the head end of the motor. Fittings and short oil-filled lines connect the pressure ports to their respective transducers.

Specifications and capability of the Test and Evaluation Laboratory equipment used for pressure and thrust measurements on TX-33 motors are as follows:

1. Transducers

A. Pressure Transducers

Pressure transducers used for the measurement of motor chamber pressure and pyrogen pressure have less then 0.25% combined hysteresis and linearity. Temperature compensation is 0.0035%/°F. The natural frequency of the high frequency pressure transducer is at least 15,000 cps.

B. Thrust Transducers

The main and preload thrust transducers have less than 0.2% combined hysteresis and linearity. Temperature compensation is 0.0008%/°F.

2. Recording Equipment

A. Oscillograph Recording System

Consolidated Electrodynamics Corporation (CEC) Model Recorders are used almost exclusively. A full range of galvanometers is used ranging in frequency band pass from DC to 5 KCPS. The following schedule is normally used with the assigned data.

Data	CEC Galvanometer	Band Pass CPS
Motor Chamber Pressure	7-346	0.190
Igniter Chamber Pressure	7-362	0-2500
Main Motor Thrust	7-343	0-200
Preload Thrust	7-348	0-60

Three inches of galvanometer deflection are used for the maximum values of pressure and thrust. This span coupled with paper shrinkage and expansion limits the accuracy of the oscillograph record. Resolution is approximately $\pm$ 1/40 inch in 3 inches.

B. Digital Systems

Pressure and thrust are acquired with a Packard Bell Computer Corporation digital data handling system designed and fabricated specifically for the Army Test and Evaluation Laboratory. This system can acquire up to 150 channels of data and transmit these data by microwave link to an IBM 7094 computer. This transmission of data during static test permits data reduction to be performed immediately after the test. The sample rate of the system is 15,000 samples/second. The code used with this system is 14 bit binary. The maximum resolution of this system is one bit in 9999 bits or 0.001%. The linearity is 0.01%. The transducers become the limiting factor when determining the accuracy of data obtained with the system. Special attention must be given to determining the sample rate and associated frequency response with the digital system. One thousand uniformly distributed samples/second/channel are used with TX-33 data acquisition. Using an established 8 sample/cycle for frequency response determination, then 0 to 125 cps is established as the frequency response of digital data.

TX-33 Test Data Reduction

Pressure and thrust definitions reported for data recorded during the static firings of TX-33-35 (XM 33E5) rocket motors are taken from Thiokol Standard Definitions and Model Specification SP-425 definitions. Until recently, all pressure and thrust data were taken from the oscillograph records by utilizing analog techniques. Presently, data is being recorded by digital and analog systems. Dual independent channels of pressure and thrust are being recorded during static firings.

Two oscillograph traces are available to Thiokol, each of which contains one channel of pressure and one channel of thrust. Each channel on the oscillograph trace has an electrical calibration recorded prior to motor ignition and again following motor operation. This consists of from 5 to 6 step levels. Linearity of calibration between steps normally remains within $\pm$0.5% of full-scale deflection. Full-scale deflection is chosen as that step level which corresponds with the average pressure and thrust during motor operation.

This level is used as a deflection factor, D.F. (psi/inch or lbs./inch), when reading integrals or amplitudes. When a thrust or pressure average falls between two calibration steps, the average of the steps is taken for full scale and for determining deflection factors. If calibration linearity based on full scale exceeds $\pm$ 1% non-linearity between steps, the alternate oscillograph trace is utilized if more linear. When both oscillograph traces indicate a calibration non-linearity exceeding $\pm$ 1%, calibration steps are plotted and data are read from a non-linear curve.

Integrals taken from an oscillograph trace are determined as follows:

$$\frac{\text{Area x D. F.}}{\text{Recorder speed}} = \int P dt \text{ or } \int F dt$$

Area = area under curve as read with a polar planimeter ($in.^2$)

D. F. = deflection factor taken from calibration (psi/inch or lbs./inch)

Speed of Recorder = speed of oscillograph recorder (inches/sec.)

Speed of the recorder is determined by measuring the length of the trace under the total area of the pressure or thrust curve and dividing the length by total operating time or

$$\frac{\text{Total length (inches)}}{\text{Total time (seconds)}} = \text{in/sec.}$$

A point is then chosen at approximately one-half of total operating time. The time from ignition to this point is read plus the length in inches. By dividing this length by the speed of the recorder, there should be a correlation of $\pm$0.003 second with the midpoint time. If this speed is nonuniform, the pressure and thrust curves are marked off in positions and speed is determined for each portion of the area read.

Data are taken from the alternate oscillograph trace as a check for correlation. When digital data are available, these data are used as a check for correlation. All pressure and thrust curves are plotted. Completed data are forwarded to the Engineering Department for review before final data are released.

The digital printout from the Packard Bell System provides a tabulation of the following data:

1. Time
2. Pressure data points (psia)
3. Thrust data points
4. Cumulative pressure integrals
5. Cumulative thrust integrals

TX-3 Static Tests

Specifications and capability of Thiokol equipment used for recording pressure-time data from TX-3 motor static tests are as follows:

1. Transducers

Pressure transducers used in the measurement of TX-3 motor chamber pressure have less than 0.25% combined hysteresis and linearity. Temperature compensation is 0.005%/°F from 15 to 115°F.

2. Recording Equipment

A. Oscillograph Recording System

Consolidated Electrodynamics Corporation recorders are used for data acquisition. The accuracy and frequency limitations are as described for the Army Test and Evaluation Laboratories system used for TX-33 tests.

B. Digital System

A Systems Engineering Laboratories digital system was designed and installed in the Thiokol test facility. An IBM 7070 computer is used for data reduction. One thousand samples/second/channel are used for data acquisition. The system uses a 15 bit binary coded decimal code. Linearity is 0.1%. Maximum resolution is one bit in 7999 bits. The transducers become the limiting factor in determining the accuracy of data obtained with this system.

TX-3 Test Data Reduction

TX-3 batch check data are recorded simultaneously by digital and analog systems. Digital tapes consist of two channels of recorded pressures, each independent of the other. Oscillograph traces consist of two channels of recorded pressure, each independent of the other. Data from the digital system are used in test evaluation. The analog system is used for redundancy. Necessary information pertinent to final data output for each motor tested is transposed to standard forms. Such information, along with the digital data tapes, is transferred to the computer facilities where it is key punched and fed into the programs when processing data tapes. This program is identified as G-2133. Final output from program G-2133 is returned to the Data Reduction Group for verification. The validity of digital data is further verified by reducing redundant data from the oscillograph recordings. This consists of randomly selecting 10% of the TX-3 motors tested and reducing the data by analog techniques.

When digital data are not acquired and analog recordings are the primary data source for reduction of TX-3 data, procedures are the same as applied to the TX-33-35 motor.

In order to maintain accuracy in data reduction techniques, the following procedures have been established.

1. Calibration curves and deflection factors are checked by one individual and verified by another.

2. Redundant data are never reduced by an individual who has reported the primary data. Data from each individual should correlate within ± 1.0%.

3. Integrals under the plotted curves of data transposed from oscillograph records should be within ± 1.0% of integrals read directly from the oscillograph trace.

4. All analog data should compare within ± 1.0% of digital data when such correlation is performed.

5. A minimum of two channels per system is recorded for pressure or thrust in order to provide correlation. This correlation between channels should remain within ± 1.0% when data are analog and ± 0.5% when data are digital.

6. A computer program has been established as a validity check for TX-3 reported data. This program screens and displays record errors and performance abnormalities in the TX-3 data.

7. Electrical calibrations are given preference over dead load calibrations. When dead load calibrations are used, electrical calibrations are taken immediately following such in order to provide correction factors due to a change in gage voltage or amplifier gain.

Test Temperature

Temperature conditioning of the TX-33 motor is performed at the Army Test and Evaluation Laboratory environmental facilities. In accordance with the test requirements specified by Thiokol, the motors are subjected to the required temperature ± 5°F for a minimum conditioning time of 6 days.

The motor assembly is removed from the conditioning chamber, transported to the test site, and then static tested. Thiokol test requirements specify that the test shall be completed within 1-1/2 hours after removal from the pre-test conditioning chamber. Up until immediately prior to test, motor cavity temperature is monitored.

Temperature conditioning of the TX-3 ballistic test motor is performed at Thiokol in environmental facilities adjacent to the test facilities. The conditioning temperatures are maintained to within ± 5.0% of the required test temperature.

The TX-3 ballistic test motor is temperature conditioned for a minimum of 8 hours prior to static testing. Insulated carrier boxes are also conditioned at the same temperature. The motors are placed in the carrier boxes prior to removal from the conditioning chamber and transported to the static test site. It is required that all TX-3 motors be tested within 20 minutes after removal (in carrier boxes) from the conditioning chamber and within 5 minutes after removal from the carrier box. The motors are returned to the conditioning chamber if either of these times is exceeded.

Weighing

The equipment and procedures used by Thiokol to determine the reported weights of the Castor motor are discussed in this section. The section is subdivided into a discussion of each of the component weights. Where more than one weighing operation is involved to determine a component weight, statistical techniques are employed to estimate the error involved. All scales used to measure component weights of the Castor motor are accurate to within 0.1% of the full scale range.

The motor case weight is determined by a direct weighing of the empty motor case prior to the application of liner and insulation. A Fairbanks Morse scale, graduated in two pound increments, with a capacity of 2,000 pounds is used. The scale is calibrated every 60 days and has an accuracy of 0.1% of the full scale deflection. The nominal weight of the Castor motor case is 803 pounds. Based on the reported scale accuracy, a maximum scale error of $\pm$ 2 pounds, approximately $\pm$ 0.25% of the measured value, is possible.

The liner weight is determined by weighing the liner material before and after each lining operation, the difference between these two weights representing the liner weight applied to the motor case. A Toledo scale, graduated in 0.1 pound increments, with a capacity of 200 pounds is used. The scale is calibrated every 90 days and has an accuracy of 0.1% of the full scale deflection. A total of six coats of liner is applied to each motor, involving twelve weighing operations. Based only on the scale accuracy, a weighing error of $\pm$ 0.2 pound could be encountered in each of the twelve measurements. The total weight error can be estimated best by a statistical addition of the weighing errors where the total variance is equal to the square root of the sum of the individual variances. This approach estimates the maximum total weight error to be 0.69 pound or 0.41% of the nominal 170 pounds liner weight.

The weight of the forward and aft insulation is determined by obtaining the difference in material weight before and after installing the insulation. The forward and aft insulation weights are determined using shadowgraph scales, graduated in 0.005 pound increments, with a capacity of 22 pounds and 75 pounds, respectively. Both of these scales are calibrated every 90 days and are accurate to 0.1%. Based on the reported scale accuracy, each weighing operation required to determine the weights of the forward and aft insulation could result in a maximum error of $\pm$ 0.022 pound and $\pm$ 0.075 pound, respectively. A statistical consideration of the four weighing operations involved yields an estimate of the total weight error of 0.11 pound.

The nozzle assembly is weighed separately on a Toledo scale, graduated in 2 pound increments, with a capacity of 1,000 pounds. The scale is calibrated every 60 days and is accurate to 0.1% of full scale deflection. The nominal weight of the nozzle assembly is 521 pounds. Based on the reported scale accuracy, a maximum scale error of $\pm$ one pound, approximately $\pm$ 0.20% of the measured value, is possible.

The total assembly weight (the total weight of all components except the nozzle closure) is determined by direct measurement using an 11,500 pound capacity Toledo scale which is graduated in 2 pound increments. The scale is calibrated at 60 day intervals and is accurate to 0.1% of full scale deflection. Based on the reported scale accuracy, a maximum scale error of 11.5 pounds, approximately $\pm$ 0.13% of the measured weight, is possible.

The pyrogen unit is weighed separately using a 75 pound capacity Toledo scale graduated in one ounce increments. The nominal weight of the pyrogen unit is 14 pounds. The scale is calibrated at 90 day intervals and is accurate to within 0.1% of the scale range. Based on the reported scale accuracy, a maximum scale error of 0.075 pound, approximately 0.5% of the measured value, is possible.

The pyrogen ring and nozzle closure are weighed separately using a 20 pound capacity Trinner scale graduated in 0.01 pound increments. The nominal weights of the pyrogen ring and nozzle closure are 5 pounds and 7 pounds, respectively. The scale is calibrated at 90 day intervals and has an accuracy within 0.1% of scale range. Based on the reported scale accuracy, a maximum scale error of $\pm$ 0.02 pound is possible.

The propellant weight is determined by subtracting from the total assembly weight the weight of the case, nozzle, liner, insulation, pyrogen unit and pyrogen ring. Since the error in the reported propellant weight is a result of each of the component errors, a statistical combination of these errors can be used to estimate the propellant weight accuracy. The total error in each of the component weights is assumed to be the result of two factors: 1) scale accuracy and 2) reading accuracy.

The scale accuracy has been previously reported in the discussion of each component. The accuracy of reading a given scale is a function of the scale graduation. In developing an estimate of the reading error, it was assumed that the error would not exceed one-half of the graduation, i.e., the scale could be read at least to the nearest graduation.

Statistically combining these two sources of error to obtain the total error in the reported weight yields the following:

COMPONENT	SCALE ERROR (lb)	READING ERROR (lb)	TOTAL ERROR (lb)
Case	± 2.0	± 1.0	± 2.236
Liner	± 0.69	± 0.17	± 0.710
Insulation	± 0.11	± 0.00	± 0.110
Nozzle assembly	± 1.0	± 1.0	± 1.414
Total motor assembly	± 11.5	± 1.0	± 11.545
Pyrogen unit	± 0.075	± 0.03	± 0.081
Pyrogen ring	± 0.02	± 0.00	± 0.020

Assuming that the total errors reported in the above table are three sigma errors, then the standard deviation for the weight error is one-third the root-sum-square of the tabulated total error values.

The standard deviation of the error in the reported propellant weight is estimated to be ± 3.96 pounds. Since the nominal propellant weight is 7321 pounds, the standard deviation expressed as a percentage is 0.054%.

7.1.3 THIRD STAGE

7.1.3.1 Static Test Instrumentation

The X259 motors are static fired at simulated altitude conditions at AEDC and at sea level conditions at Allegheny Ballistics Laboratory (ABL). The discussion which follows concerns the sea level firings only, since AEDC instrumentation is discussed in Paragraph 7.2.

The pressure and force measurements are recorded on the ABL x-range Data Acquisition System using oscillograph and analog to digital magnetic tape equipment. The digital tape is transcribed to engineering units and plotted by the computers. The transducers used in these tests are of the resistance strain gage type and their response to pressure or force and shunt calibration is accurate to 0.1%. The digital recording equipment is repeatable to one part in 1000 in response to shunt calibration applied to the transducers.

The transducers used at ABL were purchased from BLH, Alinco, and Revere. These transducers were purchased to Hercules Specifications HXS 1-86 and HXS 1-87, which describe a transducer with accuracy of 0.1% for the expected firing uses and environments.

The X259 is static fired in a roller stand while contained in a motor corset which allows for chamber expansion. The method of hold down is the use of large diameter straps tied to the firing bay floor. The estimated error in thrust measurements is 1.0%, allowing for the uncertain error contributed by the firing stand.

7.1.3.2 Weighing

The X259 motor assembly and component weights are derived from a series of weighings conducted during the motor processing at ABL. These

weighings are conducted using load cells and scales. A breakdown of the weighings and accuracies is shown below:

	One sigma (percent)
Chamber weighing	0.07
Nozzle weighing	0.09
Igniter weighing	0.21
Chamber grain assembly weighing	0.04
Propellant weight	0.04
Total motor assembly weighing	0.06

The chamber and nozzle are weighed on scales accurate to 0.2 lb. upon receipt from the vendor. The chamber is barrier coated with epoxy resin and embedded. The resin weights and embedment powder installed into the chamber are weighed on scales accurate to 0.2 lb. The chamber is cast and cured and the chamber-grain assembly is weighed after machining with a 3000 lbs. load cell accurate to 0.1%. The propellant grain weight is obtained by subtracting the chamber, barrier coat and embedment resin, and handling ring weights from the chamber-grain assembly weight. The total propellant weight is obtained by adding the igniter propellant weight to the propellant grain weight.

The total loaded motor weight of the motor is measured prior to shipment. This weight is obtained using 2000 lb. load cells accurate to 0.1% of the full readings, and subtracting the weights of the two handling rings, each known to an accuracy of 0.2 lb.

7.1.4 FOURTH STAGE

7.1.4.1 Static Firing Instrumentation

X258 motors are static fired at simulated altitude conditions at AEDC and sea level conditions at ABL. The most recent X258 static firings (at AEDC) were conducted with the motor spinning at 200 rpm to simulate the radial forces on the motor during flight. At the present time, only AEDC pressure and thrust data have been utilized for flight performance analysis. The AEDC instrumentation system is discussed in Paragraph 7.2.

7.1.4.2 Weighing

The X258 motor assembly and component weights are derived from a series of weighings conducted during the motor processing at ABL. These weighings are conducted using 500 lb. load cells and scales. A breakdown of the weighings and accuracies is shown on the following page.

	One sigma (percent)
Chamber weighing	0.052
Post embedment chamber weighing	0.074
Nozzle assembly weighing	0.014
Igniter assembly weighing	0.048
Chamber-propellant assembly weighing	0.032
Propellant weight	0.034
Total motor assembly weighing	0.044

The chamber weighing is conducted upon receipt of the chamber from the vendor. This weighing is performed on scales accurate to 0.01 lb. The nozzle assembly weighing is also conducted upon its receipt from the vendor using scales accurate to 0.01 lb.

The chamber is then prepared for hydrotest and subsequent casting by adding a barrier coat of epoxy resin and a layer of embedment resin and casting powder. This assembly is weighed on scales accurate to 0.01 lb. The assembly is then cast and cured, and after machining the chamber grain assembly is weighed on scales accurate to 0.5 lb. The propellant grain weight is obtained by subtracting the inert chamber weight from the chamber-grain assembly weight. The inert chamber weight is obtained by subtracting the weight of embedment powder from the post-embedment chamber weight. The total propellant weight is obtained by adding the igniter propellant weight to the propellant grain weight.

The total loaded weight of the motor is measured prior to shipping the motor. This weight is obtained using two 500 lb. load cells, each of which is accurate to 0.1% of the applied load. The weight of the two handling rings, which is accurate to 0.01 lb. per ring, is subtracted from the measured value to give a total motor weight.

7.2 ARNOLD ENGINEERING AND DEVELOPMENT CENTER INSTRUMENTATION

Practically all measurement transducers are of the strain gage type, the exceptions to this rule are in temperature sensing and the basic time correlation generator. Temperature sensing is accomplished by the standard thermocouples method and with a Pace 150°F reference junction.

The various pressures are monitored by units manufactured by Teledyne or Stathem depending upon the pressure range required. If the pressure is equal to or greater than 50 psia, a Teledyne bonded strain gage unit is used; but if the pressure is equal to or less than 50 psia, then a Stathem unbonded strain gage unit is used. By going to the bonded strain gage for the higher pressures, a high frequency response with a very small, if any, loss in sensitivity is achieved; however, for the small pressure ranges, some frequency response is sacrificed by using the unbonded strain gage but a higher sensitivity to pressure changes is achieved. All of the pressure transducers are calibrated before and after each test in the Calibration Lab against standards which are checked by the NBS on a periodic basis.

Thrust levels are measured by strain gage load cells manufactured by Revere or BLH and a minimum of four cells is used per test run. The load cells are also calibrated before and after each test firing. This is accomplished under simulated conditions of the test firing. The actual test motor is installed on the cradle in the test cell and the cell pressure is reduced to the test altitude to simulate the actual firing conditions. Test weights are used on the end of a balance arm with a 10:1 ratio from the balance point, and this calibration force is applied directly to the motor cradle with the motor installed. The weights are calibrated by using a special load cell in place of the test load cells. The special load cell is precalibrated by NBS weights. This special cell has its own force readout gage and therefore is a self-contained force measuring device. At the time the test cell load weights are being calibrated with the special load cell, the force of the weights is applied, through the balance arm, directly to the special load cell. After the weights have been calibrated, the load cells to be used during the test firing are installed and electrically as well as mechanically connected for the test. By applying the force of the calibrated weights to the motor cradle the entire system is calibrated. The estimated maximum difference or delta between the pre- and post-run calibrations is 0.05% of maximum range.

The temperature monitoring system has a very small series resistor in the line to provide a means of calibrating the monitoring equipment. By applying accurate current steps through the series resistor and monitoring the voltage drop across the resistor, the entire temperature circuitry is calibrated and also checked for continuity. No actual calibration of the sensor and monitoring system is performed using heat or cold applications to the thermocouple. The standard temperature versus voltage characteristics of the thermocouple is used for data reduction. The voltage calibrations are used only to define the gain or sensitivity of the recording system.

Motor weighing is performed on a platform type scale with a stated accuracy of 0.25%. The weighing is done before the motor is placed in the test cell and also after the test run when the motor is removed from the test cell.

An individual power supply is used for each measurement channel reducing the problems of cross-talk, ground loops and power surges.

The data received from the measuring sensor may be recorded on a CEC oscillograph, strip chart or tape recorder. The oscillograph and the strip chart record the analog data in real time and are useful for quick look analyses or to define the time some instantaneous event occurred. This method of data reduction is less accurate, however, than the rate pulse tape recorder method which feeds directly into the 7074 or 1102 computers for data analyses. The oscillograph has the least accuracy due to problems of sensitivity and readability. This accuracy will run a little over 1.0% in most cases. The strip chart units have a better readout ability and greater sensitivity, and therefore the accuracy will be about 50% better

than that of the oscillograph. The tape recorded data, since it is adaptable to a direct computer routine without manual interpretation, is definitely the most accurate method of data recording.

A high degree of accuracy is accomplished at AEDC through the use of multiple, redundant, measurement sensors for all critical measurements. The calibration data received from the pre-test and post-test run calibrations, for each of the redundant sensors, are fed into the computer and examined for abnormal deviations among the data from each sensor. Abnormal values are rejected and the remaining data from each sensor is smoothed by integration. The smoothed data from all sensors are compared by the computer. The best average curve is then defined, plotted, and the computed accuracy is provided according to the amount of scatter in the data from each sensor and the differences in smoothed data between sensors.

The actual test run data are handled in the same way as the calibration data in the computer. The data are examined for abnormal deviations among the data from each sensor. Any abnormal deviations are compared with any in the original calibration data as well as with any in the data from redundant sensors used for the same measurement. Through this comparison technique, the outlying deviations in the data can be defined as a real excursion of performance or as a discrepancy within one sensor system. If the deviation is not real, then it is rejected and the remaining data are smoothed by the computer. The computer then integrates all redundant measurement data and again takes the statistical average of the data as being the actual data information. Again, the computer is fed all calibration as well as test data and an accuracy is defined for the measurement.

The accuracy of the AEDC test facility has been represented (Reference 5) by one sigma errors of 0.15% in thrust integral measurements and 0.13% in pressure integral measurements when in-place calibration is used.

7.3 SCOUT VEHICLE INSTRUMENTATION

7.3.1 TELEMETER

The telemetry system is an 18 channel PAM-FM-FM system.

PAM commutation consists of a double deck 30 x 5 switch. Cross-strapping of switch points is used to provide sampling rates for the required frequency response. The range of response is from 1 to 5 cps for the functions monitored.

Functions monitored primarily for motor performance evaluation are:

Measurement	Commutated Channels Deck A	Deck B	Contin. Chans.	SCO (KC)	Location
Head-cap Pres. 1st Stage	-	1	1	30.00	Lower "B" Trans.
N_2 Pres., 2nd Stage	-	1			Transition "B"
N_2 Pres., 3rd Stage	-	1			Upper "C" Trans.
0, 1/2 & Full Scale Calib.	-	5			Transition "D"
Head-cap Pres. 2nd Stage	3	-		40.00	Lower "C" Trans.
Head-cap Pres. 3rd Stage	3	-			Head-cap Adapter
Long. Accel.	-	-	1	14.50	Transition "D"
N_2 Amb. Temp.		1 of 4		30.00	Upper "C" Trans.

Calibration curves are provided for end instruments, sub-carrier oscillators and other telemetry equipment. Copies of calibration curves are supplied with each telemetry system. End instrument signal simulators, to provide three-point calibration of measurement data channels and to simulate OFF-ON functions (relay and switch) actuations, etc., are provided for use in systems tests and pre-launch checkout.

7.3.2 TRANSDUCERS

7.3.2.1 Head-cap Pressure

Head-cap pressure transducers are the absolute pressure, bourdon-tube type. The response time to 63% of the applied pressure is 50 milliseconds or less. The specified error limits are:

Error Source	Error Limit +% of 800 psi Range
Static pressure	0.9
Temperature, 0-165°F	2.0
Vibration, 16-35 "g," 25-2000 cps	
Peak (except resonance)	1.0
Peak (resonance)	2.0
Acceleration Sensitivity (% per "g")	
Lateral and Transverse Axes	0.05
Longitudinal Axis	0.004

7.3.2.2 Longitudinal Acceleration

Longitudinal acceleration transducers of a -4 "g" to + 20 "g" range have the following accuracy characteristics:

Error Source	Error Limit
Output AC ripple	1% rms or less of full scale
Linearity	1% or less of accel. span (best straight line)
Hysteresis	0.1% or less of accel. span
Resolution	Continuous
Balance control	± 10% or more of full scale from zero "g" condition
Natural frequency	135 cps nominal
Damping	60% to 85% at 75°F (nominal)
Cross talk	0.010 G/G

7.3.3 COMPARISON OF HEAD-CAP PRESSURE WITH LONGITUDINAL ACCELERATION, TELEMETRY DATA

Both head-cap pressure and longitudinal acceleration are related to the total vacuum impulse delivered by a motor in flight. Head-cap pressure integrals should vary from motor to motor by no more than can be attributed to actual variation in 1) throat area, 2) characteristic velocity, 3) propellant weight and 4) average error in head-cap pressure measurement throughout burning time. Longitudinal acceleration integrals should vary among vehicles, for a given stage, by no more than the actual variation in 1) vacuum specific impulse, 2) variation in stage mass, 3) thrust misalignment, 4) aerodynamic and jet vane drag, 5) ambient pressure at the nozzle exit, 6) propellant weight and 7) error in measurement of longitudinal acceleration throughout burning time.

A limit on the amount of actual variation in the head-cap pressure integrals can be estimated conservatively by assuming that characteristic velocity varies as much as specific impulse, and combining this variable with the variations of throat area and propellant weight. The Algol and the Castor both afford sufficient data for investigation:

Variable	Estimate of Actual Variation			
	Algol		Castor	
	σ, %	σ^2	σ, %	σ^2
Specific Impulse	0.18	0.031	0.094	0.01
Throat Area	0.38	0.144	0.56	0.31
Propellant Weight	0.23	0.053	0.20	0.04
Sum		0.228		0.36
Pressure Integral	0.48		0.60	

The variation in integral values of head-cap pressure acquired by telemetry is illustrated in Figures 42 and 43 . Allowing for the actual variation in pressure data, the error in measurement can be estimated:

Mode	Variation in Head-cap Pressure			
	Algol		Castor	
	σ,%	σ^2	σ,%	σ^2
Measured	1.87	3.50	1.89	3.57
Estimate Actual	0.48	0.23	0.60	0.36
Difference		3.27		3.21
Estimated Error	1.8		1.8	

The error in measurements of longitudinal acceleration has not been estimated in this same manner. However, the acceleration data have been a basis for calculating a vacuum impulse value for flight motors, and an allowance for variation in actual vacuum impulse will net an estimate of the error in such calculations of impulse:

Variable	Estimate of Actual Variation			
	Algol		Castor	
	σ,%	σ^2	σ,%	σ^2
Vacuum Specific Impulse	0.18	0.031	0.094	0.01
Propellant Weight	0.23	0.053	0.20	0.04
Sum		0.084		0.05
Vacuum Impulse	0.29		0.22	

The variation in vacuum impulse, calculated from longitudinal acceleration telemetry, is illustrated in Figures 44 and 45 . The error contribution to the apparent variation is estimated to be:

Mode	Variation in Vacuum Impulse			
	Algol		Castor	
	σ,%	σ^2	σ,%	σ^2
Apparent	2.47	6.10	2.07	4.28
Estimated Actual	0.29	0.08	0.22	0.05
Difference		6.02		4.23
Estimated Error	2.5		2.06	

Some portion of this error combination is not assignable to error in measuring longitudinal acceleration. The contribution of errors in the attributes (previously numbered 2, 3, 4, and 5) has not been established.

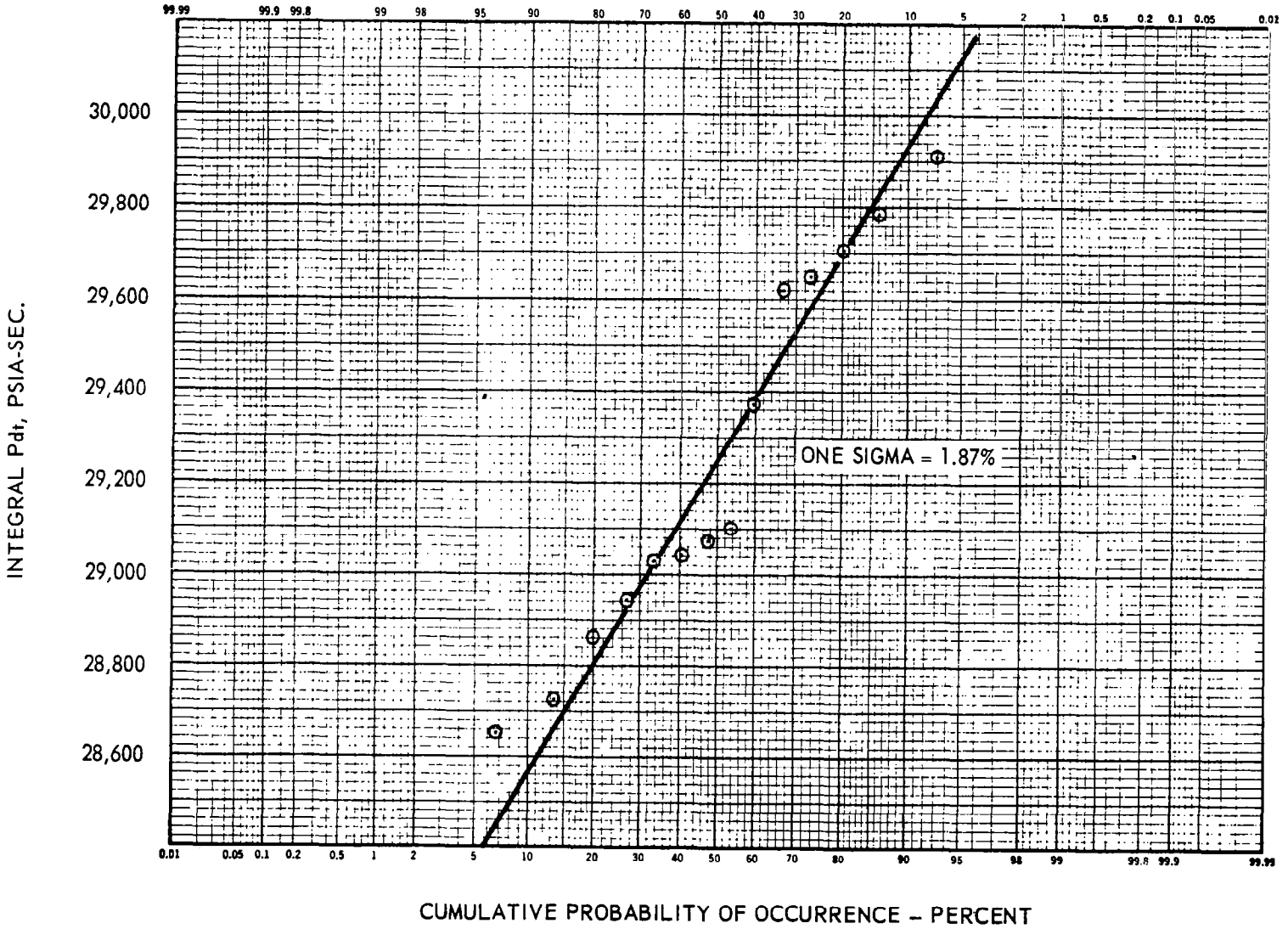

FIGURE 42 ALGOL FLIGHT DATA, VARIATION IN HEAD-CAP PRESSURE INTEGRAL

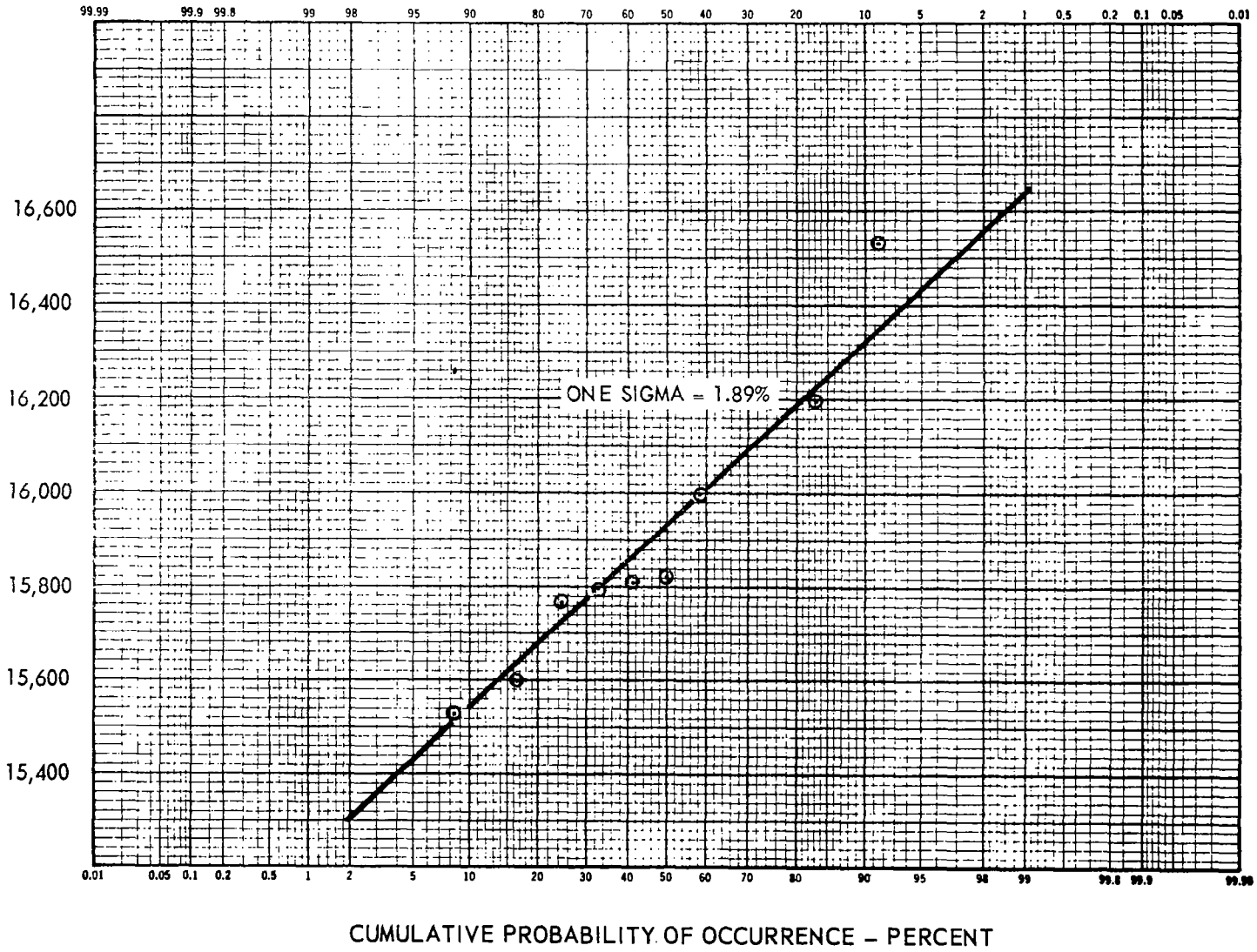

FIGURE 43 CASTOR FLIGHT DATA, VARIATION IN HEAD-CAP PRESSURE INTEGRAL

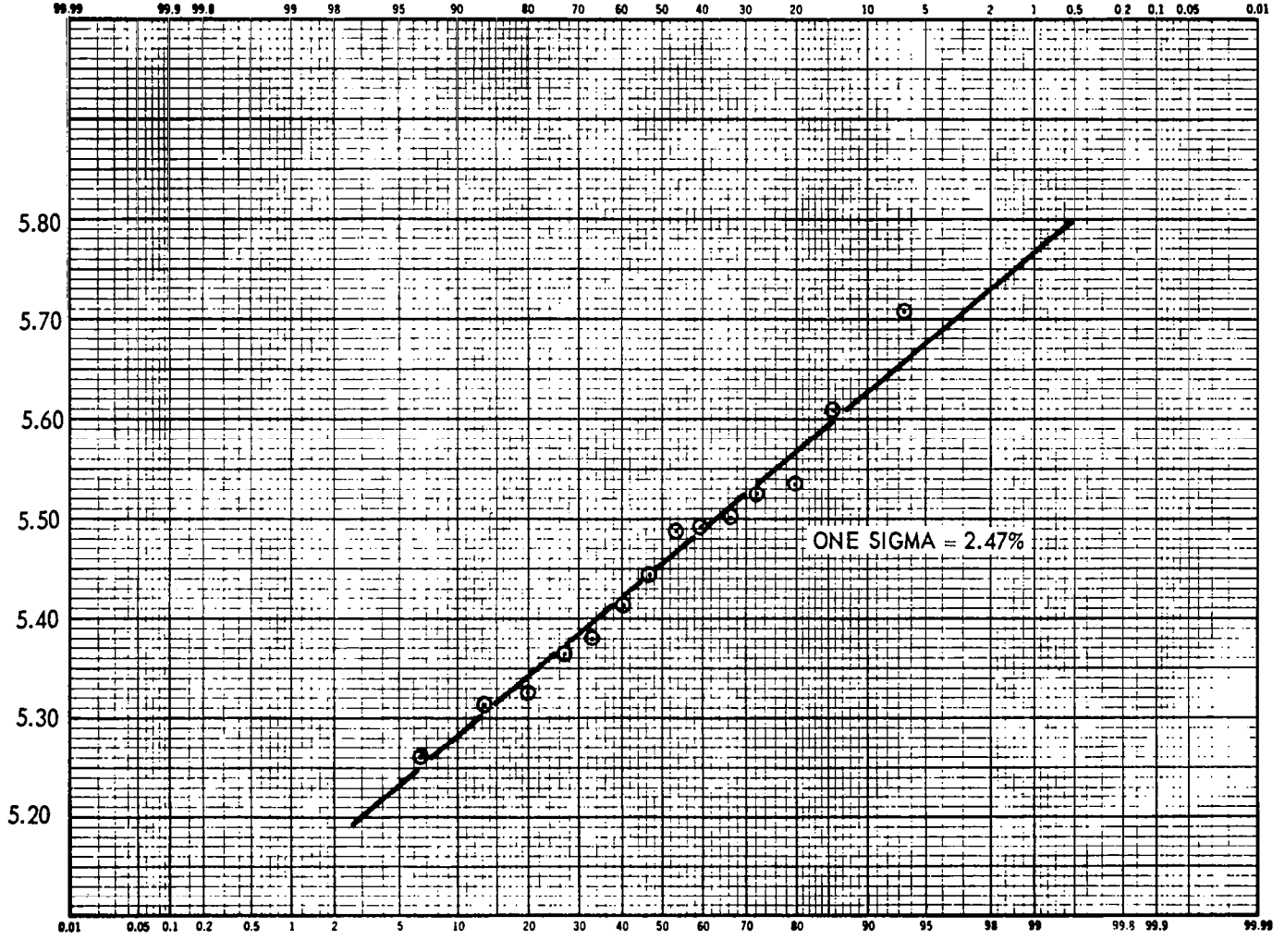

FIGURE 44 ALGOL FLIGHT DATA, VARIATION IN APPARENT VACUUM IMPULSE

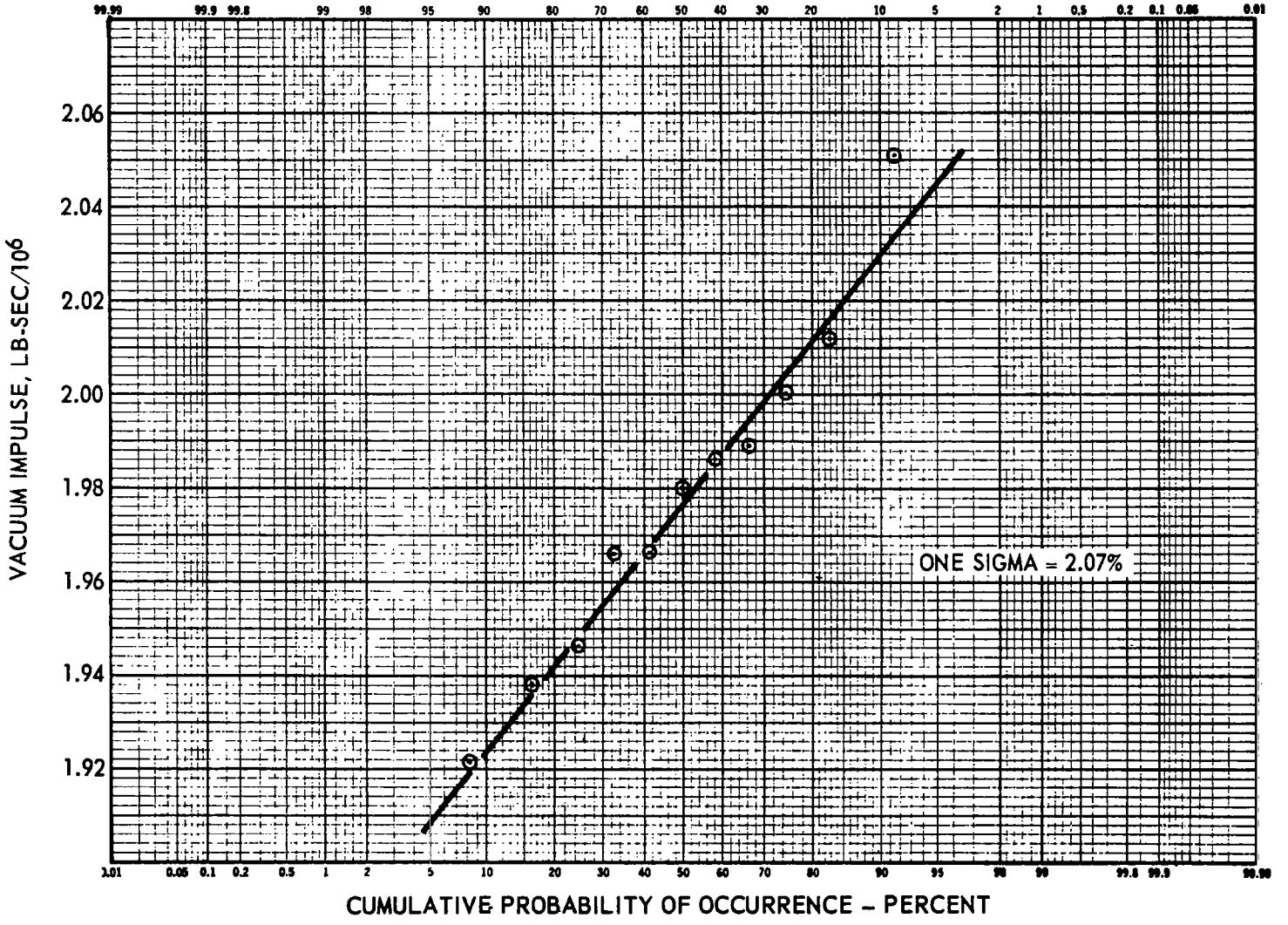

FIGURE 45 CASTOR FLIGHT DATA, VARIATION IN APPARENT VACUUM IMPULSE

8.0 SPECIAL STUDIES

8.1 FIRST STAGE

8.1.1 EFFECTS OF PROPELLANT WEIGHT VARIATION

The propellant weight for 18 Algol motors is correlated with the total impulse and with the pressure integral in Figures 46 through 48. Also, the total impulse is correlated with the pressure integral in Figures 49 and 50. The theoretical or predicted values for the parameters follow the dashed lines. The results are summarized below:

		STANDARD DEVIATION - PERCENT	
		STATIC	FLIGHT
Propellant Weight	Lb	0.085	0.227
Total Impulse	LBF-Sec	0.537	2.053
Pressure Integral	PSIA-Sec	0.826	1.253

DATA SOURCES: 8 STATIC TEST MOTORS
10 FLIGHT MOTORS

These results indicate that the measurement of pressure integral for static and flight motors is accomplished with about the same accuracy. However, the measurement of total impulse of flight motors shows four times the error in measurement of total impulse for static motors.

8.1.2 PROPELLANT WEIGHT VERSUS PROPELLANT DENSITY

The propellant weights for 21 Algol motors are compared with the average propellant densities for the motors in Figure 51. The variation of the weight values is almost four times that of the density values. Also, there is very little correlation of the data with the theoretical line.

8.1.3 STATIC TEST SPECIFIC IMPULSE VERSUS CHAMBER PRESSURE

The specific impulse values for the statically tested Algol motors are correlated with the web average pressures of the motors in Figure 52. The best-fit line through the data is also the theoretical relationship for the parameters. If this relationship were used to predict the specific impulse of the static test motors, the standard deviation of the measured specific impulse values would be 0.53 lbf/lbm, one sigma, and the coefficient of variation would be 0.24%.

8.1.4 ACTUAL VARIATION IN SPECIFIC IMPULSE (VACUUM)

The factors which contribute to a variation of vacuum specific impulse are listed in Table 16. The standard deviations about the nominal values of these factors were determined from experimental data wherever

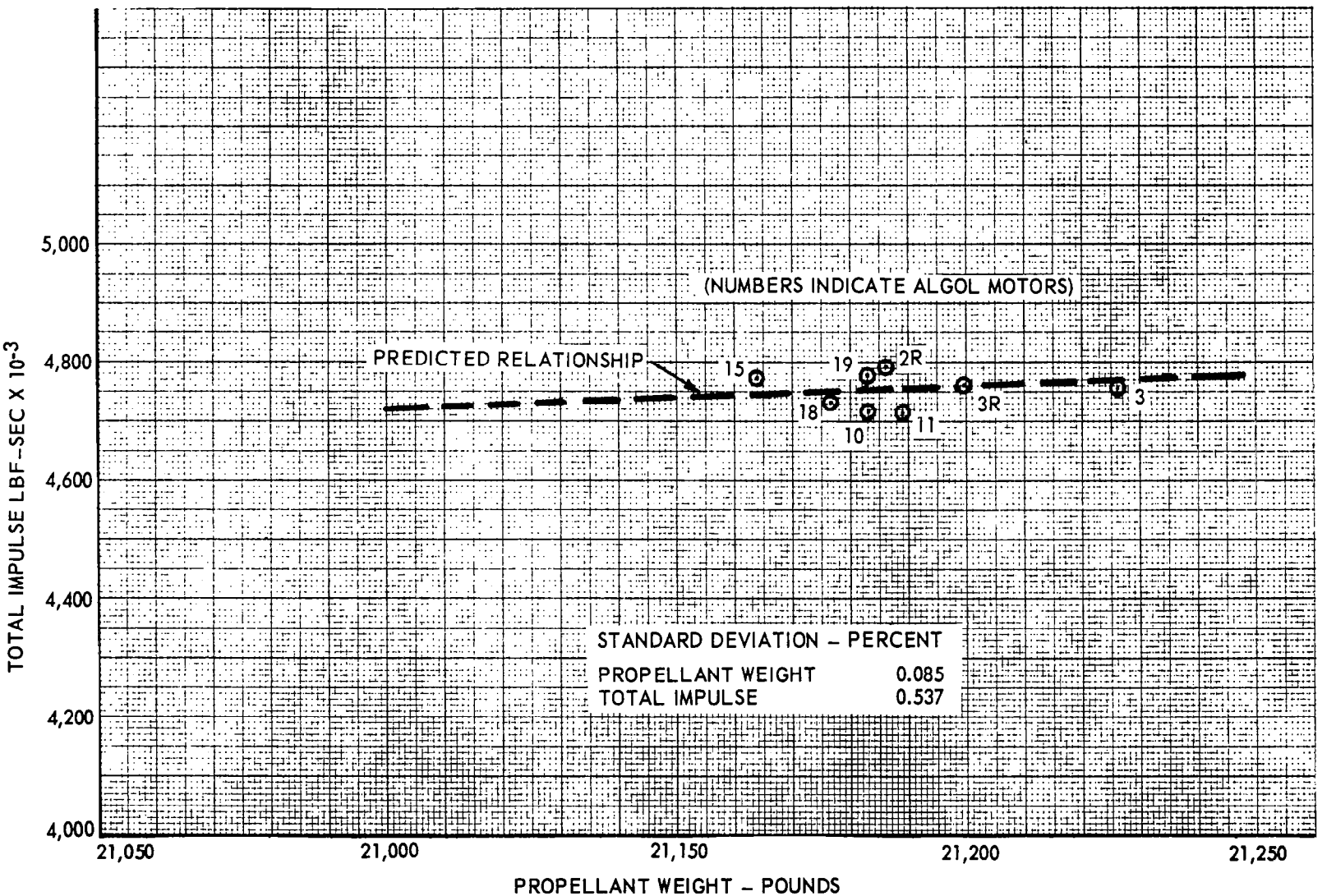

FIGURE 46 ALGOL IIA IMPULSE VS PROPELLANT WEIGHT — STATIC TEST DATA

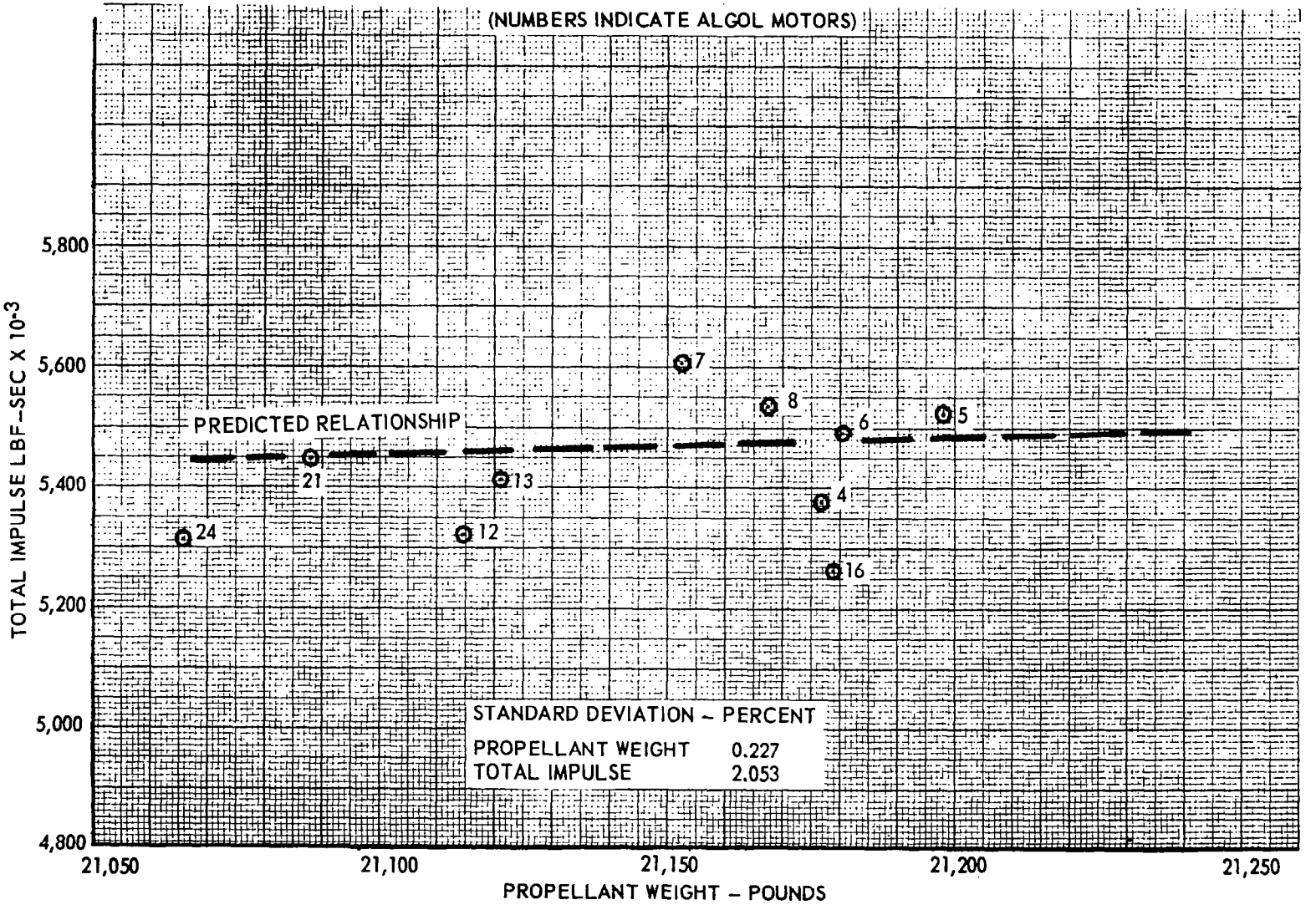

FIGURE 47 ALGOL IIA VARIABLES STUDY TOTAL IMPULSE VS PROPELLANT WEIGHT — FLIGHT DATA

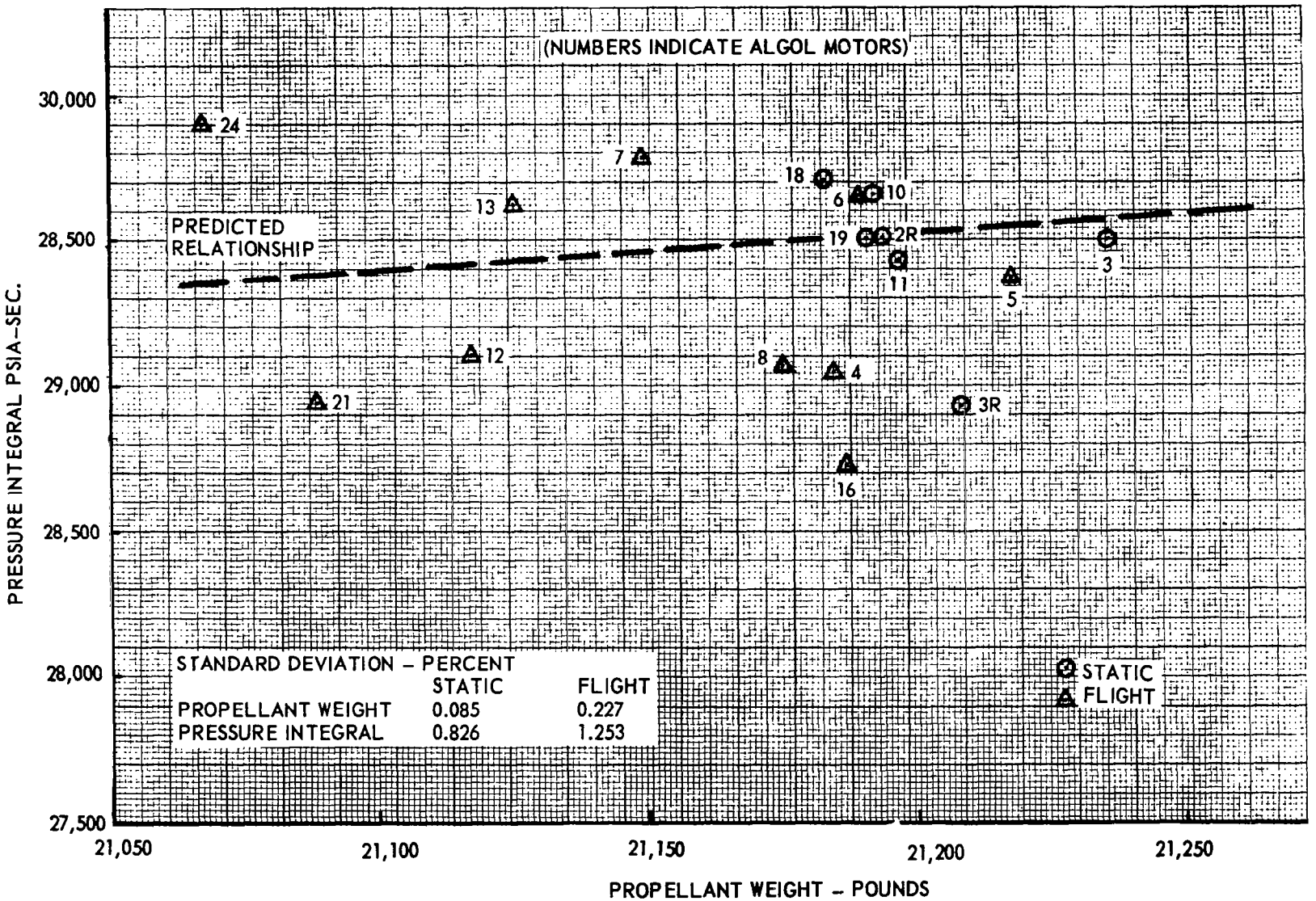

FIGURE 48 ALGOL IIA PRESSURE INTEGRAL VS PROPELLANT WEIGHT

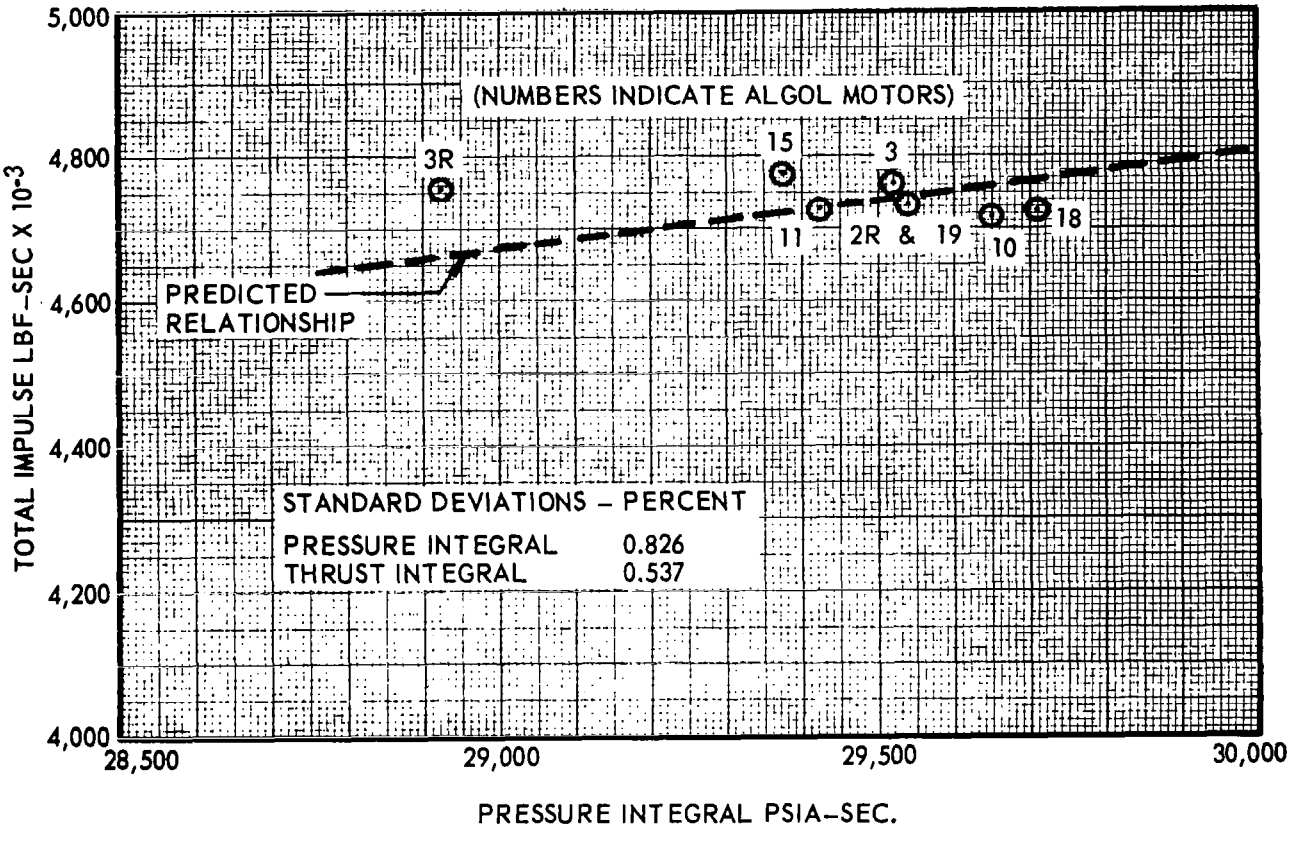

FIGURE 49 ALGOL IIA TOTAL IMPULSE VS PRESSURE INTEGRAL — STATIC TEST DATA

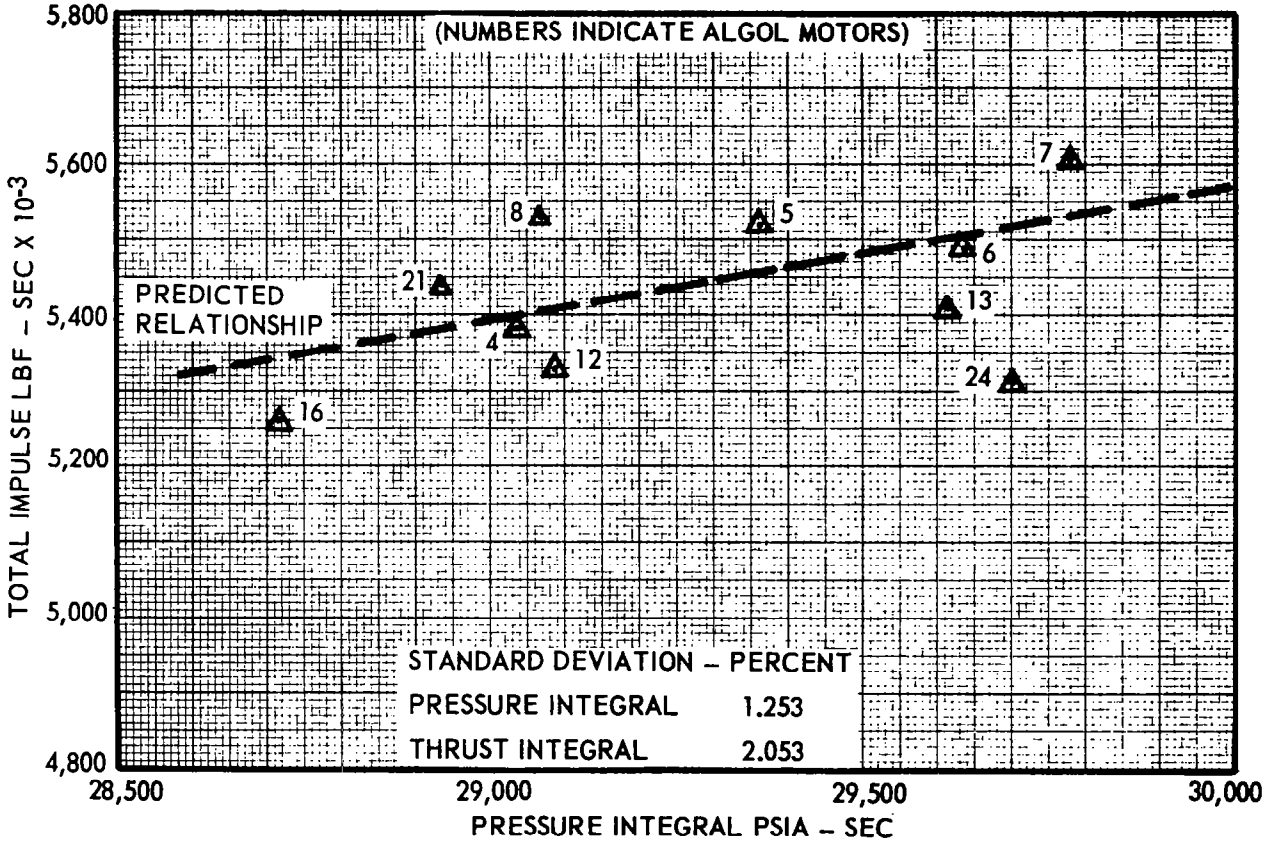

FIGURE 50 ALGOL IIA TOTAL IMPULSE VS PRESSURE INTEGRAL — FLIGHT DATA

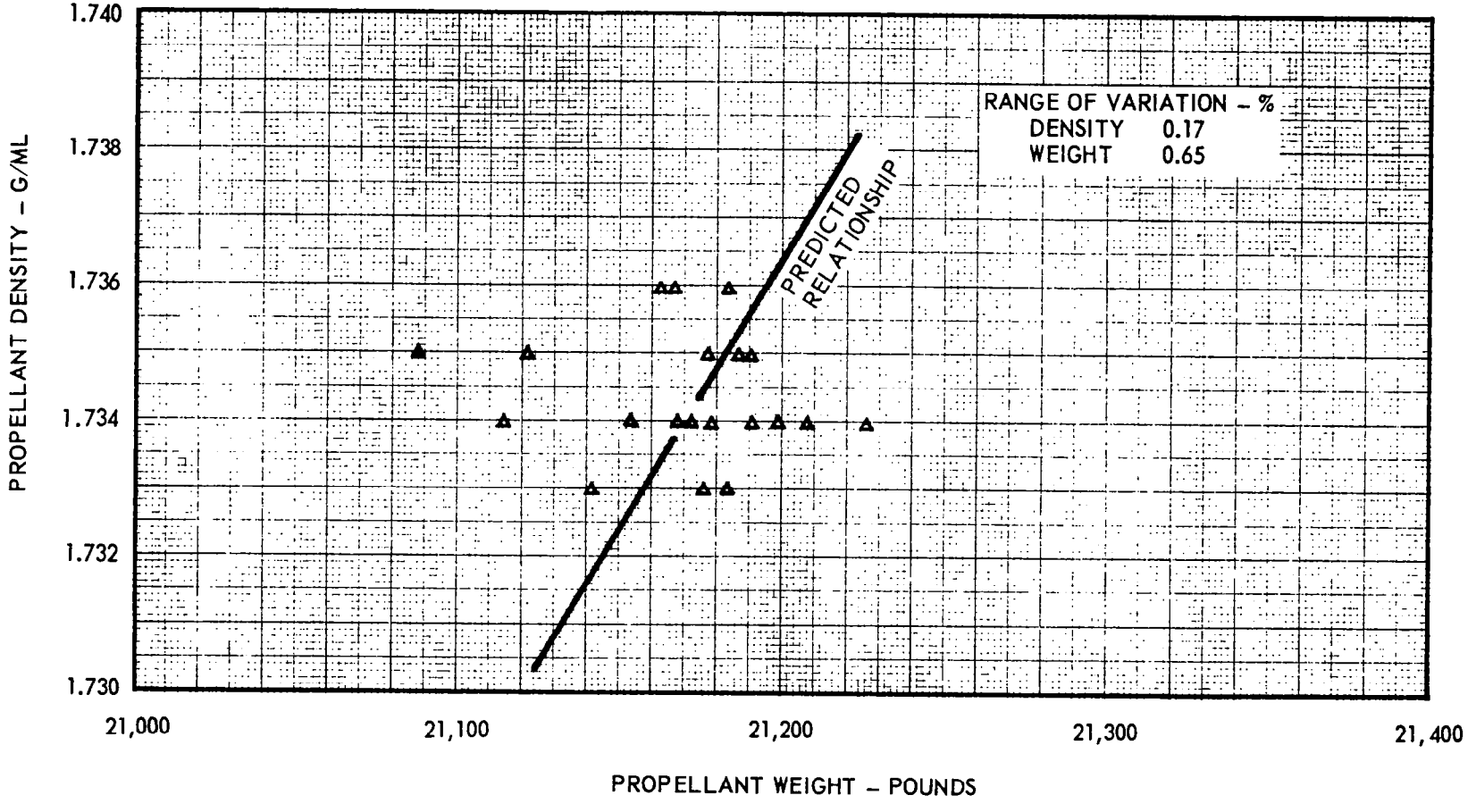

FIGURE 51 ALGOL IIA AVERAGE PROPELLANT DENSITY VS PROPELLANT WEIGHT

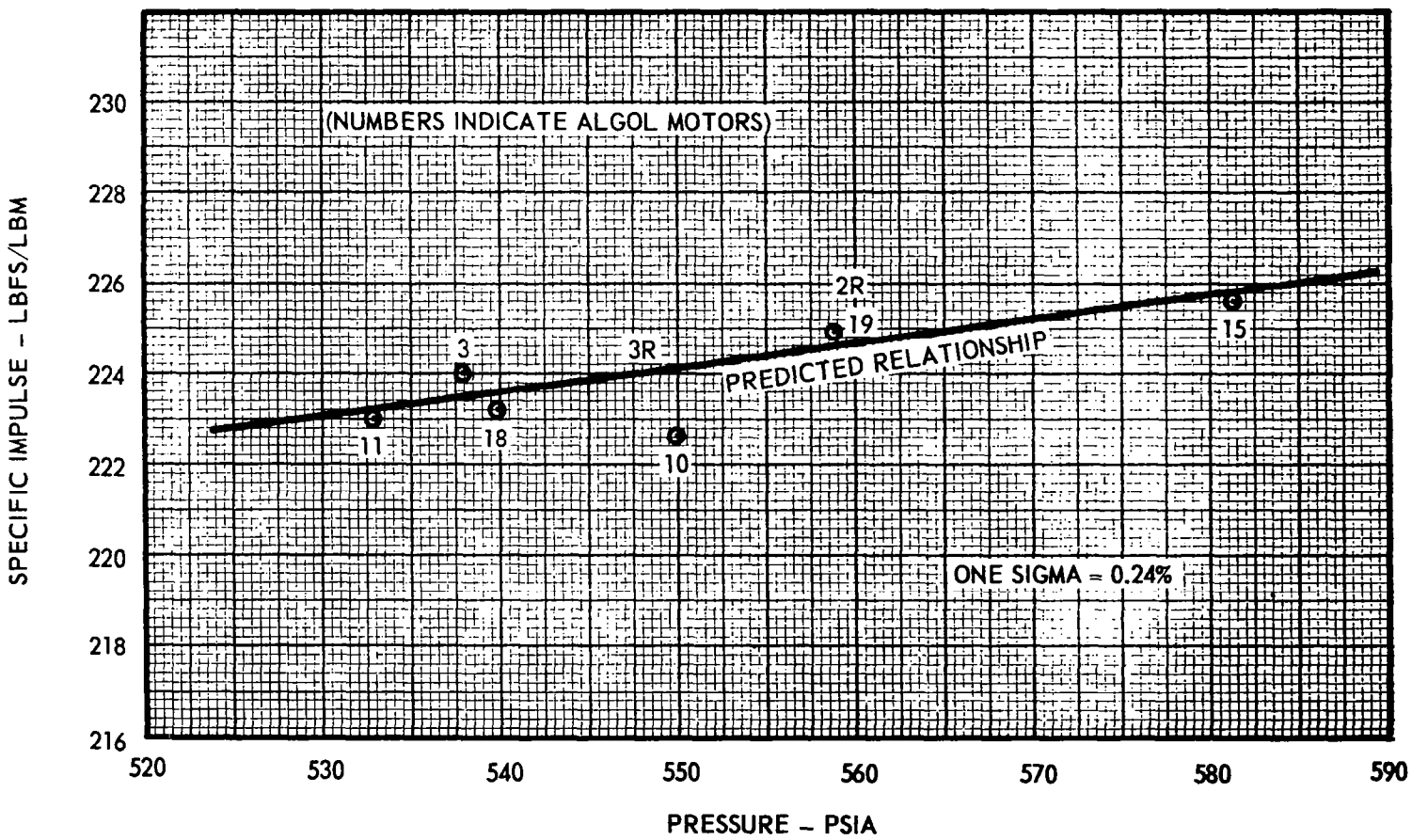

FIGURE 52 ALGOL II STATIC TEST SPECIFIC IMPULSE VS PRESSURE

possible or were selected to represent the expected maximum variation of the parameter. The resultant one sigma percentage effects upon specific impulse are tabulated. A root-square-summation of these contributing effects yields 0.17%, one sigma.

This value of 0.17%, one sigma, is comparable with the observed experimental value of 0.24%, one sigma, for static test data mentioned earlier, since the experimental value also includes weight, thrust, and pressure measurement errors. See Section 7.0, Instrumentation Systems. If the variances of the weight and thrust measurement error are subtracted from the variance of the experimental value, the resultant standard deviation estimated for vacuum specific impulse corrected for the effect of sea level ambient pressure is 0.18%, one sigma.

		1σ	σ^2
	Experimental I_{SP}	0.24%	0.0576
(minus)	Weighing error	0.06%	0.0036
(minus)	Thrust error	0.14%	0.0196
			0.0344

$(0.0344)^{1/2}$ = 0.18% I_{SP} variation, one sigma

TABLE 16
ALGOL II
ANALYSIS OF VACUUM SPECIFIC IMPULSE VARIATION

Contributing Factors	Nominal	One Standard Deviation	Data Source	One Sigma Percentage Effect, %
Propellant Temperature	77°F	± 5°F	Experimental	± 0.0024
Nozzle Expansion Ratio	7.135	±0.027	Experimental	± 0.0300
Nozzle Half-Angle	17°	± 0°20'	Theoretical	± 0.0800
Chamber Pressure	550psia	± 20 psia	Theoretical	± 0.0490
Inert Weight Consumed	216 lb.	± 35 lb.	Experimental	± 0.0820
Propellant Ingredients				
Oxidizer Weight	Specification	± 0.5%	Theoretical	± 0.0740
Aluminum Weight	Specification	± 0.5%	Theoretical	± 0.0740
Specific Impulse (Vacuum)	Root-Square-Summation			± 0.17

8.1.5 RETEST OF BURNING RATE EXPONENT AND TEMPERATURE SENSITIVITY VALUES FOR ALGOL IIB PROPELLANT

8.1.5.1 Introduction

A series of twenty 10KS-2500 test motors was fired at temperatures of 40, 80, and 120°F and nominal pressures of 350, 550, and 850 psia to obtain burning rate exponent and temperature sensitivity values for the Algol IIB propellant.

Burning rate exponent and temperature sensitivity values are required in the prediction of Algol II motor performance in flights of the Scout launch vehicle. The values are used to correct burning rate data for deviations in the motor chamber pressure and motor temperature. The values are applied to Algol II motor performance data and also to 10KS-2500 test motor burning rate data in constructing burning rate prediction correlations. The values in use on the Algol program were determined five years ago from propellant tests using 3KS-500 test motors. The present Algol program utilizes 10KS-2500 test motors to measure propellant burning rates. The change from 3KS-500 test motors to 10KS-2500 test motors was made some time ago to utilize the more accurate burning rate measuring device.

An investigation of the Scout Motor Performance Analysis and Prediction Study disclosed reason for doubt of the validity of the established values as applied to current propellant mixes and to 10KS-2500 test motor data. An error, in either the burning rate exponent value or the temperature sensitivity value, in representing a true value for a current propellant in a 10KS-2500 motor would contribute to errors in the Algol II motor performance prediction. This test program was conducted to confirm the values of the coefficients now being used and to provide a needed burning rate comparison between the round bore and keyhole bore configurations of the 10KS-2500 test motor.

8.1.5.2 Test Methods

The 10KS-2500 test motors were fabricated in accordance with AGC Drawing No. 383773 and the process and inspection procedures for 10KS-2500 motors. The propellant for all of the motors was mixed in one full-scale 2,200 pound batch, using the propellant formulation and process and inspection procedures identical to those used in the manufacture of Algol IIB motors. Of the twenty motors, fourteen were P/N 383773-9 neutral burning keyhole configuration motors and six were P/N 383773-19 progressive burning motors. The nozzle throats were specially sized, not in accordance with the drawings, to produce the nominal web average chamber pressures shown in Table 17. The motors were conditioned at three temperatures (40°, 80° and 120°) and were fired at the conditioning temperature. Oscillograph record data were collected for each test firing and reduced to complete the Test Data Sheet (Form AGC3-100-611) in the same manner as normally employed for 10KS-2500 test motors used on the Algol II-B production program. The pertinent portion of the data is summarized in Table 17. The data were reduced by the method given in Paragraph 4.1.2.1.

TABLE 17

ALGOL IIB 10KS-2500 TEST MOTOR PATTERN

RUN	GRAIN TEMP. °F	NOMINAL PRESSURE psia	TOTAL PRESSURE INTEGRAL psia-sec	WEB AVERAGE PRESSURE psia	EFFECTIVE WEB BURN TIME sec	WEB LENGTH in.	BURNING RATE in/sec
			KEYHOLE BORE MOTORS				
3	40	350	4822	391	11.937	2.160	.1809
4	40	350	4903	392	12.108	2.171	.1793
11	40	550	6747	588	11.107	2.157	.1942
12	40	550	6794	591	11.128	2.175	.1955
17	40	850	9500	866	10.619	2.180	.2053
18	40	850	9512	873	10.547	2.152	.2040
8	80	550	6850	609	10.888	2.174	.1997
9	80	550	6824	613	10.776	2.158	.2003
5	120	350	4874	416	11.341	2.186	.1928
6	120	350	4892	421	11.248	2.177	.1935
13	120	550	6748	613	10.656	2.174	.2040
14	120	550	6690	621	10.428	2.137	.2049
19	120	850	9488	940	9.771	2.170	.2221
20	120	850	9365	915	9.907	2.181	.2201
			ROUND BORE MOTORS				
1	80	350	3092	372	7.938	1.434	.1807
2	80	350	3117	381	7.813	1.440	.1843
7	80	550	4414	574	7.344	1.450	.1944
10	80	550	4426	577	7.326	1.448	.1977
15	80	850	6015	838	6.855	1.449	.2114
16	80	850	5989	835	6.849	1.445	.2110

8.1.5.3 Results

The slope of the line through the burning rate versus pressure data is the burning rate exponent, n.

$$n = \left((\ln r_2 - \ln r_1) / (\ln P_2 - \ln P_1) \right) \quad (1)$$

where r_1 and r_2 are the calculated burning rates of the propellant under pressure conditions P_1 and P_2 for a constant propellant temperature.

The value of n was determined to be 0.17 utilizing the keyhole bore test motor data in Figure 53.

The temperature sensitivity coefficient, π_K, is defined as:

$$\pi_K = 100 \left((\ln r_2 - \ln r_1)/(T_2 - T_1) \right) = \%/°F \quad (2)$$

where r_1 and r_2 are the burning rates of a motor at temperatures T_1 and T_2. The data are for a constant K_n condition.

At the nominal 850 psia, r_2 = .221, r_1 = 0.205, T_2 = 120°F and T_1 = 40°F. Thus, $\pi_K = 100 \left((\ln 0.205 - \ln .221)/(120-40) \right) = 0.10$ %/°F.

8.1.5.4 Discussion

The established values for n and π_K which have been used to date on the Algol II program are 0.22 and 0.11%/°F, respectively. The measured values are 0.17 and 0.10%/°F. Use of the new values yields converted burning rate data which differ only slightly from converted data computed with the established values. For example, in a typical calculation to convert an Algol burning rate at 500 psia to a burning rate at 550 psia, the standard condition:

$$(r_2/r_1) = (P_2/P_1)^n$$

if r_1 = 0.210 in/sec, P_1 = 500 psia, and P_2 = 550 psia

using n = 0.22, $r_2 = 0.210\ (550/500)^{0.22} = 0.214$ in/sec at 550 psia

or using n = 0.17, $r_2 = 0.210\ (550/500)^{0.17} = 0.213$ in/sec at 550 psia

Also, in a typical calculation to convert an Algol burning rate at 60°F and 550 psia to a burning rate at 80°F and 550 psia, since π_K is defined at a constant K_n condition:

$$r_2 = r_1\ (e)^{\pi_K (T_2 - T_1)}$$

$$P_2 = P_1\ (e)^{\pi_K (T_2 - T_1)}$$

and $$r_3 + r_2\ (P_3/P_2)^n$$

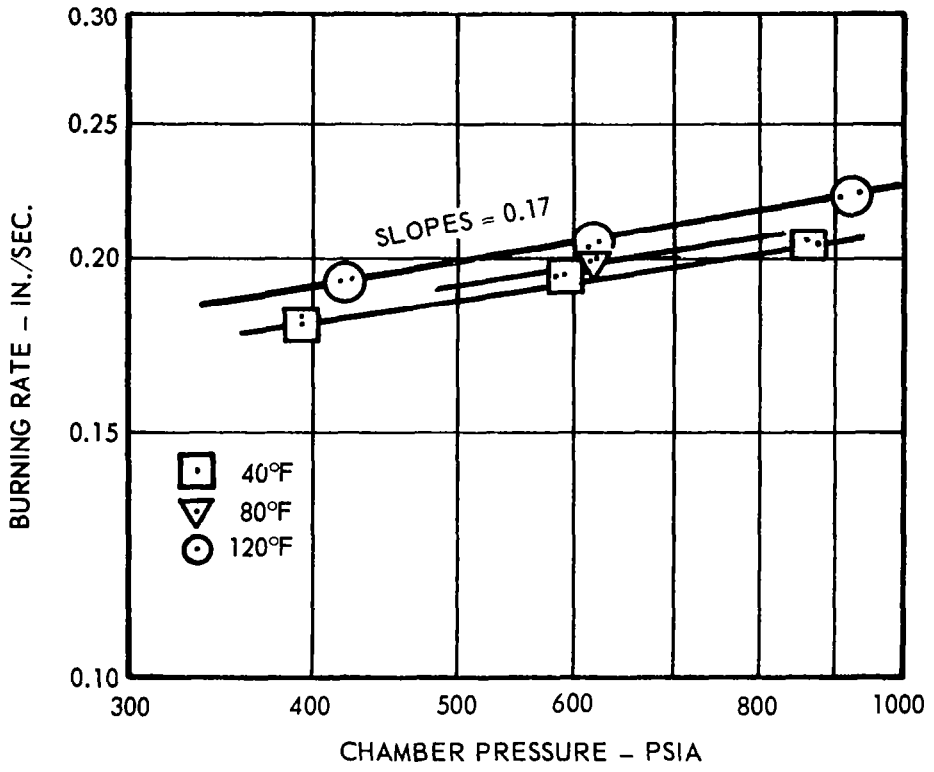

FIGURE 53 ALGOL IIB 10KS–2500 KEYHOLE BORE TEST MOTOR DATA

if r_1 = 0.210 in/sec, P_1 = 550 psia, P_3 = 550 psia,

T_1 = 60°F and T_2 = 80°F

Using π_K = .11%/°F $r_2 = 0.210\ (e)^{0.0011\ (80-60)} = 0.215$ in/sec

$P_2 = 550\ (e)^{0.0011\ (80-60)} = 562$ psia

and $r_3 = 0.215\ (550/562)^{0.22} = 0.214$ in/sec at 550 and 80°F

Or using π_K = .10%/°F $r_2 = 0.210\ (e)^{0.0010(80-60)} = 0.214$ in/sec

$P_2 = 550\ (e)^{0.0010(80-60)} = 561$ psia

and $r_3 = 0.214\ (550/561)^{0.22} = 0.213$ in/sec at 550 and 80°F

8.2 SECOND STAGE

8.2.1 ACTUAL VARIATION IN SPECIFIC IMPULSE

The reproducibility of the specific impulse of solid propellant rocket motors has been the subject of much controversy in recent years. The relatively small real variation of specific impulse and the relatively large inaccuracies normally encountered in the measurement of specific impulse have resulted in estimates of excessive impulse variability. These estimates are often many times as large as the real impulse variation. Many studies have been conducted in an attempt to estimate the true impulse reproducibility. Normally, these studies have used one or both of the following approaches:

1. A statistical analysis of static test data where controlled tests were conducted using the best instrumentation available.

2. A theoretical analysis of each known contributor to impulse variation using statistical techniques to combine the factors.

The Thiokol Chemical Corporation conducted a study in 1961 using the first approach to evaluate the reproducibility of impulse (Reference 6). In this study data from approximately 420 motors, representing eight different motor programs, with a range of propellant weights from three pounds to 5900 pounds were collected and evaluated. The motor programs selected for this study utilized modern data recording techniques. Strain gauge thrust transducers, high speed magnetic tape, and digital data systems were common to all. Dual channels of thrust and pressure instrumentation were available for all motors.

The derived standard deviations of specific impulse within the various motor programs ranged from 0.20% to 0.70%. In an attempt to determine if these estimates of impulse reproducibility were indicative of the real variation of specific impulse, a correlation was made between the characteristic velocity, C*, and specific impulse. The basis of this approach was that two independent measurement systems, pressure and thrust, were involved in deriving C* and impulse data. Therefore, agreement between the two parameters would indicate that the observed differences in impulse were real. The impulse/C* relationship was uncorrelated and, thus, represented measurement error with no recognizable amount of real variation among motors. The conclusion drawn from this study was that the basic propellant variability is too small to isolate from experimental error, even with instrumentation and test controls of high accuracy.

A theoretical analysis of the contributors to the ballistic variability of large solid propellant rocket motors was conducted by Thiokol in 1964 (Reference 7). The report presenting the results of this study quotes a standard deviation of specific impulse of 0.22% under sea level test conditions. The variation of vacuum specific impulse would be expected to be considerably smaller since the effect of chamber pressure on the thrust coefficient is eliminated in a vacuum test situation.

The variation of specific impulse of the Castor I motor has been calculated by two methods. The first method consisted of calculating the standard deviation of the specific impulse measured for a series of sea level static test motors. Figure 54 is a plot of the measured specific impulse versus the web average chamber pressure of fourteen statically tested Castor I motors. Specific impulse was plotted as a function of pressure in order to account for the effect of chamber pressure on the thrust coefficient. Where motors were tested at other than 77°F, the specific impulse derived was adjusted to 77°F based on an estimate of the temperature sensitivity of C* (.005%/°F).

A standard deviation of the measured specific impulse of 1.04% was calculated from these data. It should be noted that the collection of data shown in Figure 54 was obtained over a six year period using analog data reduction techniques. The estimate of specific impulse variability obtained by this approach is believed to be primarily a measure of the measurement and data reduction errors, and is unacceptable as an indication of the real variability of specific impulse.

The other means of estimating the variability of the specific impulse of the Castor I motor consisted of estimating the effect of each contributor to impulse variations and statistically combining these effects. Since the Castor motor of the Scout vehicle operates under near vacuum conditions in its flight environment, only those factors which contribute to a variation of vacuum specific impulse were considered. Table 18 lists the contributing factors to variations of vacuum specific impulse and shows the effect of each factor. The standard deviation of vacuum specific impulse is estimated to be 0.094% by a statistical combination of the impulse deviations shown in Table 18 . This is believed to be a reasonable estimate of the true variability of vacuum specific impulse.

TABLE 18

VARIATION OF VACUUM SPECIFIC IMPULSE

Contributing Factor	Mean	Standard Deviation	Data Source	% Effect of Standard Deviation on Specific Impulse
Propellant Temperature, °F	77	5	Experimental	0.0250
Nozzle Expansion Area Ratio	15.642	0.0873	Experimental	0.0271
Nozzle Divergent Angle	21°41'	0°01'	Dwg. Dim.	0.0051
Inert Material Consumed, lb	131	10.2	Experimental	0.0697
Effect of Propellant formulation Differences on C*, ft/sec	5063	2.33	Thermo-chemical Calculation	0.0460
Effect of Chamber Pressure Variation on C*, ft/sec (P_c = 507 ± 15)	5063	1.06	Thermo-chemical Calculation	0.0210
Vacuum Specific Impulse	Root-Square-Summation			0.094

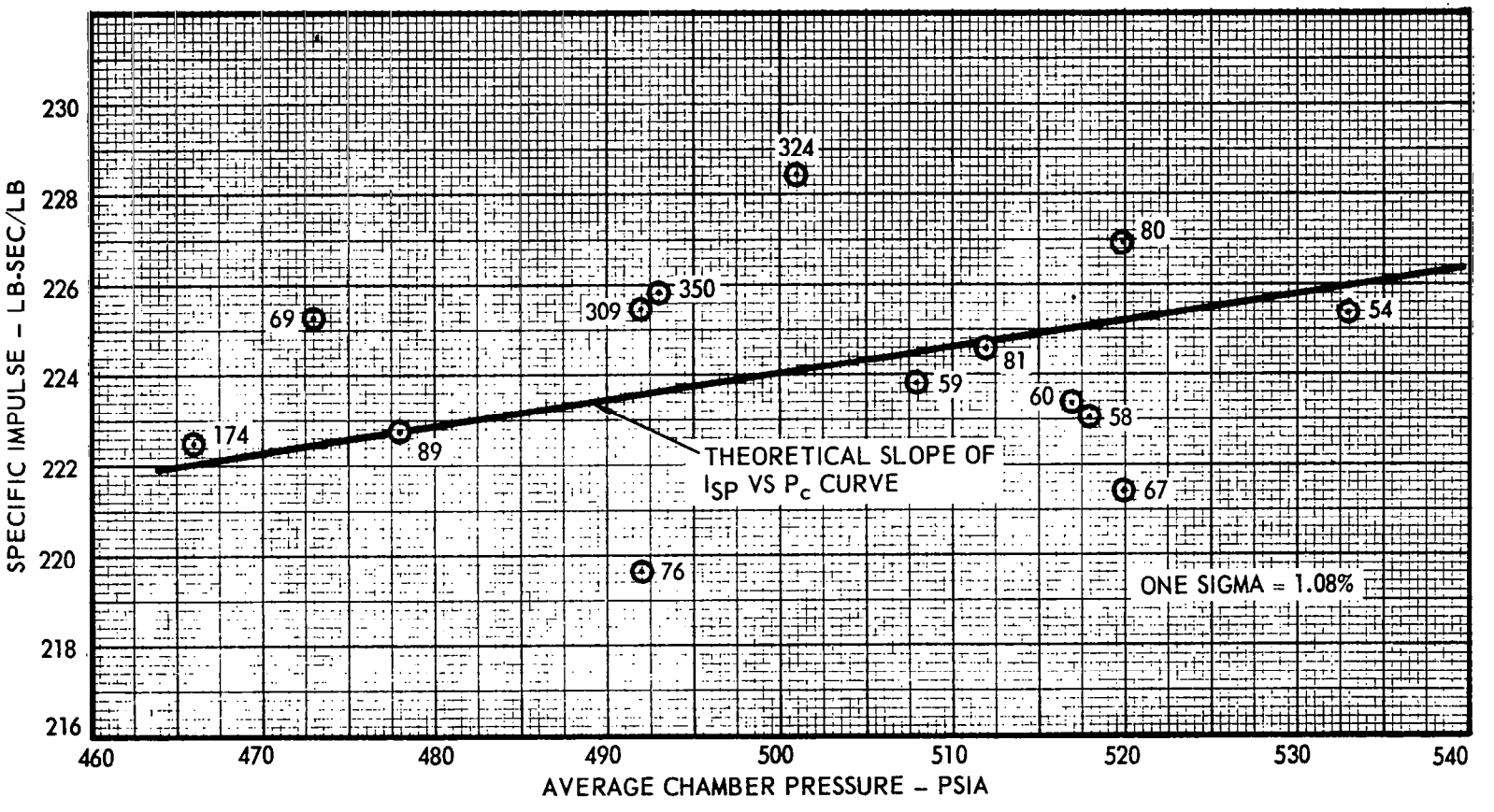

FIGURE 54 CASTOR I STATIC TEST SPECIFIC IMPULSE VERSUS CHAMBER PRESSURE

8.3 THIRD AND FOURTH STAGE

8.3.1 VARIATION IN POWDER/SOLVENT RATIO

The Powder/Solvent Ratio is a ratio of the amount of casting powder put into the rocket chamber prior to casting to the amount of casting solvent introduced into the powder-filled chamber during the casting operation. A series of test motors (20 total) were utilized in determining if any ballistic variations were caused by the variation of the Powder/Solvent Ratio. These motors were static fired at 60°F; a plot of percent solvent versus burn time is shown in Figure 55 . The results show no significant effect of solvent percent on burn time.

8.3.2 VARIATION IN PROPELLANT DENSITY

An investigation was conducted at ABL to determine what variation exists in the propellant density between individual X259 and X258 rocket motors. Since only a limited amount of data was available for density calculations, the pre-machining propellant weight and the weights of the casting powder were used in determining the densities. The actual volume of propellant could not be used to determine density since not all the necessary dimensional data were available. A total of thirteen X258 motors and fifteen X259 motors were investigated. The determined densities are shown in Tables 19 and 20 . Shown below are the results of the statistical analyses of the data shown in Tables 19 and 20.

Group of Motors	Powder Lot	Average Density (lbs/in^3)	% Variation (one sigma)
13 X258	Z1-143	0.06278	0.18
10 X259	Z1-193	0.06385	0.20
4 X259	Z1-169	0.06298	0.25
All X259	---	0.06358	0.66

Because of the method used to calculate the densities, it was necessary to check the weighing system and casting powder density and solvent density calculations to determine the precision of the results in Tables 19 and 20. The total variation (one sigma) for the X258 and X259 (each powder lot) motors is $\pm 0.18\%$ and $\pm 0.22\%$, respectively. These total variations are due to the weighing errors and errors in density determinations of the casting powder and solvent. Most of this variation is due to the error in measuring casting powder density. The errors involved in this method make up approximately 90% of the total variation of the propellant density between motors in one powder lot. However, the variation in propellant density between different powder lots is 0.69% or approximately three times the other variation. This is due to the variation in casting powder density. Based on available X259 ballistic data utilizing different powder lots, no errors in performance prediction can be attributed to this difference in densities.

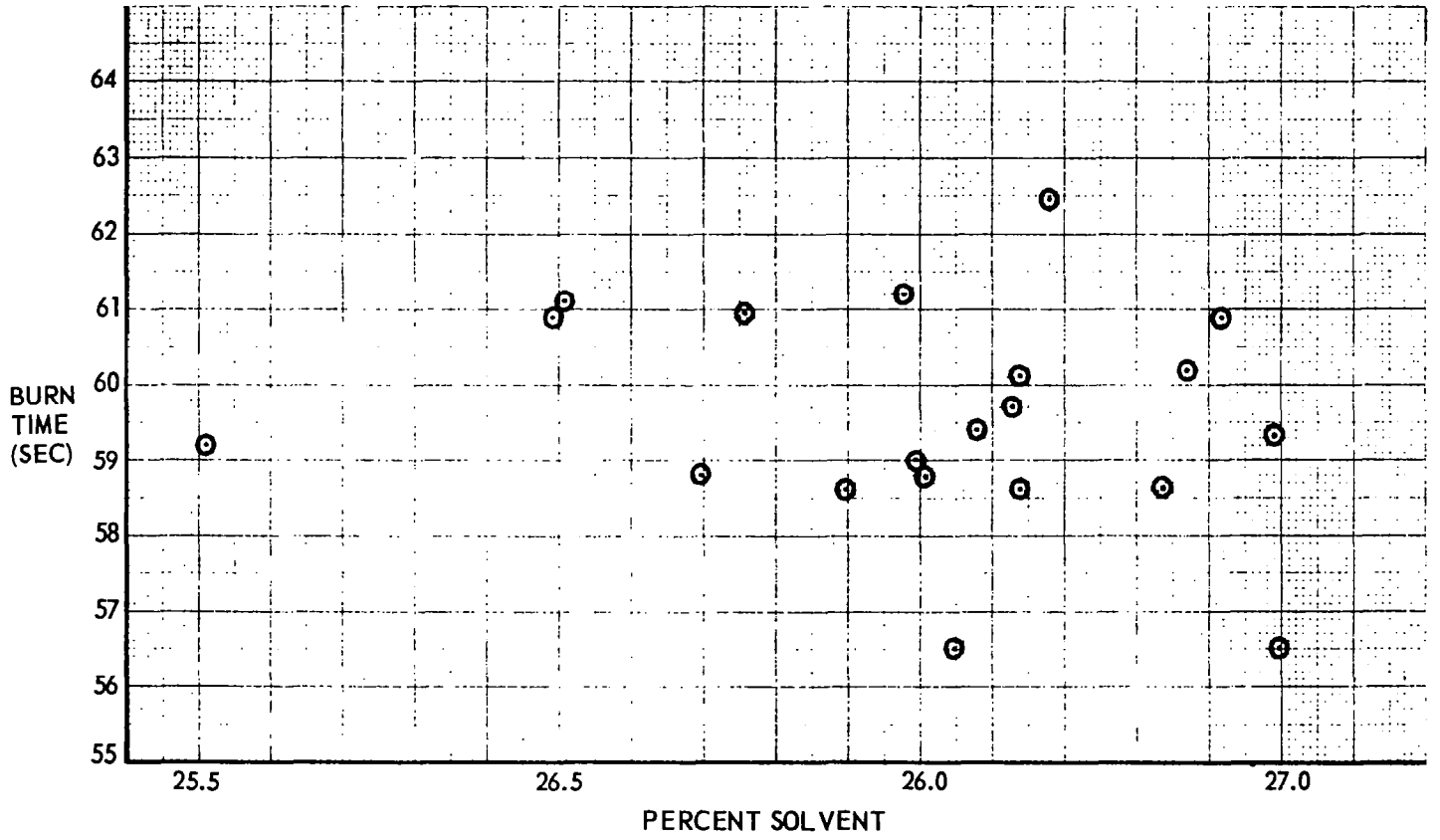

FIGURE 55 BURN TIME VS POWDER/SOLVENT RATIO (PERCENT SOLVENT) – NOMINAL 60 SEC. TEST MOTOR

TABLE 19

X259 PROPELLANT DENSITY

Motor Serial Number	Powder Lot	Powder Density (ρ_{pwd}) gm/cm^3	Solvent Density (ρ_{sol}) gm/cm^3	Average Propellant Density (ρ_{prop}) lbs/in^3
HPC-108	Z1-169	1.879	1.4557	0.06301
HPC-109	Z1-169	1.879	1.4536	0.06287
HPC-111	Z1-169	1.879	1.4511	0.06234
HPC-119	Z1-169	1.879	1.4556	0.06318
HPC-102	Z1-193	1.911	1.4556	0.06394
HPC-106	Z1-193	1.911	1.4493	0.06370
HPC-114	Z1-193	1.911	1.4553	0.06408
HPC-115	Z1-193	1.911	1.4558	0.06391
HPC-117	Z1-193	1.911	1.4543	0.06382
HPC-118	Z1-193	1.911	1.4555	0.06394
HPC-122	Z1-193	1.911	1.4502	0.06370
HPC-128	Z1-193	1.911	1.4567	0.06387
HPC-134	Z1-193	1.911	1.4562	0.06388
HPC-145	Z1-193	1.911	1.4508	0.06367

TABLE 20

X258 PROPELLANT DENSITY

Motor Serial Number	Powder Lot	Powder Density (ρ_{pwd}) gm/cm^3	Solvent Density (ρ_{sol}) gm/cm^3	Average Propellant Density (ρ_{prop}) lbs/in^3
RH-34	Z1-143	1.879	1.4520	0.06267
RH-35	Z1-143	1.879	1.4531	0.06280
RH-36	Z1-143	1.879	1.4549	0.06281
RH-40	Z1-143	1.879	1.4512	0.06275
RH-41	Z1-143	1.879	1.4540	0.06276
RH-42	Z1-143	1.879	1.4531	0.06292
RH-45	Z1-143	1.879	1.4525	0.06280
RH-46	Z1-143	1.879	1.4508	0.06285
RH-47	Z1-143	1.879	1.4553	0.06263
RH-55	Z1-143	1.879	1.4553	0.06270
RH-56	Z1-143	1.879	1.4553	0.06273
RH-58	Z1-143	1.879	1.4567	0.06261
RH-59	Z1-143	1.879	1.4552	0.06300

8.3.3 TIP-OFF AND THRUST MISALIGNMENT

Among the factors different in the flight environment than in static test are tip-off and coning and the effects of spin stabilization. Figure 56 shows those factors which contribute to tip-off and subsequent coning. Case I is misalignment of the nozzle centerline with the geometric centerline of the chamber. Case II is when there is nonperpendicularity between the motor attachment plane and the motor payload centerline. Case III is misalignment of the grain inside the chamber, which might cause a tip-off effect. Case IV is off-center ejection of mass from the nozzle during ignition.

Manufacturing tolerances and inspection procedures control the misalignments and keep them minimized, and ignition effects are probably most responsible for tip-off. In the X248, tip-off was a problem and caused coning of about 3.0 degrees. However, in the X258, tip-off has not been observed. The differences in tip-off between the X248 and the X258 probably can be explained by the difference in ignition systems between the X248 and X258. The X248 utilized a pyrotechnic type igniter which contained pellets and propellant strips mounted on two sides of a resonance suppressor paddle. The differences in ignition characteristics on each side of the paddle and the ejection of pieces of pellet cage and wiring, etc., contributed to X248 tip-off. The X258 employs a single pyrogen igniter on the center line of the motor. This has apparently eliminated the problem of ignition tip-off.

8.3.4 SPIN AND LONGITUDINAL ACCELERATION EFFECTS

Several cases of unusual ballistic behavior have been reported in rocket motors under the influence of spin-stabilization and/or acceleration loading in flight, notably in the Sidewinder, the Tartar-Terrier gas generator, the X248 and the X258. Figure 57 shows a comparison of pressure-versus-time curves for the X258 in static test and in spin test. In the spin mode the pressure levels and burn times vary by about 15% from static test. The subject of spin effects on ballistic performance has been controversial and a variety of test results and conclusions has been reported. Therefore, the literature was surveyed to gain additional information on the subject. All the motor contractors--Hercules, Thiokol, and Aerojet--have conducted spin testing or acceleration testing on propellant grains.

Aerojet tested its 15-inch diameter spherical motors at spin rates of 900 rpm. Burn times from these tests revealed no change in burn rate due to spinning. Aerojet has also tabulated burn times on eleven of its 30KS 8000 rocket motors used in flight tests in which spin rates of 600 rpm were measured. It was Aerojet's conclusion, based on limited data, that the nominal burning rates of the 15-inch spherical motor and the 30 KS 8000 motor showed no significant change when operating under these spin conditions.

Thiokol/Elkton Division centrifuged end-burning charges to acceleration loads as high as 750 g's (Figure 58 and Reference 8). Two propellants were used--both a conventional and a non-conventional high-burning rate propellant--and the test data showed that both propellants exhibited an

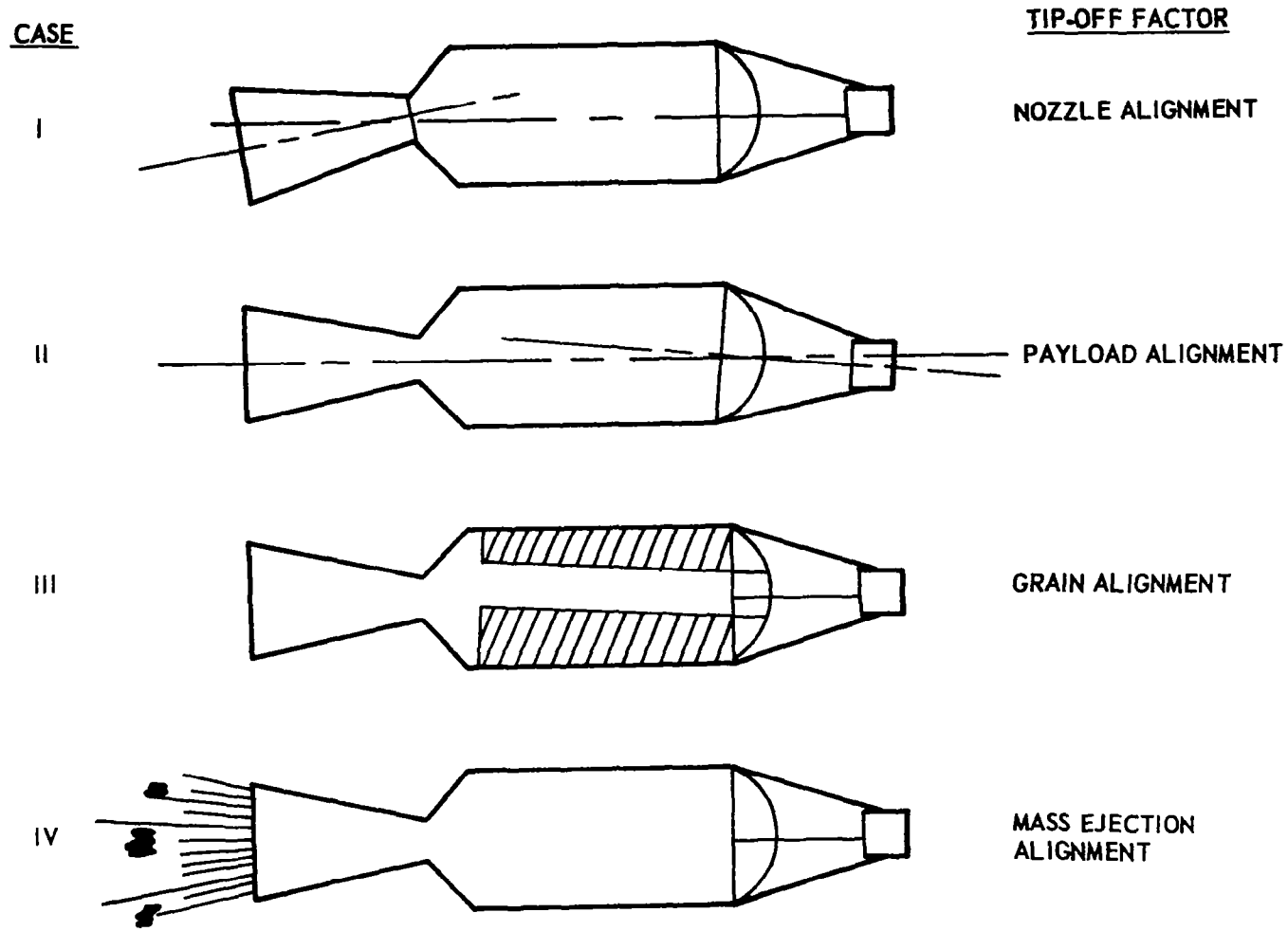

FIGURE 56 ALIGNMENT FACTORS AFFECTING TIP-OFF

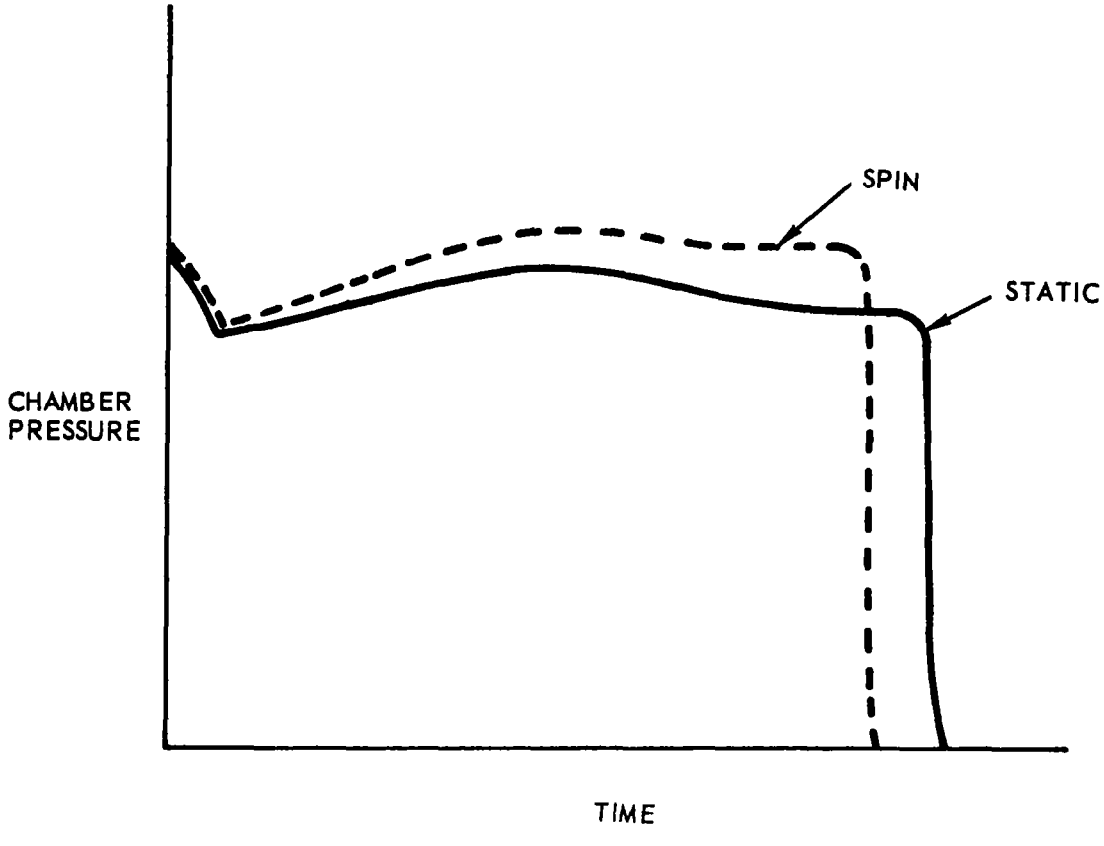

FIGURE 57 TYPICAL EFFECT OF SPINNING ON X258 PERFORMANCE

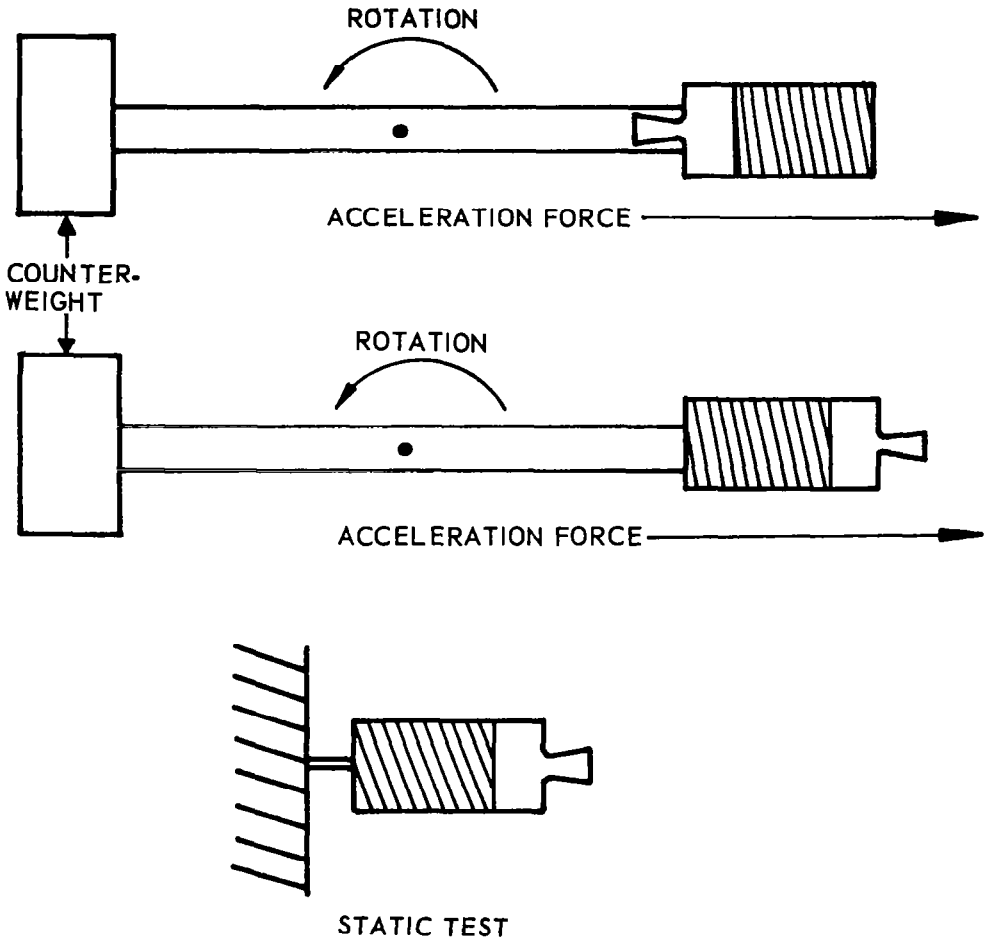

FIGURE 58 CENTRIFUGE TEST ARRANGEMENTS

increased burning rate when acceleration forces were directed toward the propellant burning surface. Thiokol/Huntsville Division collaborated with Douglas Aircraft in test firing its TX-3 motor in a Douglas centrifuge (Reference 9). The accuracy of the pressure measurement was affected by instrumentation difficulties, which may have masked some of the acceleration effects, but the tests demonstrated that those effects were small if present at all.

Hercules/ABL also conducted extensive testing on a variety of propellants on its ballistic centrifuge (Reference 10). The motors were of an end-burner configuration and were tested with acceleration forces directed toward the burning surface and away from it. The centrifuge test results were then compared with static test results. The following comments apply only to propellants most similar to X258 and X259 formulation--that is, a high-energy aluminized double-base propellant--from the combustion of which a relatively high concentration of solid material is exhausted. In these tests which imposed acceleration loads of about 40 g's on the grain, chamber pressure was monitored. Testing here was also limited, but the following observations were made: 1) there were no ignition difficulties caused by 40 g's acceleration on any of the tests; 2) in the tests where acceleration forces were directed away from the burning surface, chamber pressures were lower and burning times longer; and 3) combustion efficiency, as suggested by the discharge coefficient, was highest when acceleration forces were directed toward the surface and lowest where acceleration forces were directed away from the surface.

Although the results were inconclusive as to the mechanism of the effect of acceleration on propellant burning, a plausible explanation was proposed. In the tests where acceleration forces were directed toward the burning surface, chamber pressures and burning rates were higher because of increased residence time of the non-gaseous combustion products within the chamber. When exhaust streams are subjected to acceleration forces which deflect the normal direction of flow, the particle residence time is increased, and combustion goes further to completion within the chamber. See Figure 59.

It was also proposed that increased residence time of the solid particles near the propellant surface could enhance the burning rate by increasing the heat transfer to the propellant surface.

From the test results surveyed so far, there is one point outstanding, i.e., that no generalization can be applied to cover all motors and all propellants. Each propellant and each grain configuration reacts differently to acceleration forces. For example, a Hercules Bacchus motor, the BE-3, which is smaller than the X258 and is cast with a different propellant but with a similar grain configuration, has shown no increase in burning rate while spinning at 600 rpm.

Since this phenomenon is present in the X258, further studies are being conducted to investigate it.

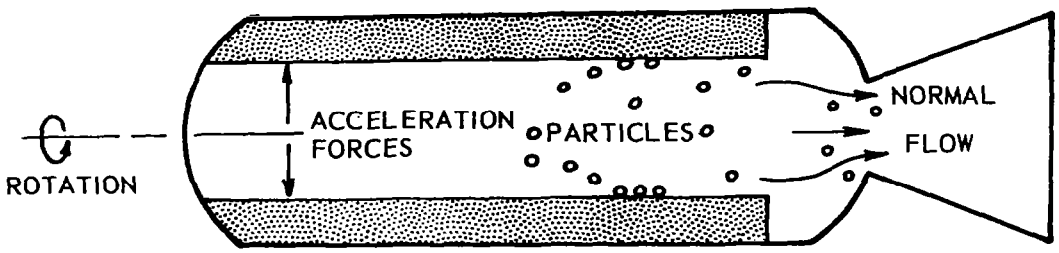

FIGURE 59 INCREASED BURNING RATE MECHANISM

8.3.5 X259 PERFORMANCE VARIABLES

The X259 motor has two impulse values which are used in predicting flight performance. These two values are caused by the different nozzle expansion ratios which have been used because of two different classes of burning rate propellants. When the higher rate propellant was utilized, the nozzle throat diameter was increased to reduce the chamber pressure to correspond to that of the low burning rate propellant. The two specific impulse values used are 278.8 lbf sec/lbw. for the high rate propellant and 281.4 lbf sec/lbw. for the normal (or low rate) propellant. The 281.4 lbf sec/lbw. impulse value was measured at AEDC while the 278.8 lbf sec/lbw. impulse value was calculated from the first value, using the revised expansion ratio. The variation of specific impulse measurements at AEDC (5 tests) was 0.14% (one sigma). This variation included thrust measurement errors. Since all of the test values used for predicting third stage motor performance are derived from AEDC data, the accuracy and variability of these measurements are dependent on the AEDC measuring system (see Paragraph 7.2).

Another important factor in performance variability is the measuring accuracy in weighing the different motor assemblies and components. In a recent survey conducted at ABL, the accuracy of the X259 total assembly and propellant weight is 0.06% (one sigma).

A consumable weight for each X259 motor is derived from propellant weight plus the inert weight expended during motor operation. The inert weight expended is a measured value taken from AEDC tests. An average of the before and after firing weights of these tests was 25 lbs. with a one sigma standard deviation of 1.1 lbs.

The total accuracy of the nominal consumable weight remaining value used in predicting performance (including propellant weight error) is calculated using a root-square-summation. The accuracy was determined to be (one sigma) 0.15%.

8.3.6 X259 BURN RATE VARIATION

The X259 motor burn rate variation is dependent on separating the motors into two distinct groups. One group contains propellant using casting powder which exhibits a "normal" (or low) burning rate while the other group contains propellant using casting powder which exhibits a "high" burning rate. The burning rates for both groups of propellants are shown below:

NORMAL RATE PROPELLANT		HIGH RATE PROPELLANT	
Powder Lot	Burning Rate (in/sec)	Powder Lot	Burning Rate (in/sec)
Z1-91	0.302	Z1-193	0.323
Z1-109	0.312	Z1-193	0.326
Z1-109	0.304	Z1-207	0.332
Z1-151	0.306		
Z1-169	0.306		
Z1-246	0.300		
Avg.	0.305	Avg.	0.327
C.V. (one sigma)	1.3%	C.V. (one sigma)	1.4%

Based on the above data, the burning rate variation when the propellant rates are separated is 1.3% and 1.4%. The average burning rate for all of the powder lots together is 0.311 in/sec with a variation of 3.8%.

Since X259 performance calculations are made keeping these powder lots separate, the error in predicting burn rate is treated by a summation of the population variances. This gives a 1.8% variation.

8.3.7 X258 PERFORMANCE VARIABLE

The X258 specific impulse was measured at AEDC during simulated altitude test firings. The average value measured was 281.2 lbf sec/lbw with a variation of 0.57% (one sigma). This large variation in measured specific impulse could possibly be caused by the different test environments the X258 has undergone at AEDC. These different environments consisted of static tests and 200 rpm spinning tests. An extensive study of the X258 propellant and the effect of spin and longitudinal forces on its performance has been proposed.

The impulse data presently being used were obtained from tests on motors which are no longer being produced. A number of changes were made to the X258 flight design in an attempt to keep structural integrity in the chamber after firing and to eliminate a possible sliver of unburned propellant in the forward dome. Insulation material was incorporated into the cylindrical section of the chamber and the length of the grain inhibitor tube was reduced. This temporary fix was incorporated into the "C" motor. A new version of the X258, known as the "E" motor, contains a one piece insulator. New ballistic nominals will be generated for this model of the X258, based on AEDC 200 rpm spin firings at simulated altitude conditions.

The consumable weight for each X258 motor is derived by taking into account a possible 4.1 lb. of unburned propellant and/or undischarged aluminum when using propellant weight and adding 5.7 lbs. of inerts consumed. The inerts consumed is an average of "before" and "after" weight measurements of one static test and the three 200 rpm AEDC spin test motors. The standard deviation inerts consumed in these tests was 1.7 lbs. The root-square-summation of propellant weight accuracy and inert consumption variation calculates 0.36% (one sigma) for the total consumable weight.

8.4 VARIATION IN MOTOR TAIL-OFF CHARACTERISTICS

The portion of the thrust curve which appeared to be most variable was the tail-off transient during which thrust decays. In general, the importance of unpredicted deviations in the shape of the thrust curve diminish with successively higher stages of the vehicle.

As a test of the importance of the errors, the predicted thrust curves of the first three stages of Scout S-118 were modified to have alternate shapes, "fast" and "slow" tail-off rates (Figure 60). The modifications of tail-off were comparable to the extreme deviations that had been encountered in flights. To assist in the analysis of the test results, the extremes were constructed to be symmetrical about the nominal tail-off. All three conditions provided the same impulse, and special weight-remaining data were calculated for the extremes.

These three tail-off conditions for the motors were inputs to a trajectory computation and error analysis. The resultant effect on a two sigma error allowance for a typical orbital mission is:

Altitude Deviation (2 sigma, N.M.I.)	Without Tail-off Error	With Tail-off Error
Perigee	30.0	31.4
Apogee	81.0	83.3

The increment of error was considered to be insufficient justification for a very difficult, expensive and uncertain effort to predict deviations in the shape of the analog curves. Involved in such an effort would be the testing and correlating of interactant effects of 1) mix-to-mix differences in burning rate, 2) the resultant increments of increased burning surface area, 3) inconsistencies among motors in web thickness, 4) differences in the rate of exposure of inert materials, 5) differences in port flow velocities, and 6) temperature gradients in the propellant.

8.5 ANALYSIS OF TRAJECTORY PREDICTION ACCURACY

8.5.1 INTRODUCTION

The accuracy of the new procedures for predicting the flight performance of Scout motors is difficult to evaluate. Telemetry data and radar data are poor bases for measuring the error in predicting the impulse of any one Scout stage during the boost trajectory. Orbit tracking radar data are credited with sufficient accuracy, given several measures of the orbit characteristics, to determine the payload injection conditions better than by any other available means.

This analysis compares predicted boost trajectories, injection conditions and orbit characteristics with the Scout performance as determined from radar data. Predicted trajectories for Scouts S-113, S-122, S-123, S-125, S-128 and S-134 were computed on three bases:

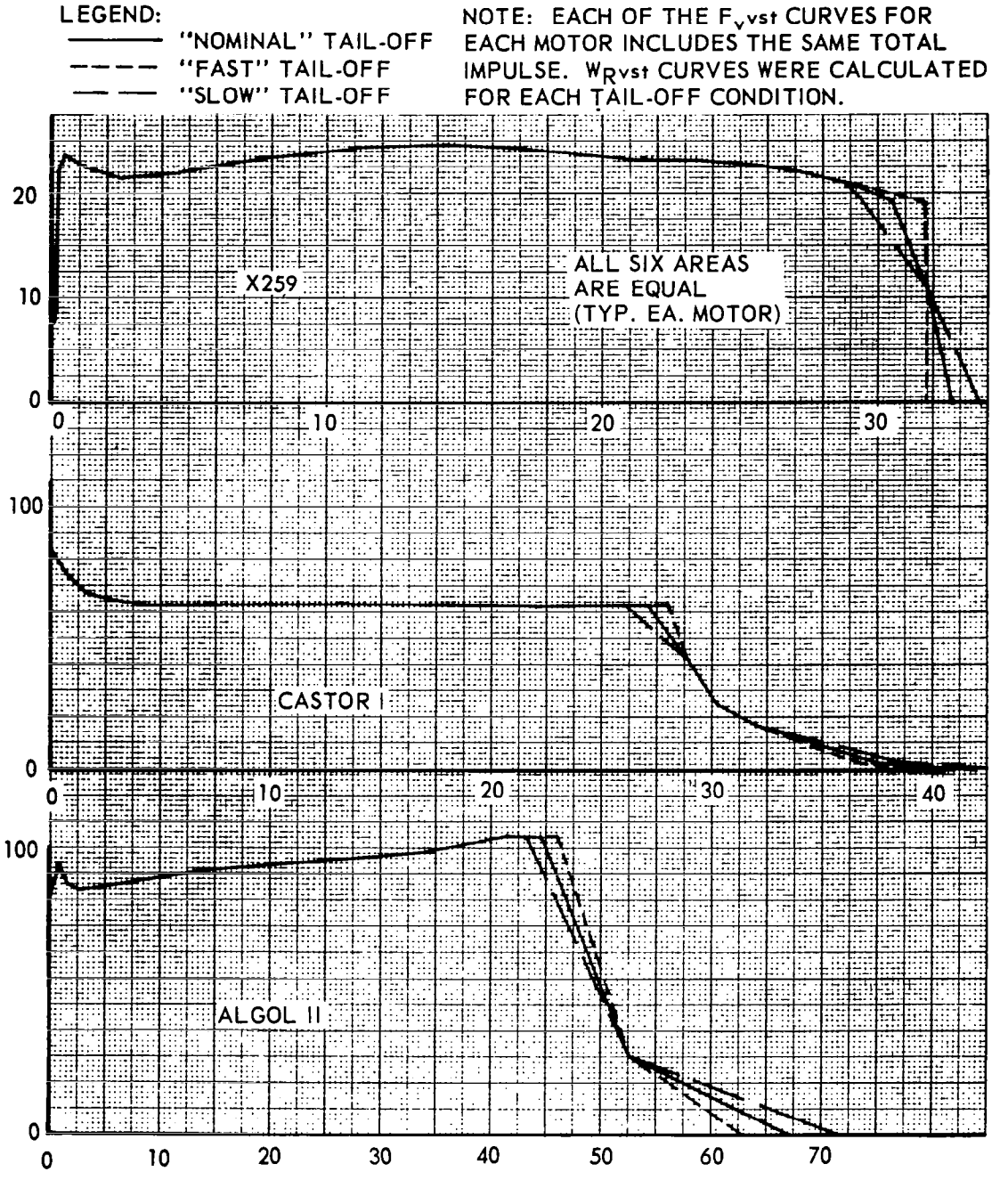

FIGURE 60 ALTERNATE TAIL-OFF RATES

1. Original preflight predictions of motor performance (past procedures) and preflight predictions of vehicle weight, drag, winds, etc. (Referred to as "Predicted, Pre-flight.")

2. Postflight, repredictions of motor performance (new PAPS procedures), and preflight predictions of the vehicle and flight conditions. (Referred to as "Repredicted, Pre-flight.")

3. Postflight, repredictions of motor performance, and postflight measures of actual vehicle weight, drag, winds, etc. (Referred to as "Repredicted, Post-flight.")

The Scout trajectory computed for each of the three combinations of prediction inputs is compared with radar based Scout performance at ignition of the second, third and fourth stages as well as at injection of the payload into orbit. Also, orbit characteristics are compared.

8.5.2 METHOD

Pre-flight and post-flight trajectories using repredicted motor data were calculated for each vehicle. These trajectories are compared with the pre-flight trajectory originally predicted for each vehicle. At stage ignition times, trajectory parameters are compared with radar data, when available; at injection, trajectory parameters are compared with the injection conditions computed from the orbit data derived from Goddard Space Track Bulletins.

Repredicted pre-flight trajectories incorporate the current second and third stage control fuel consumption weights of 35 and 4.5 pounds, respectively. The original pre-flight calculations for some of the earlier vehicles utilized the then current values of 90 and 10 pounds, respectively. Vehicle weight changes resulting from differences in total and consumed weights between predicted and repredicted motors have been included.

Repredicted post-flight trajectories include vehicle disturbances such as winds and atmospheric deviations, weight changes, and thrust misalignment. To provide the most accurate post-flight trajectory possible, telemetry records were reviewed to isolate vehicle disturbances, as indicated by displacement errors, which may not have been available for the usual post-flight analysis conducted after launch.

Results are presented as (1) tabulations of velocity, altitude, and flight path angle for predicted, repredicted, and post-flight trajectories at stage ignition and injection, and (2) tabulations of orbit data from Goddard Space Track Bulletins. These tabulations are compared with radar data where available. Vehicle S-128, which experienced a failure near second stage ignition, is compared by plots of predicted, repredicted, and radar trajectories during first stage flight.

Trajectory data plots and motor performance curves for vehicle S-125 are shown as typical data. See Figures 61 through 71.

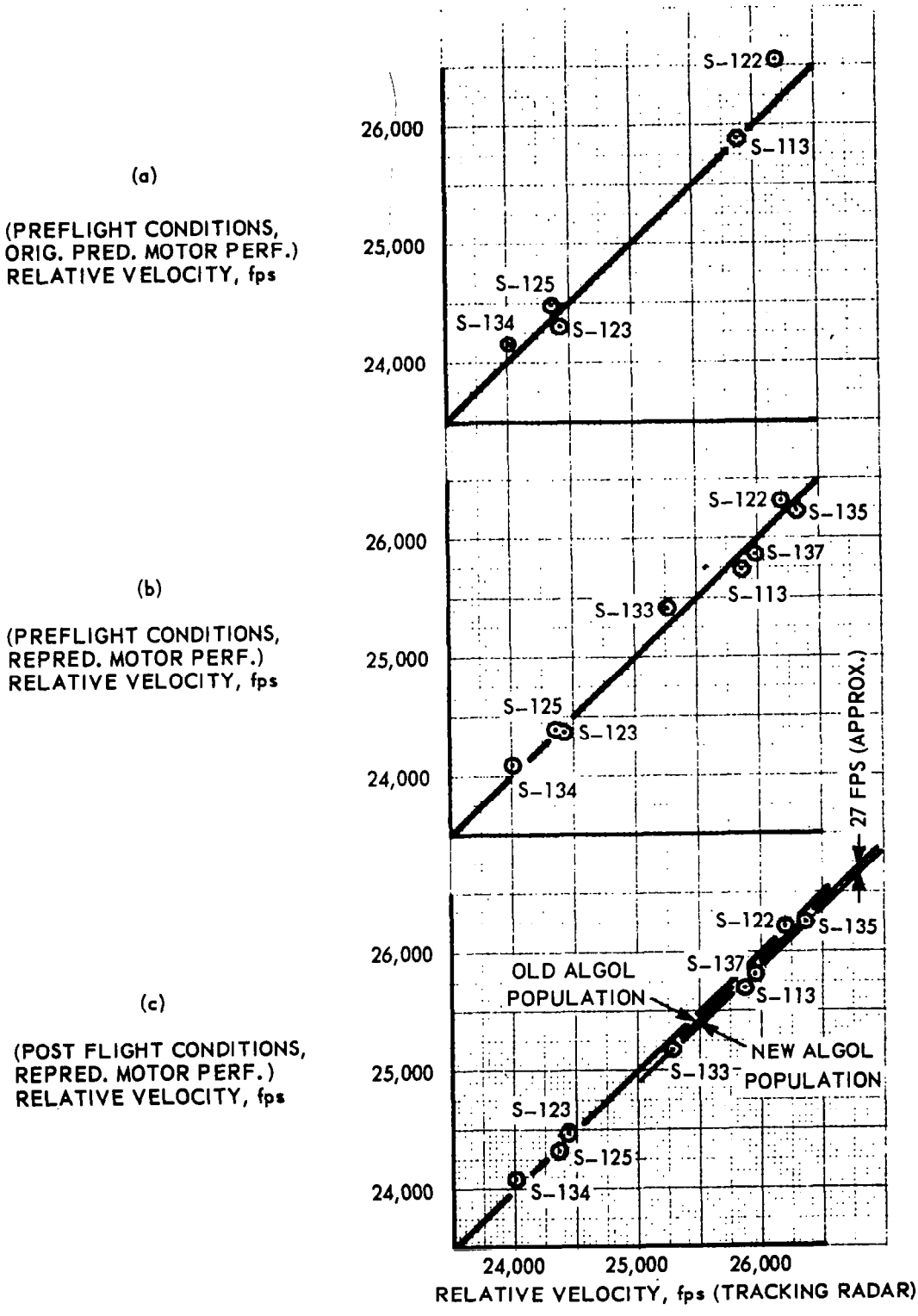

FIGURE 61 INJECTION VELOCITY CORRELATIONS

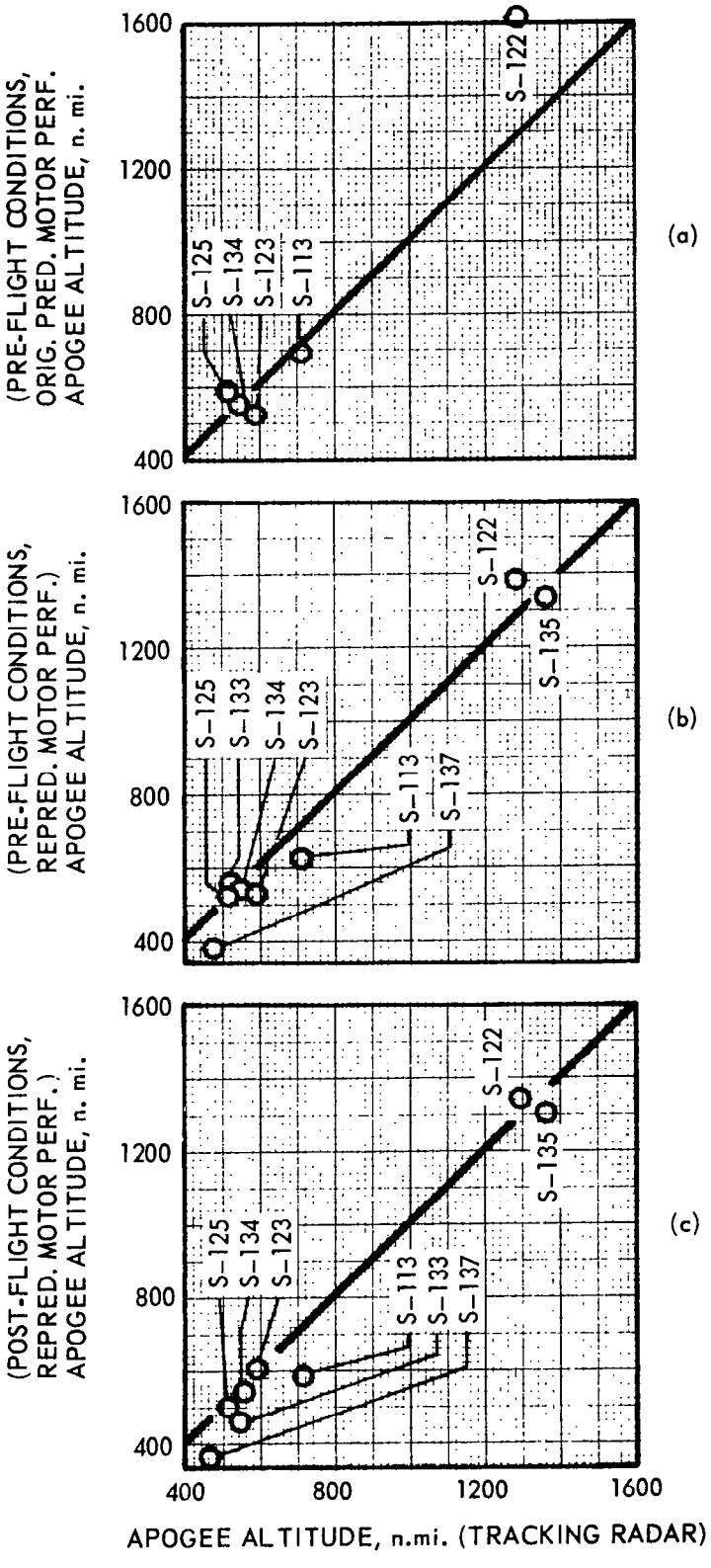

FIGURE 62 APOGEE ALTITUDE CORRELATIONS

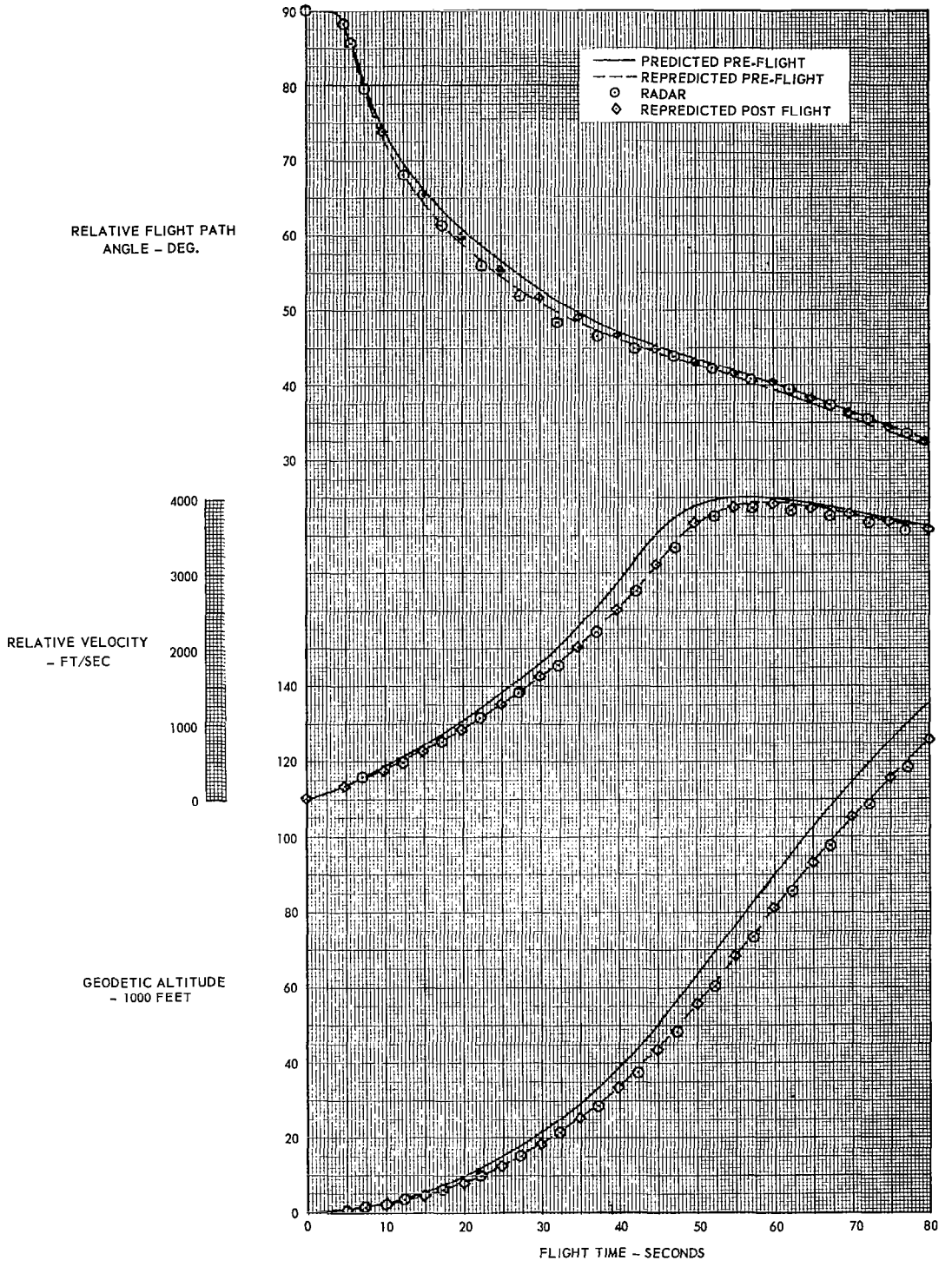

FIGURE 63
SCOUT S–128
HISTORY OF TRAJECTORY PARAMETERS – FIRST STAGE

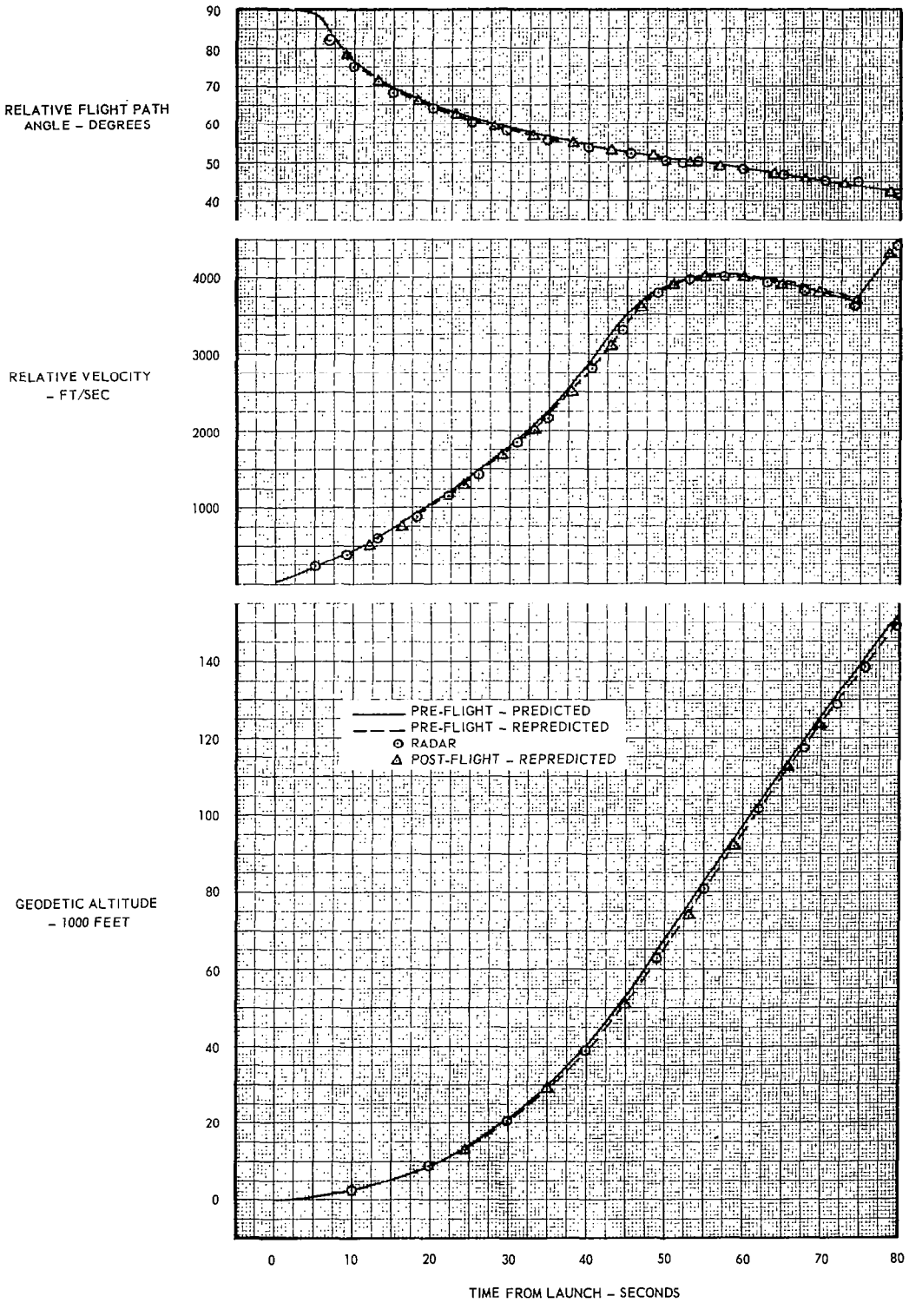

FIGURE 64
SCOUT S–125
TRAJECTORY PARAMETERS – FIRST STAGE TIME HISTORY

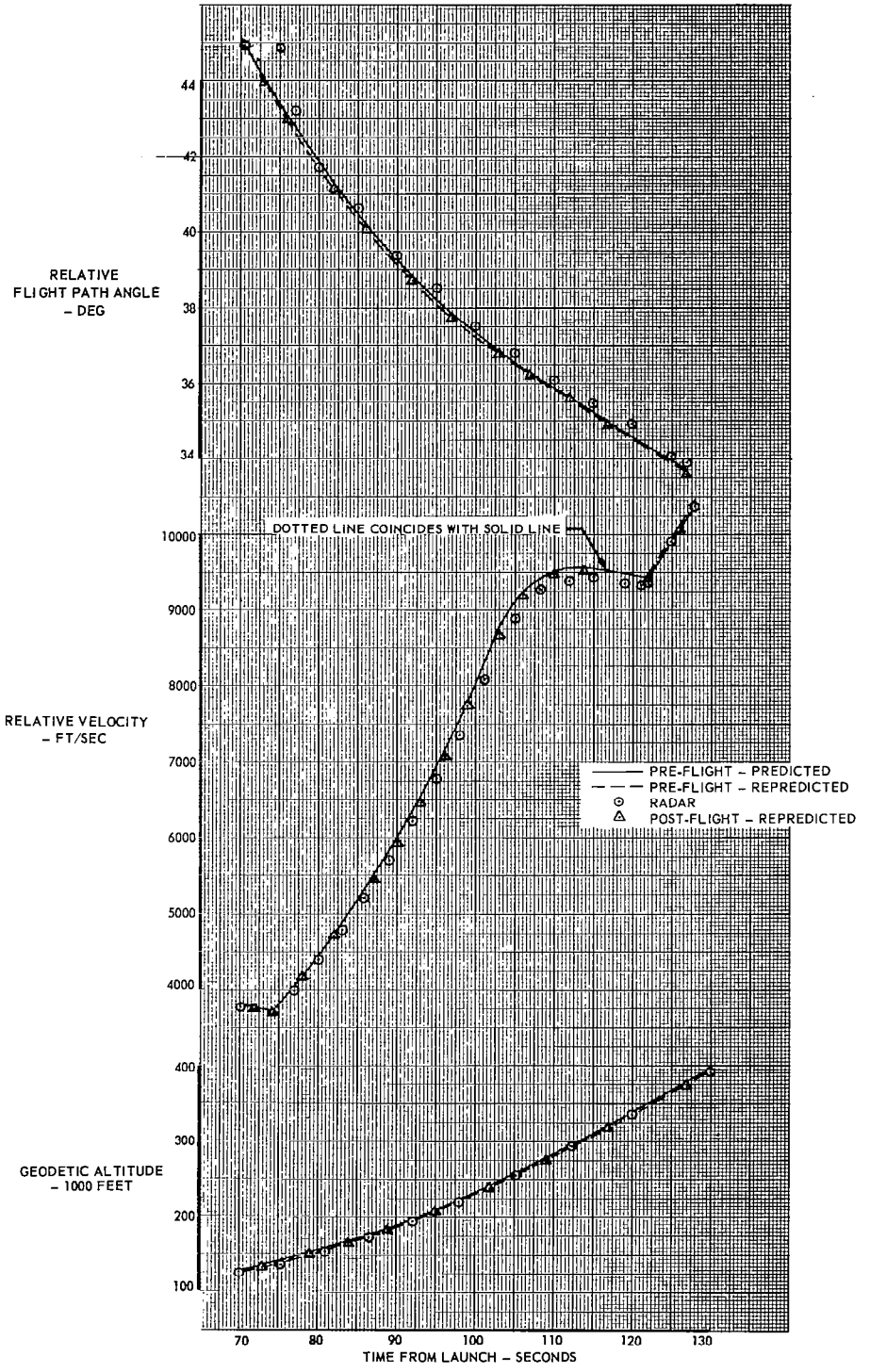

FIGURE 65
SCOUT S–125
TRAJECTORY PARAMETERS – SECOND STAGE TIME HISTORY

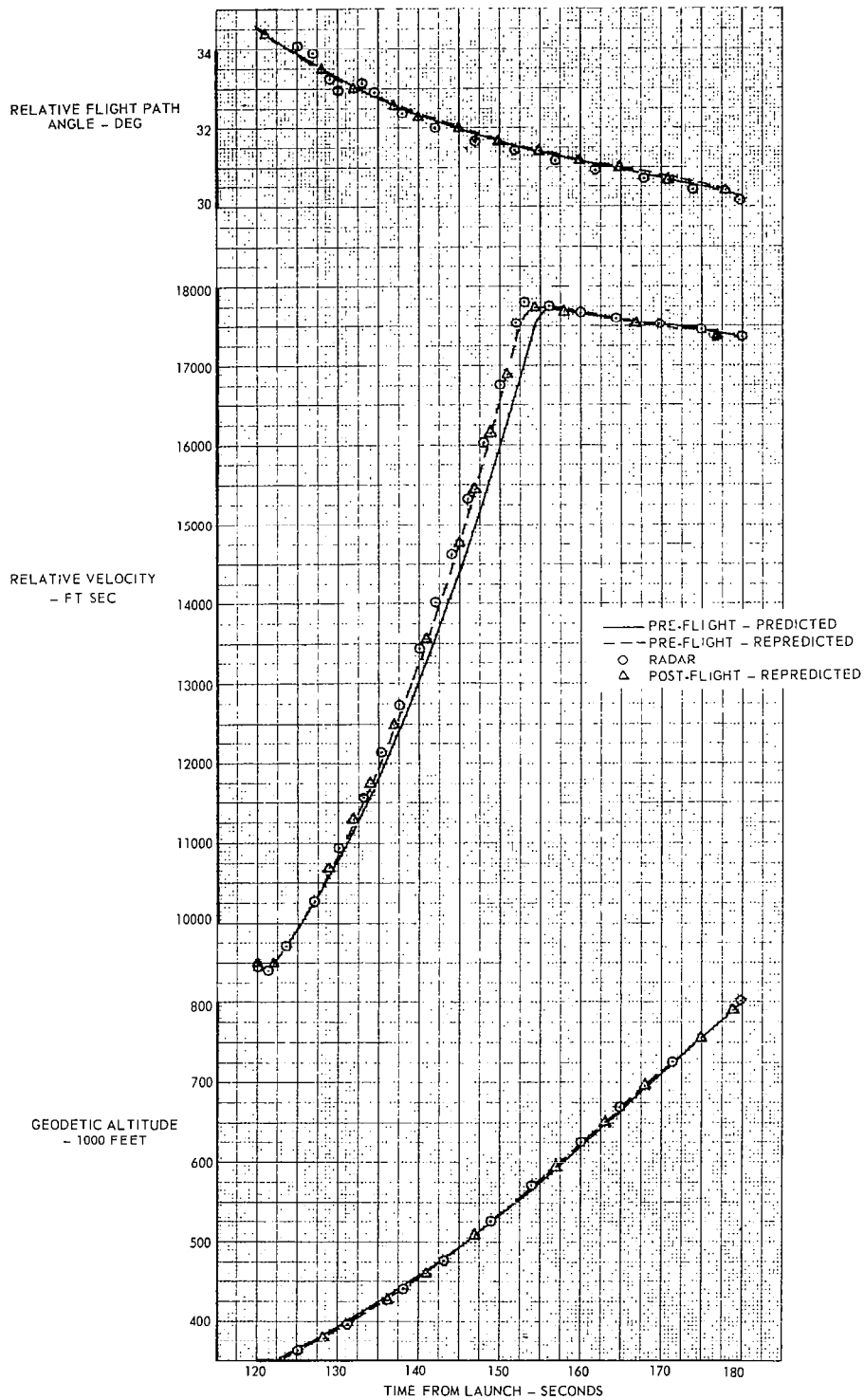

FIGURE 66
SCOUT S –125
TRAJECTORY PARAMETERS – THIRD STAGE TIME HISTORY

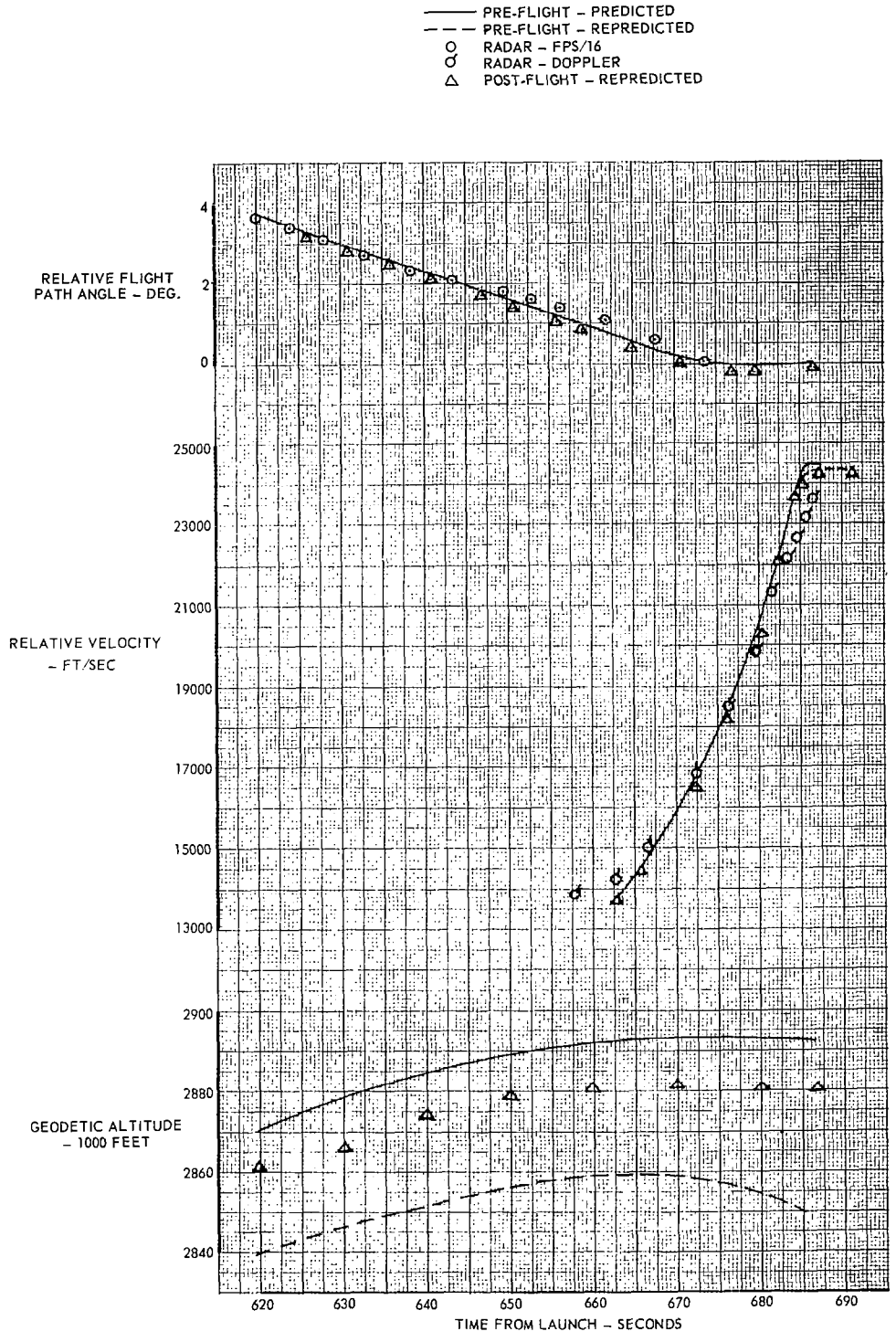

FIGURE 67
SCOUT S–125
TRAJECTORY PARAMETERS – FOURTH STAGE TIME HISTORY

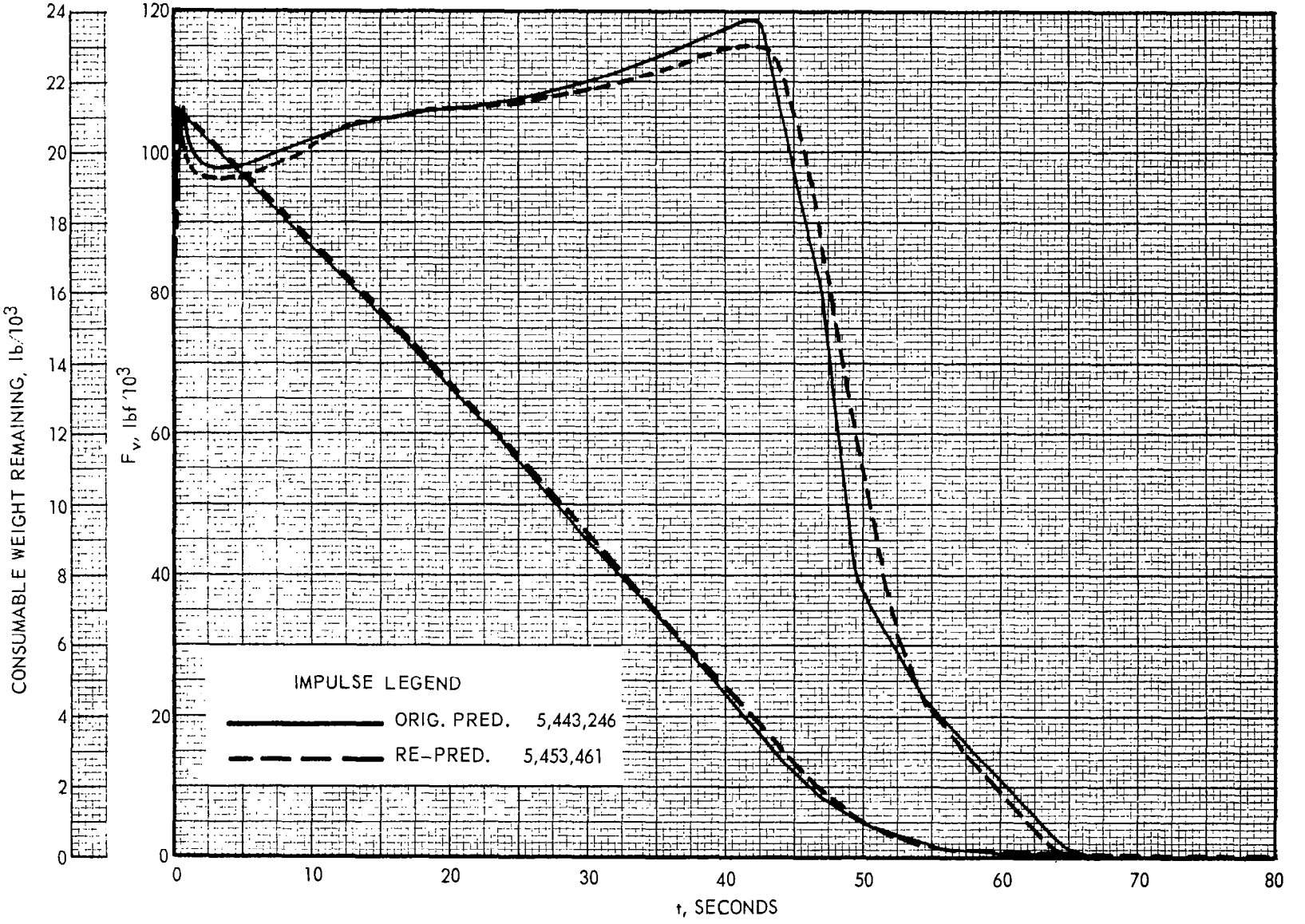

FIGURE 68 S-125 ALGOL IIA S/N 24 PERFORMANCE PREDICTIONS

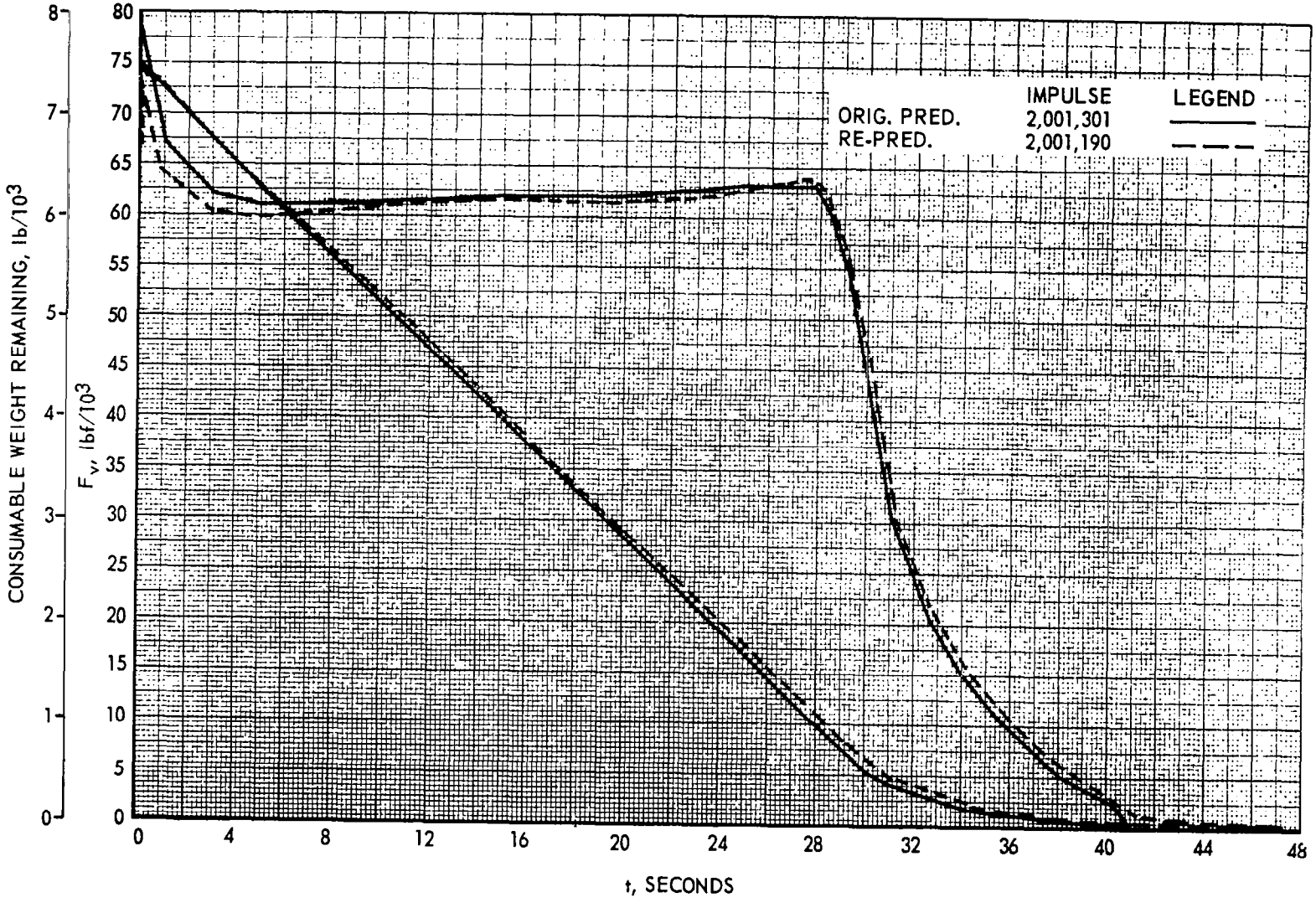

FIGURE 69 S-125 CASTOR I S/N 182 PERFORMANCE PREDICTIONS

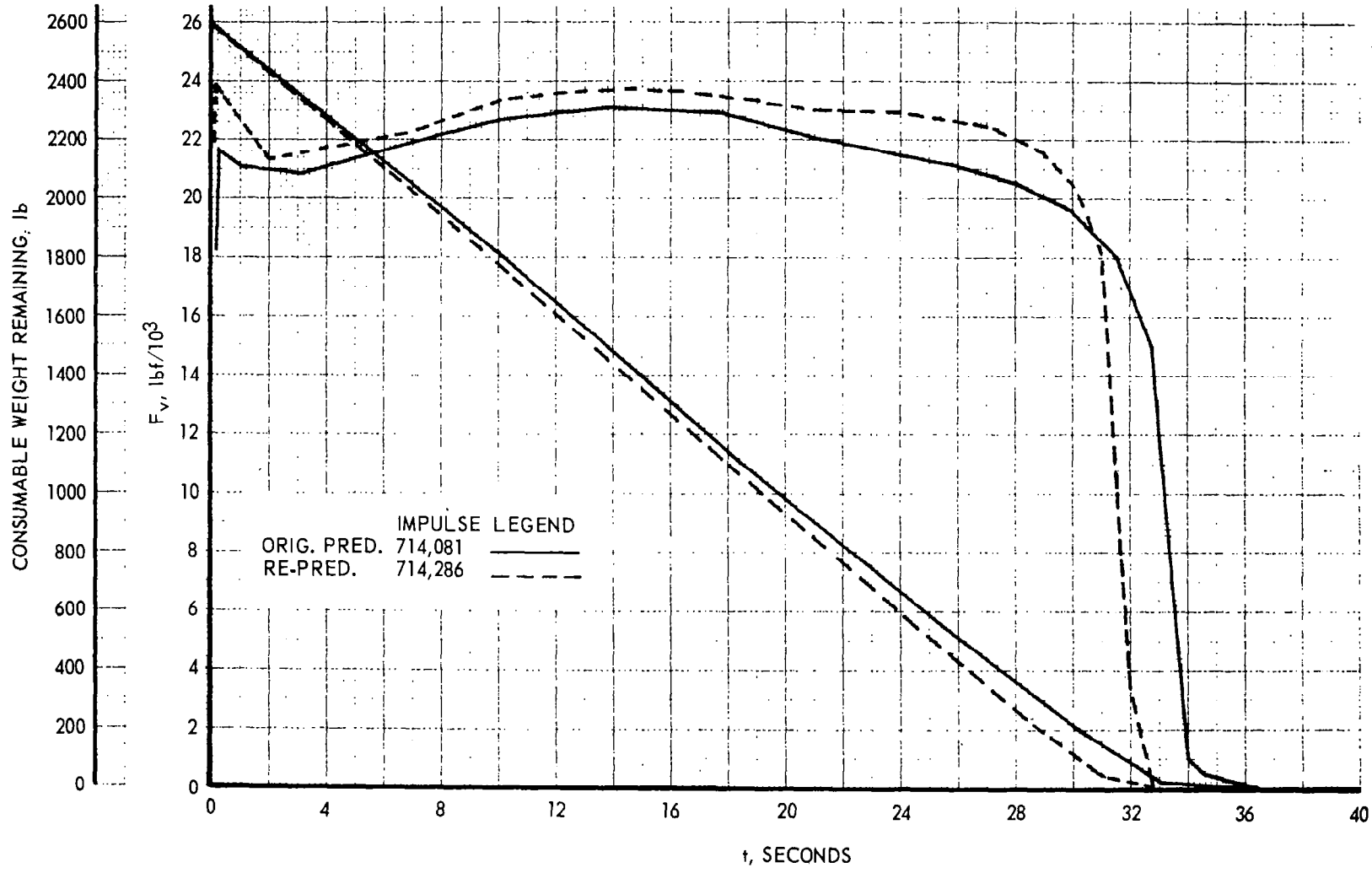

FIGURE 70 S-125 X259 S/N HPC-146 PERFORMANCE PREDICTIONS

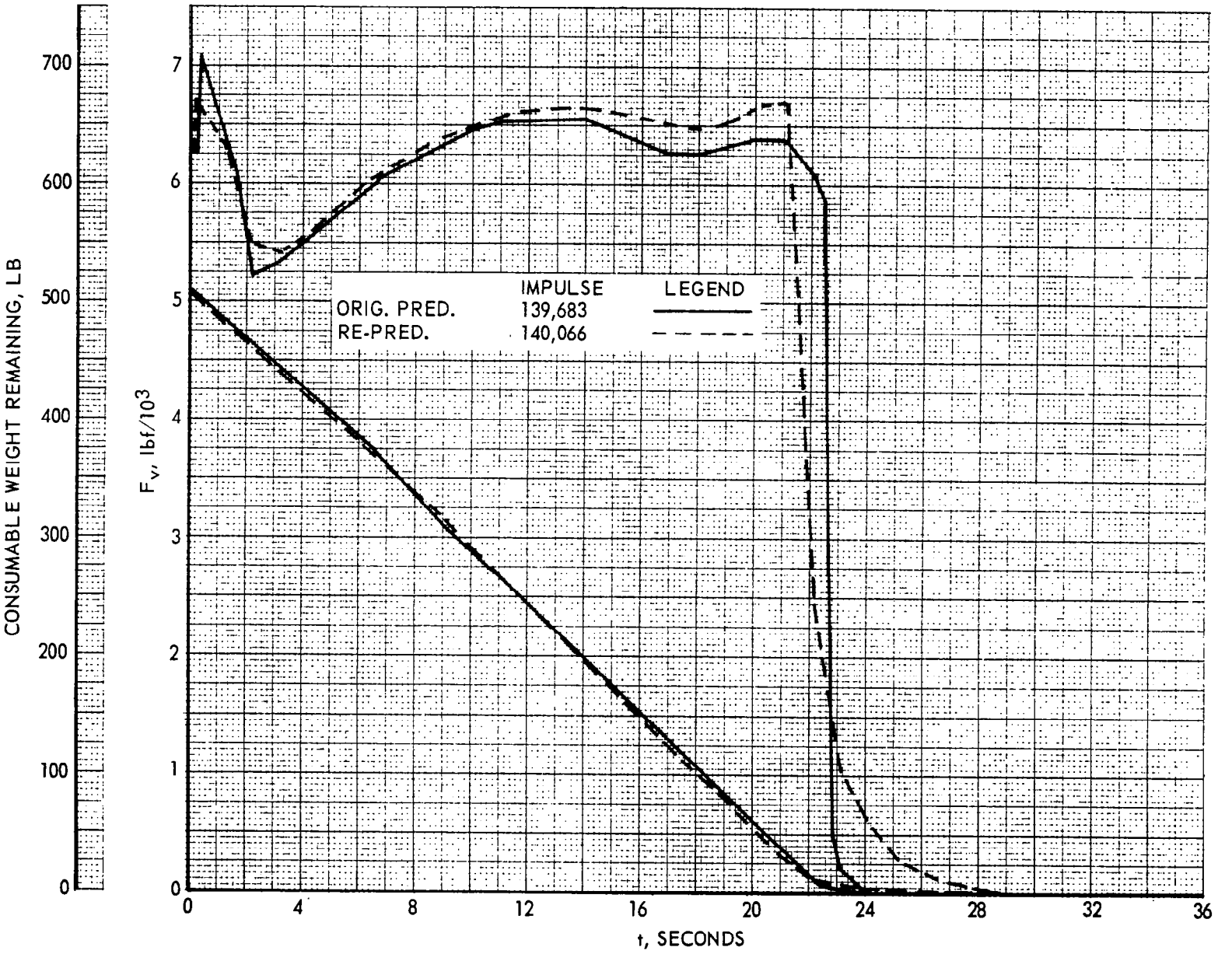

FIGURE 71 S-125 X258 S/N RH-55 PERFORMANCE PREDICTIONS

8.5.3 DISCUSSION OF RESULTS

The disagreement (as a bias and standard deviation) in the correlation of results from each type of pre-flight input and the post-flight inputs with the results from Goddard data can be compared for an indication of relative accuracies among the two types of pre-flight inputs and the post-flight inputs. All the bias and standard deviation values include the small error in the Goddard data. Also, the values involve a mixture of mission requirements. The bias and standard deviation values are not measures of Scout performance errors. They are appropriate only for this analysis.

Because complete trajectories were computed, an individual assessment of each stage is not presented. Injection conditions would be affected by anomalies in any one of the four stages. The radar data tabulated at stage ignition provide some basis for estimating stage performance but it must be remembered that radar data accuracy is often questionable, particularly in the vicinity of stage ignition or burnout.

Following is a summary of the results obtained for each vehicle.

Vehicle S-113

The repredicted post-flight trajectory includes a pitch up displacement of 0.8 degree in the second stage.

It is evident from the comparison shown in Table 21 that the predicted pre-flight trajectory is in much closer agreement with the injection conditions and orbit data calculated from Goddard Space Track Bulletins than the trajectory incorporating repredicted engine data.

Up to stage 4 ignition, there is little difference between the predicted and repredicted trajectories. The largest deviation occurs at stage 3 ignition and radar data appear to correlate with repredicted data. At fourth stage ignition, predicted pre-flight velocity is approximately 22 fps lower and altitude is 1.3 n. mi. lower than repredicted pre-flight data. But at injection, repredicted pre-flight velocity is approximately 149 fps less than predicted while the altitude deviation is unchanged. If the velocity decrement between repredicted pre-flight and post-flight trajectories is applied to the predicted pre-flight injection velocity and if repredicted post-flight injection altitude is assumed to be correct (since it appears that the repredicted trajectory is the more accurate up to stage 4 ignition), the resulting injection conditions would closely match Goddard data. It may be concluded, therefore, that the repredicted fourth stage performance is too low.

TABLE 21
SCOUT VEHICLE S-113
TRAJECTORY AND ORBIT DATA
TRAJECTORY PARAMETERS AT EVENT TIMES

EVENT	TRAJECTORY	TIME SEC.	RELATIVE VELOCITY FPS	GEODETIC ALTITUDE N. MI.	RELATIVE FLT PATH ANGLE-DEG.
STG II IGN	Predicted pre-flight	92.52	3361.0	25.7	32.431
	Repredicted pre-flight	92.52	3353.3	26.0	32.606
	Repredicted post-flight	92.47	3359.0	25.9	32.420
	Radar (FPS-16)	92.45	3320.0	25.9	32.99
STG III IGN	Predicted pre-flight	137.42	9228.6	47.4	21.607
	Repredicted pre-flight	137.42	9319.8	47.4	21.568
	Repredicted post-flight	137.39	9319.1	47.6	21.910
	Radar (FPS-16)	137.40	9270.0	47.8	22.10
STG IV IGN	Predicted pre-flight	510.54	15894.2	224.8	.445
	Repredicted pre-flight	510.54	15916.1	226.1	.542
	Repredicted post-flight	510.54	15880.7	229.3	.707
	Radar		not available		

INJECTION CONDITIONS

EVENT	DATA SOURCE	TIME SEC.	INERTIAL VELOCITY FPS	ALTITUDE* N. MI.	INERTIAL FLT PATH ANGLE-DEG.
STG IV B.O.	Predicted pre-flight	534.54	25882.	226.9	-0.029
	Repredicted pre-flight	539.54	25733.	228.3	0.067
	Repredicted post-flight	539.54	25701.3	231.8	0.155
	Goddard Space Track Bulletins**		25864.4	232.8	0.733

ORBIT DATA*

DATA SOURCE	APOGEE N. MI.	PERIGEE N. MI.
Predicted pre-flight	696.2	226.9
Repredicted pre-flight	601.5	228.3
Repredicted post-flight	592.4	231.4
Goddard Space Track Bulletins**	710.5	227.6

STAGE IGNITION WEIGHT - LB. (INCLUDING PAYLOAD)

STAGE	PREDICTED	REPREDICTED	POST-FLIGHT
1	38,579.95	38,594.95	38,594.95
2	13,940.32	13,940.32	13,940.32
3	4,190.72	4,190.72	4,190.72
4	807.99	807.99	807.99

*Based on mean earth radius
**Computed from average of several bulletins

Vehicle S-122

The post-flight trajectory includes atmospheric deviations, weight changes, and pitch and yaw displacements as determined from telemetry records. The available wind data, recorded approximately 4 hours before launch, were not considered a true representation of winds actually experienced by the vehicle and were therefore omitted from the post-flight analysis. The vehicle disturbances represented by the displacements shown on telemetry records made a significant contribution to the higher altitude and lower velocity than were predicted at injection. These displacement errors were all in a pitch up direction and of magnitudes 1.0, 1.0, and 0.6 degrees for the first, second, and third stage boost phases, respectively.

Table 22 shows that repredicted motor data provide a closer approximation to the injection conditions and orbit data derived from Goddard Space Track Bulletins.

Predicted, repredicted and radar data (compared with post-flight) compare well up to fourth stage ignition. At injection it is obvious that the repredicted pre-flight trajectory agrees more closely to Goddard data in velocity than does the predicted trajectory. Changes simulated in the post flight trajectory result, at fourth stage ignition, in a velocity loss of approximately 66 fps with a corresponding increase in altitude. At injection, post-flight velocity is 64 fps higher than indicated by Goddard data while altitude is approximately 1.3 n. mi. lower. It is apparent that the repredicted fourth stage performance is a much better approximation of the estimated performance calculated from Goddard data than is the predicted performance. A small decrease in repredicted fourth stage performance would eliminate the velocity deviation while a more accurate simulation of vehicle disturbances would correct the altitude deviation. Orbit data essentially confirm these conclusions.

Vehicle S-123

The repredicted post-flight trajectory includes winds, atmospheric deviations, weight changes, and a pitch down displacement of 0.75 degree during third stage boost.

As shown in Table 23, both predicted and repredicted pre-flight trajectories agree closely. The repredicted trajectory is the better of the two when compared with Goddard data. The apparent better correlation of the repredicted trajectory to the Goddard data may be attributed almost entirely to repredicted fourth stage performance which adds approximately 22 fps to injection velocity. It must be remembered, however, that this increment of velocity is well within the accuracy usually expected of radar and tracking data.

The pitch down disturbance which was recorded during third stage boost is the primary cause for the higher than predicted injection velocity and lower than predicted injection altitude, clearly indicated by the post-flight trajectory data.

TABLE 22
SCOUT VEHICLE S-122
TRAJECTORY AND ORBIT DATA
TRAJECTORY PARAMETERS AT EVENT TIMES

EVENT	TRAJECTORY	TIME SEC.	RELATIVE VELOCITY FPS	GEODETIC ALTITUDE N. MI.	RELATIVE FLT PATH ANGLE-DEG.
STG II IGN	Predicted pre-flight	85.01	3499.2	25.0	36.662
	Repredicted pre-flight	85.01	3502.7	24.9	36.606
	Repredicted post-flight	85.01	3480.3	25.3	37.920
	Radar (FPS-16)	84.90	3475.0	25.1	37.370
STG III IGN	Predicted pre-flight	132.50	9432.1	52.6	26.223
	Repredicted pre-flight	132.50	9409.0	52.2	26.131
	Repredicted post-flight	132.50	9370.7	53.4	27.102
	Radar (FPS-16)	132.50	9345.0	52.9	26.85
STG IV IGN	Predicted pre-flight	580.33	15464.9	322.2	0.640
	Repredicted pre-flight	580.33	15449.4	318.7	0.436
	Repredicted post-flight	580.33	15383.8	320.4	0.375
	Radar (FPS-16)	580.40	15375	322.6	N.A.

INJECTION CONDITIONS

EVENT	DATA SOURCE	TIME SEC.	INERTIAL VELOCITY FPS	ALTITUDE* N. MI.	INERTIAL FLT PATH ANGLE-DEG.
STG IV B.O.	Predicted pre-flight	606.33	26561.7	325.7	0.0
	Repredicted pre-flight	609.33	26308.6	321.9	-0.094
	Repredicted post-flight	609.33	26252.3	323.2	-0.430
	Goddard Space Track Bulletins **		26186.3	324.5	0.250

ORBIT DATA*

DATA SOURCE	APOGEE N. MI.	PERIGEE N. MI.
Predicted pre-flight	1616.4	322.1
Repredicted pre-flight	1385.0	321.9
Repredicted post-flight	1344.1	322.2
Goddard Space Track Bulletins**	1294.9	326.2

STAGE IGNITION WEIGHT - LB. (INCLUDING PAYLOAD)

STAGE	PREDICTED	REPREDICTED	POST-FLIGHT
1	38,549.49	38,549.49	38,552.99
2	13,861.85	13,861.85	13,858.35
3	4,107.77	4,107.77	4,109.27
4	729.07	729.07	728.87

*Based on mean earth radius
**Computed from average of several bulletins

TABLE 23

SCOUT VEHICLE S-123

TRAJECTORY AND ORBIT DATA

TRAJECTORY PARAMETERS AT EVENT TIMES

EVENT	TRAJECTORY	TIME SEC.	RELATIVE VELOCITY FPS	GEODETIC ALTITUDE N. MI.	RELATIVE FLT PATH ANGLE-DEG.
STG II IGN	Predicted pre-flight	77.85	3532.9	22.3	44.963
	Repredicted pre-flight	77.85	3537.5	21.7	44.638
	Repredicted post-flight	77.75	3528.4	21.6	44.591
	Radar (FPS-16)	77.75	N.A.	21.2	N.A.
STG III IGN	Predicted pre-flight	125.36	9243.8	56.8	35.504
	Repredicted pre-flight	125.36	9237.2	55.9	35.325
	Repredicted post-flight	125.35	9236.5	55.8	35.288
	Radar (FPS-16)	125.32	9212.0	55.6	35.460
STG IV IGN	Predicted pre-flight	679.80	13301.6	491.7	0.468
	Repredicted pre-flight	679.80	13308.6	490.1	0.402
	Repredicted post-flight	679.97	13389.6	482.5	0.069
	Radar (FPS-16)	680.00	N.A.	483.2	0.060

INJECTION CONDITIONS

EVENT	DATA SOURCE	TIME SEC.	INERTIAL VELOCITY FPS	ALTITUDE* N. MI.	INERTIAL FLT PATH ANGLE-DEG.
STG IV B.O.	Predicted pre-flight	703.80	24296.4	495.2	-0.140
	Repredicted pre-flight	708.80	24325.3	493.5	-0.163
	Repredicted post-flight	708.97	24447.0	485.9	-0.043
	Goddard Space Track Bulletins**		24442.0	486.5	0.25

ORBIT DATA*

DATA SOURCE	APOGEE N. MI.	PERIGEE N. MI.
Predicted pre-flight	519.6	491.5
Repredicted pre-flight	532.6	490.5
Repredicted post-flight	586.7	485.8
Goddard Space Track Bulletins**	588.5	483.4

STAGE IGNITION WEIGHT - LB. (INCLUDING PAYLOAD)

STAGE	PREDICTED	REPREDICTED	POST-FLIGHT
1	38,692.65	38,723.65	38,717.95
2	13,900.27	13,900.27	13,894.57
3	4,116.20	4,116.20	4,117.50
4	718.69	718.69	717.59

*Based on mean earth radius

**Computed from average of several bulletins

Vehicle S-125

The repredicted post-flight trajectory calculation includes a pitch up displacement of 0.70 degree during second stage boost.

Repredicted pre-flight data are in better agreement with Goddard data than are the predicted, as indicated in Table 24 . Post-flight injection velocity is approximately 24 fps less than velocity calculated from Goddard data while the altitude difference is less than one n. mi. This velocity decrement appears to be approximately the same decrement (compared to radar) observed at fourth stage ignition between predicted and repredicted pre-flight data and indicates a) that repredicted third stage performance should be a fraction higher, and b) the repredicted fourth stage performance appears to simulate the stage performance inferred from Goddard data. The higher post-flight injection altitude and lower velocity result from the pitch up disturbance which occurred during second stage boost.

Orbit data reflect the close agreement between repredicted and Goddard data. For this particular orbit, the assumption of an injection path angle of 0.34 degree, as is indicated by Goddard data, applied to the post-flight injection velocity and altitude would result in a perigee altitude of 459.4 n. mi. and an apogee altitude of 507.3 n. mi.

Vehicle S-128

A failure occurred in the neighborhood of second stage ignition during the flight of this vehicle. Repredicted motor evaluation is therefore restricted to the first stage and calculated trajectories are compared to radar data in Figure 63 .

The repredicted post-flight trajectory includes measured winds, post-flight weights, and a first stage thrust misalignment. From Figure 63 it is immediately apparent that the repredicted trajectory is a better estimate of the vehicle performance indicated by radar data than is the predicted trajectory. It would appear, from the radar data, that the repredicted thrust during tail-off is too high and over-all thrust level may be a little high.

Vehicle S-134

Measured winds, post-flight weights, and a first stage thrust misalignment are incorporated in the repredicted post-flight trajectory. A post-flight increase of about 58 pounds in second stage inert weight results in a decrease in velocity at stage 3 ignition of about 55 fps.

First stage moment disturbances, which included thrust misalignment, were in the pitch up direction. No vehicle disturbances for subsequent stages were included in the post-flight trajectory.

Unlike the vehicles evaluated in preceding paragraphs, S-134 shows appreciable differences between the predicted and repredicted pre-flight

TABLE 24

SCOUT VEHICLE S-125

TRAJECTORY AND ORBIT DATA

TRAJECTORY PARAMETERS AT EVENT TIMES

EVENT	TRAJECTORY	TIME SEC.	RELATIVE VELOCITY FPS	GEODETIC ALTITUDE N. MI.	RELATIVE FLT PATH ANGLE-DEG.
STG II IGN	Predicted pre-flight	74.43	3694.2	22.6	43.652
	Repredicted pre-flight	74.43	3678.4	22.1	43.376
	Repredicted post-flight	74.36	3668.9	22.0	43.417
	Radar (FPS-16)	74.35	3670	22.2	N.A.
STG III IGN	Predicted pre-flight	121.92	9453.1	57.1	34.346
	Repredicted pre-flight	121.92	9412.7	56.1	34.154
	Repredicted post-flight	121.86	9396.6	56.3	34.654
	Radar (FPS-16)	121.85	N.A.	56.3	N.A.
STG IV IGN	Predicted pre-flight	663.10	13736.1	476.1	0.673
	Repredicted pre-flight	663.10	13719.7	470.3	0.347
	Repredicted post-flight	663.31	13651.5	474.4	0.466
	Radar (Doppler)	663.00	13670	N.A.	N.A.

INJECTION CONDITIONS

EVENT	DATA SOURCE	TIME SEC.	INERTIAL VELOCITY FPS	ALTITUDE* N. MI.	INERTIAL FLT PATH ANGLE-DEG.
STG IV B.O.	Predicted pre-flight	692.10	24482	479.8	0.01
	Repredicted pre-flight	692.10	24399.4	473.7	-0.182
	Repredicted post-flight	692.31	24335.7	477.8	-0.164
	Goddard Space Track Bulletins		24359.5	478.6	0.34

ORBIT DATA*

DATA SOURCE	APOGEE-N. MI.	PERIGEE-N.MI.
Predicted pre-flight	591.5	479.8
Repredicted pre-flight	521.0	470.3
Repredicted post-flight	495.0	470.8
Goddard Space Track Bulletins**	520.5	465.4

STAGE IGNITION WEIGHT - LB. (INCLUDING PAYLOAD)

STAGE	PREDICTED	REPREDICTED	POST-FLIGHT
1	38,515.0	38,552.80	38,552.80
2	13,867.65	13,867.65	13,867.65
3	4,103.54	4,103.54	4,103.54
4	720.49	720.49	720.49

* Based on mean earth radius

** Computed from average of several bulletins

trajectories prior to stage 4 ignition. From Table 25, it appears that the predicted trajectory more closely approximates radar data for the first two stages. At stage 4 ignition, the biggest difference between the two trajectories is in altitude. If the performance of the first two repredicted stages was reduced to agree with radar data, the total impulse of the third stage repredicted motor would have to be higher to produce a trajectory corresponding to radar data. The thrust level of this repredicted motor is higher than originally predicted; this higher thrust level appears reasonable inasmuch as the higher altitude at fourth stage ignition may be attributed to the higher path angle which results from the higher thrust level.

At injection, the deviations between the predicted and repredicted trajectories are essentially the deviations observed at stage 4 ignition; therefore, the effect of repredicted and predicted fourth stage motors is virtually the same. While repredicted total impulse is higher, the additional "inert weight" resulting from unconsumed propellant cancels out the potential increase in velocity.

The post-flight injection velocity is about 40 fps higher than calculated from Goddard data while altitude differences are negligible.

It is interesting to note that individually, the repredicted motors and radar data do not agree as well when compared stage by stage as do the predicted motors, and yet the repredicted injection conditions more closely approximate the injection conditions calculated from Goddard data.

TABLE 25

SCOUT VEHICLE S-134

TRAJECTORY AND ORBIT DATA

TRAJECTORY PARAMETERS AT EVENT TIMES

EVENT	TRAJECTORY	TIME SEC.	RELATIVE VELOCITY FPS	GEODETIC ALTITUDE N. MI.	RELATIVE FLT PATH ANGLE-DEG.
STG II IGN	Predicted pre-flight	74.05	3619.7	22.5	46.082
	Repredicted pre-flight	74.05	3668.0	22.8	46.242
	Repredicted post-flight	73.97	3643.1	22.8	47.146
	Radar (FPS-16)	73.90	3600.0	23.3	47.20
STG III IGN	Predicted pre-flight	121.54	9342.6	58.5	36.965
	Repredicted pre-flight	121.54	9424.8	59.1	37.072
	Repredicted post-flight	121.43	9341.6	59.1	37.361
	Radar (FPS-16)	121.45	9250	59.8	37.70
STG IV IGN	Predicted pre-flight	701.82	13076.3	534.5	0.617
	Repredicted pre-flight	701.82	13047.8	539.5	0.807
	Repredicted post-flight	701.99	13008.8	540.0	0.768
	Radar (projected radar data)	702.00	13000.0	537.4	0.50

INJECTION CONDITIONS

EVENT	DATA SOURCE	TIME SEC.	INERTIAL VELOCITY FPS	ALTITUDE* N. MI.	INERTIAL FLT PATH ANGLE-DEG.
STG IV B.O.	Predicted pre-flight	725.82	24138.8	538.2	-0.017
	Repredicted pre-flight	730.82	24101.3	543.4	0.073
	Repredicted post-flight	730.99	24064.7	543.8	0.009
	Goddard Space Track Bulletins**		24024.3	544.3	-0.40

ORBIT DATA*

DATA SOURCE	APOGEE-N. MI.	PERIGEE-N. MI.
Predicted pre-flight	542.3	537.7
Repredicted pre-flight	545.4	530.8
Repredicted post-flight	543.9	510.0
Goddard Space Track Bulletins**	555.4	474.0

STAGE IGNITION WEIGHT - LB. (INCLUDING PAYLOAD)

STAGE	PREDICTED	REPREDICTED	POST-FLIGHT
1	38,668.89	38,685.39	38,753.90
2	13,858.61	13,776.11	13,844.62
3	4,091.88	4,091.88	4,093.89
4	714.89	714.89	714.89

* Based on mean earth radius

** Computed from average of several bulletins

8.5.4 IMPROVEMENT IN INJECTION AND ORBIT ACCURACY

COMPARISON OF INJECTION CONDITIONS
WITH GODDARD DATA
(REF. FIGURE 61)

Vehicle	Deviation from Goddard Data at Injection: Predicted Pre-flight	Repredicted Pre-flight	Repredicted Post-flight
S-113 Alt-n. mi.	-5.9	-4.5	-1.0
Velocity-fps	+17.6	-131.4	-163.1
Path Angle-deg.	-0.762	-0.666	-0.578
S-122 Alt-n. mi.	+1.2	-2.6	-1.3
Velocity-fps	+375.4	+122.3	+66.0
Path Angle-deg.	-0.25	-0.344	-0.680
S-123 Alt-n. mi.	+8.7	+7.0	-0.6
Velocity-fps	-145.6	-116.7	+5.0
Path Angle-deg.	-0.39	-0.413	-0.293
S-125 Alt-n. mi.	+1.2	-4.9	-0.8
Velocity-fps	+122.5	+38.9	-23.8
Path Angle-deg	-0.33	-0.522	-0.504
S-134 Alt-n. mi.	-6.1	-0.9	-0.5
Velocity-fps	+114.5	+77.0	+40.3
Path Angle-deg.	+0.383	+0.473	+0.409

	PAPS Predicted Pre-Flight	PAPS Predicted Post-Flight
S-133 Alt-n. mi.	-9.5	+4.1
Velocity-fps	+63.0	-120.0
Path Angle-deg.	-0.49	-0.24
S-135 Alt-n. mi.	-4.8	-4.2
Velocity-fps	-36.4	-44.6
Path Angle-deg.	+0.17	+0.37
S-137 Alt-n. mi.	-0.5	+2.0
Velocity-fps	-121.4	-143.2
Path Angle-deg.	+0.412	+0.612

Statistical Measures of Deviations at Injection*

Injection Characteristic	Pred., Pre-flight Bias	Pred., Pre-flight Std. Dev.	Repred & PAPS Pred. Pre-flt. Bias	Repred & PAPS Pred. Pre-flt. Std. Dev.	Repred., Post-flt. Bias	Repred., Post-flt. Std. Dev.
Altitude-n.mi.	-0.2	6.1	-2.6	4.8	-0.3	2.4
Velocity-fps	+47.0	124.0	-13.1	102.0	47.9	86.0
Path Angle-deg.	-0.17	0.46	-0.17	0.45	0.11	0.50

*The tabulated values are not representative of Scout performance errors for any specific mission.

COMPARISON OF ORBIT WITH GODDARD DATA
(REF. FIGURE 62)

Vehicle		Deviation from Goddard Tracking Data: Predicted Pre-flight	Repredicted Pre-flight	Repredicted Post-flight
S-113	Perigee-n. mi.	-0.7	+0.7	+3.8 (-2.4)*
	Apogee-n. mi.	-14.3	-109.0	-118.1 (-111.5)
S-122	Perigee-n. mi.	-4.1	-4.3	-4.0
	Apogee-n. mi.	+321.5	+90.1	+49.2
S-123	Perigee-n. mi.	+8.1	+7.1	+2.4
	Apogee-n. mi.	-68.9	-55.9	-1.8
S-125	Perigee-n. mi.	+14.4	+4.9	+5.4 (-6.0)*
	Apogee-n. mi.	+71.0	+0.5	-24.6 (-13.2)*
S-134	Perigee-n. mi.	+63.7	+56.8	+36.0 (+20.4)*
	Apogee-n. mi.	-13.1	-10.0	-11.5 (+3.9)*

		PAPS Predicted Pre-Flight	PAPS Predicted Post-Flight
S-133	Perigee-n. mi.	-7.3	+6.1
	Apogee-n. mi.	+6.9	-65.5
S-135	Perigee-n. mi.	-4.6	-4.1
	Apogee-n. mi.	-50.4	-54.3
S-137	Perigee-n. mi.	+2.6	+4.8
	Apogee-n. mi.	-78.4	-83.1

Statistical Measures of Deviation from Orbit*

Orbit Characteristic	Pred., Pre-flt. Bias	Pred., Pre-flt. Std.Dev.	Repred. and PAPS Pred. Pre-flt. Bias	Repred. and PAPS Pred. Pre-flt. Std. Dev.	Repred., Post-flt. Bias	Repred., Post-flt. Std. Dev.
Perigee-n. mi.	+16.3	25	+7.0	21	+2.2	8.6
Apogee-n. mi.	+59	139	-26	62	-35	53

*The tabulated values are not representative of Scout performance errors for any specific mission.

8.5.5 CONCLUSIONS

Over-all, the repredicted motor data analyzed show an improvement over the originally predicted motor data. The significance of the improvement is somewhat obscured by the relatively large error sources elsewhere than in motor predictions, evidenced by the large reduction in error by using post-flight data.

9.0 CONCLUSIONS

Over-all, the repredicted motor data analyzed show an improvement over the originally predicted motor data. The significance of the improvement is somewhat obscured by the relatively large error sources elsewhere than in motor predictions, evidenced by the large reduction in error by using post-flight data.

As a result of the PAPS effort, pitch programs for Scout trajectories can be designed with significantly less error. Improvements in the prediction of Scout motor performance include:

A. Burn Rate

	One Sigma Error, Percent Used in Error Analysis		
Motor	NASA	LTV	PAPS
Algol II	1.65	3.2	1.4
Castor I	1.65	2.5	1.0
X259	1.65	5.0	1.8

B. Specific Impulse

	One Sigma Error, Percent Used in Error Analysis		
Motor	NASA	LTV	PAPS
Algol II	0.5	0.34	0.18
Castor I	0.5	0.75	0.094
X259	0.5	0.69	0.14

C. Consumable Weight Remaining

(1) The new procedure for predicting consumable weight remaining versus time obtains a more accurate prediction of the stage velocity increment:

Motor	Burnout Velocity (Ideal), fps, Error Avoided by Change to PAPS Procedure from Prior Procedure
Algol II	3
Castor I	19
X259	(No Change)

(2) The new procedure for the X258 predicts unburned propellant (4.1 pounds). This has not been confirmed.

Estimates of prediction errors which will be encountered in applying the new procedures can be summarized:

	One Sigma, Percent				
Motor	Specific Impulse	Propellant Weight	Total Inerts	Burn-out Weight	Burn Rate
Algol II	0.18	0.06	0.076	1.54	1.4
Castor I	0.094	0.054	0.061	0.73	1.0
X259	0.14	0.06	0.072	0.15	1.8
X258	0.60	0.034	0.056	0.36	1.8*

*estimated

Improvements in predicting Algol II and Castor I burn times have been made by:

A. Changing from the "tangent angle bisector" technique for determining web burn time to the "effective" burn time method.

B. Improving control of, or correcting for, variables in the burn rate test motor system.

C. Determining for the Castor I motor (and confirming a result discovered prior to this study) a K_n condition for the burn rate test motor data that produced the best burn rate correlation with the Castor I burn rate.

The actual variation in specific impulse is much smaller than the apparent variation that is indicated by the differences among measured values obtained from motor firings. As a result, Scout orbit errors attributed to specific impulse variation have been unrealistically large in past error analyses.

The flight performance of the Algol II, Castor I and X259 motors is not significantly different from static test performance.

The accuracies of flight telemetry pressure and acceleration data are roughly the same although the natures of the errors appear different somewhat. Neither type of data is sufficiently accurate for evaluating a normal deviation in impulse for any one motor. However, an apparent impulse discrepancy that persists through consecutive flights of a motor might be discovered due to a significant change in the average of both pressure integrals and thrust integrals derived from acceleration data.

The error in head-cap pressure telemetry data normally is more constant (in percent) throughout the motor burning time than is the error in thrust data based upon acceleration telemetry.

Flight motor temperature data, when available, is sufficiently accurate to permit evaluation of burn rate effects from motor temperature deviations. However, the performance effects of past magnitudes of temperature deviations at launch are relatively unimportant by comparison, for instance, with the normal error in the burn rate prediction procedures. If burn rate prediction accuracy is a special payload requirement, then motor temperatures should be controlled (to the nominal temperature) accordingly.

A recognition of the sensitivity of some types of burning rate correlations to changes in oxidizer particle size is essential in order to avoid significant prediction errors due to deliberate or inadvertent changes in the oxidizer grind ratio.

REFERENCES

1. ORBITAL ERROR ANALYSIS OF THE SCOUT RESEARCH VEHICLE, C. H. Woodling, Jarrell R. Elliott and Paul J. Spull, NASA TN D-1639 May 1963.

2. MISSION ERROR ANALYSIS FOR THE SCOUT VEHICLE, Chance Vought Corp., Astronautics Division, Report No. 23.41, 30 November 1962.

3. BALLISTIC EFFECT OF PYROLYZED LINER IN SOLID PROPELLANT MOTOR FIRINGS, J. L. Gordon, Aerojet-General Corporation, ARS Journal, May 1960.

4. INSTRUMENTATION ACCURACY AND MEASUREMENT PRECISION FOR PERFORMANCE CALCULATION OF SOLID ROCKET MOTORS, Aerojet-General Corporation Technical Memorandum 156A, SRO (Revised), 12 June 1964.

5. AEDC TEST FACILITIES HANDBOOK (5th Edition), Arnold Engineering and Development Center.

6. SPECIAL REPORT, REPRODUCIBILITY OF TOTAL IMPULSE IN SOLID PROPELLANT ROCKET MOTORS, Thiokol Chemical Corp., Huntsville Division Report No. C-A-61-118A (Confidential).

7. FINAL REPORT, STATISTICAL STUDY OF LARGE SOLID MOTOR PARAMETER VARIANCE, Thiokol Chemical Corp., Huntsville Division Report No. 22-64.

8. EXPERIMENTAL EVALUATION OF SOLID PROPELLANT ROCKET MOTORS UNDER ACCELERATION LOADS, John L. Horton, II, Thiokol Chemical Corporation, Elkton Division, Journal of Spacecraft and Rockets, Vol. I, No. 6, Nov.-Dec., 1964.

9. ANALYSIS OF EXPERIMENTAL RESULTS OBTAINED FROM SOLID PROPELLANT MOTORS TESTED UNDER HIGH ACCELERATION CONDITION, Thiokol Chemical Corporation, Huntsville Division Report C-64-5538B.

10. ACCELERATION EFFECTS ON PROPELLANT BURNING, M. D. Eirich, Hercules Powder Co., ABL/EPA-8 October 1962.

APPENDIX A

RECOMMENDED TESTING/STUDIES

1. ERROR IN PREDICTING FOURTH STAGE PERFORMANCE

A program is recommended to alleviate the small but important error in predicting the large velocity increment of the Scout fourth stage. Several variables have been accused of contributing, singly or in combination, to the fourth stage performance variability. The candidates for investigation include:

a. Longitudinal acceleration interacting with X258 spinning.

b. Extinction of burning in the X258 motor before all the propellant is consumed.

c. Retention of alumimum and/or aluminum oxide in the X258 motor.

d. Actual variation in X258 specific impulse.

Correlations between any of these variables and the measurements of fourth stage performance are presently considered inadequate.

A reliable resolution of the problem will require that a correlation involving an X258 variable be based upon X258 data -- not only upon data acquired by another test vehicle. The alternative is significant advancement in the state of the science/art, because 1) reliable correlation of spinning conditions and longitudinal accelerations with their effects on the performance of a given motor design cannot (from experience) be presumed to apply to a motor of another design, even if the propellant composition is the same, and 2) the burning rate of propellant is sensitive (correlated) not only to the propellant composition and motor K_n but also to differences in size and physical design features of the combustion chamber and nozzle. Thus, any use of a vehicle other than the X258 in experiments probably will require a confirmation (and modification) of the test results by repeating key experiments using the X258. Only by developing reliable, accurate theory for predicting differences in propellant pyrolysis rates and combustion reactions according to differences in motor design and operating conditions can the X258 be replaced as the vehicle with which correlation data is acquired.

The program should be initiated by completing the list of candidate error sources. This is emphasized by the recent announcements of previously ignored amounts of alumimum oxide residues in X258 motors after firing at AEDC. It is recommended that all such pertinent information be acquired by re-examination of fired X258 motors, review of X258 manufacturing and test data, and review of X258 and fourth stage flight performance data. The results should be analyzed on the basis that each change in X258 manufacturing practices may require a different correlation with stage performance.

2. ERROR IN PREDICTING FIRST STAGE BURN TIME

A program is recommended to establish a more reliable basis for the Algol II burn rate prediction correlation. Data for motors 31 (static test), 32 (S-133), 33 (S-135) and 34 (S-137) indicate that the burn rates of these motors were all about three percent lower than predicted by the original correlation involving prior Algol II and 10 KS 2500 burn rates. The original correlation would not have forecast four such prediction errors in fewer than about one thousand firings, and the occurence in consecutive order was highly improbable according to the correlation. The probable cause of the recent, "consistent" error was an unacknowledged sensitivity of the burn rate correlation to a coincidental change in the proportions of fine and coarse oxidizer fractions.

The basis for a more reliable correlation is a K_n condition for test motor burn rate data which has been confirmed to yield a correlation that is insensitive to such changes as oxidizer particle size conditions. This best K_n condition is selected from within a range of K_n conditions that have been applied simultaneously to propellant burn rate tests in each of several mixes that are cast into each of a series of Algol II motors. This series of Algol II motors must involve significant changes in oxidizer particle size. As the Algol II motors are fired, in static tests (and/or flights), the burn rates are correlated with the burn rates from related test motor data for each of selected K_n conditions throughout the range available.

The range of test motor K_n conditions should include the same K_n as the Algol II motor and a K_n which will obtain a test motor burn rate that is approximately the same as the burn rate of the related Algol II. One or more intermediate K_n conditions are recommended to assure against significant errors in assuming the burn rate test data to fit the equation, $r = c\ (P)^n$. The number of test motors, among the mixes in an Algol II, that have a given K_n should provide tests for at least two-thirds of the mixes; and the number of replicates, per K_n, per mix, should be sufficient to avoid a standard error of the mean greater than one-half percent, by demonstration. This error in burn rate values and evaluations of mix-to-mix average values for a K_n condition should be based upon a constant K_n for the burn rate values.

The program can be accomplished by the special testing of propellant in motors made for flight. The requisite changes in oxidizer particle size (confirmed by significant changes in the burning rate exponent) can be accomplished deliberately, with an acceptance of the prediction error that results. (The effect of the deliberate changes on Algol II burn rate can be minimized, for a given change in the burning rate exponent, by the manner of changing the oxidizer particle size).

An alternate procedure, costing more but saving time and flight prediction errors, could be to produce special Algol II motors for static testing. These would involve only the practical extremes of oxidizer particle size changes among them. The least number required would be one at each extreme and these would be adequate if the results could be forecast. Not being so, an additional two motors probably would be required to assure confident results.

The tests of Algol II motors and the test motors should not involve significant differences from the nominal temperature for Algol II flight performance. Changes in oxidizer particle size conditions can affect the temperature sensitivity of burning rate and the burning rate exponent, and any significant differences in temperature would require additional test motor firings for each of the K_n conditions in order to "pool" all the data at the nominal temperature.

3. ERROR IN PREDICTING THIRD-STAGE BURN TIME

A study program is recommended to further improve the accuracy in predicting X259 burn time. The latest prediction procedure does not involve the propellant test motor data that is acquired for acceptance of a powder lot.

Potentially, a prediction of burn time for the X259 motors made from a powder lot could be more precise than when based upon a single X259 static test if the same burn rate correlation concept advocated for the Algol II, and which was confirmed by the PAPS procedure for Castor I, is applied with the available X259 propellant test motor data. These data do include requisite changes in burning rate exponent among powder lots. A careful review and screening of the data and a comparison of lot-average X259 burn rate correlations with test motor burn rate values for each of selected K_n conditions within the available range would yield a best burn rate correlation and K_n condition. If the K_n is not at one extreme of the available range, the prediction accuracy obtainable with the "best" K_n is optimum for this procedure (and the level of precision in the test data) and can be compared with the accuracy of the procedure based upon an X259 static test. If the "best" K_n is at an extreme of the available range, additional testing to extend the K_n range would be needed to achieve optimum prediction accuracy based upon powder lot test motor data. A recommendation for such testing should be based upon the results of the correlation study.

4. CASTOR II BURN TIME PREDICTION PROCEDURES

It is recommended that the propellant burn rate testing and correlation concepts, as confirmed for Castor I, and underlying previous recommendations 2 and 3, be applied to the Castor II motor.

NOTE: The concept is most expediently and economically applied during R & D of a new motor. It is recommended that new procurement contracts for any motor require the burn time prediction procedure to be based upon the subject concept unless the trajectory sensitivity to burn time prediction errors is unimportant or the motor manufacturing practice permits testing (for each temperature specified) two or more of a "uniform population" of the motor type as samples for burn rate evaluation.

5. ERROR IN FLIGHT MOTOR PERFORMANCE TELEMETRY DATA

A program is recommended to determine the sources of the largest errors that result in a combined error greater than one percent, one sigma, in the unpredicted variation of the integrals of head-cap pressure and apparent vacuum thrust (as calculated from longitudinal acceleration data). The

suspected sources of error should include calibration practices, tape recording and tape copies, ground station equipment and operating practices.

The program should provide recommendations for coordinated changes to the telemetry and ground station systems that will reduce the unpredicted variation in both types of integrals to within one percent, one sigma, and reduce the variation in the ratio of apparent vacuum thrust to head-cap pressure for each motor type to within 1.4 percent after accumulation (to within the "equilibrium pressure" interval) of any fraction of the pressure integral.

6. PERFORMANCE EFFECTS OF CONFIGURATION DIFFERENCES

A program is recommended to extend the state of the science/art in predicting the differences in behavior of a propellant when burned in motors of different size or configuration. Such a program should be planned and supervised by individuals who are abreast of the current state of the basic mechanism of propellant pyrolysis and combustion reaction and who are acquainted with solid motor manufacturing and operating variables. The individuals should have access to test facilities and test vehicles required to obtain conclusive results through each phase of the program.

APPENDIX B

DETERMINATION OF

PROPELLANT WEIGHT FLOW RATE

1. BACKGROUND

The flight thrust, versus time, of a Scout propulsion motor has been calculated from telemetry data from instantaneous head-cap pressure and acceleration measurements. Past practice adopted a nominal value of inertia weight remaining versus time. Telemetry data, pre-flight data and/or other nominal data provide the other required values. To solve for the motor thrust an instantaneous value for propellant weight remaining is needed and was calculated from the head-cap pressure data. Propellant flow rate was assumed to vary, during motor burning, in direct proportion to the head-cap pressure.

This assumption would be approximately correct if the internal inerts flow rate varied in direct proportion to propellant flow rate but such is not the case. Other important features of motor performance which prevent high accuracy in propellant flow rate and, hence, in thrust are the changes in nozzle throat area and in the motor port velocity (which causes port pressure drop and a resulting increase in head-end pressure that is independent of propellant flow rate and thrust). Actually, internal inerts flow rate varies independently of propellant flow rate in such a degree that a significant improvement in the accuracy of thrust values probably can be achieved by acknowledging the disproportionate change in internal inerts flow rate during motor burning.

2. PROPELLANT FLOW RATE

C^* for any propellant may be calculated from $C^* = \frac{P\ g\ At}{w}$

Reference 3 presents evidence that the specific impulse of pyrolized inerts can be represented as one-half the specific impulse of the propellant alone. This supports an approximation that the C^* of the gas from pyrolized inerts, in a propellant inert gas mixture, is one-half the C^* of the propellant alone.

The concentration of inert gas in the total gas flow may change during burning of a motor. The effect on the C^* of the mixture may be assumed to be linear as described in the following sketch.

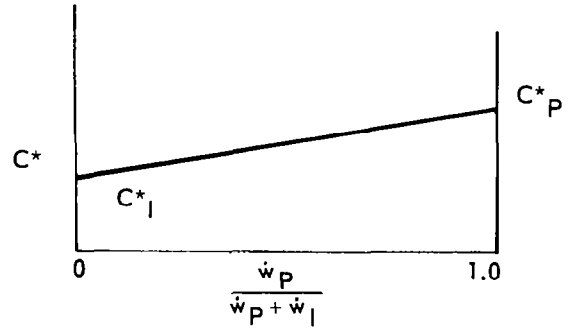

then

$$C^* = \frac{C^*_P}{2} \left(\frac{\dot{w}_P}{\dot{w}_P + \dot{w}_I + 1} \right) \tag{2}$$

Now rewriting Equation 1 and letting $\dot{w} = \dot{w}_P + \dot{w}_I$

$$\frac{P_g A_t}{C^*} = \dot{w}_P + \dot{w}_I \tag{3}$$

Dividing both sides by $\dot{w}_P$

$$\frac{P_g A_t}{c^* \dot{w}_P} = \frac{\dot{w}_P + \dot{w}_I}{\dot{w}_P} \tag{4}$$

Substituting Equation 2 and solving for $\dot{w}_P$

$$\dot{w}_P = \frac{P_g A_t}{C^*_P} - \frac{\dot{w}_I}{2} \tag{5}$$

However

$$C^* W_c = C^*_P W_P + C^*_I W_I \tag{6}$$

and since $C^*_I = \frac{C^*_P}{2}$ (7)

$$C^* W_c = C^*_P W_P + \frac{C^*_P}{2} W_I \tag{8}$$

Substituting Equation 8 in Equation 5

$$\dot{w}_P = \left[\frac{P_g A_t}{C^* (W_P + W_I)} (W_P + \frac{W_I}{2}) \right] - \frac{\dot{w}_I}{2} \tag{9}$$

APPENDIX C

CALCULATION OF THE INSTANTANEOUS WEIGHT-REMAINING OF MOTOR CONSUMABLES

1. BACKGROUND

Appendix A presented the primary basis (vehicle weight-remaining and longitudinal acceleration) for evaluating Scout motor thrust in flight. Also presented were the influences of changing motor conditions (during burning time) on the propellant weight flow rate.

The past practice of determining the instantaneous weight-remaining, W_R, of motor internal consumables is given by the equation

$$W_R = \left[W_P + W_{IN} \right] \left[1 - \frac{\int_o^t P dt}{\int_o^{tT} P dt} \right] \qquad (1)$$

This equation implies that the propellant weight flow rate at a given instant is given by

$$\dot{w}_P = \left((W_P + W_I)_N \quad P / \int_o^{tT} P dt \right) - \dot{w}_{IN} \qquad (2)$$

In these equations there is no provision for inputs of the changes in motor conditions during burning time. Hence, a more comprehensive equation is required for more accurate evaluation of Scout motor thrust in flight.

2. EQUATION DERIVATION

Let $C^*_I = Q\, C^*_P$ (3)

where C^*_I and C^*_P = characteristic velocities of the flowing products of pyrolysis of the consumable inerts and the propellant, respectively

Q = proportionality constant, calculated from C^*_I / C^*_P, or as estimated

In the derivation of Equation 9 of Appendix B, the specific approximation, $C^*_I = C^*_P/2$, was used. By adopting the generalized approximation in Equation 3, above, a more general form of Equation 9 is derived:

$$\dot{w}_P = \frac{g P_c (A_t)_N \left[W_P + Q W_{IN} \right]}{\bar{C}^*_c \left[W_P + W_{IN} \right]} - Q \dot{w}_{IN} \qquad (4)$$

Where

P_c = stagnation pressure at nozzle entrance

$$\bar{C}^*_c = g\bar{A}_t \left(\int_o^{t_T} P_c dt \right) / \left[W_P + W_{IN} \right]$$

Flight measurements of motor performance are limited to headcap pressure and the total pressure integral but nominal tables of instantaneous values of changing motor conditions can be prepared. Neglecting individual motor discrepancies from the nominals, it is assumed that the following quantities are unchanged from the nominals in any motor:

$$\frac{P_c}{\bar{P}}, \quad \int_o^{t_T} P_c dt, \quad \int_o^{t_T} P dt, \quad A_t, \quad \bar{A}_t, \text{ and } \dot{w}_I$$

Equation 4 can have these nominals substituted, obtaining

$$\dot{w}_P = \frac{C_N \, P \, W_P + Q\dot{W}_{IN}}{\int_o^{t_T} P dt} - Q\dot{w}_{IN} \qquad (5)$$

Where

$$C_N = \left[\frac{P_c}{P} \right]_N \left[\frac{A_t}{\bar{A}_t} \right]_N \Bigg/ \left[\frac{\int_o^{t_T} P_c dt}{\int_o^{t_T} P dt} \right]_N \qquad (6)$$

Equation 5 can be modified further to calculate the instantaneous weight remaining of consumable motor materials by adding the nominal flow rate of inerts to obtain the total rate of consumption. Integrating with respect to time and deducting the result from the total consumables, yields:

$$W_R = W_P + W_{IN} - \frac{\bar{C}_N \left(\int_o^{t} P dt \right) \left[W_P + QW_{IN} \right]}{\int_o^{t_T} P dt} + QW_{ID_N} - W_{ID\,N} \qquad (7)$$

where $W_{ID_N} = \int_o^{t} \dot{w}_{IN} dt$, the discharged weight of inerts.

$$\bar{C}_N = \left(\int_o^{t} C_N dt \right)/t$$

Equation 7 reduced, becomes

$$W_R = W_P + W_{IN} - \frac{\bar{C}_N \left(\int_o^{t} P dt \right) \left[W_P + QW_{IN} \right]}{\int_o^{t_T} P dt} + W_{IDN} (Q-1) \qquad (8)$$

This equation permits input of any value of Q. If Q is assigned a value of unity, Equation 8 reduces to

$$W_R = \left[W_P + W_{IN} \right] \left[1 - \frac{\bar{C}_{Ni} \left(\int_o^{t} P dt \right)}{\int_o^{t_T} P dt} \right] \qquad (9)$$

If each of the quantities that comprise C_{Ni} are assigned values of unity, Equation 9 reduces to

$$W_R = \left|W_P + W_{IN}\right| \left[1 - \frac{\int_0^t P\,dt}{\int_0^{t_T} P\,dt}\right] \tag{10}$$

which is the equation that has been standard in practice.

Equation 8 provides a means for more accurately evaluating the instantaneous motor consumable-weight remaining (and motor thrust) in flight. Hence, the error in pre-flight predictions of motor performance can be evaluated more accurately; and the discrepancy between post-flight methods (mass-acceleration, radar, etc.) of computing the vehicle trajectory can be more accurately evaluated.

The improvement realized in applying these equations to post-flight evaluations of motor performance depends, of course, upon the accuracy of:

1. The nominal values which represent the conditions of the motor in flight.

2. The measured values of head-cap pressure which represents the performance of the motors in flight.

3. The measured values of longitudinal acceleration, the predictions of drag, and the values for weight of vehicle components in flight.